

**UNIVERSIDADE FEDERAL DO ESPÍRITO SANTO**

**CENTER OF TECHNOLOGY**

**GRADUATE PROGRAMME IN ENVIRONMENTAL ENGINEERING**

**YASMIN KAORE LAGO KITAGAWA**

**STUDY OF CHILDREN'S EXPOSURE TO AIR POLLUTION IN THE  
METROPOLITAN REGION OF VITÓRIA**

**ESTUDO DA EXPOSIÇÃO DE CRIANÇAS À POLUIÇÃO ATMOSFÉRICA NA  
REGIÃO METROPOLITANA DE VITÓRIA**

**VITÓRIA**

**2022**

YASMIN KAORE LAGO KITAGAWA

**STUDY OF CHILDREN'S EXPOSURE TO AIR POLLUTION IN THE  
METROPOLITAN REGION OF VITÓRIA**

*A thesis submitted to Programa de Pós-Graduação em Engenharia Ambiental of the Centro Tecnológico da Universidade Federal do Espírito Santo, for the degree of Doctor in Environmental Engineering.*

Supervisor: Prof. Davidson Martins Moreira, Dr.

Co-supervisor: Prof. Erick Giovani Sperandio Nascimento, Dr.

**VITÓRIA**

**2022**

Ficha catalográfica disponibilizada pelo Sistema Integrado de Bibliotecas - SIBI/UFES e elaborada pelo autor

---

L177s LAGO KITAGAWA, YASMIN KAORE, 1990-  
Study of children's exposure to air pollution in the Metropolitan Region of Vitória / YASMIN KAORE LAGO KITAGAWA. - 2022.  
225 f. : il.

Orientador: Davidson Martins Moreira.  
Coorientador: Erick Giovani Sperandio Nascimento.  
Tese (Doutorado em Engenharia Ambiental) -  
Universidade Federal do Espírito Santo, Centro Tecnológico.

1. Poluição urbana. 2. Ar - Poluição. 3. Atmosfera. 4. Química atmosférica. 5. Modelos químicos. I. Martins Moreira, Davidson. II. Sperandio Nascimento, Erick Giovani. III. Universidade Federal do Espírito Santo. Centro Tecnológico. IV. Título.

CDU: 628

---




UNIVERSIDADE FEDERAL DO ESPÍRITO SANTO  
CENTRO TECNOLÓGICO  
PROGRAMA DE PÓS-GRADUAÇÃO EM ENGENHARIA AMBIENTAL

# ESTUDO DA EXPOSIÇÃO DE CRIANÇAS À POLUIÇÃO ATMOSFÉRICA NA REGIÃO METROPOLITANA DE VITÓRIA


**Yasmin Kaore Lago Kitagawa**

**Banca Examinadora:**

 Documento assinado digitalmente  
DAVIDSON MARTINS MOREIRA  
Data: 07/07/2022 14:40:32-0300  
Verifique em <https://verificador.itl.br>

---

**Prof. Dr. Davidson Martins Moreira**  
Orientador - PPGEA/CT/UFES

 Documento assinado digitalmente  
ERICK GIOVANI SPERANDIO NASCIMENTO  
Data: 07/07/2022 11:47:30-0300  
Verifique em <https://verificador.itl.br>

---

**Prof. Dr. Erick Giovanni Sperandio Nascimento**  
Coorientador – SENAI CIMATEC

 Documento assinado digitalmente  
JANE MERI SANTOS  
Data: 06/07/2022 15:33:36-0300  
Verifique em <https://verificador.itl.br>


---

**Prof.<sup>a</sup> Dr.<sup>a</sup> Jane Meri Santos**  
Examinadora Interna – PPGEA/UFES

 Documento assinado digitalmente  
Taciara Toledo de Almeida Albuquerque  
Data: 07/07/2022 11:33:34-0300  
Verifique em <https://verificador.itl.br>


---

**Prof.<sup>a</sup> Dr.<sup>a</sup> Taciana Toledo de Almeida Albuquerque**  
Examinadora Interna – PPGEA/CT/UFES

 Documento assinado digitalmente  
GILBERTO FERNANDO FISCH  
Data: 30/06/2022 16:39:50-0300  
Verifique em <https://verificador.itl.br>

---

**Prof. Dr. Gilberto Fernando Fisch**  
Examinador Externo – INPE

 Documento assinado digitalmente  
LUIZ CLAUDIO GOMES PIMENTEL  
Data: 04/07/2022 07:35:55-0300  
Verifique em <https://verificador.itl.br>

---

**Prof. Dr. Luiz Claudio Gomes Pimentel**  
Examinador Externo – UFRJ

**Elisa Valentim Goulart**  
Coordenadora do Programa de Pós-Graduação em Engenharia Ambiental  
UNIVERSIDADE FEDERAL DO ESPÍRITO SANTO

Vitória/ES, 28 de junho de 2022



## ACKNOWLEDGEMENT

I would like to thank God for the blessing of living healthy, and, for somehow showing me that everything has a purpose and it is worth it! I truly believe that I became a better person during the graduate process.

I would like to thank my parents and my sister, despite my absence at home for over 10 years including my undergraduate studies and the time I lived abroad because of my studies, they always encouraged me so much for pursuing studying, not to give up, they cheered for my accomplishments and had patience with me till finish this PhD.

I would like to thank my advisors, Dr. Davidson Moreira and Dr. Erick Nascimento, for trusting me and my work, even in the challenging moments. The distance between us in no way interfered with the student-advisor relationship and the development of our work.

I also would like to thank my coworkers, especially Dr. Taciana Toledo and Dr. Rizzieri Pedruzzi, for their friendship and for sharing their knowledge and time. Thank you for all the support, advice, and lots of laughs. I will always remember and carry you guys with me.

A special thank you to Dr. Prashant Kumar, who has opened the doors of the Global Centre for Clean Air Research (GCARE) at the University of Surrey and supported me as a visiting researcher and encouraged me to be a better researcher.

I would like to thank all my friends and professors from NQualiAr, SENAI-CIMATEC, and GCARE, which have supported me with advice and partnership, helped me fix some issues, process my data, implement the models, among other activities to carry out my studies. I am not citing the names here to not be unfair and forget someone. Anyway, thank you so much my friends from academia and all other friends from Brazil and around the world for sending good energies and cheering for me.

Thank to the Coordenação de Aperfeiçoamento de Pessoal de Nível Superior (CAPES) together with the Programa Institucional de Internacionalização (CAPES-PrInt) for grating this study. Thank you to the Supercomputing Center for Industrial Innovation (OGUM CIMATEC) for allowing me to perform my simulations. Thank you to ArcelorMittal Tubarão for funding the ASMA-Vix project.

## ABSTRACT

This study estimates exposure and inhaled dose to air pollutants of children residing in a tropical coastal-urban area, namely the Metropolitan Region of Vitória (MRV), highly influenced by industrial and urban emissions, located in Southeast Brazil. The air pollutant concentration data were provided by the chemistry and transport Community Multiscale Air Quality (CMAQ) model together with the Integrated Source Apportionment Method (ISAM) tool. The simulations were performed over three months (November/2019, December/2019, and February/2020) using a local inventory, which was processed by the Sparse Matrix Operator Kernel Emission (SMOKE). The meteorological fields were provided by the Weather Research and Forecasting (WRF-Urban) model while the boundary (BCON) and initial (ICON) conditions were performed by the global atmospheric chemistry model GEOS-Chem. Sensitivity analyses were conducted to investigate the relationship between air pollutant concentrations and the configuration of the lowest model level height ( $z = 4$  m,  $z = 10$  m,  $z = 20$  m) using the multi-layer urban canopy model BEP (Building Effect Parameterisation), totalizing nine simulations for each model. Once the air pollutant concentrations were predicted by the numerical modelling system, the personal exposure was calculated using information from the time-activities diaries of the children, and *I/O* ratios were also employed to consider the amount of time they spent indoors. In total, eight exposure scenarios were assessed, one was using data from the fixed monitoring station nearby children's residences, and three used the CMAQ model. In addition, each one considered two approaches (*i*) assuming no indoor correction and (*ii*) using *I/O* values to represent differences between indoor and outdoor concentrations. The scenarios were compared with NO<sub>2</sub> personal monitors ( $12.3 \pm 5.1 \mu\text{g}/\text{m}^3$ ) worn by twenty-one children and revealed that the use of *I/O* correction benefitted exposure results using the monitoring station ( $9.3 \pm 2.7 \mu\text{g}/\text{m}^3$ ). On the other hand, it has not benefitted exposure results using the CMAQ model, in which the most suitable performance was found with the configuration  $z = 20$  m without *I/O* adjustment ( $15.9 \pm 2.0 \mu\text{g}/\text{m}^3$ ). The exposures to O<sub>3</sub>, PM<sub>10</sub>, PM<sub>2.5</sub>, and PM<sub>1</sub> were qualitatively estimated since there were no personal observations. Nevertheless, the results were presented comparing both indirect methods (monitoring station and model). The dose assessment considered two approaches for PM<sub>2.5</sub> and PM<sub>1</sub>, namely the average daily potential dose (ADD<sub>pot</sub>) and the respiratory deposition dose (RDD). The inhaled dose intake by boys tended to be higher than girls because boys usually breathe faster than girls. However, the results showed how this assessment is highly influenced by personal data (e.g. age, gender, respiratory parameters, and physical activities). Finally, the source apportionment

assessment revealed that the greatest contributors to children's exposure were the boundary conditions, the vehicular exhausts, the industrial point sources, the shipping sector, and the road dust resuspension, suggesting that emissions control policies have to integrate different levels of government. In conclusion, the exposure of children to air pollutants estimated by the numerical model in this work was comparable to other studies found in the literature, showing one of the advantages of using the modelling approach since some air pollutants are poorly spatially represented and/or are not routinely monitored by environmental agencies in many regions. Additionally, the ISAM showed to be a powerful tool that could aid local, state, and federal authorities to make decisions.

**Keywords:** children, personal exposure, NO<sub>2</sub>, fine particles, source apportionment; air quality modelling.

## LIST OF ACRONYMS

ADD <sub>pot</sub>	Average daily potential dose
ADMS	Atmospheric Dispersion Modelling System
ANNs	Artificial Neural Networks
AOD	Aerosol Optical Depth
AQG	Air Quality Guidelines
AQMBC	Air Quality Model Boundary Condition tool
BC	Black Carbon
BCON	Boundary Conditions
BEP	Building effect parameterisation
BFM	Brute Force Method
BMI	Body Mass Index
BVOCs	Biogenic Volatile Organic Compounds
BW	Body weight
C	The concentration of the pollutant
C1	Campaign 1 in the Andorinhas district between November 2-17, 2019
C2	Campaign 2 in the Maruípe district between December 4-19, 2019
C3	Campaign 3 in the Itararé district between February 12-19, 2020
CALPUFF	California Puff Model
CAMx	Comprehensive Air Quality Model with Extensions
CATT-BRAMS	Coupled Aerosol and Trace Gas Transport Model to the Brazilian Developments of the Regional Atmospheric Modelling System
CLM4	Community Land Model 4
CMAQ	Community Multiscale Air Quality model
CMB	Chemical Mass Balance
CTMs	Chemical Transport Models
CO	Carbon monoxide
COPD	Chronic Obstructive Pulmonary Disease
DARS	Data Attribute Rating System
DF	Deposition Fraction
d <sub>p</sub>	Median particle diameter
E	Exposure
EC	Elemental Carbon
ECMWF	European Centre for Medium-Range Weather Forecasts
EDGAR	Emissions Database for Global Atmospheric Research-Hemispheric Transport of Air Pollution
EEA	European Environmental Agency
EIIP	Emission Inventory Improvement Programme
EMEP	European Monitoring and Evaluation Programme
ERA5	Global atmospheric reanalysis
ERI	Emission Reduction Impacts
<i>f</i>	Breathing Frequency

FAC2	Fraction of predictions within a factor of two of observations
FARM	Flexible Air quality Regional Model
FEF <sub>25-75</sub>	Forced Expired Flow at 25–75% FVC
FEV1	Forced Expiratory Volume in 1 second
FVC	Forced Vital Capacity
GAM	Generalized Additive Model
GEOS-Chem	Global chemical transport model
GIS	Geographic Information Systems
HAPEM	Hazardous Air Pollutant Exposure Model
HFX	Sensible heat flux
HRs	Hazard Ratios
ICON	Initial Conditions
IF	Inhalable Fraction
I/O ratio	The air pollutant indoor/outdoor ratio
IDW	Inverse Distance Weighting
IOA	Index of Agreement
IR	Inhalation Rate
ISAM	Integrated Source Apportionment Method
LAI	Leaf Area Index
LSM	Land Surface Model
LT	Local Time
LULC	Land Use and Land Cover
LUR	Land use regression models
MAGE	Mean absolute gross error
MB	Mean bias
MCIP	Meteorology-Chemistry Interface Processor
MDA8	Maximum daily 8-hr average for ozone
MEGAN	Model of Emissions of Gases and Aerosols from Nature
ML	Machine Learning
MLR	Multiple Linear Regression
MODIS	Moderate Resolution Imaging Spectroradiometer
MRV	Metropolitan Region of Vitória
NMB	Normalized mean bias
NME	Normalized mean error
NO <sub>2</sub>	Nitrogen dioxide
NO <sub>x</sub>	Nitrogen oxides
O <sub>3</sub>	Ozone
PBL	Planetary Boundary Layer
PM	Particulate matter
PM <sub>0.1</sub> or UFP	Ultrafine particles
PM <sub>1</sub>	Particulate matter with a diameter of 1 µm or less
PM <sub>10</sub>	Particulate matter with a diameter of 10 µm or less

PM <sub>2.5</sub>	Particulate matter with a diameter of 2.5 µm or less
PMF	Positive Matrix Factorization
PMSS	Parallel Micro-Swift-Spray
PNC	Particle Number Concentration
PROCONVE	Control of Air Pollution by Automotive Vehicles
PRONAR	National Programme for Control of Air Quality
PSAT	Particle Source Apportionment Technology
PFT	Plant Functional Type
<i>r</i>	Pearson correlation coefficient
RDD	Respiratory Deposition Dose
RH <sub>2</sub>	2-meter relative humidity
RMSE	Root mean square error
RRTMG	Rapid Radiative Transfer Model
RT	Total Respiratory Resistance
SACZ	South Atlantic Convergence Zone
SASH	South Atlantic Subtropical High
SHEDS	Stochastic Human Exposure and Dose Simulation
SLUCM	Single-Layer Urban Canopy Model
SMOKE	Sparse Matrix Operator Kernel Emission
SO <sub>2</sub>	Sulfur dioxide
SVR	Support Vector Regression
T <sub>2</sub>	2-meter surface temperature
UCM	Urban Canopy Model
USEPA	U.S. Environmental Protection Agency
VEG	Vegetation Coverage
V <sub>max50</sub> and V <sub>max75</sub>	Maximal flow at 50 and 75% expired vital capacity
VOCs	Volatile organic compounds
VR	Ventilation Rate
VT	Tidal Volume
WD <sub>10</sub>	10-meter wind direction
WHO	World Health Organization
WRF	Weather Research and Forecasting model
WRF-Chem	Weather Research and Forecasting model coupled with Chemistry
WS <sub>10</sub>	10-meter wind speed
XGBoost	Extreme Gradient Boosting
<i>z</i>	Model height

## LIST OF FIGURES

Figure 1. Environmental epidemiologic studies design based on CDC (2012) and Nieuwenhuijsen (2015). The classification with blue lines is based on Andersen (2020).	26
Figure 2. Relationship among health effects, exposure estimates, and air pollution. Based on Nieuwenhuijsen (2015).	35
Figure 3. The relative size of particles. Source: Ang <i>et al.</i> (2020).	40
Figure 4. The exposure process, defined by (Furtaw, 2001).	41
Figure 5. The respiratory system. Source: Guarneri and Balmes (2014)	43
Figure 6. Predicted total and regional deposition for adults in light exercise. Alv (alveolar) and TB (tracheobronchial). Source: Hinds (1999)	44
Figure 7. Hourly variation of NO <sub>2</sub> concentrations at four microenvironments and its effect on spatiotemporal variation on personal exposure. Source: Mölter (2012).	45
Figure 8. Schematic diagram of the key factor influencing indoor air pollution and the home as a microenvironment. Source: Vallero (2014b).	46
Figure 9. Location of Espírito Santo State in Brazil (upper left) and the location of the Metropolitan Region of Vitória in Espírito Santo State (lower left). The location of the air quality stations (AQS) used to evaluate the performance of the WRF-Urban and CMAQ-ISAM models.	70
Figure 10. Location of the selected children of the ASMA-Vix project and the location of their schools, main roads, and industries in the city of Vitória.	74
Figure 11. Hourly time series of observed WS10 in November/December 2019 and February 2020 at the surface meteorological stations in the MRV.	79
Figure 12. Boxplots of observed WS10 in November/December 2019 and February 2020 at the surface meteorological stations in the MRV. The diamonds represent the outliers, the bars represent the minimum and maximum values, and the lines represent the mean values.	79
Figure 13. Hourly temperature comparing the observations among the stations in the MRV.	80
Figure 14. Hourly relative humidity comparing the observations among the stations in the MRV.	80
Figure 15. Observed accumulated daily precipitation at ST02 (Carapina) and INMET stations.	82
Figure 16. The synoptic weather charts of CPTEC/INPE on November 13, 2019.	82
Figure 17. Schematic representation of the various models and methods used in the present work to evaluate the exposure of children that reside in the Metropolitan Region of Vitória (MRV), Brazil.	83
Figure 18. Geopotential height across the D03 domain from the south (S) to north (N) from the bottom to the model top and within the first 500 m.	88
Figure 19. Land use classes of MODIS used as input data for the WRF model and MCIP processor. 2: Evergreen broadleaf forest (dark green), 8: Woody savannas (light pink), 9: Savannas (light green), 10: Grasslands (orange), 12: Croplands (yellow), 13: Urban and Built-up (red), 14: Natural Vegetation Mosaic (purple).	90
Figure 20. Spatial distribution of the monthly mean leaf area index (LAI) during November and December 2019 and February 2020 over the D03 domain.	92
Figure 21. Spatial distribution of the monthly mean of isoprenes and terpenes emissions (moles/s) during November and December 2019 and February 2020 over the D03 domain.	93
Figure 22. Monthly temporal profile used by the SMOKE.	95

Figure 23. Weekly temporal profile used by the SMOKE. ....	95
Figure 24. Hourly temporal profile used by the SMOKE. ....	95
Figure 25. Chemical speciation of the main sources, which <i>S</i> represents the stacks labelled as point sources and <i>Ship</i> the shipping sector. The names of the species are described as follows, which <i>P</i> means particulate: <i>PAL</i> : aluminum, <i>PCA</i> : calcium, <i>PCL</i> : chloride, <i>PEC</i> : elemental carbon, <i>PFE</i> : iron, <i>PK</i> : potassium, <i>PMN</i> : manganese, <i>PMOTHR</i> : all other unspiciated particulates, <i>PNCOM</i> : non-carbon organic matter, <i>PNH4</i> : ammonium, <i>PNO3</i> : nitrate, <i>POC</i> : organic carbon, <i>PSI</i> : silica, <i>PSO4</i> : sulfate, <i>PTI</i> : titanium, <i>PNA</i> : sodium, <i>PMG</i> : magnesium, <i>PH2O</i> : particle-bound water.....	97
Figure 26. Location of the top ten largest emission sources of PM <sub>2.5</sub> according to the local emission inventory (IEMA, 2019), which are represented by the point sources and shipping sector. The yellow dots are the air quality stations. ....	97
Figure 27. Comparison of average boundary conditions of the particles from the GEOS-Chem simulation in November 2019 and the CMAQ default fixed values available in version 5.3.2. The bars represent minimum and maximum values.....	101
Figure 28. Comparison of average boundary conditions of the gases from GEOS-Chem simulation in November 2019 and the CMAQ default fixed values available in version 5.3.2. The bars represent minimum and maximum values.....	103
Figure 29. Vertical and horizontal patterns of the four boundary conditions of the D03 domain for O <sub>3</sub> and NO <sub>x</sub> in November 2019. ....	104
Figure 30. Comparison of WS10 hourly time series (left) and mean hourly variation (right) for observed (black line) and modelled by the WRF-Urban varying the lowest model height for each monitoring site. ....	120
Figure 31. Comparison of the averages of statistical indices for each station and configuration, considering the three months together, for WS10. ....	122
Figure 32. Comparison of the averages of statistical indices for each station and configuration, considering the three months together, for WD10. ....	126
Figure 33. Comparison of T2 hourly time series (left) and mean hourly variation (right) for observed (black line) and modelled by the WRF-Urban varying the lowest model height for each monitoring site. ....	128
Figure 34. Comparison of RH2 hourly time series (left) and mean hourly variation (right) for observed (black line) and modelled by the WRF-Urban varying the lowest model height for each monitoring site. ....	129
Figure 35. Comparison of the averages of statistical indices for each station and configuration, considering the three months together, for T2.....	131
Figure 36. Comparison of the averages of statistical indices for each station and configuration, considering the three months together, for RH2.....	131
Figure 37. Boxplots of hourly observed NO <sub>2</sub> , O <sub>3</sub> , PM <sub>2.5</sub> , and PM <sub>10</sub> for each station and month. ....	134
Figure 38. Comparison of observed and modelled 24-h average NO <sub>2</sub> (left) and mean hourly variation (right) for each monitoring station and model's configuration. The red line represents the final standard of WHO 2021 (25 µg/m <sup>3</sup> ).....	137
Figure 39. Comparison of observed and modelled MDA8 O <sub>3</sub> (left) and mean hourly variation (right) for each monitoring station and model's configuration. The red line represents the final standard of WHO 2021 (100 µg/m <sup>3</sup> ).....	138



Figure 40. Comparison of observed and modelled 24-h average PM <sub>2.5</sub> (left) and mean hourly variation (right) for each monitoring station and model's configuration. The red line represents the final standard of WHO 2021 (15 µg/m <sup>3</sup> ). .....	140
Figure 41. Comparison of observed and modelled 24-h average PM <sub>10</sub> for each monitoring station and model's configuration. The red line represents the final standard of WHO 2021 (45 µg/m <sup>3</sup> ). .....	141
Figure 42. NME and NMB for 24-h averages of NO <sub>2</sub> , PM <sub>2.5</sub> , and PM <sub>10</sub> . The NME (NMB) goal (green line) and criteria (red line) considered <35% (<±10%) and <50% (<±30%), respectively. For MDA8 O <sub>3</sub> , NME (NMB) goals and criteria were <15% (<±5%) and < 25% (<±15%), respectively. ....	143
Figure 43. Comparison of children's hour-mean exposure estimates using data from the ASMA-Vix station and the CMAQ model during Campaign 1 (November 2-17, 2019) in Andorinhas. The red line represents the concentration detected in the passive samplers wore by the children. The suffix I/O indicates that concentrations were adjusted for home and school microenvironments. ....	149
Figure 44. Comparison of children's hour-mean exposure estimates using data from the ASMA-Vix station and the CMAQ model during Campaign 2 (December 4-19, 2019) in Maruípe. The red line represents the concentration detected in the passive samplers wore by the children. The suffix I/O indicates that concentrations were adjusted for home and school microenvironments. ....	151
Figure 45. Comparison of children's hour-mean exposure estimates using data from the ASMA-Vix station and the CMAQ model during Campaign 3 (February 12-19, 2020) in Itararé. The red line represents the concentration detected in the passive samplers wore by the children. The suffix I/O indicates that concentrations were adjusted for home and school microenvironments. ....	152
Figure 46. Comparison of the children personal exposure to NO <sub>2</sub> measured by the passive samplers (green), and estimated using data from the ASMA-Vix station (yellow) and the CMAQ model with three different heights. The diamond (lines) represent the mean (median) values, the circles represent the outliers, and the bars represent the minimum and maximum values. ....	154
Figure 47. Average daily exposure of children to a) PM <sub>10</sub> , b) PM <sub>2.5</sub> , c) O <sub>3</sub> , and d) PM <sub>1</sub> using the information of their daily routines and data from the ASMA-Vix station and the CMAQ model with three different heights. The diamond (lines) represent the mean (median) values, the circles represent the outliers, and the bars represent the minimum and maximum values. ....	157
Figure 48. Boxplot of the hourly PM <sub>2.5</sub> inhaled dose of children (unadjusted for body weight) considering (a) no I/O correction and (b) with I/O correction using data from the monitoring station and the CMAQ model with $z = 20$ m. ....	161
Figure 49. Boxplot of the hourly simulated PM <sub>1</sub> inhaled dose of children (unadjusted for body weight) considering (a) no I/O correction and (b) with I/O correction using data from CMAQ model $z = 20$ m. ....	162
Figure 50. Children's potential average daily dose (ADD <sub>pot</sub> ) of a) PM <sub>2.5</sub> with I/O correction, b) PM <sub>2.5</sub> with no I/O correction, and c) PM <sub>1</sub> using data from the monitoring station and the CMAQ model $z=20$ m. The diamond (lines) represent the mean (median) values, the circles represent the outliers, and the bars represent the minimum and maximum values. ....	163
Figure 51. Respiratory deposition doses (RDD) throughout the respiratory tract of boys and girls during sleeping and light exercises for a) PM <sub>2.5</sub> with I/O correction, b) PM <sub>2.5</sub> with no I/O	

correction, and c) PM <sub>1</sub> using data from the monitoring station and the CMAQ model z=20 m. .....	165
Figure 52. Contributions of different sectors to NO <sub>2</sub> concentrations for each campaign during a) weekdays and b) weekends. The numbers in the pie chart indicate the percentage of the most relevant sectors. ....	169
Figure 53. Contributions of different sectors to O <sub>3</sub> concentrations for each campaign during a) weekdays and b) weekends. The numbers in the pie chart indicate the percentage of the most relevant sectors. ....	170
Figure 54. Contributions of different sectors to PM <sub>2.5</sub> concentrations for each campaign during a) weekdays and b) weekends. The numbers in the pie chart indicate the percentage of the most relevant sectors. ....	171

## LIST OF TABLES

Table 1. Study designs in environmental epidemiology. Based on WHO (1991).....	36
Table 2. Summary and comparison of recommended long- and short-term AQG levels. Source: WHO (2021). .....	39
Table 3. Summary of the methods used to assess air pollutant concentrations. Based on Jerrett <i>et al.</i> (2005) and Hoek (2017). .....	48
Table 4. A detailed description of the experimental campaigns of the ASMA-Vix project. ...	72
Table 5. Summary of the experimental campaigns of the ASMA-Vix project. ....	74
Table 6. The location of the meteorological and air quality station in the MRV. The amount of paired data points used to compare observed and simulated data is also presented. M1 and M2 are exclusively meteorological stations. ....	76
Table 7. Observed wind roses at meteorological stations in the MRV. ....	77
Table 8. The spatial configuration adopted and physical parameterization schemes in the WRF-Urban simulations. ....	87
Table 9. Land use classification of MODIS and the occupation (%) of each class in the D03. ....	90
Table 10. The total emission of atmospheric pollutants by source (IEMA, 2019).....	94
Table 11. Inhalation rates (m <sup>3</sup> /h) for children that attended the ASMA-Vix project as a function of their activities and age, based on Yoon <i>et al.</i> (2020). ....	113
Table 12. The mean inhalation rates for males and females by age group and body mass index. Source: (Brochu <i>et al.</i> , 2011; Brochu <i>et al.</i> , 2014).....	114
Table 13. Mean ventilation rate (m <sup>3</sup> /min) for children that attended the ASMA-Vix project as a function of their activities and age, based on USEPA (2009). ....	115
Table 14. The I/O ratios adopted in the present study. ....	117
Table 15. Comparison of the wind speed performance of the present study with others found in the literature review. The values of this study were averaged among the stations.....	124
Table 16. Observed and simulated wind roses at the Airport station for each month.....	125
Table 17. Comparison of the temperature performance of the present study with others found in the literature review. The values of this study were averaged among the stations. ....	132
Table 18. Comparison of NO <sub>2</sub> performance of the present study with others found in the literature review. The values of this study were averaged among the stations. ....	145
Table 19. Comparison of O <sub>3</sub> performance of the present study with others found in the literature review. The values of this study were averaged among the stations.....	146
Table 20. Statistical analysis of exposure methods .....	153
Table 21. Comparison of the exposure to air pollutants of the present study with others found in the literature review. The values are presented in terms of mean ± standard deviations. The values of this study were presented with I/O correction. ....	160

## SUMMARY

<b>1. INTRODUCTION</b> .....	17
<b>2. OBJECTIVES</b> .....	24
<b>3. REVIEW OF THE LITERATURE</b> .....	25
<b>3.1 EPIDEMIOLOGICAL STUDIES DESIGNS</b> .....	25
<b>3.2 ASPECTS OF AIR POLLUTION EXPOSURE</b> .....	38
<b>3.3 METHODS TO EVALUATE AIR POLLUTANT CONCENTRATIONS</b> .....	47
<b>3.4 CHILDREN PERSONAL EXPOSURE TO AIR POLLUTION</b> .....	58
<b>4. METHODOLOGY</b> .....	69
<b>4.1 THE ASMA-VIX PROJECT</b> .....	69
<b>4.2 THE CLIMATOLOGICAL AND METEOROLOGICAL DESCRIPTION OF THE STUDY AREA</b> .....	75
<b>4.3 MODELLING APPROACH</b> .....	83
<b>4.3.1 WRF-URBAN MODEL</b> .....	84
<b>4.3.2 BIOGENIC EMISSIONS</b> .....	89
<b>4.3.3 SMOKE PROCESSOR</b> .....	93
<b>4.3.4 BOUNDARY AND INITIAL CONDITIONS</b> .....	98
<b>4.3.5 CMAQ MODEL</b> .....	105
<b>4.4 PERFORMANCE EVALUATION OF WRF-URBAN/CMAQ MODELS</b> ....	109
<b>4.5 EXPOSURE AND DOSE ASSESSMENT</b> .....	110
<b>5. RESULTS AND DISCUSSION</b> .....	118
<b>5.1 THE WRF-URBAN VALIDATION</b> .....	118
<b>5.1.1 WIND SPEED AND DIRECTION</b> .....	118
<b>5.1.2 TEMPERATURE AND RELATIVE HUMIDITY</b> .....	127
<b>5.2 THE CMAQ MODEL EVALUATION</b> .....	132
<b>5.3 PERSONAL EXPOSURE TO NO<sub>2</sub>: COMPARISON WITH PERSONAL DATA</b> .....	147
<b>5.4 CHILDREN EXPOSURE TO O<sub>3</sub> AND PARTICULATE MATTER</b> .....	156
<b>5.5 INHALATION DOSE ASSESSMENT OF PARTICULATE MATTER</b> .....	161
<b>5.6 SOURCES CONTRIBUTIONS TO THE CHILDREN'S PERSONAL EXPOSURE</b> .....	166
<b>6. CONCLUSIONS</b> .....	172
<b>7. REFERENCES</b> .....	176

## 1. INTRODUCTION

Air pollution has been considered one of the main environmental risks over the past decades because it can cause harmful effects on human health, particularly cardiovascular and pulmonary diseases, affecting populations' life expectancy and causing premature deaths (Pope *et al.*, 2002; Pope and Dockery, 2006; Crouse *et al.*, 2012; Lim *et al.*, 2012; Cesaroni *et al.*, 2013; Han *et al.*, 2016; Prüss-Ustün *et al.*, 2016; Miller and Newby, 2020). Children, pregnant women, the elderly, and those with pre-existing health conditions are most sensitive to the health impacts of air pollution because of their physiological characteristics (EEA, 2019).

With respect to children, they are affected by air pollution as they are still developing their immune systems (Kim *et al.*, 2013; WHO, 2018), and due to their heights. As children are shorter than adults, they are closer to the ground and, therefore, they can be more exposed to higher levels of pollution, such as from vehicle exhaust (Schwartz, 2004; Nakashima *et al.*, 2014; Kumar and Goel, 2016; Kumar *et al.*, 2017; Mudway *et al.*, 2019; Palazzi *et al.*, 2019; Sharma and Kumar, 2020). In addition, children have faster respiratory rates than adults, and thus, children inhale a higher volume of air per body weight, suggesting a higher intake of biological and chemical contaminants (Foos *et al.*, 2008; Brochu *et al.*, 2011; Brochu *et al.*, 2014). Epidemiological studies have indicated that either short- and long-term exposure to air pollution can negatively affect lung function, brain development and induce cardiorespiratory, allergic, and depressive disorders diseases in children and adolescents (Brunekreef *et al.*, 1997; Gauderman *et al.*, 2004; Guarnieri and Balmes, 2014; Schultz *et al.*, 2017; Sharma and Kumar, 2018; Zou *et al.*, 2018; Herting *et al.*, 2019; Huang *et al.*, 2019; Xu *et al.*, 2020).

Nitrogen dioxide (NO<sub>2</sub>), ground-level ozone (O<sub>3</sub>), and particulate matter (PM) are some of the air pollutants capable of harming human health (EEA, 2019). In addition, these air pollutants also have economic consequences because they affect agricultural crop yields, influence the visibility and the efficiency of solar photovoltaic panels, and directly affect Earth's climate by scattering and absorbing solar and terrestrial radiation, as well as indirectly through cloud formation (Boucher *et al.*, 2013; Zhao *et al.*, 2013; Zhou *et al.*, 2018; Maji *et al.*, 2019; Feng *et al.*, 2019; Nascimento *et al.*, 2020).

NO<sub>2</sub> is formed by combustion processes that occur in automobile engines, power plants, and domestic and industrial activities. A fact that was well-pictured in the first semester of 2020, during the COVID-19 crisis, when NO<sub>2</sub> levels were directly impacted because of the restricted

movements measures, decreasing NO<sub>2</sub> concentrations between 30% and 60% when compared to previous periods (Baldasano, 2020; Dantas *et al.*, 2020; Salma *et al.*, 2020; Jephcote *et al.*, 2021). Exposure to NO<sub>2</sub> has been associated with irritation of the eyes, nose, and throat, triggering of asthma, and reduced lung function (Koenig, 1999; Jerrett *et al.*, 2008; Hernández-Cadena *et al.*, 2009; Hesterberg *et al.*, 2009; Schultz *et al.*, 2012; Kim *et al.*, 2013). O<sub>3</sub> is formed by chemical reactions triggered by solar radiation which involve hydrocarbons, nitrogen oxides (NO<sub>x</sub>), and volatile organic compounds (VOCs). Exposure to ground-level ozone can provoke oxidative stress and inflammatory responses in the lungs and airways (Kreit *et al.*, 1989; Arjomandi *et al.*, 2015; Huang *et al.*, 2019; Bruyn and Vries, 2020; Hu *et al.*, 2020). PM is a complex mixture of solid and liquid particles suspended in the air, directly emitted into the atmosphere, or formed through gas-to-particle conversion processes (Seinfeld and Pandis, 2006; Heal *et al.*, 2012; Kumar *et al.*, 2014). Different particulates are commonly classified by their size: PM<sub>10</sub> (mass concentrations of particles smaller than 10 μm), PM<sub>2.5</sub> (fine particles), and PM<sub>0.1</sub> (ultrafine particles). Fine and ultrafine particles have been widely investigated because of their characteristics to be inhalable, which can reach the lungs and cause adverse health effects (Schultz *et al.*, 2017; Habre *et al.*, 2018; Hou *et al.*, 2020; Xu *et al.*, 2020). It also caught great attention during the COVID-19 pandemic because suspended air particles exhaled by infected people can be an important route in the mechanism of SARS-CoV-2 transmission (Kumar and Morawska, 2019).

When considering the adverse health effects due to air pollution, a key point of these studies relies heavily on knowledge of the concentrations of these air pollutants. The traditional approach uses average concentrations of the nearest monitoring station as a surrogate of personal exposure, assuming homogeneity among air pollution concentrations within the area surrounding the monitoring station, or even within the whole city (Horie and Stern, 1976; Ott, 1982; Dockery *et al.*, 1993). However, substantial challenges persist in obtaining good quality data for air quality indicators given the often-limited resource availability (Andries *et al.*, 2019). In South America, the deficiency or scarcity of information about emission data and measurement campaigns is usually faced by researchers and decision-makers (Alonso *et al.*, 2010; Andrade *et al.*, 2017). For instance, Brazil which occupies almost half of the South American continent has only 1.7% of the cities covered by air monitoring networks fixed at ground level (ISS, 2019), which mostly do not include PM<sub>2.5</sub> and are located only in some cities in the Southeast of Brazil (Peláez *et al.*, 2020). It is worth mentioning that PM<sub>2.5</sub> was included as a criteria pollutant in Brazil only in 2018, and its standard was divided into four stages, but

the deadlines for its implementation are not yet defined and the initial standard is still permissive compared to the World Health Organization (WHO) guidelines (Andreão and Albuquerque, 2021). In addition, ultrafine particles are not yet subject to monitoring. In this context, the air monitoring network poorly realistically represents the air quality status in Brazil. This lack of knowledge of temporal and spatial characteristics of the atmospheric parameters limits further studies that investigate potential air pollution control strategies and improvement of the risk assessments associated with air pollution exposure (Hu *et al.*, 2016).

To overcome this shortcoming, air pollutant concentration data have been derived by various approaches such as statistical methods, artificial intelligence algorithms, land use regression (LUR) models, satellite observations, atmospheric dispersion models, and chemical transport models (CTMs), or a combination of these methods. These approaches are very useful to areas that do not have monitoring station networks or have poorly spatial distribution. The choice of the approach will depend on the study design, but its performance is still compared to data that are measured at the ground-level station networks. LUR models, statistical and computational intelligence methods have relatively low costs and easy implementation, but they require a large amount of historical data. In addition, they cannot predict concentrations during periods of unusual emissions (e.g., the COVID-19 pandemic) and/or meteorological conditions that deviate significantly from the historical record (Baklanov and Zhang, 2020). Satellite remote-sensing data can provide complete spatial coverage and a vertically integrated measure of atmospheric components, however, close to the ground, where human beings live, its accuracy can significantly vary, leading to erroneous analyses (Alvarado *et al.*, 2019). In addition, satellite observations also have higher spatiotemporal resolution when compared to other approaches and can be highly affected by the presence of clouds, for instance. Dispersion models can provide a more detailed resolution of the spatial variations of air pollutant concentrations, however, they cannot properly treat photochemical transformations (Monticelli *et al.*, 2021). CTMs require computational power and multiple information (e.g. emission inventories, initial and boundary conditions, parameterization schemes, meteorological fields, and others), making their use sometimes unfeasible. However, they are the ones that have the ability to consider the major processes affecting air pollution formation and dispersion, especially the chemical reactions in gaseous and aerosol phases. Critical air pollutants, such as PM secondary components, O<sub>3</sub>, and NO<sub>2</sub>, are identified as having a photochemical origin or being strongly affected by photochemical processes (Isakov *et al.*, 2007). In addition, CTMs were designed for air quality regulation and management purposes, being able to do direct

linkages between emissions sources and resultant pollution (Appel *et al.*, 2020; Baklanov and Zhang, 2020).

One of the directives of air quality management is the abatement of pollution at its source. For that, extensive information is needed on the main pollution sources over a region as well as the environmental characteristics of this region to determine whether air pollution levels are due to the sources themselves, or natural factors such as climate conditions, or transboundary contributions, or a combination of these factors. Source apportionment methodologies aim at understanding the origin of the pollution and are generally used for the identification and quantification of the sources that contribute most to concentration levels. In addition, it also can inform on the efficiency of mitigation strategies, identify possible measures to be applied to a category of sources, and evaluate scenarios for future emissions (Thunis *et al.*, 2019).

Receptor-oriented models, commonly represented by the chemical mass balance (CMB) and positive matrix factorization (PMF), apportion the measured mass of an air pollutant at a given site to its emission sources by solving a mass balance equation (Mircea *et al.*, 2020). These models can quantify the source contributions based on physical and chemical characteristics (fingerprints) measured at the sampling site, linking the pollutant emissions with specific sources, and do not depend on emission inventories, meteorological and chemical processors. However, their application needs the expertise of the user to interpret the source profiles, which can lead to misinterpretation due to inability or inexperience (Santos *et al.*, 2017; Galvão *et al.*, 2019; Galvão *et al.*, 2020).

Source-oriented modelling techniques are usually based on the application of chemistry-transport models (CTMs), which follow two main approaches. The first is the sensitivity analysis, also known as the brute force method (BFM) or the emission reduction impacts (ERI), which involves zeroing out emissions from a particular source category and determining its contribution by subtracting the zero-out run and the base run with all source categories. However, in this approach, the balance of chemical reactions can be altered due to the nonlinearity of pollutants, e.g. PM<sub>2.5</sub> and O<sub>3</sub>. The second technique is the tagged species (or mass-transfer method), in which a tag is used to classify a category/sector/activity/geographical origin of the precursors and then follow their atmospheric fate. Examples of this approach are the Particle Source Apportionment Technology (PSAT) within the Comprehensive Air Quality Model with Extensions (CAMx), and the Integrated Source Apportionment Method (ISAM)



with Community Multiscale Air Quality Model (CMAQ) model. This approach is capable of apportioning source contributions from multiregional and multisectoral emissions simultaneously based on a single model run, whereas BFM requires a series of simulations to perform the same task (Burr and Zhang, 2011; Cohan and Sergey, 2011; Kwok *et al.*, 2013; Kwok *et al.*, 2015; Clappier *et al.*, 2017; Collet *et al.*, 2018; Han *et al.*, 2018; Albuquerque *et al.*, 2019; Thunis *et al.*, 2019; Mircea *et al.*, 2020; Maciel *et al.*, 2021).

Seeking a more strategic approach to managing the ambient concentrations in the Metropolitan Region of Vitória (MRV), state of Espírito Santo, Brazil, some works have treated the subject. Santos *et al.* (2017) used the CMB model to quantify the main source contributors of settleable particle (coarser particles with diameters greater than 10  $\mu\text{m}$ ), as a result of the annoyance of local dwellers and constant complaints to the local environmental agency (Machado *et al.*, 2015). Later, Galvão *et al.* (2019) used the PMF receptor model to perform the source apportionment analysis on  $\text{PM}_{10}$  and  $\text{PM}_{2.5}$ . Both studies revealed industrial sources as the main contributors of particles in the MRV, mainly those related to the pelletizing and steel industries. Indeed, the MRV is a complex coastal urban and industrialized area in southeastern Brazil with significant problems of air pollution and public health. Epidemiological studies have shown a positive correlation between ambient air pollution and hospital admissions in Vitória city (Souza *et al.*, 2014; Freitas *et al.*, 2016; Nascimento *et al.*, 2017; Souza *et al.*, 2018; Nascimento *et al.*, 2020). For instance, the increase of 8  $\mu\text{g}/\text{m}^3$ , 4  $\mu\text{g}/\text{m}^3$ , and 6  $\mu\text{g}/\text{m}^3$  in the  $\text{PM}_{10}$ ,  $\text{PM}_{2.5}$ , and  $\text{SO}_2$  concentrations were associated with a 14%, 6%, and 28% increase in the relative risk (RR) of hospital admission for respiratory diseases in children under 12 years old, respectively (Nascimento *et al.*, 2017; 2020). In addition, the prevalence of asthma and rhinitis among children in Vitória is higher than the Brazilian national average (Serpa *et al.*, 2014). However, a small number of avoided deaths and hospital admissions have been found for the MRV (Andreão *et al.*, 2018; Fernandes *et al.*, 2020). According to the authors, this was a result of not exceeding the air quality limits established by the WHO, but which was also related to the low number of air quality monitoring stations and/or lack of concentration data (for instance,  $\text{PM}_{2.5}$  is monitored only in two sites in the MRV). Although the ambiguous results, these findings indicate that air pollution levels in the MRV may affect public health even in low concentrations.

The aforementioned studies performed in the MRV were determined through air quality direct measurements. Although they are undoubtedly valuable, they are also limited to a location and

require intensive sampling and analysis. That is why numerous studies have based their results on the use of computational and numerical methods because they can be extrapolated in time and space. Both approaches are useful to estimate people's exposure to air pollution, however, these methods provide information of the pollutant concentrations in the ambient air, aiding as an indicator of local pollution and may represent a minimum value that would be found in a region (Andréão *et al.*, 2018). Meantime, each individual has a unique air pollution exposure profile, meaning that these approaches cannot replace, in terms of accuracy and representativeness, instrumental personal exposure measures that would be directly carried out according to the daily activities of each individual. Measurements with personal monitors can differ greatly from estimates using fixed monitoring stations and/or numerical models because they consider that individuals spend their time exclusively in the outdoor ambient, which is an erroneous assumption since people usually spend the majority of their time in indoor environments, such as at home, schools, offices, transit routes, among others (Ott, 1982; Kornartit *et al.*, 2010; Hannam *et al.*, 2013; Demirel *et al.*, 2014; Smith *et al.*, 2016; Rivas *et al.*, 2017; Almeida *et al.*, 2018; Niu *et al.*, 2018; Brand *et al.*, 2019; Tran *et al.*, 2020; Lei *et al.*, 2020; Lung *et al.*, 2020). For instance, in household air pollution, people are exposed to the same pollutant but from different sources. Indoor sources are related to daily human activities such as cooking, walking, cleaning, burning candles, smoking, the use of unpaved areas, building deterioration, among others (Viana *et al.*, 2011; Amato *et al.*, 2014; Rivas *et al.*, 2014; Goel *et al.*, 2015, 2021). In the absence of indoor sources, the indoor air pollution is a result of ventilation and airtightness of the spaces, people's activities, and dust resuspension (Hänninen *et al.*, 2011; Pallarés *et al.*, 2019; Shrestha *et al.*, 2019; Chen *et al.*, 2020; Faria *et al.*, 2020). Therefore, understanding personal exposure includes understanding both indoor and outdoor air pollution.

Since there is no consensus on the best approach for estimating exposure, and results can vary significantly depending on the approach adopted, the model used, spatial and temporal resolution, air pollutants, study area, and health outcomes (Jerrett *et al.*, 2005; Bravo *et al.*, 2012; Zhang *et al.*, 2012; Baklanov and Zhang, 2020; Gariazzo *et al.*, 2021), the present study aims to estimate the exposure and inhaled dose to ambient air pollution (PM<sub>10</sub>, PM<sub>2.5</sub>, PM<sub>1</sub>, NO<sub>2</sub>, and O<sub>3</sub>) of children living in the tropical coastal-urban area of Vitória, Espírito Santo, using a numerical modelling approach together with a source apportionment assessment. The modelling approach was compared with data collected from wearable passive samplers during experimental campaigns performed by the 'ASMA-Vix' study

(<https://qualidadedoar.ufes.br/asmavix>). The ‘ASMA-Vix’ project has been approved by the national ethics committee under the registration number CAAE: 09214519.1.0000.5071. This comparison allowed us to evaluate whether the predicted ambient concentrations could be used as a reliable surrogate of personal exposures in air pollution health effect studies in the study area. In addition, three different configurations with the modelling system were also conducted to assess the air pollutant concentrations at different heights because human beings, especially children, breathe in a zone close to the ground. To date, the present work is the first study using the state of the art of computational numerical modelling to investigate children’s exposure to air pollutants in Brazil.

This Ph.D. thesis begins by giving a general introduction to the epidemiological studies designs used in the field of air pollution and how they have estimated people’s exposure to air pollutants. The review considers the aspects of air pollution exposure, especially concerning the space-time activities of children. Then, it is presented all the models used to estimate the air pollutant concentration together with the study area and the climatological and meteorological conditions of the region. Finally, the results of the models’ performance, source apportionment assessment, and the estimate of the personal exposure and inhaled dose to air pollutants of children using the modelling approach are presented, followed by the general and remarkable conclusions and suggestions/recommendations for future studies. Furthermore, the contents presented in this Ph.D. thesis have been already published in three papers (Kitagawa *et al.*, 2021, 2022a, 2022b), and one more paper is in formulation.

## 2. OBJECTIVES

The main objective of this study consists of using a specific chemical transport model coupled with a source apportionment tool to assess the exposure to ambient air pollutants of children living in a tropical coastal-urban area highly influenced by industrial and vehicular emissions. To achieve this main objective, the following specific objectives were drawn:

- To use the state of the art in atmospheric modelling to emulate the dispersion of PM<sub>10</sub>, PM<sub>2.5</sub>, PM<sub>1</sub>, NO<sub>2</sub>, and O<sub>3</sub> over MRV.
- To validate modelled results with measurements at fixed meteorological and air quality monitoring stations.
- To investigate the impacts of three different model heights on air pollutant concentrations.
- To estimate the exposure and dose of children using modelled results and observed data at a fixed air quality station and compare the results with data collected from wearable passive samplers during experimental campaigns.
- To perform a sensitivity test regarding the indoor and outdoor ratios to consider the amount of time that children spend indoors.
- To identify and quantify the main contributors of air pollutant concentrations that contribute to children's exposure.

### **3. REVIEW OF THE LITERATURE**

#### **3.1 EPIDEMIOLOGICAL STUDIES DESIGNS**

Epidemiology is the study of the distribution (frequency and pattern) and determinants (causes and risk factors) of health-related states and events in specified populations, and the application of this study to the control of health problems. Frequency refers to the number of health events and the relationship of that number to the size of the population. The resulting rate is used to compare disease occurrence across different populations. Pattern refers to the occurrence of health-related events by time (annual, seasonal, weekly, daily, hourly, weekday versus weekend), place (geographic variation, urban/rural differences, and location of work sites or schools), and person (age, sex, marital status, socioeconomic status, behaviors, and environmental exposures). Determinants are the causes and other factors that influence the occurrence of a disease and other health-related events. An illness does not occur randomly in a population, it happens when the right accumulation of risk factors or determinants exists in an individual. To search for these determinants, epidemiologic studies are carried out to provide answers to such events (CDC, 2012).

Environmental epidemiology focuses on determining whether a health outcome is a result of exposures arising from our daily environment (e.g. air, water, diet, soil). A subset of environmental epidemiology is air pollution epidemiology which is concerned with health effects related to exposure to air pollution and is typically divided into two major areas, short- and long-term studies. Short-term studies, also called time-series studies, examine health effects related to acute or short-duration exposures to air pollution, by studying whether variations in air pollution levels over hours, days, or weeks can trigger adverse health effects, such as cough, headache, irritation of the eyes, nose, and throat, allergic reactions, asthma symptom aggravation, wheezing, among others. Long-term studies examine whether exposure of months, years, decades, and lifetimes to air pollution explains the risk of developing a chronic disease, such as asthma, chronic obstructive pulmonary disease, cardiovascular disease, diabetes, stroke, cancers, and premature death. Long-term air pollution studies use cohort, case-control, and cross-sectional designs (Andersen, 2020).

In traditional epidemiology, however, study designs fall into two other major categories, descriptive and analytical epidemiology studies (Figure 1). Descriptive epidemiology studies tend to use synonyms of the five W's to characterize an epidemiologic event, that is definition

(what), person (who), place (where), time (when), and causes/risk factors/modes of transmission (why/how). From these observations, hypotheses are developed about the causes of these patterns and about the factors that increase the risk of a disease. The need for further investigation to search for causes and effects is performed by the analytic epidemiology, which quantifies the association between exposures and outcomes and tests hypotheses about causal relationships (Thomas, 2009; CDC, 2012). Note that cross-sectional studies may be either descriptive or analytical, in which descriptive studies, most aim to provide estimates of the prevalence of disease, whereas analytical studies aim to assess associations between different variables (Kesmodel, 2018).

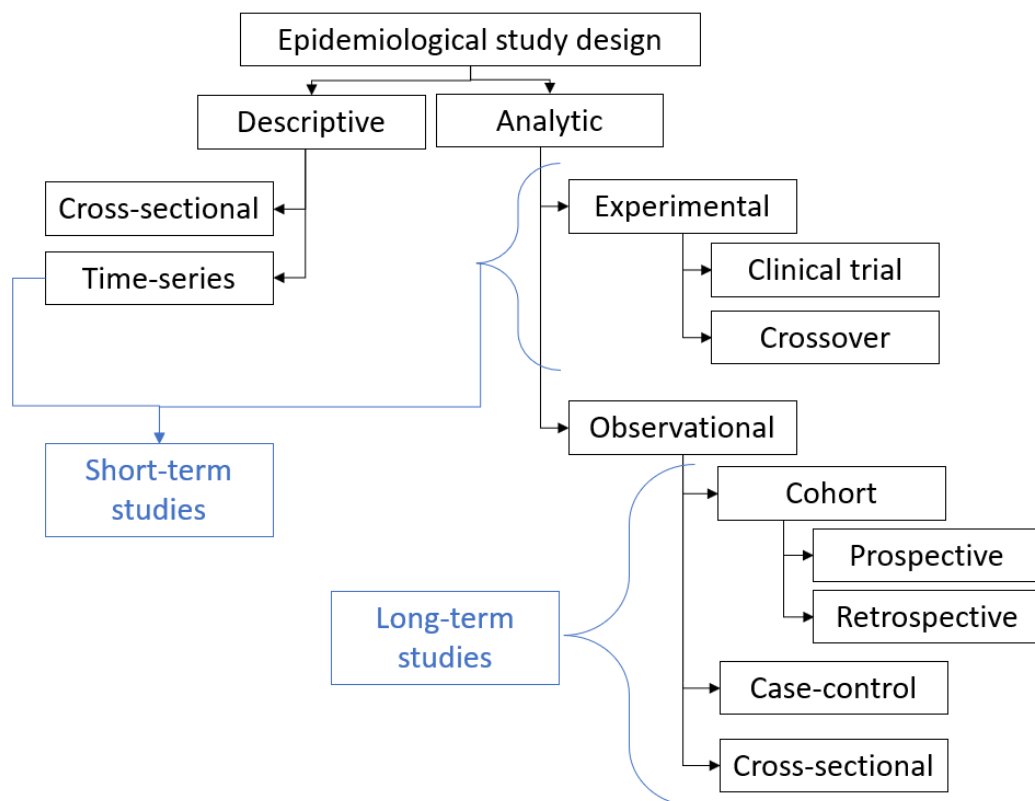


Figure 1. Environmental epidemiologic studies design based on CDC (2012) and Nieuwenhuijsen (2015). The classification with blue lines is based on Andersen (2020).

When the investigator determines, through a controlled process, the exposure for an individual and tracks him over time to detect the effects of the exposure, the study is characterized as an experimental study. Experimental studies on human health effects of air pollutants usually are performed through clinical trials or in studies of occupationally exposed workers. Workers have

historically been exposed to much higher concentrations of air pollutants than the general population. Therefore, the elevated, long-term exposures experienced by workers can provide insight into the toxicity of air pollution components. Whereas clinical studies typically involve controlled experiments of human volunteers in exposure chambers (National Research Council, 2002). The studies of Koenig *et al.* (1981), Kreit *et al.* (1989), and Barck *et al.* (2005) are examples of experimental studies. Koenig *et al.* (1981) estimated several pulmonary functions of eight adolescents with asthma being exposed to 1 ppm of sulfur dioxide (SO<sub>2</sub>) with 1 mg/m<sup>3</sup> of sodium chloride (NaCl) droplet aerosol (at 22° C and relative humidity ≥ 75%) after 30 min at rest and after 10 min of moderate exercise on a treadmill. No statistically significant functional changes were seen after 30 min exposure at rest, but the total respiratory resistance (R<sub>T</sub>), the maximal flow at 50 and 75% expired vital capacity (V<sub>max50</sub> and V<sub>max75</sub>), and the forced expiratory volume in 1 second (FEV<sub>1</sub>) were reduced postexercise due to the increase of inspiratory flow rates which induced greater penetration of SO<sub>2</sub>. Kreit *et al.* (1989) also compared measurements of pulmonary functions before and after nine asthmatics and nine normal subjects (18–35 years old) being exposed to filtered and purified air and 0.4 ppm O<sub>3</sub> within a stainless steel chamber (at 22°C and 50% relative humidity) with alternating 15-min periods of rest and exercise on a cycle ergometer. The experimental study demonstrated that exposure to 0.4 ppm O<sub>3</sub> was associated with a statistically significant decrease in forced vital capacity (FVC), FEV<sub>1</sub>, and forced expired flow at 25–75% FVC (FEF<sub>25-75</sub>) in both normal and asthmatic subjects. However, this decrease was greater in asthmatics, indicating that asthmatics developed greater airway obstruction, which was also supported by a significant increase in airway resistance only in asthmatics. In the same way, Barck *et al.* (2005) evaluated whether exposure to NO<sub>2</sub> was associated with an increased inflammatory response to allergens in the airways. For that, eighteen subjects (23–48 years old) with mild allergic asthma were exposed, in randomized order, to purified air or 500 mg/m<sup>3</sup> NO<sub>2</sub> for 15 min on day 1, and twice for 15 min on day 2. Birch or timothy pollen was inhaled 3–4 h after the NO<sub>2</sub> exposures on both days. Exposure to NO<sub>2</sub> enhanced the inflammatory response in sputum and blood that were induced by the allergens inhaled, despite symptoms and pulmonary function were equally affected by NO<sub>2</sub>+allergen or purified air+allergen. Experimental studies allow the exposure and the response to be assessed by detecting subclinical changes and determining whether an exposure has an effect. On the other hand, it usually includes a limited sample size, typically excluding children, elderly people, and those with relatively severe diseases. In addition, only acute

exposures are being assessed, it is difficult in replicating the entire mix of ambient pollutants, and needs approval from an ethics committee (National Research Council, 2002).

More recently, natural experimental studies have been carried out, also referred to as crossover studies. An example includes 28 healthy volunteers (18–60 years) riding a bicycle on a busy highway and also in a market square without traffic in Barcelona, Spain, to investigate blood pressure in response to a 2 h traffic-related air pollution exposure in a real-world situation (Kubesch *et al.*, 2015). The author reported that cycling at high air pollution exposure levels increased systolic and diastolic blood pressure more than at low air pollution levels. A similar experimental design asked participants (60 years and older) healthy ( $n = 40$ ), with chronic obstructive pulmonary disease (COPD) ( $n = 40$ ), and with ischaemic heart disease ( $n = 39$ ) to do a 2 h walk either along a commercial street in London (Oxford Street) or in an urban park (Hyde Park) (Sinharay *et al.*, 2018). Participants with COPD reported more cough, sputum, shortness of breath, and wheeze after walking down Oxford Street compared with Hyde Park. In addition, walking in Hyde Park led to an increase in lung function in all participants, irrespective of their disease status.

Observational analytic epidemiology studies simply observe the exposure and disease status of each study participant without controlling the exposure process, that is the subjects are exposed under natural conditions. The main study designs are cohort and case-control studies.

A cohort study is similar in concept to the experimental study because a cohort (group) of individuals with exposure to a substance and a cohort without exposure are followed over time to compare the occurrence of a disease. It differs from the experimental study because the investigator does not determine the exposure status of the participants. After some time, the disease rate in the exposed group is compared with the disease rate in the unexposed group (baseline). If the disease rate is substantively higher in the exposed group compared to the unexposed group, the exposure is said to be associated with illness (CDC, 2012). These studies are typically considered the gold standard in air pollution epidemiology because they are designed to account for other factors such as smoking, physical activity, body mass index, alcohol use, and diet, among others (rather than air pollution levels and mortality or morbidity) (Andersen, 2020). This study can be prospective (follow-up) in which cohorts are identified based on current exposures and followed into the future; or retrospective, in which the exposure and the outcomes have already occurred, and the cohorts are identified based on past exposure



conditions (data come from past records) and study follow-up proceeds forward in time. Examples of cohort studies are those carried out by Cerza *et al.* (2019), Olaniyan *et al.* (2020), Elten *et al.* (2020), and Silva *et al.* (2014).

Cerza *et al.* (2019) evaluated the association between exposure to air pollution and hospitalization for dementia through a cohort study in Rome, Italy. For that, they selected 350844 individuals (free of dementia) aged 65–100 years at inclusion (October/2001) and followed them until December 2013. The individuals who were hospitalized for the first time for dementia and its subtypes (7497 for vascular dementia, 7669 for Alzheimer's disease, and 7833 for senile dementia) were selected to have their exposure to be estimated at their residence location using LUR models for nitrogen oxides ( $\text{NO}_x$ ,  $\text{NO}_2$ ) and particulate matter ( $\text{PM}_{10}$ ,  $\text{PM}_{2.5}$ , soot) and a CTM for  $\text{O}_3$ . Their results showed a positive association between exposure to  $\text{NO}_x$  and  $\text{O}_3$  and hospitalization for dementia. Exposure to  $\text{NO}_x$ ,  $\text{NO}_2$ ,  $\text{PM}_{10}$ , and  $\text{PM}_{2.5}$  was positively associated with vascular dementia and negatively associated with Alzheimer's disease, whereas hospitalization for senile dementia was positively associated with exposure to  $\text{O}_3$ .

Olaniyan *et al.* (2020) investigated the association between ambient air pollution and respiratory morbidities through a prospective cohort study among 590 primary school children (average age of 10 years) in the Western Cape, South Africa. The baseline testing was conducted between February and September 2015, and the school children were follow-up over twelve months (till September 2016). Lung function parameters ( $\text{FEV}_1$ , FVC,  $\text{FEV}_1/\text{FVC}$ , and  $\text{FEF}_{25-75}$ ) and airway inflammation measurements were considered only from participants free of disease at baseline. Annual  $\text{NO}_2$  and  $\text{PM}_{2.5}$  concentration levels were estimated for each child's home using a LUR model. Despite the  $\text{NO}_2$  ( $16.62 \mu\text{g}/\text{m}^3$ ) levels being below the local standard guidelines, increases new cases of asthma-associated outcomes (which included ocular-nasal symptoms, wheezing, asthma symptom score, and airway inflammation) after 12 months, independent of co-exposure to  $\text{PM}_{2.5}$

Elten *et al.* (2020) conducted a retrospective cohort study in Ontario, Canada, between April 1991 and March 2014 to investigate the association between inflammatory bowel disease and exposures to  $\text{NO}_2$  (from a LUR model),  $\text{PM}_{2.5}$  (from satellite data),  $\text{O}_3$  (from an interpolation technique), and redox-weighted oxidant capacity ( $\text{O}_x$ ) (calculated as the weighted average of  $\text{NO}_2$  and  $\text{O}_3$  concentrations) during pregnancy and from birth until the age of 18. 2218789 newborns were included in the study, of whom 2491 developed inflammatory bowel disease

during follow-up. Statistically significant positive associations were detected for O<sub>x</sub> during the second trimester of pregnancy and childhood, suggesting an increase in the risk of being diagnosed with inflammatory bowel disease before 18 years of age. However, no association for any of the three individual pollutants investigated was found, suggesting the potential of pollutants to cause oxidative stress is more relevant to inflammatory bowel disease development than their individual concentrations.

A retrospective cohort study was also carried out in the cities of Mato Grosso, Brazil, to investigate the association between biomass burning that usually occurs between July and October in Amazon and low birth weight (Silva *et al.*, 2014). Concentrations of PM<sub>2.5</sub> and carbon monoxide (CO) were estimated through the Coupled Aerosol and Trace Gas Transport Model to the Brazilian Developments of the Regional Atmospheric Modelling System (CATT-BRAMS Model). A total of 6147 singleton live births were included between July 2004 and December 2005, of which 193 (3.1%) were low birth weight. The study concluded that maternal exposure to air pollution during the second and third trimesters of pregnancy was associated with low birth weight.

In the case-control studies, individuals with a disease (case) are compared with similar individuals without the disease (controls) to determine if there is an association of the disease with prior exposure to an agent. The control group provides an estimate of the baseline in population. If the amount of exposure among the case group is substantially higher than the control group, then illness is said to be associated with that exposure. In a cohort study, subjects are grouped based on their exposure, then they are followed to document the occurrence of a disease. Whereas in a case-control study, subjects are enrolled according to whether they have the disease or not, then they are tested to determine their prior exposure. As an example of case-control studies, we can find those performed by Liu *et al.* (2021), Wang *et al.* (2020), Deygas *et al.* (2021), and Vinceti *et al.* (2016).

Liu *et al.* (2021) performed a population-based case-control study in Liaoning province, China, to evaluate the association between maternal SO<sub>2</sub> exposure and the risk of oral clefts. The study involved 3086 patients with oral clefts and 7950 controls from January 2010 to December 2015. SO<sub>2</sub> concentration data were acquired from 77 air monitoring stations, and each pregnant woman was assigned to the mean of all air monitoring stations in her city. They found positive associations between maternal SO<sub>2</sub> exposure during 3 months before conception and the first

and second months of pregnancy and oral clefts. Similarly, Wang *et al.* (2020) found significant associations between PM<sub>2.5</sub> exposure and pediatric rheumatic diseases during pregnancy and infancy in Taiwan. The study consisted of infants born between 2004 and 2014 who were followed from conception to the end of 2015. There were 2363 cases of incident pediatric rheumatic diseases in children and 23 630 (10:1) children served as controls. A linear mixed-effect model was used to incorporate 3-km satellite-based aerosol optical depth (AOD), meteorological variables, and land-use data to predict daily PM<sub>2.5</sub> concentrations during each week of pregnancy (40 weeks) and after birth to one year (52 weeks) for each infant according to their maternal address in the postcode level.

In France, another case-control study carried out from 1990 to 2011 significantly associated an increase in the risk of breast cancer and cumulative exposure to atmospheric polychlorinated biphenyls (Deygas *et al.*, 2021). Each case was individually matched to one control, randomly selected by incidence density at the time of the case diagnosis, thus 5222 women with primary incident breast cancer cases were matched to 5222 controls (no previous diagnosis of any cancer). The annual exposures for each woman using their postal codes were estimated based on hourly polychlorinated biphenyl concentrations that were modelled by the air quality model CHIMERE.

In another population-based case-control study carried out in Reggio Emilia, Northern Italy, from January 1998 to December 2006, 228 cases of birth defects and 228 referent newborns were under investigation whether maternal exposure to PM<sub>10</sub> and benzene from vehicular traffic during early pregnancy would be associated with excess congenital anomalies risk (Vinceti *et al.*, 2016). Both pollutants were modelled by a dispersion model, the CALifornia LINE Source Dispersion Model, at the geocoded maternal residence at a height of 2 m. Results of this study show a tendency towards an overall higher risk of congenital anomalies among women exposed during pregnancy to higher levels of PM<sub>10</sub>, while no such association emerged for benzene.

Cross-sectional studies have been mainly used to understand the prevalence of a disease in clinical research. Prevalence refers to the proportion of persons in a population who have a particular disease regardless of when they first developed the disease. It is important to distinguish prevalence from incidence, which the latter refers to the number of new cases that develop in a given period of time. Cross-sectional studies measure outcomes and exposures of the study subjects at a single point in time (do not follow individuals over time). Hence, there

is no time dimension as all data are collected and mostly refer to the time at or around the time of the data collection. Because of that, it is relatively difficult to establish causal relationships from a cross-sectional study. Even though, cross-sectional studies may be also used for analytical purposes whether the health outcome is assessed for potential associations with exposures or risk factors (Wang and Cheng, 2020). Furthermore, these studies can be examples of ecological studies because they produce risk estimates at the population level (when personal characteristics at an individual level are not used) (Andersen, 2020). Zheng *et al.* (2021), Bont *et al.* (2019), Tu *et al.* (2021), and Clifford *et al.* (2018) can be referred to as cross-sectional studies.

Zheng *et al.* (2021) performed a cross-sectional analysis with children and adolescents (9–17 years,  $n = 36456$ ) between September and November 2019 in Jiangsu province, China, to examine the association between exposure to NO<sub>2</sub>, O<sub>3</sub>, PM<sub>10</sub>, and PM<sub>2.5</sub> and obesity. A multivariate regression model was used to estimate the effects of three-year (2016–2018) average concentrations of air pollutants on obesity. The concentrations came from 124 ground monitoring stations and the exposure level was estimated by the nearest air monitoring station of the address of each selected school (between 0.3 and 5.6 km, with a median of 3.5 km). These monitoring stations were mandated to be away from traffic roads, industry sources, or residential sources of emissions, thus reflecting the background pollution concentration in the selected districts. Obesity measurements were taken using the children's Body Mass Index (BMI) according to the WHO, which includes data of age, sex, weight, and height. The authors suggested that higher concentrations of PM<sub>2.5</sub>, NO<sub>2</sub>, and O<sub>3</sub> were associated with a likelihood of obesity.

The association between levels of NO<sub>2</sub>, PM<sub>10</sub>, PM<sub>2.5</sub>, elemental carbon (EC), and ultrafine particles (UFP) and overweight and obese in 2660 children (7-10 years) was also explored in Barcelona, Spain, through a cross-sectional study in 2012 (Bont *et al.*, 2019). The air pollutant concentrations were estimated for the geocoded postal address of each participant using a LUR model together with measurements in schoolyards. Children were classified as normal, overweight, and obese also using the BMI for children. Children exposed to higher levels of UFP at schools were 30% more likely to be overweight or obese than those exposed to low levels. Exposure to medium levels of NO<sub>2</sub>, PM<sub>2.5</sub>, and EC at also schools was associated with an increase in the odds of being overweight or obese.

A national cross-sectional study with 2226 children, aged 7-11 years, from 12 cities in Australia, was also carried out to investigate aeroallergen sensitization due to exposure to NO<sub>2</sub> during 2007-2008 (Tu *et al.*, 2021). Exposure to NO<sub>2</sub> was estimated through a weighted mean, assuming children spend 75% of their time at home and 25% at school, using measurements from monitors near each school (within 2 km) and also with a validated satellite-based LUR model at geocoded residential and school addresses. The assessment of aeroallergen sensitization was performed through skin prick tests for aeroallergens of indoor (two types of house dust mites, cockroach, and cat allergen) and outdoor (*Alternaria*, *Aspergillus*, ryegrass, and a grass mixture) origin. The results showed that NO<sub>2</sub> exposure was associated with greater odds of sensitization to house dust mites.

Also in Australia, Clifford *et al.* (2018) evaluated the effects of exposure to ambient UFP on respiratory health and systemic inflammation among 655 children (8-11 years) from 25 primary schools in the Brisbane Metropolitan Area, between October 2010 and August 2012. Ultrafine particle number concentration was measured at each school and modelled at homes using a LUR model over one year. Health outcomes were respiratory symptoms and diagnoses, measured by questionnaire, spirometric lung function (FEV<sub>1</sub>, FVC, FEV<sub>1</sub>/FVC ratio), exhaled nitric oxide (FeNO), and serum C reactive protein (CRP). Ultrafine particle number concentration was positively associated with CRP and FeNO among atopic participants. It was reported that UFPs did not affect respiratory health outcomes in children, but did have systemic effects, detected in the form of a positive association with a biomarker for systemic inflammation.

Most aforementioned studies (cohort, case-control, cross-sectional) are classified as long-term studies in air pollution epidemiology because they assess the cumulative effects of repeated exposure to typical levels of air pollution. In contrast, short-term studies exploit day-to-day variations in air pollution as determinants of day-to-day variations in health outcomes. These studies are also referred to as time-series studies because they use routinely collected time-series data of air pollution levels and counts of a health outcome to make an association (Andersen, 2020). The modelling of this existing relationship between two variables was introduced in the early 1990s by (Schwartz and Marcus, 1990) when they examined the associations between mortality and levels of PM, SO<sub>2</sub>, and smoke during winters in London from 1958 to 1972 with the Poisson generalized additive model (GAM). Poisson distribution is commonly used because time-series data involve count variables (which can take any

nonnegative integer value, such as the number of cases of a disease in a population) (Thomas, 2009). In addition, the assumption of a disease can occur independently in different people and in the same person at different points in time justifies the use of the Poisson distribution (Flanders and Kleinbaum, 1995). Thus, this model quickly became the standard tool because they are relatively cheap and feasible, leading to an exponential increase in studies of the short-term effects of air pollution.

Pu *et al.* (2021) explored the association between  $PM_{2.5}$ ,  $PM_{10}$ , and their difference ( $PM_C$ ) and hospitalizations of children aged <18 years for pneumonia and bronchitis (lower respiratory infections) in 18 cities in southwestern China, from January 2015 to December 2016, using a quasi-Poisson GAM. Ambient air pollution data were obtained from monitoring stations for each city that had between three to six stations. To explore the immediate, delayed, and prolonged effects of the three types of size-specific PM on children's hospitalizations, it was considered the single-day lags from the current day to six days before (lag0-lag6) and the multi-day lags from the moving average of two days to seven days (lag01-lag06). The strongest effects of  $PM_{10}$  and  $PM_C$  on hospital admissions for pneumonia and bronchitis were both on lag06, whereas the strongest effect of  $PM_{2.5}$  was on lag03, lag6, and lag02.  $PM_C$  was the most significantly associated with lower respiratory infections probably due to  $PM_C$  deposition in the upper respiratory tract of the lungs. Also using a quasi-Poisson GAM, Rodrigues *et al.* (2021) estimated the effects of  $PM_{10}$  concentrations on childhood (0–4 years, 5–9 years, and 10–14 years) asthma admissions from 2009 to 2015 in the Lisbon Metropolitan Area, Portugal.  $PM_{10}$  concentrations were obtained from the monitoring stations in the study area. They also considered the delay association between exposure and outcome in the relationship between hospital admissions and environmental variables. They found that an increase of  $1 \mu\text{g}/\text{m}^3$  of  $PM_{10}$  was associated with an increased risk of asthma-related hospital admission on the order of 2%. Similarly, Baek *et al.* (2021) investigated the relationship between ambient air pollution ( $PM_{10}$ ,  $O_3$ ,  $NO_2$ ,  $CO$ , and  $SO_2$ ) and medical care visits for atopic dermatitis in children (aged <19 years) from January 2012 to December 2015 in Incheon, Republic of Korea. The study treated the daily number of medical care visits for atopic dermatitis with the Poisson GAM, which included air pollutant levels, ambient temperature, relative humidity, day of the week, national holidays, and seasons. Air pollutants data were obtained from monitoring stations. The results showed that higher  $PM_{10}$ ,  $O_3$ , and  $SO_2$  were associated with a significantly increased risk of a medical care visit for atopic dermatitis on lag0, but  $NO_2$  and  $CO$  concentrations were not.

These and many other epidemiological studies have consistently reported the association between chronic and acute exposure to ambient air pollution and adverse health effects, becoming a valuable tool for mapping the health burden related to air pollution and for the development of air pollution control policies (Andersen, 2020). However, it also could be observed that there is heterogeneity between them in terms of measurement of exposure/outcome, study design, data sources, sample size, air pollutants of interest, time and spatial resolutions, population, area of study, among others. A summary of the characteristics of the air pollution epidemiology study designs is presented in Table 1. All the study designs require exposure estimates to be able to estimate the risk associated with the substance of interest (Figure 2). The methods to obtain exposure estimates are often classified as direct and indirect and the choice of a method depends on the aim of the study and, more often, on the financial resources available. Exposure estimates can consider ambient air pollution monitors in the area in which the subjects live, or models to predict the concentrations. In addition, questionnaires are useful to get information related to where and when people carry out their daily activities. Alternatively, a representative sample of the group can also be personally monitored. It is expected that the individual estimates provide the best exposure estimates, however, this may not be true because of the variability in exposure and the limited number of samplers (Nieuwenhuijsen, 2015). Some aspects involving exposure assessment to air pollution are discussed in the following sections.

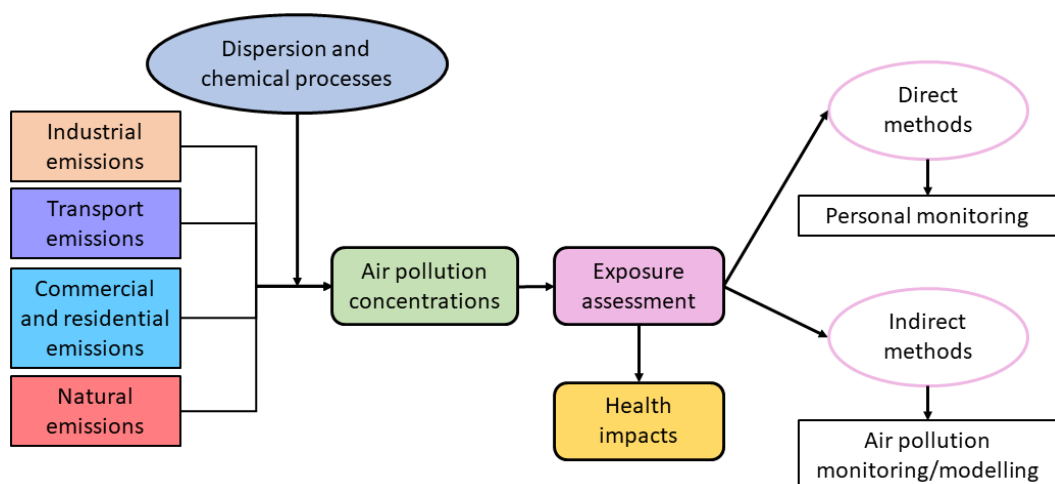


Figure 2. Relationship among health effects, exposure estimates, and air pollution. Based on Nieuwenhuijsen (2015).

Table 1. Study designs in environmental epidemiology. Based on WHO (1991).

<b>Study design</b>	<b>Population</b>	<b>Exposure</b>	<b>Health effect</b>	<b>Confounders</b>	<b>Problems</b>	<b>Advantages</b>
<b>Experimental study</b>	special groups	Controlled and already known	To be measured during the study	Can be controlled by randomisation of subjects	Expensive; ethical considerations; study subjects compliance required	Well accepted results; strong evidence for causality or efficacy of intervention
<b>Retrospective cohort study</b>	Special groups; workers, patients, insured persons	Records of past measurement	Records of past or current diagnosis	Often difficult to measure because of its retrospective nature; depends on the availability of previously obtained data (e.g. past smoking habits)	Need to rely on records that may not be accurate	Less expensive and quicker than a prospective study; can be used to study exposures that no longer exist
<b>Prospective cohort study</b>	Community or special groups; exposed versus non-exposed	Defined at outset of study (can change during the study)	To be determined during the study	Usually easy to measure	Expensive and time consuming; exposure categories can change; high dropout rate possible	Can estimate incidence and relative risk; can study many diseases in one study; can describe associations that suggest cause-effect relationships
<b>Case-control study</b>	Usually small groups; diseased (cases) versus nondiseased (controls)	Records or interview	Known at start of the study	If confounders can be identified and measured they may be addressed	Difficult to generalise due to small study groups; some incorporate biases	Relatively cheap and quick; particularly useful for studying rare diseases



<b>Cross-sectional study</b>	Communities or special groups; exposed versus non-exposed	Current	Current	Usually easy to measure	Hard to establish cause relationship; current exposure may be irrelevant to current disease	Can be done quickly; can use large populations; can estimate prevalence
<b>Time-series study</b>	Large community; susceptible groups	Current (e.g. daily) changes in exposure	Current (e.g. daily) variations in mortality	Often difficult to sort out; e.g. effects of influenza	Many confounding factors; often difficult to measure	Useful for studies on acute effects

### 3.2 ASPECTS OF AIR POLLUTION EXPOSURE

Air pollution is characterized by the presence of airborne substances (solids, liquids, or gases) that occur in concentrations high enough to threaten the health of people and animals, harm vegetation and structures, or toxify a given environment (Salvador, 2018). Air pollution affects agricultural crop yields, causes material damage, generates acid rain, influences visibility, changes the efficiency of solar photovoltaic panels, and directly affects Earth's climate by scattering and absorbing solar and terrestrial radiation, as well as indirectly through cloud formation (Boucher *et al.*, 2013; Zhao *et al.*, 2013; Adrees *et al.*, 2016; Grøntoft, 2018; Zhou *et al.*, 2018; Maji *et al.*, 2019; Z. Feng *et al.*, 2019; Nascimento *et al.*, 2020). Air pollution also has acute and chronic effects on human health, in particular, respiratory and cardiovascular diseases, which included irritation of the eyes, nose, and throat, acute respiratory infections, exacerbation of asthma, chronic bronchitis, lung cancer, lung function reduction, strokes, among others (Pope *et al.*, 2002; Lim *et al.*, 2012; Prüss-Ustün *et al.*, 2016; EEA, 2019).

Air pollutants differ by chemical composition, reactions, emissions, persistence in the environment, spatial and temporal scales, and impacts on human health and/or on the environment (Fino, 2018). It is important to note that air pollutants rarely occur alone in the atmosphere, suggesting that their effects may be associated with more than one pollutant or a mixture of pollutants. Environmental agencies around the world, such as those in the U.S., Canada, and European Union generally divide air pollutants into criteria pollutants and hazardous air pollutants. Both types are hazardous, but the criteria pollutants are those that are used to designate the ambient air quality of a region, based on common standards; whereas hazardous air pollutants are usually restricted spatially to hot spots, such as industrial and urban areas (Vallero, 2014c). They may be also categorized as either primary (air pollutants directly emitted to the atmosphere) or secondary (pollutants formed in the atmosphere from precursor gases). The so-called criteria pollutants are particulate matter (PM), O<sub>3</sub>, CO, SO<sub>2</sub>, NO<sub>2</sub>, and lead (Pb). Although air pollutants can usually be classified by their chemical composition, particles are categorized according to their physical properties. The WHO establishes air quality standards for the air pollutants in outdoor air because of its public health perspective. Table 2 shows a comparison of the 2005 air quality guidelines (AQG) and the 2021 AQG levels for the criteria pollutants. The lowering of the air quality guidelines (except for SO<sub>2</sub>) was based on a systematic review of evidence on literature over past years which pointed out that exposure to these air pollutants, even at low levels, can cause adverse health effects. These reductions aim

to be translated to have a positive health impact. In addition, efforts to improve air quality can mitigate climate impacts (WHO, 2021).

Table 2. Summary and comparison of recommended long- and short-term AQG levels. Source: WHO (2021).

<b>Pollutant</b>	<b>Averaging time</b>	<b>2005 AQG [<math>\mu\text{g}/\text{m}^3</math>]</b>	<b>2021 AQG [<math>\mu\text{g}/\text{m}^3</math>]</b>
<b>SO<sub>2</sub></b>	24-hour	20	40
<b>CO</b>	24-hour	-	4
<b>NO<sub>2</sub></b>	Annual	40	10
	24-hour	-	25
<b>O<sub>3</sub></b>	peak season	-	60
	8-hour	100	100
<b>PM<sub>2.5</sub></b>	Annual	10	5
	24-hour	25	15
<b>PM<sub>10</sub></b>	Annual	20	15
	24-hour	50	45

<sup>a</sup> 99th percentile (i.e. 3–4 exceedance days per year).

<sup>b</sup> Average of daily maximum 8-hour mean O<sub>3</sub> concentration in the six consecutive months with the highest six-month running-average O<sub>3</sub> concentration

Sources of air pollutants can be categorized as natural and anthropogenic emissions, however, because the same chemical compounds from a natural source (e.g. a volcano) can cause the same adverse effects as when they are emitted by anthropogenic sources. Examples of anthropogenic sources include the energy production sector, fuel combustion (industrial, commercial, institutional, and residential), industrial processes and product use (cement, iron and steel production, construction and demolition, pulp and paper industry, etc), agriculture, landfill, shipping, aircraft, road traffic, nonroad sources (off-road vehicles and other machinery, e.g. gardening, railways), among others.

SO<sub>2</sub> is usually generated by the combustion of sulfur-containing fossil fuels (principally coal and heavy oils), whereas volcanoes and oceans are its major natural sources. CO comes from the incomplete combustion of fossil fuels and biomass burning. NO<sub>2</sub> is formed by combustion processes of mobile and stationary sources, lightning, biomass burning, and from the oxidation of ammonia by photochemical processes in oceans and by some terrestrial plants. O<sub>3</sub> is formed

by chemical reactions triggered by solar radiation which involve hydrocarbons,  $\text{NO}_x$ , and VOCs. VOCs are emitted in the manufacture of paints, combustion activities, solvent use, cleaning products, extraction and distribution of fossil fuels, as well as natural biogenic emissions. PM is a complex mixture of small particles and liquid droplets that are suspended in the air, which vary in size (Figure 3) and composition and are produced by a wide variety of natural and anthropogenic sources such as fossil fuel combustion of industries, power plants, incinerators, motor vehicles, construction activity, sea spray, volcanic eruptions, wildfires, and natural windblown dust. Mineral dust (silicon, iron, aluminium, magnesium, calcium), biogenic organic particles (pollen, spores, plant fragments), and sea salt contribute more to the coarse fraction, whereas ammonium ( $\text{NH}_4^+$ ), sulfate ( $\text{SO}_4^{2-}$ ), nitrate ( $\text{NO}_3^-$ ), organic carbon (OC), and elemental carbon (EC, also called black carbon) contribute more to the fine fraction. OC can be directly emitted from sources or produced from atmospheric reactions involving gaseous organic precursors. EC can be produced only in a combustion process and is therefore solely primary. PM is also constituted of trace elements, such as lead, nickel, vanadium, chromium, and manganese (Finlayson-Pitts and Pitts, 2000; Seinfeld and Pandis, 2006; Vallero, 2014a; Fino, 2018; Salvador, 2018).



Figure 3. The relative size of particles. Source: Ang *et al.* (2020).

After being released into the environment by a source, the pollutant undergoes the dispersion process that depends on meteorological dynamic and thermal factors (wind direction and speed and temperature) but also on the terrain features (whether it is on flat or mountainous land or in

a valley). Throughout the dispersion process is when people come into contact with the pollutants, referred to as exposure. Ott (1982) defined the concept of human exposure as “*the event when a person comes into contact with a pollutant of a certain concentration during a certain period of time*”. If the pollutant is uptake into the body, it is referred to as a dose. Furtaw (2001) defined the difference between these two terms by explaining the exposure process (Figure 4). “*A pollutant is released into the environment from a source. Once the chemical is in the environment, it is transported through space and time into multiple media (air, water, soil, surfaces, and so forth). Various transformations may occur, such as degradation, chemical reaction, deposition, volatilization, and so forth. These transport and transformation processes will result in various concentrations of the chemical within environmental media as functions of time. Exposure then occurs when humans contact the pollutant-bearing media in the course of human activities. If the chemical of interest subsequently crosses the outer boundary and enters the human body, a dose occurs*”. Exposure may result in a dose, but a dose cannot occur without exposure.



Figure 4. The exposure process, defined by (Furtaw, 2001).

Exposure assessment considers the first four steps in Figure 4 (from source to dose). The physical course a pollutant takes from the source to an individual is often referred to as *exposure pathway*, whereas the way the air pollutant enters the body is often referred to as *exposure route* (e.g., inhalation, ingestion, absorption). The exposure to air pollutants can depend upon the duration (e.g. in hours or days) or amount (kg/day ingested), the concentration (e.g. in  $\mu\text{g}/\text{m}^3$ ), and frequency (e.g. times per week). Any of these factors can be used as an exposure index in epidemiological studies, but they can also be combined to obtain a new exposure index, e.g. by multiplying duration and concentration to obtain an index of cumulative exposure (Nieuwenhuijsen, 2015).

Estimation of exposure is also classified according to the length of exposure. Long-term exposure is associated with constant background concentrations, or persistent exposure in the

day-to-day work-transport-home environment, or from the accumulation of many short-term exposure episodes. The long-term analysis is related to chronic health effects, morbidity, and mortality of a population. From an air-pollution control perspective, the benefit of a long-term analysis is to understand long-term spatial and temporal trends, improve planning and perceive the need for action for mitigation strategies. Short-term episodes are related to natural disasters or severe pollution episodes and acute health effects. Short-term studies of air pollution episodes lead to a better understanding of the source-receptor relationship, and transformation and transport of air pollutants. Moreover, it can improve short-term air quality forecasting and signal imminent disaster response capabilities (Sorek-Hamer *et al.*, 2020).

For exposure assessments by the inhalation route, it is necessary to take into account the breathing characteristics of the individual and the chemical and physical characteristics of the pollutant. The respiratory system from the head airways (nose, mouth, pharynx, and larynx) through the tracheobronchial region (from the trachea to the terminal bronchioles) is covered with a layer of mucus that is in continuous motion and aims to protect the alveolar region of the lungs (Figure 5). Thus, if particles settle on the mucus, are moved up, and are ultimately swallowed. Larger particles are generally removed by these ciliated surfaces, whereas fine and ultrafine particles are more likely to reach the alveolar region where gas exchange occurs (and also reach the bloodstream) than coarse particles because of their particle size. Because the alveolar region is not coated with a protective mucus layer, the clearance time for deposited particles is much greater than in the upper respiratory tract; hence the potential for health effects is much greater (Hinds, 1999; Finlayson-Pitts and Pitts, 2000).

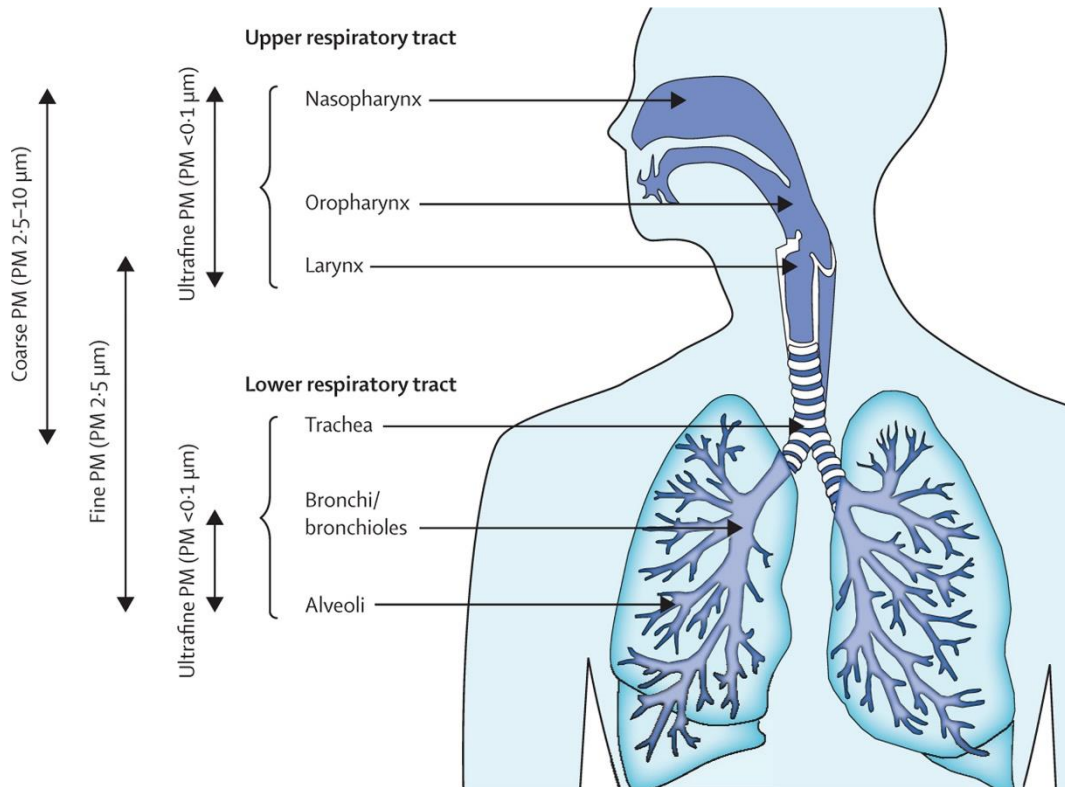


Figure 5. The respiratory system. Source: Guarnieri and Balmes (2014)

The deposition of particles on the human tract not only depends on particle size but also on the gender, age, breathing rates (frequency), and tidal volume (the amount of air breathed in with each normal breath) of the individual. Figure 6 shows the deposition of particles in various regions of the respiratory tract and the total deposition as a function of particle diameter. Total deposition reflects deposition in two or more regions. Deposition in any region is affected by deposition in the preceding regions. Thus, only particles that are inhaled can be deposited in the head airways, and only particles passing beyond the head airway region can be deposited in the tracheobronchial region, and so on. The deposition fraction of  $PM_{10}$  in the head airway region can be quite large, so it is not surprising that health effects could be associated with these particles (Hinds, 1999; Finlayson-Pitts and Pitts, 2000).

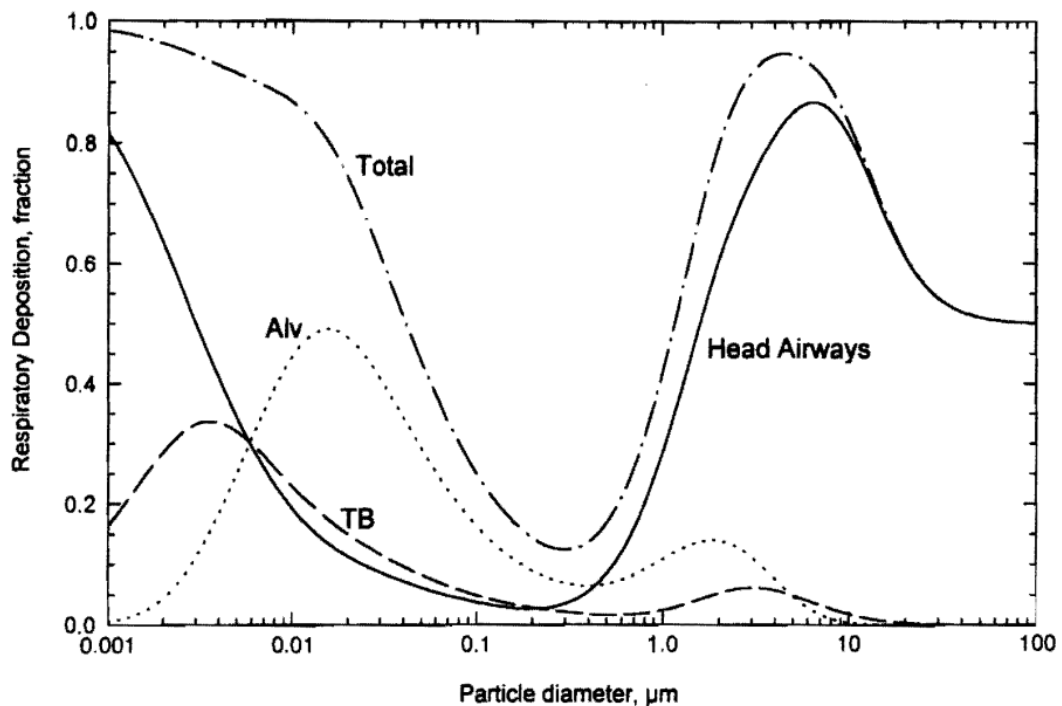


Figure 6. Predicted total and regional deposition for adults in light exercise. Alv (alveolar) and TB (tracheobronchial). Source: Hinds (1999)

Together with the definition of human exposure, Ott (1982) also introduced the concept of microenvironment which is the location or classes of locations in which a person is spatially homogeneous exposed to a pollutant concentration. This concept was also presented to explain that it would be necessary to have knowledge of the air pollutant concentrations in all locations that a person attends throughout the day since either air pollution and people are not static in time and space, making the exposure assessment more complex the greater the number of factors to be considered. So, understanding the daily time-activity pattern of individuals is important in exposure assessments. An example of this is shown in Figure 7, in which an individual (shown as the dotted line and black arrows) spends an amount of time in one location and then moves to another location throughout the day. The total exposure of this person will therefore depend on the time spent in each location (microenvironment) and the concentrations during the time spent in this location. Examples of microenvironments are home, bedroom, kitchen, living room, schools, classroom, playground, travel routes and modes, bus, car, subway, workplaces, offices, etc.



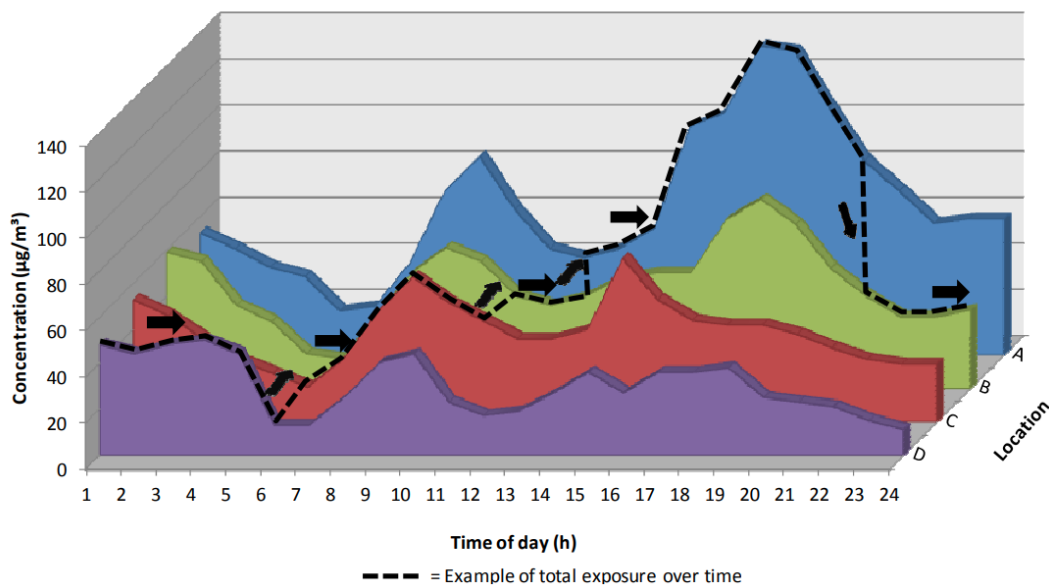


Figure 7. Hourly variation of NO<sub>2</sub> concentrations at four microenvironments and its effect on spatiotemporal variation on personal exposure. Source: Mölter (2012).

People spend most of their time indoors, which the amount of time can vary by whether the person is employed or not, in what type of job, how far is the job from its house, gender, the season of the year, whether they live alone or have children (Klepeis *et al.*, 2001; Kousa *et al.*, 2002). In the case of children, they also spend most of their time indoors such as at home, bedroom, living room, school, classrooms (Mölter *et al.*, 2012; Smith *et al.*, 2016; Pañella *et al.*, 2017; Cunha-Lopes *et al.*, 2019; Tu *et al.*, 2021). Indoor sources are related to daily human activities such as cooking, walking, cleaning, burning candles, natural and mechanical ventilation use, smoking, the use of unpaved or leisure areas, building deterioration, among others (Viana *et al.*, 2011; Amato *et al.*, 2014; Rivas *et al.*, 2014; Goel *et al.*, 2015, 2021). In the absence of indoor sources, indoor air pollution is a result of ventilation and airtightness of spaces, people's activities, and dust resuspension (Figure 8) (Hänninen *et al.*, 2011; Pallarés *et al.*, 2019; Shrestha *et al.*, 2019; Chen *et al.*, 2020; Faria *et al.*, 2020). Infiltration of air pollutants from the outdoor environment to the indoor air is also subject of study and usually is expressed in terms of indoor/outdoor (I/O) ratios. That is the concentrations inside a place are divided by the concentrations outside of the place's location. Not considering this variability may cause substantial exposure misclassification. Indoor air pollutants concentrations can be also enhanced due to complex urban landscapes, the distance of pollutant sources, and meteorological conditions (Milner *et al.*, 2005).

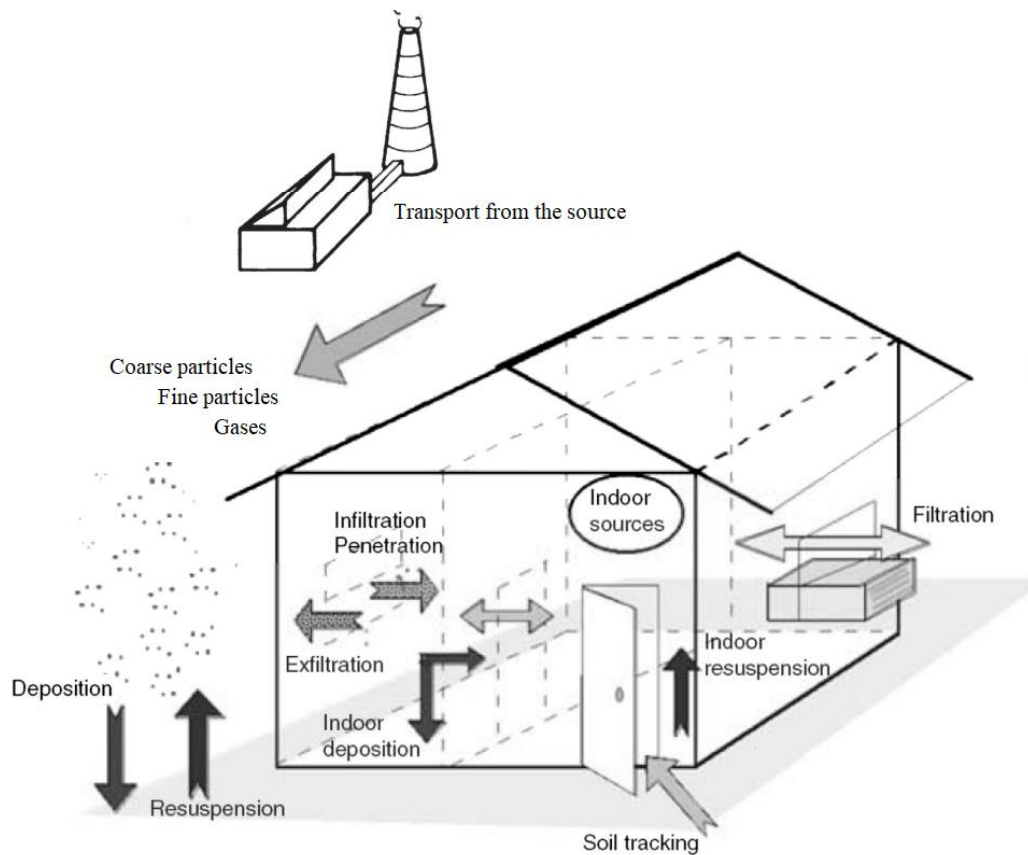


Figure 8. Schematic diagram of the key factor influencing indoor air pollution and the home as a microenvironment. Source: Vallero (2014b).

One crucial factor in determining people’s exposure to air pollution is to know the concentrations of air pollutants they are exposed to. Various methods of estimating concentrations have been applied and the most often used has been measurements from fixed air quality stations. However, measurements at a station at a fixed site generally do not realistically represent the pollutant concentrations people are in reality exposed to. In addition, many areas do not have monitoring station networks or they are poorly spatial distributed, such as the case of several regions in South America (Peláez *et al.*, 2020). In Brazil, only 1.7% of Brazilian municipalities have air quality monitoring stations (ISS, 2019). In this sense, several computational approaches were developed in order to estimate air pollutants concentrations, and then, have a better representation of the exposure indices. These approaches are further discussed in the coming section.

### 3.3 METHODS TO EVALUATE AIR POLLUTANT CONCENTRATIONS

The methods of estimating air pollutants concentrations have significantly improved over time since computational costs decreased and science and technology advanced. Generally, air pollutants concentrations can be directly measured through air quality stations/monitors or estimated indirectly by computational techniques. A summary of these methods is shown in Table 3 and was built based on the review papers of Jerrett *et al.* (2005) and Hoek (2017). Note that all approaches presented in Table 3 are indirect methods to estimate the exposure indices to air pollution (Figure 2). Direct methods of measuring exposure include portable monitoring equipment, which can be classified as passive or active. Active portable monitoring equipment is costly and leads to altered behaviour while individuals must carry relatively little robust and expensive equipment. Passive equipment is more robust but gives a cumulative concentration that does not allow measuring peak values or other exposure over a short time period (Clench-Aas *et al.*, 1999).

Table 3. Summary of the methods used to assess air pollutant concentrations. Based on Jerrett *et al.* (2005) and Hoek (2017).

Methods	Principle	Strengths	Weaknesses
<b>Air quality monitors</b>	Measured values that are usually from surface-monitoring stations	A routine monitoring network includes low cost, consistency of monitoring methods, and often a long period of monitoring.	<p>Lack of characterization of intra-urban contrasts related to traffic emissions and other local sources, because networks are typically not spatially dense enough.</p> <p>It usually measures regulated pollutants and generally does not measure ultrafine particles and black carbon, for example.</p> <p>Surface monitoring may be affected by differences in monitoring methods among regions/countries and the selection of monitoring sites.</p>
<b>Interpolation</b>	It uses data from multiple stations and assigns more weight to stations that are at a shorter distance from the receptor point (e.g. residential address), using nearest neighbour, kriging, inverse distance weighting (IDW), or other geostatistical methods.	<p>It provides a spatially more resolved pattern than a simple average. It can be a useful option for areas with relatively few local sources, such as rural areas. However, the assumed smooth spatial change of concentration may be too simple in urban areas.</p> <p>It is relatively easy to apply the method.</p> <p>Low input data demand compared to other methods</p>	<p>It depends on the existence of multiple stations in the area of interest.</p> <p>This approach might be too simplistic for urban areas that are characterized by high spatial variability of air pollutants.</p>

<b>Satellite monitoring</b>	<p>Monitoring methods are based on the absorption and scattering of specific wavelengths of sunlight.</p> <p>Satellite monitoring of aerosol optical depth (AOD) contributed significantly to observations of NO<sub>2</sub> and fine particles that are measured by the ozone-monitoring instrument (OMI). Despite satellite observations of ozone are less useful, because of the high concentrations in the stratosphere, limiting the reliability of assessing surface concentrations from total column concentrations.</p>	<p>Data can be available globally, in contrast to surface-monitoring data that are available in a more limited number of countries and often concentrated in urban areas.</p> <p>It can provide a vertically integrated measure of atmospheric components.</p>	<p>The concentrations are assigned to the entire population of the grid cells (at least 0.1° x 0.1° ≈ 123 km<sup>2</sup>), and thus, smaller-scale variation is lost.</p> <p>Coarser spatial and temporal resolution, interference by clouds, and the characterization of a single time of the day (satellites pass each location of the earth at the same time).</p>
<b>Land use regression modelling</b>	<p>It is derived by combining air quality monitors and collection of variables related to geographic information systems (GIS), which can potentially predict the measured spatial variation (e.g. land use, altitude, meteorology, traffic, roads data)</p>	<p>It provides spatially more resolved predictions.</p> <p>It has a relatively low cost and easy implementation.</p>	<p>It also needs a dense air quality monitoring network.</p> <p>LUR is an empirical approach in contrast to dispersion/chemical transport models which are based upon physical principles and actual emission data. This explains the difficulty to transfer LUR models from one study area to another.</p> <p>It cannot predict concentrations during periods of unusual emissions (e.g., the COVID-19 pandemic) and/or meteorological conditions that deviate significantly from the historical record</p>

<b>Dispersion modelling</b>	Modelling of dispersion of emission from source to receptors using deterministic models	Fine spatial scale compare to CTMs It is helpful for air quality management purposes.	Do not treat chemical processes and reactions. Validation with monitoring data is an important requirement for its application. It requires multiple information as well as CTMs.
<b>Chemical transport modelling</b>	Modelling the dynamics of atmospheric pollutants considering dispersion plus chemical transport.	It can consider the reactivity of the chemicals in the atmosphere, such as the formation of O <sub>3</sub> and PM. Useful to prognosticate air contaminants that are not routinely monitored by environmental agencies because they are not regulated yet. It is helpful for air quality management purposes.	It requires higher computational power and multiple information (emission inventories, initial and boundary conditions, parameterization schemes, meteorological fields, and others), making its use sometimes unfeasible.

Previous studies characterized exposure to air pollution by assigning the average concentration measured at one or a few central sites within a city. For example, one of the most highly cited research articles, Dockery *et al.* (1993) positively correlated mortality rates and outdoor air pollution of people living in six American cities using six monitoring sites. Similarly, numerous other studies used fixed monitoring stations as a surrogate of exposure (Horie and Stern, 1976; Spix *et al.*, 1998; Lee *et al.*, 2014; Baek *et al.*, 2021; Liu *et al.*, 2021; Pu *et al.*, 2021; Rodrigues *et al.*, 2021; Zheng *et al.*, 2021).

However, to characterize intra-urban contrasts and/or to cover a broader spatial area, approaches beyond air monitoring stations were developed, including interpolation methods, satellite remote sensing, LUR models, computational algorithms, dispersion models, and CTMs. They are usually classified into deterministic models (i.e. physical) and stochastic models (i.e. statistical), despite, nowadays, it is common to refer to the latter as “traditional” statistical method due to arising of the artificial intelligence methods, considered as a third category. Stochastic models describe the statistical relationships among variables and have been developed from traditional multiple linear regression methods. Whereas, artificial intelligence methods have emerged in recent years and include machine learning methods such as artificial neural networks (ANNs) and deep learning. Deterministic models describe the relationship between variables mathematically based on knowledge of the physical, chemical, and biological mechanisms (Liao *et al.*, 2021).

The interpolation models in general estimate the value at an unmeasured location as a weighted average of the measurements at surrounding monitoring stations. They are either deterministic (such as inverse distance weighting (IDW), polynomial interpolations, splines) or stochastic geostatistical techniques (e.g. kriging and its many iterations) (Jerrett *et al.*, 2005; Xie *et al.*, 2017). For example, Deng *et al.* (2016) applied the IDW method to estimate the concentrations of SO<sub>2</sub>, NO<sub>2</sub>, and PM<sub>10</sub> using measurements obtained from ambient air quality monitoring stations in Changsha, China. Their study suggested an association between maternal exposure to traffic-related pollutant NO<sub>2</sub> during pregnancy and childhood asthma, allergic rhinitis, and eczema. Similarly, Guo *et al.* (2021) investigated the influence of individual exposure to NO<sub>2</sub>, SO<sub>2</sub>, PM<sub>10</sub>, and PM<sub>2.5</sub> on children’s health in Wuhan, China. They assessed the daily exposure over 2013-2014 at the kindergarten locations also using the IDW method and data of five monitoring sites. They showed that NO<sub>2</sub>, PM<sub>10</sub>, and PM<sub>2.5</sub> were significantly associated with childhood allergic diseases. In comparison, Michael *et al.* (2018) analyzed temporal trends and

spatial patterns of O<sub>3</sub> concentrations over Houston, Texas, by comparing the results from the IDW and kriging methods based on O<sub>3</sub> observations and meteorological measurements from monitoring sites. They stated that kriging methods tend to smooth the true spatial process, consequently, they may not be able to resolve small scale spatial trends, such as titration of O<sub>3</sub> near NO<sub>x</sub> sources. In addition, its results depend on the representativeness of the sampling data for the region of interest, thus, a sparse network may limit the accuracy of the results. Nevertheless, the kriging methods performed better, showing greater consistency in the generated surfaces, fewer interpolation errors, and lower biases (Michael *et al.*, 2018).

Satellite observations provide better spatial coverage, but currently at the price of low temporal coverage and rather crude spatial resolution – especially if used for estimating personal exposure and to refer to variability among individuals that live in the same vicinity (Sorek-Hamer *et al.*, 2020). Satellite-based monitoring cannot directly measure ground-level PM<sub>2.5</sub> concentration. Instead, it can provide aerosol optical depth (AOD) products that together with observation- and simulation-based methods produce surface PM<sub>2.5</sub> concentrations (Andreão and Albuquerque, 2021). Alvarado *et al.* (2019) have estimated daily-average PM<sub>2.5</sub> concentrations for cities in low- and middle-income countries and reported that the uncertainties tended to be very large (21–77% for the statistical methods, and 48–85% for the CTM-based methods). Despite its known limitations, satellite observations have been employed extensively for assessing PM concentrations in different temporal and spatial study designs (Sorek-Hamer *et al.*, 2020). For instance, Anderson *et al.* (2012) used satellite-based observations by combining AOD obtained from spectroradiometers on the satellite Terra and aerosol vertical profiles obtained from the global CTM GEOS-Chem to estimate PM<sub>2.5</sub> and NO<sub>2</sub> concentrations and, thus, investigate the effects of ambient air pollution on childhood asthma prevalence, but they found no strong association. They suggested that the association between childhood asthma prevalence with air pollution may be local-dependent. In contrast, Wang *et al.* (2020) positive associated exposure to PM<sub>2.5</sub> during pregnancy (11–40 weeks) and infancy (1–14 weeks after birth) with pediatric rheumatic diseases using 3-km satellite-based AOD retrievals also from the Terra and Aqua satellites combined with the meteorological variables from reanalysis data, land-use variables, and a linear mixed effect model to predict daily PM<sub>2.5</sub> concentrations in Taiwan.

Statistical techniques do not consider physical and chemical processes and use historical monitoring data to predict air pollutant concentrations. LUR models are empirical models that



have been widely used, especially in community health studies for capturing the smaller-scale variability. They are based on the principle that pollutant concentrations at any location depend on the environmental characteristics of the surrounding area. The models are developed through the construction of multiple regression equations describing the relationship between the pollutant measurements at the monitoring stations or at sampling locations (the dependant variable) and the predictor variables (independent variables) that are usually obtained through Geographic Information Systems (GIS), such as traffic intensity, road length, distance to the major road, road type, population density, land cover, wind speed, among other variables that can be judged to be relevant (Hoek *et al.*, 2008; Xie *et al.*, 2017).

LUR models have generally been applied in European and North American cities. For example, Boniardi *et al.* (2019a) used several LUR models to investigate the spatial distribution of black carbon (BC) in the catchment area of an elementary school in Milan, Italy. The models were built using data from 35 monitoring sites that were selected based on the proximity to/intensity of traffic sources and the school. They used more than 100 variables (road and traffic variables, population variables, land-use variables) to develop the LUR models that had different configurations to explain the BC distribution variability for warm and cold seasons as well as during the morning rush hours (from 7 am to 9 am). The LUR models showed that BC variability is well resolved only by traffic variables and the use of variables from 2011 may not properly take into account the urban transformations that happened in the last few years. In addition, during the cold season, there was a lack of explanatory variables that properly account for the contribution of heating systems to BC concentrations. Later, Boniardi *et al.* (2019b) used the same LUR model (for morning rush hours in the cold season) to assess its reliability in estimating BC exposure during home-to-school commuting (between 7:30 am and 8:30 am) of 43 children (aged 6 to 11) from January 14 to February 19, 2019. The children had to wear a shoulder bag equipped with a personal BC monitor in the breathing zone together with a GPS device, and they also filled an activity diary. On average, the LUR model ( $6365 \pm 3676 \text{ ng/m}^3$ ) underestimated (29% less) the measured personal exposure ( $9003 \pm 4864 \text{ ng/m}^3$ ); however, the correlation between the two methods was high ( $r = 0.74$ ). Despite the good agreement, the authors highlighted that the exposure BC estimates were based on the LUR model developed using data measured by fixed monitoring sites from the previous study. In addition, the traffic variables that they used to develop the model were only available as annual estimates. Hence, daily traffic conditions were not represented.

Marcon *et al.* (2021) compared the performance of the LUR model developed for Western Europe within the ELAPSE study (Effects of Low-Level Air Pollution: A study in Europe) and the kriging method to model concentrations of NO<sub>2</sub> and formaldehyde using measurements obtained from passive sampling collected at 25 sites during 10 weeks (2017– 2018) in the municipality of Viadana, Italy. Dependent variables were the routine air quality data for NO<sub>2</sub> and PM<sub>2.5</sub> and monitoring data for BC, whereas predictor variables (independent variables) included satellite data, dispersion model estimates, land cover, and traffic indicators. They suggested that despite the differences in methodology (kriging *vs* LUR), both results indicated that children living closer to the chipboard industry (< 1.7 km) were more exposed than the children living farther away (> 3.5 km).

Hannam *et al.* (2013) compared estimates of personal NO<sub>x</sub> and NO<sub>2</sub> exposure of 85 pregnant women from Manchester and Blackpool, England, with exposure estimates derived from ten different techniques: (i) nearest stationary monitor to home, (ii) average of the closest monitor to home and workplace, (iii) DEFRA model, (iv) IDW, (v) ordinary kriging, and (vi) a LUR model. In addition, modelling techniques were adjusted to provide monthly and daily values. The use of different methods aimed to examine if the techniques had different performances in both geographic areas. The personal exposure was measured with the Ogawa passive samplers over 48 hours period. The geometric mean levels of personal exposure were 17.3±16.4 µ/m<sup>3</sup> for NO<sub>2</sub> and 52.2±54.6 µ/m<sup>3</sup> for NO<sub>x</sub>, being exposure higher in Manchester. The techniques most correlated with personal exposure were monthly adjusted DEFRA ( $r_{\text{NO}_2} = 0.61$ ,  $r_{\text{NO}_x} = 0.60$ ), which estimated personal exposure as 18.85 µ/m<sup>3</sup> for NO<sub>2</sub> and 28.38 µ/m<sup>3</sup> for NO<sub>x</sub>. Ordinary kriging and IDW also had a good agreement ( $r_{\text{NO}_2} = 0.60$ ,  $r_{\text{NO}_x} = 0.62$ ) with the Ogawa samplers.

Hoek *et al.* (2008) reviewed 25 LUR studies evaluating the differences among them with respect to the number and distribution of monitoring sites, the use of routine versus purpose-designed networks, temporal resolution, the predictor variables (traffic variables, population or address density, land use, altitude, and topography, meteorology, and location), and the performance of the LUR models for different pollutants (NO<sub>2</sub>, NO<sub>x</sub>, PM<sub>2.5</sub>, and VOCs). The study suggested that most applications have been to NO<sub>2</sub> because of the ease of monitoring of this pollutant. In addition, the authors pointed out that the performance of the method in urban areas is typically better or equivalent to geostatistical methods such as kriging and conventional dispersion models. Besides, compared to dispersion models, the LUR method requires less

detailed input data at the expense of the need to obtain monitoring data for a sufficiently large number of sites.

The statistical approach takes advantage of the spatial and temporal correlations that are present in the air pollution concentration time series. However, statistical linear methods may not show satisfactory performance because of the nonlinear nature of air pollutants, which require a more sophisticated non-linear mathematical approach. Machine Learning (ML) methods can be employed to overcome this limitation. The most common learning algorithms are Random Forest, Gradient Boosting Machine, Artificial Neural Networks, Support Vector Regression, Cubist Regression, Kernel-Based Regularized Least-Squares, and Ensemble Approaches (Géron, 2019; Ren *et al.*, 2020). Alimissis *et al.* (2018) evaluated the performance of both non-linear (ANNs) and linear (multiple linear regression – MLR) approaches to model concentrations of NO<sub>2</sub>, NO, O<sub>3</sub>, CO, and SO<sub>2</sub> using data from air quality monitoring stations located in the greater area of Athens, Greece. The results showed that the ANN models had higher predictive ability than the MLR schemes, especially where the air quality network density was sparse, leading to a decreased degree of spatial correlations among the monitoring sites. Ren *et al.* (2020) also compared the performance of several ML algorithms, among linear and nonlinear models, to estimate daily maxima of 8-hour averages of ambient O<sub>3</sub> across the US. Overall, nonlinear ML methods achieved higher prediction accuracy than linear models (nearly 10%-40% decrease of predicted RMSE). For example, random forest (RMSE = 7.33 ppb and R<sup>2</sup>= 0.71) and extreme gradient boosting (XGBoost; RMSE = 7.74 ppb and R<sup>2</sup>= 0.67) were the two best performing ML models, and LASSO (RMSE = 8.68 ppb and R<sup>2</sup>= 0.59) was one of the best performing among linear models.

Wong *et al.* (2021) integrated LUR models and ML algorithms, such as Deep Neural Network, Random Forest, and XGBoost, for improving the accuracy of NO<sub>2</sub> variation predictions. They used daily average NO<sub>2</sub> data from 2000 to 2016 collected through 70 fixed air quality monitoring stations in Taiwan. The LUR model was developed using several geospatial and land-use data. XGBoost was the most efficient algorithm and yielded the best model performance (R<sup>2</sup>=0.84, RMSE = 3.95 ppb, MSE = 15.6 ppb) compared to Deep Neural Network (R<sup>2</sup>=0.81, RMSE = 4.3 ppb, MSE = 18.4 ppb), Random Forest (R<sup>2</sup>=0.78, RMSE = 4.7 ppb, MSE = 21.8 ppb), and LUR alone (R<sup>2</sup>=0.65, RMSE = 5.9 ppb, MSE = 34.4 ppb). ML algorithms were also used to improve numerical simulations of PM<sub>2.5</sub> and its chemical components (OC, EC, NO<sub>3</sub><sup>-</sup>, NH<sub>4</sub><sup>+</sup>, and SO<sub>4</sub><sup>2-</sup>) over the Beijing-Tianjin-Hebei region, China. To improve the

prediction accuracy of the WRF-CAMx model, the MLR model, random forest, and support vector regression (SVR) model were assessed. The prediction accuracy of the MLR optimized model was slightly better than that of the WRF-CAMx model. However, there were substantial discrepancies between the observed and predicted data. Random forest and SVR models exhibited better prediction performance, with  $r$  values of 0.71–0.82, and error indices 17–79% lower than that of the WRF-CAMx model (Lv *et al.*, 2021).

In contrast to statistical methods, dispersion and chemical transport models (CTMs) simulate the physical and chemical processes of the dispersion and transformation of atmospheric pollutants to predict the pollutant concentrations associated with emission sources, topography, meteorology, as well as their spatial and temporal variations. CTMs numerically solve the physical and chemical equations and can be time-consuming due to the computationally expensive chemical mechanisms. The core of a CTM is the propagator consisting of all subroutines that are needed to update the current concentrations for a one-time step ahead. For each time step, it uses actual weather conditions, concentrations, and emissions as inputs, until it reaches the desired model prediction time. The predictability of CTMs suffers from uncertainties in characterizing the chemical mechanisms, emissions data, and meteorological processes (Vlasenko *et al.*, 2021).

The representative deterministic models are the Community Multiscale Air Quality modelling system (CMAQ), the California Puff Model (CALPUFF), the Atmospheric Dispersion Modelling System (ADMS) model, and the Weather Research and Forecasting model coupled with Chemistry (WRF-Chem) model. For instance, Isakov *et al.* (2009) combined CMAQ and AERMOD results with population exposure models, namely the Hazardous Air Pollutant Exposure Model (HAPEM) and the Stochastic Human Exposure and Dose Simulation (SHEDS) model to estimate benzene and PM<sub>2.5</sub> concentrations, respectively. HAPEM and SHEDS use census demographic data to simulate a representative population and combine air pollutant concentrations with human activity pattern data to estimate population exposures. The average hourly concentrations from the CMAQ model (12 km horizontal resolution) were added to the hourly concentrations calculated by the AERMOD local plume model at 318 receptors in the modelling domain. Modelled exposures based on the hybrid approach (CMAQ+AERMOD) were much higher and had a wider variability when compared to CMAQ results only, which the former may enhance the spatiotemporal analysis of exposures within a community.

Monticelli *et al.* (2021) applied CALPUFF to model NO<sub>2</sub> concentrations near homes and schools of children living in the MRV, Brazil. Modelled and observed concentrations were used to estimate children's exposure to NO<sub>2</sub> and the results were compared with passive samplers worn by the children. In terms of mean, the monitoring station provided results closer to the passive samplers, however, the spatial-temporal variability, as well as the minimum and maximum values, was best captured with CALPUFF. Khreis *et al.* (2018) used the ADMS-Urban atmospheric dispersion model to estimate NO<sub>x</sub> and NO<sub>2</sub> concentrations and thus, correlated them with the annual number of childhood asthma cases in Bradford, UK. The ADMS results were compared to estimates derived from the LUR model based on passive samplers placed at 41 sites over 14 days. Using the ADMS model, they estimated that an average of 18% of all childhood asthma cases in Bradford are attributable to NO<sub>2</sub>, and 24% using the LUR model. Andreão *et al.* (2020) used the WRF-Chem to quantify daily and annual PM<sub>10</sub> and PM<sub>2.5</sub> concentrations in 102 Brazilian cities because the monitoring network in Brazil is sparse. Then, they computed how many deaths and hospitalizations would be avoided due to respiratory and circulatory system diseases.

Other studies applied alternative deterministic models but which have the same purpose. Klompmaker *et al.* (2021) evaluated associations between mortality rates and air pollution levels based on two stochastic models (Dutch LUR and European-wide hybrid), and a deterministic Dutch dispersion model. All these models showed positive associations of air pollutants with mortality due to natural causes, cardiovascular disease, respiratory disease, and lung cancer, but the strength of the associations differed between the three models. The hybrid and the dispersion models were generally more strongly associated with all mortality outcomes, whereas air pollutants modelled with LUR were only significantly associated with lung cancer mortality. The spatial variability of PM<sub>2.5</sub> and BC exposure was smaller for LUR compared to hybrid and dispersion models. NO<sub>2</sub> exposure variability was similar for the three methods. The study concluded the choice of the model may contribute to heterogeneity in effect estimates from cohort studies of long-term exposure to outdoor air pollution and mortality.

Similarly, Gariazzo *et al.* (2021) used three different approaches to estimate population long-term exposure to NO<sub>2</sub> and PM<sub>10</sub> and associated with mortality rates of natural-cause, cardiovascular, and respiratory diseases in Rome, Italy. Their study aimed to investigate if the results would have significant differences among the different models and resolutions. Air pollutant concentrations were estimated at different resolutions at 4 m, 200 m, and 1 km through

the micro-scale dispersion model PMSS (Parallel Micro-Swift-Spray), Random Forest, and the CTM Flexible Air quality Regional Model (FARM), respectively. There were significant differences when exposure was estimated and expressed per interquartile ranges. However, the differences in terms of hazard ratios (HRs) values for non-accidental and cardiovascular mortalities due to either NO<sub>2</sub> or PM<sub>10</sub> exposures were not statistically significant. These results imply that computational efforts required to estimate exposure at very fine resolution, using sophisticated model techniques like PMSS, do not provide significant differences in HRs of long-term health effects assessment with respect to simpler and less resolved computational modelling approaches, like CTM or machine learning methods.

Although all approaches presented in this section have their limitations, researchers in most cases are doing the best work that technology, available data, or indeed time or known methods allowed them to do. In addition, the use of more sophisticated model techniques does not necessarily provide significant differences or improvements in the results (Gariazzo *et al.*, 2021). However, as mentioned, each individual has a unique air pollution exposure profile, meaning that these approaches cannot replace, in terms of accuracy and representativeness, instrumental personal exposure measures that would be directly carried out according to the daily activities of each individual. Measurements with personal monitors can differ greatly from estimates using fixed monitoring stations or numerical models because both consider that individuals spend their time exclusively in the outdoor ambient, which is an erroneous assumption since people usually spend the majority of their time in indoor environments, such as at home, schools, offices, transit routes, among others. For this reason, the next section was dedicated to a literature review of studies that evaluated the personal exposure of children to air pollutants.

### **3.4 CHILDREN PERSONAL EXPOSURE TO AIR POLLUTION**

In a series of papers, Buonanno *et al.* (2012, 2013a; 2013b) reported the personal exposure and dose of children (8–11 years old) living in Cassino, Italy, to ultrafine particles (UFP, <0.1 µm) and BC. The portable apparatus wore by children was composed of a BC monitor (microAeth® AE51, Magee Scientific), a GPS tracking device, and three hand-held UFP counters (NanoTracer, Philips), which the latter measured (i) particle number concentration (PNC, up to  $1 \times 10^6$  part/cm<sup>3</sup> in the diameter range of 10–300 nm), (ii) nanoparticle surface area (µg<sup>2</sup>/cm<sup>3</sup>),

and (iii) mean diameter of the particle number size distribution. Activity diaries were also used to track children's activities throughout the day. The daily average PNC measured on a personal scale was equal to  $58 \times 10^3$  part/cm<sup>3</sup>, and for BC was equal to  $5.1 \mu\text{g}/\text{m}^3$ . As interpreted by Buonanno *et al.* (2013), the average personal UFP exposure experienced by children was very high and was comparable to concentrations measured in street canyons and roadsides, as reported by Morawska *et al.* (2008), which determined mean concentrations for several environments, such as clean background, rural, urban background, urban, street canyon, roadside, on-road, and tunnel environments as 2.6, 4.8, 7.3, 10.8, 42.8, 48.2, 71.5,  $167.7 \times 10^3$  part/cm<sup>3</sup>, respectively. With regard to dose, the mean daily inhaled dose of particle number and BC concentrations were  $3.35 \times 10^{11}$  part/day and  $39.2 \mu\text{g}/\text{day}$ , respectively. For all children, the lowest PNC values were registered during sleeping time and the highest occurred during eating time. Furthermore, the sleeping time presented a higher mode diameter range (84–136 nm) compared to the eating time (67–84 nm) because of the presence of more aged particles. Children were also exposed to high PNC during their time spent on transport, with an average ranging from  $55 \times 10^3 \pm 24 \times 10^3$  part/cm<sup>3</sup> to  $68 \times 10^3 \pm 28 \times 10^3$  part/cm<sup>3</sup> in the urban area, and  $21 \times 10^3 \pm 82 \times 10^3$  part/cm<sup>3</sup> in the rural site.

Mazaheri *et al.* (2014) carried out similar experiments with schoolchildren (8–11 years old) living in the Brisbane Metropolitan Area, Australia. A similar device to Buonanno *et al.* (2012, 2013a; 2013b) was used, the Philips Nanotracers, to measure PNC and it was carried by children around the waist using a dedicated belt. A diary survey was developed for recording children's daily activities. The mean and standard error of exposure to PNC in each of the four environments were:  $10.5 \times 10^3 \pm 58.8$  part/cm<sup>3</sup> (home),  $8.53 \times 10^3 \pm 0.13 \times 10^3$  part/cm<sup>3</sup> (school),  $13.7 \times 10^3 \pm 0.30 \times 10^3$  part/cm<sup>3</sup> (commuting), and  $8.66 \times 10^3 \pm 0.28 \times 10^3$  part/cm<sup>3</sup> (other). An important feature described in the study design was all classrooms used natural ventilation all year round and no heating systems were used during winter or on cooler days, which is a similar assumption for classrooms in Brazil. The authors concluded that inhaled alveolar surface area doses in the Italian schools were approximately 1.5–5 times higher than in Brisbane, Australia. Later, Mazaheri *et al.* (2019) evaluated UFP concentrations (with the same equipment) over 24 h for 24 children (9–13 years old) in the city of Heshan, the Pearl River Delta region, southern China. Natural ventilation was used in all the indoor microenvironments, which made the infiltration of outdoor particles indoors a natural process. However, the authors highlighted the impact of adults' smoking and the use of mosquito repellent incense at home on children's exposure because the highest average exposure ( $12.6 \times 10^3$  part/cm<sup>3</sup>) was found to occur at

home, especially during sleeping hours, based on the collected questionnaire data. The results also showed significant differences between the concurrently measured PNC using fixed-site and personal monitors, hourly average personal PNC was lower than ambient PNC by  $51.8 \times 10^3 \text{ part/cm}^3$  (65%), which demonstrated that fixed-site monitoring does not provide a realistic estimate for personal exposures.

Möller *et al.* (2012) carried out personal monitoring campaigns with children from a secondary school (12–13 years) in Greater Manchester, England. Participating children were asked to wear a passive sampler (Ogawa & Co., USA) on their school blazers for two consecutive weekdays, with the sampler being exchanged after the first day. In addition to wearing the personal monitors, the children were asked to complete a time-activity diary for the same time period. Because only four urban monitoring stations within the Greater Manchester area were available at the time of the campaign, a LUR model specifically developed for the Greater Manchester area was employed to provide outdoor  $\text{NO}_2$  concentrations. I/O ratios were also used for schools (I/O = 0.5), went on walking/cycling (I/O = 1.0), went by car/bus (I/O = 2.0), and a model parameterised for the UK was adopted for I/O at homes. With the data collected, the authors formulated a ‘microenvironmental exposure model’ which consisted of three main environments (home, school, journey) which are further subdivided into indoor or outdoor, and in the case of the home into kitchen, living room, and child’s bedroom. The mean exposure estimated by their microenvironmental exposure model ( $19.6 \pm 4.7 \mu\text{m}^3$ ) was the most similar to the mean personal exposure measured by Ogawa samplers ( $20.4 \pm 7.9 \mu\text{m}^3$ ). Meanwhile, the personal exposure would be overestimated if it was used only the nearest urban monitor ( $28.6 \pm 15.0 \mu\text{m}^3$ ) or modelled LUR data ( $31.2 \pm 5.4 \mu\text{m}^3$ ). In this sense, the study demonstrated that modelling based on time spent in microenvironments provides a better estimate of personal exposure than an outdoor model or the nearest urban monitor.

Rivas *et al.* (2016) evaluated personal BC exposure of 45 schoolchildren (7–10 years old) living in Barcelona, Spain, using a portable MicroAeth AE51 (AethLabs, USA) over 48 h. Children carried the instrument in a belt bag, with the inlet tube always exposed and placed in the breathing zone. Children filled a time-activity diary reporting every time they changed location and activity. Children spent 6% of their time commuting but received 12% of their daily BC exposure (mean of  $3.3 \mu\text{g/m}^3$ ), due to cooccurrence with road traffic rush hours and the proximity to the source. Children received 33% of their daily-integrated BC exposure at school ( $1.5 \mu\text{g/m}^3$  in the classroom and  $1.4 \mu\text{g/m}^3$  in the school playground) where they spent 31% of



their time. Home (58% of their time,  $1.3 \mu\text{g}/\text{m}^3$ ) and others (6% of their time,  $1.4 \mu\text{g}/\text{m}^3$ ) were responsible for the 50% and 6% BC dose, respectively. Beyond that personal BC concentrations were 20% higher than in fixed stations at schools, but in the warm season, the fixed stations agreed better with personal measurements than during the cold season.

Paunescu *et al.* (2017) reported daily (24 h) personal BC and UFP individual exposure of 96 children ( $9 \pm 0.2$  years old) living in Paris, France. Time spent in each microenvironment came from space-time-activity questionnaires filled by the families, and Google Maps was used to geocode all addresses. The parameters were measured by portable devices microAeth® AE51 (Aethlabs, San Francisco, CA, USA) and DiSCmini® (Matter -aerosol; Wohlen, Switzerland) located inside a backpack with the inlet in the breathing zone. The total BC (UFP) exposure during school, home, transportation, and extra-curricular activities were 53% (65%), 33% (23%), 12% (10%), and 2% (2%). The results also showed that BC exposure concentration was higher during trips, principally subway/train (BC=  $3.75 \pm 1.77 \mu\text{g}/\text{m}^3$ ; UFP=  $29.1 \pm 16.6 \times 10^3 \text{ part}/\text{cm}^3$ ) and bus (BC=  $3.32 \pm 1.25 \mu\text{g}/\text{m}^3$ ; UFP=  $32.6 \pm 14.9 \times 10^3 \text{ part}/\text{cm}^3$ ). On the other hand, UFP exposure concentration was higher during indoor activities, mainly during eating at restaurants (BC=  $2.40 \pm 1.19 \mu\text{g}/\text{m}^3$ ; UFP=  $98.2 \pm 175.8 \times 10^3 \text{ part}/\text{cm}^3$ ) and on trips (BC=  $1.97 \pm 1.29 \mu\text{g}/\text{m}^3$ ; UFP=  $34.3 \pm 33.1 \times 10^3 \text{ part}/\text{cm}^3$ ), but the most significant UFP peaks occurred during cooking at home.

Pañella *et al.* (2017) also assessed daily (24 h) personal BC and UFP individual exposure of asthmatic ( $n=50$ ) and non-asthmatic children ( $n=50$ ) ( $9 \pm 0.7$  years old) in Catalonia, Spain. Time spent in each microenvironment was derived by the geolocation provided by the smartphone together with the portable devices microAeth® AE51 (Aethlabs, San Francisco, CA, USA) and DiSCmini® (Matter -aerosol; Wohlen, Switzerland) located inside a backpack with the inlet in the breathing zone. Asthmatics and non-asthmatics essentially spent the same amount of time at home (BC=  $1.54 \mu\text{g}/\text{m}^3$ ; UFP=  $10 \times 10^3 \text{ part}/\text{cm}^3$ ), at school (BC=  $1.65 \mu\text{g}/\text{m}^3$ ; UFP=  $10.2 \times 10^3 \text{ part}/\text{cm}^3$ ), on transportation (BC=  $3.34 \mu\text{g}/\text{m}^3$ ; UFP=  $19.1 \times 10^3 \text{ part}/\text{cm}^3$ ), and in other microenvironments (BC=  $2.20 \mu\text{g}/\text{m}^3$ ; UFP=  $14.2 \times 10^3 \text{ part}/\text{cm}^3$ ). The highest concentrations were attributed to transportation, despite it was the microenvironment where the children spent the least time over a day. In conclusion, the authors suggested that interventions should be tailored to the general population rather than to subgroups defined by a disease.

Karakatsani *et al.* (2017) followed 188 children, between 10 to 11 years old, for 5 weeks in the two major cities of Greece, namely Athens and Thessaloniki, to assess O<sub>3</sub> weekly exposure. The personal exposure was measured with Ogawa samplers (Ogawa & Co. USA Inc., Pompano Beach, FL) which were worn by children continuously on their chests. In high (low)-ozone areas, O<sub>3</sub> personal measurements were 10.8±7.8 µg/m<sup>3</sup> (8.2±6.7 µg/m<sup>3</sup>) and 5.9±6.6 µg/m<sup>3</sup> (4.7±4.8 µg/m<sup>3</sup>) in Athens and Thessaloniki, respectively. O<sub>3</sub> personal measurements were much lower than outdoor measurements at schools (range of 35.2±20.7 µg/m<sup>3</sup>– 64.3±20.1 µg/m<sup>3</sup>) or fixed sites (24.6±13.8 µg/m<sup>3</sup>– 63.8±16.4 µg/m<sup>3</sup>), reflecting the amount of time spent indoors, where ozone concentrations are lower.

Zhang *et al.* (2018) performed a PM<sub>2.5</sub> exposure assessment with 57 children (aged 8–12 years) in Shanghai, China. Like the other studies, they conducted a questionnaire survey to collect information about the children's lifestyles. PM<sub>2.5</sub> concentrations at school were measured in several microenvironments (e.g. classrooms, main corridors, and the playgrounds) from 8 a.m. to 4 p.m. with TSI DUSTTRAK™ DRX (Model 8533, TSI Inc. Paul, MN, USA) device. During the off-campus period (from 4 p.m. to 6 a.m. the next day), PM<sub>2.5</sub> concentrations were measured by a set of real-time laser diode photometers (SidePak™ AM510, TSI Inc, USA), which were placed in small bags. A sampling air inlet was fixed in the vicinity of the students' breath zone. The median of the PM<sub>2.5</sub> exposure levels in the different microenvironments and corresponding fractional time of all students was 3014.13 (µg.h)/m<sup>3</sup>, with an average of 155.74±72.73 µg/m<sup>3</sup>. They concluded that PM<sub>2.5</sub> concentrations in the schools greatly exceeded the daily standard of PM<sub>2.5</sub> Ambient Air Quality Standards of China (75 µg/ m<sup>3</sup>).

Personal exposure assessment to UFP was also carried out by Nyarku *et al.* (2019) with 61 schoolchildren (11–16 years old) from Accra, Ghana. The researchers also used the Three Aerasure NanoTracers (NT Model PNT1000; Philips, The Netherlands) to conduct the measurements. The mean UFP concentration and the mean (median) daily exposure were 53.30 ×10<sup>3</sup> part/cm<sup>3</sup> and 44.67 ×10<sup>3</sup> (41.0 ×10<sup>3</sup>) part/cm<sup>3</sup> per hour per day. The highest mean exposure was received at home because the open burning of trash is a common practice in the study area. In addition, many households burn mosquito coils at night as a means of keeping mosquitos out of their bedrooms.

Cunha-Lopes *et al.* (2019) quantified daily exposure to BC (with the MicroAeth AE51 (AethLabs, USA)) and sized-fractioned PM<sub>2.5</sub> (SKC five-stage Sioutas Cascade Impactor (SKC

Inc., USA)) of nine children (7–10 years old) residing in Lisbon, Portugal. Each child carried a trolley with three portable monitoring devices with the air inlet tube placed in the breathing zone. The equipment was carried for three days and recorded the time spent in their activities and respective microenvironments. The average exposure to PM<sub>2.5</sub> (19 µg/m<sup>3</sup>) was higher than that registered by the nearest fixed urban background station (11 µg/m<sup>3</sup>), evidencing the importance of assessing the personal daily exposure. The average exposure to PM<sub>1</sub>, PM<sub>0.5</sub>, and PM<sub>0.25</sub> was 14 µg/m<sup>3</sup>, 11 µg/m<sup>3</sup>, and 7.7 µg/m<sup>3</sup>, respectively. Although the lowest BC concentrations were measured at home (0.89 µg/m<sup>3</sup>), it was influenced by indoor sources (e.g. cooking and candles) and by infiltration from outdoor sources. The highest BC concentrations were registered while commuting (5.1 µg/m<sup>3</sup> by car and 2.5 µg/m<sup>3</sup> on foot). The daily average BC exposure and dose were 1.3 µg/m<sup>3</sup> and 15 µg/day, which was similar to the BC background concentrations of European cities.

George *et al.* (2020) conducted experiments with 46 children (aged 10–12 years), which carried the aethalometer (microAeth® model AE51, AETHLABS, San Francisco, USA) for a 24 h period on a typical school day in Singapore to measure BC concentrations. The aethalometer was placed in a shoulder bag, with the hose of the monitor affixed to the strap of the bag such that its tip was at the child's shoulder level. The mean BC exposure on a typical school day was 3.34±174.4 µg/m<sup>3</sup>/min. The highest BC exposure occurred during commuting to and from school (5.08 µg/m<sup>3</sup>/min), compared to that when at home (2.94 µg/m<sup>3</sup>/min), at school (3.37 µg/m<sup>3</sup>/min), and during other activities (2.76 µg/m<sup>3</sup>/min).

In Milan, Italy, Boniardi *et al.* (2021) asked children (8–9 years old) to complete a time-activity diary and to wear a GPS and a shoulder bag equipped with the microAeth® AE51 (Aethlabs, San Francisco, CA, USA) to measure personal exposure to BC concentrations. They found that the personal exposure in the cold season was 3.9±3.3 µg/m<sup>3</sup>, a 3-fold higher than in the warm season (1.3±1.5 µg/m<sup>3</sup>), while exposure to BC concentrations was 2.8 µg/m<sup>3</sup> (range: 0.2–11.9 µg/m<sup>3</sup>) when considering overall data. Regardless of seasonality, transportation was the microenvironment linked with the highest mean and maximum personal BC concentrations.

Jung *et al.* (2021) considered children between 9 and 14 years old with current asthma status living in New York City, USA. Children wore BC monitors for two 24-h periods over six days sampling period. The BC concentrations were measured with the MicroAeth (Model AE51; Magee Scientific) monitor and a survey asking children if he/she went to school that day. The

levels of hourly personal BC during school hours (between 08:30 and 14:30 hours) ranged between 1.26 and 1.66  $\mu\text{g}/\text{m}^3$ . There were higher mean personal BC concentrations before (7–8 a.m.) and after school hours (3–4 p.m.), whereas the highest concentrations were observed between 7 and 9 p.m.

In Brazil, no studies involving personal exposure of children to air pollutants have been reported, however, some studies carried out with adults could be found. For example, Santos *et al.* (2016) evaluated the 24-hour personal exposure to  $\text{PM}_{2.5}$  of 101 non-smoking workers (taxi drivers, traffic controllers, and forest rangers) in São Paulo. The personal sampler was designed by the Harvard School of Public Health and installed in a shoulder bag to be carried all day and kept nearby during sleeping or bathing periods to record real 24-hour environmental exposure. The median (mean) personal exposure was 42.26  $\mu\text{g}/\text{m}^3$  ( $38.42 \pm 14.72 \mu\text{g}/\text{m}^3$ ) for taxi drivers, 23.24  $\mu\text{g}/\text{m}^3$  ( $20.75 \pm 6.49 \mu\text{g}/\text{m}^3$ ) for traffic controllers, and 36.72  $\mu\text{g}/\text{m}^3$  ( $31.83 \pm 17.17 \mu\text{g}/\text{m}^3$ ) for forest rangers. More recently, also in São Paulo, the Health District of Butantan School recruited 131 pregnant women to assess individual exposure to  $\text{NO}_2$  and  $\text{O}_3$  with passive devices, that were delivered to each patient by a community health agent 7 to 18 days before her ultrasonography. The study found a median (mean) personal exposure of 40.29  $\mu\text{g}/\text{m}^3$  ( $40.27 \pm 16.9 \mu\text{g}/\text{m}^3$ ) to  $\text{NO}_2$  and 8.12  $\mu\text{g}/\text{m}^3$  ( $8.30 \pm 1.09 \mu\text{g}/\text{m}^3$ ) to  $\text{O}_3$  (Hettfleisch *et al.*, 2021). Because  $\text{O}_3$  is consumed by nitrogen oxides in the photochemical cycle, the pollutants were inversely correlated, and thus, their results encountered that primary pollutants (represented by  $\text{NO}_2$  as a proxy variable of fresh automotive emissions) are more important in promoting adverse effects in placental tissue than secondary pollutants, in this case, represented by  $\text{O}_3$ .

In Londrina, Paraná, Carvalho *et al.* (2018) determined the personal exposure and dose of six couples with different working routines over 48 h based on mobile BC measurements with a hand-held aethalometer (models AE51, AethLabs, USA). In their study, the volunteers spent on average 67% of their time at home, 23% at work, 7% in transport, and 3% conducting other activities (shopping, gym, visiting friends, and family, etc.). The highest levels and variability were found to occur in transport (mean of  $4.01 \pm 5.35 \mu\text{g}/\text{m}^3$ ). Conversely, mean concentrations at work were lower and showed less variability (mean of  $1.42 \pm 1.45 \mu\text{g}/\text{m}^3$ ). The authors reinforced that data from fixed monitoring sites could not capture the variability of BC concentrations, especially within transport microenvironments, where the spikes occurred. Moreover, concentrations measured at fixed sites were not correlated with the personal monitoring during the day, since BC featured a large spatial variability. Also in Londrina,

Almeida *et al.* (2018) assessed the personal exposure of 30 individuals from five occupational categories to PNC for size ranges (PM<sub>1</sub>; PM<sub>2.5</sub>; PM<sub>4</sub>; PM<sub>10</sub>). The personal sampling occurred during workdays, starting from the moment they left their homes to go to work. The devices were placed in a small backpack, with the inlets externally attached to the strap near the volunteer's airways. The equipment consisted of a GPS, a particle counter monitor (Met One Instruments, Model 804, Grants Pass, U.S.A) to measure the PNC, and a mass particle monitor (Met One Instruments, Model Aerocet 831, Grants Pass, U.S.A.) to measure the PM concentrations. The personal exposure to PNC was on average higher in lower ranges (PNC<sub>0.3-0.5</sub>=93.9±55.4 part/cm<sup>3</sup>) when compared to other size intervals (PNC<sub>2.5-10</sub>=0.2±0.1 part/cm<sup>3</sup>). Volunteers in the 'education' category experienced the lowest exposure to PM (e.g. PM<sub>1</sub>=7.4±3.3 µg/m<sup>3</sup> and PM<sub>2.5</sub>=11.1±4.1 µg/m<sup>3</sup>), as opposed to those involved in 'commercial' and 'transport' activities with the highest exposure for PM<sub>1</sub> (15.5±8.5 µg/m<sup>3</sup>) and PM<sub>2.5</sub> (22.6±13.1 µg/m<sup>3</sup>), respectively.

Pacitto *et al.* (2021) performed a comparison among airborne particle concentrations, at a personal scale using a handheld particle counter, in different cities around the world (Cairo, Accra, Florianopolis, and Nur-Sultan). Exposure data characteristics of these populations revealed significant differences with respect to the high-income western countries. For example, the exposure during the cooking/eating activities was the most critical for western countries, however, for these low- and middle-income countries, it was lower or similar to those measured in other microenvironments. Several reasons could explain this finding, such as type of food, cooking activity, fuel and stoves used, and climatic conditions. An exception was Florianopolis, which according to the authors, socioeconomic conditions would explain this divergence compared to the other cities since no site-specific air quality issues typical of the other low- and middle-income countries were reported. Nevertheless, for Brazil, it was found that the median exposure to PNC values were 9.83×10<sup>3</sup> part/cm<sup>3</sup> (Sleeping & Resting), 12.1×10<sup>3</sup> part/cm<sup>3</sup> (indoor day), 13.1×10<sup>3</sup> part/cm<sup>3</sup> (outdoor day), 13.3×10<sup>3</sup> part/cm<sup>3</sup> (transport), 11.8×10<sup>3</sup> part/cm<sup>3</sup> (working), and 19.4×10<sup>3</sup> part/cm<sup>3</sup> (cooking/eating). The authors also concluded that low- and middle-income populations spend less time indoors due to climate conditions, resulting in different contributions of the microenvironments to the daily exposure and dose.

Because the objective of the present study is to investigate whether the modelled ambient concentrations could be used as a reliable surrogate of personal exposures in the study area, a

literature review was devoted to finding studies that used a dispersion and/or CTM model to assess individual exposure. For that, keywords beginning with 'personal exposure', followed by the terms: 'CTM', 'dispersion model', 'AERMOD', 'CALPUFF', 'ADMS', 'CMAQ', 'WRF-Chem', and 'CAMx', separately, were entered into the SCOPUS and Web of Science databases, filtered by the fields 'title', 'abstract', and 'keywords' and considering research articles in English. Although the literature was limited, some studies are presented hereafter.

Wang *et al.* (2009) applied two atmospheric dispersion models (ISCST3 and AERMOD) to estimate the 24-h average ambient concentrations of benzene and toluene and to compare the results with stationary sites and personal measurements from 108 participants living in Camden, New Jersey, USA. The levels of benzene and toluene concentrations predicted by ISCST3 and AERMOD were comparable to the measurements collected at the fixed sites, in which both models had similar performances but underestimated the measurement concentrations. Nevertheless, the values from fixed monitors generally showed better agreement with the personal measurements than those based on atmospheric models. The authors suggested that the dispersion modelling results for benzene and toluene might not be adequate for exposure modelling and further improvement would be needed.

Fulk *et al.* (2016) also used AERMOD to investigate if the dispersion model could be used as an approach to estimate ambient air manganese exposure concentrations for 19 children (7–9 years) living near a ferromanganese refinery in Marietta, Ohio, USA. For that, the authors used personal exposure values from the study of Haynes *et al.* (2012) that carried out the experiments through a backpack equipped with a tube connected to an air sampling pump and a modular impactor capable of sampling PM<sub>2.5</sub> for 48 h. The results indicated that modelled monthly and yearly manganese concentrations were in close agreement with the manganese measured in the PM<sub>2.5</sub> obtained from a stationary monitor placed at the refinery. However, the mean modelled values ( $27.9 \pm 46.8$  (median=8.8) ng/m<sup>3</sup>) were overestimated when compared to personal data ( $11.1 \pm 13.3$  (median=6.5) ng/m<sup>3</sup>), despite the median values being close. Nevertheless, the level of modelled manganese was found to be positively associated with the level of personal Mn, which explained more than 40% of the variability in personal exposures ( $R^2=0.42$ ).

Similarly, Physick *et al.* (2011) estimated personal exposure to NO<sub>2</sub> of 24 adults in Melbourne, Australia. The participants wore two passive samplers simultaneously attached to chest clothing, which one was worn throughout a 48-hour period and the second sampler depended

on which microenvironment (home, work, transit, or other) was being experienced. Additional pairs of samplers were placed outside of the participant's home and workplace and opened only while the volunteer was in that environment. In this way, ratios of indoor to outdoor concentrations were obtained, which homes with gas cooking adopted I/O = 0.67, and those without gas cooking used 0.47. For workplaces, it was used I/O = 0.74. Sampler measurements were compared to hourly-averaged data from fixed network monitors and an air quality model (TAPM-CTM), which used a horizontal resolution of 9, 3, and 1 km. In the vertical, model levels are at 10, 25, 50, 100, 150, and 200 m above the ground, with layer spacing gradually increasing up to the top of the model domain (which extended to 8000 m). According to the authors, the decision to use a CTM relied on an ozone case study episode in the Northern Georgia Region, USA (Bell, 2006), which showed that the MM5/CMAQ provided better estimates of exposure than fixed-network monitoring alone by increasing the spatial and temporal resolution and by providing estimates for pollutants that are not measured. In this sense, when compared to the passive samplers placed at home, the simulations predicted reasonable results, underestimating the mean NO<sub>2</sub> exposure by only 11%. However, TAPM-CTM did not perform well for the work microenvironment because of an underestimation of vehicle emissions inventory. Despite both methods underestimating the personal exposure values, the statistics for the nearest monitor approach were generally better than for the simulation approach. Thus, the authors recommended the use of values from the network monitor nearest to a person's microenvironment for calculating the personal exposure, but their findings could only be related to NO<sub>2</sub> and cities with monitoring networks of similar density to Melbourne. Conversely, Dimakopoulou *et al.* (2020) observed that personal exposure of children living in Athens and Thessaloniki to O<sub>3</sub> was better correlated using estimates from the Eulerian chemical transport model (MARS-aero) than fixed-site monitors.

As we could see throughout the literature review, there are several ways to perform the exposure assessment to air pollution, which can be based on the different modelling and measurement techniques, evaluate different population subgroups, consider space-time-activity information or/and ratios of indoor to outdoor concentrations. The current study is interested in investigating the exposure of children to air pollution in a coastal-urban area, located in the Southeast of Brazil, which has a peculiar arrangement and air pollution is not mostly exclusively emitted by vehicular sources, as occurs in most of the urban centres worldwide. The local emission inventory pointed out that the major contributor of air pollutant emissions is the industrial sources, especially those related to the pelletizing-siderurgy activities, which are located

together in the same port complex and relatively near the children's residences. Thus, by using a modelling approach together with source apportionment and sensitivity analysis, the present doctoral thesis aims not only to quantify but also address the responsibility of air quality over the region.



## 4. METHODOLOGY

### 4.1 THE ASMA-VIX PROJECT

The ASMA-Vix study was a multidisciplinary project, aimed at assessing the relationship between air pollution and children's health in the Metropolitan Region of Vitória (MRV), Espírito Santo, Southeast Brazil (Figure 9). The MRV region is a coastal, tropical, and urban-industrial area, that is composed of seven municipalities, namely: Fundão, Serra, Cariacica, Viana, Vila Velha, Guarapari, and Vitória, being Vitória the capital of the state of Espírito Santo. The MRV has a peculiar arrangement because the industrial complex (chemical, petrochemical, and mining-steel industries, landfills, civil construction, airports) are located into the urban/residential zone, where about over 2 million people live. The MRV population represents more than half of the total population of the Espírito Santo state (IBGE, 2020). Source apportionment studies in the MRV region have identified that the major emission sources are from industrial sites related to pelletizing, steel and port activities, and road traffic (Santos *et al.*, 2017; Galvão *et al.*, 2018, 2019). These anthropogenic emissions result in a mixing of air pollutants that annoy the population (Machado *et al.*, 2015). In addition, the prevalence of asthma and rhinitis among children in Vitória is higher than the Brazilian national average (Serpa *et al.*, 2014). In this context, the ASMA-Vix study was designed to investigate the respiratory function in children and adolescents with mild to moderate asthma residing in the city of Vitória in order to determine whether, and to what extent, air pollution affects asthma symptoms. For that, the selected children and adolescents have to wear passive samplers (Ogawa & Co., USA) to evaluate the levels of exposure to air pollution, which nitrogen dioxide (NO<sub>2</sub>) was chosen to be the object of monitoring. These passive samplers were wearable by twenty-one children (eight girls and thirteen boys with ages varying between 8 and 14 years old) through three monitoring campaigns (Table 4). The limited number of participants included in this pilot study in Brazil was because the ASMA-Vix project considered only children with asthma symptoms, which can be pointed out as a limitation of the study. Studies that only focus on children with asthma have small sample sizes and the extrapolation of the results could be impaired (Xu *et al.*, 2020). More detailed information about the ASMA-Vix study can be found at <https://qualidadedoar.ufes.br/asmavix>.

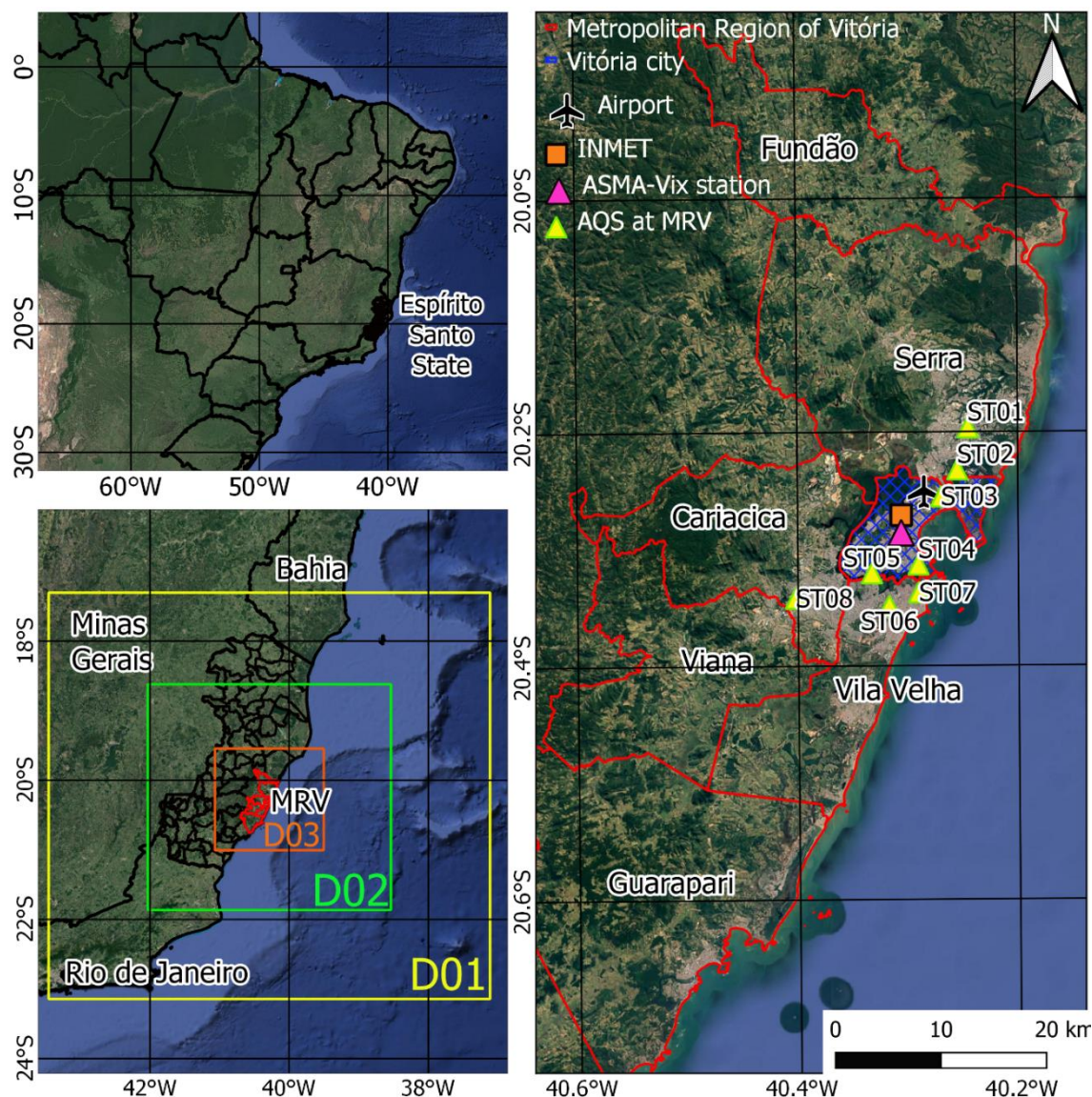


Figure 9. Location of Espírito Santo State in Brazil (upper left) and the location of the Metropolitan Region of Vitória in Espírito Santo State (lower left). The location of the air quality stations (AQS) used to evaluate the performance of the WRF-Urban and CMAQ-ISAM models.

The monitoring campaigns were performed with children living in neighbourhoods of Vitória city, namely: Andorinhas district ('Campaign 1' – C1 between November 2-17, 2019), Maruípe district ('Campaign 2' – C2 between December 4-19, 2019), and Itararé district ('Campaign 3' – C3 between February 12-19, 2020) (Table 4 and 5). In C1 and C2, the filters were changed every 5 days over three weeks, thus, each sample represented a cumulative personal exposure of 5 days to NO<sub>2</sub>. In C3, children used the personal passive samplers over one single week (7 days). The change from 5 to 7 days in the third campaign was made so that, logistically, it would be easier to change filters. In other words, the exchange of filters would occur once a week

instead of twice, aiming at the entry of more children into the project and performing more experimental campaigns. However, the 7-day model was not continued because of the interruption of all activities due to the COVID-19 pandemic. In addition, experimental data of particulate matter (PM<sub>2.5</sub> and PM<sub>10</sub>) were obtained in schools and homes (indoor measurements) of the children related to the project. The location of the neighbourhoods, schools, and children's residences are shown in Figure 10.

The description of the sampling procedures, the equipment set-up, the routine collection, and the children's profiles and their daily activities are described in Velasco (2020), Monticelli (2020), and Monticelli *et al.* (2021). Children have a highly predictable and less varied daily routine compared to adults. The selected children spent 75% and 15% of their time at home and school, respectively, totalling 90% of their time in indoor environments, and 10% outdoor including the transit routes. In addition, the majority of participants used ceiling fans and open windows throughout the day, including the sleeping hours. Sixteen children (out of 21) were walking to school and took on an average of 7 minutes in their routes for a mean distance of 444±298 m. Three children went to school using private vehicles, one using a personal vehicle that took 10 minutes to arrive at school for a distance of 2900 m, and two children using a school minibus that took 40 minutes in transit routes for a distance of 1600 m and 2700 m. Two children used the public buses to go to school for a distance of 1100 m and 2100 m, despite the close distance the latter took 40 minutes in its transit route because of a combination of walking to the bus stop, waiting, and taking the bus (Table 4).

Table 4 presents detailed information about the ASMA-Vix campaigns, informing children's characteristics and behaviours, such as their gender, age, the transport modes used by the children to go to school, the average time that they spent on commuting, the distance estimated by Google Maps, the school time they attended school, and the personal exposure of NO<sub>2</sub> (cumulative) for each child in each week. Table 5 summarized these contents by campaigns.

Table 4. A detailed description of the experimental campaigns of the ASMA-Vix project.

Campaign	Children's code	Sex	Age (years)	Mode transport home-school	Time spent during commuting home-school (min)	Distance home-school (m) (from GoogleMaps)	School time	Week	NO <sub>2</sub> data (cumulative) measured with the passive samplers [ $\mu\text{g}/\text{m}^3$ ]
<b>Campaign 1 (C1)</b> <b>W1:</b> <b>November 2-7, 2019</b> <b>W2:</b> <b>November 7-12, 2019</b> <b>W3:</b> <b>November 12-17, 2019</b>	AN.CR.01	F	11	Walking	5	300	part-time (morning)	W1	17.69
								W2	12.18
								W3	15.27
	AN.CR.02	F	10	Walking	2	170	part-time (morning)	W1	8.69
								W2	6.66
								W3	-
	AN.CR.03	F	11	Walking	2	130	full-time	W1	21.09
								W2	12.75
								W3	22.45
	AN.CR.04	F	10	Walking	10	450	part-time (afternoon)	W1	12.31
								W2	7.44
								W3	8.65
	AN.CR.05	M	11	Walking	10	450	part-time (afternoon)	W1	11.30
								W2	13.99
								W3	20.19
	AN.CR.06	M	13	Walking	3	190	part-time (afternoon)	W1	9.08
								W2	12.18
								W3	8.55
<b>Campaign 2 (C2)</b> <b>W1:</b> <b>December 4-9, 2019</b> <b>W2:</b> <b>December 9-14, 2019</b>	MA.CR.01	M	11	Walking	15	850	part-time (afternoon)	W1	10.62
								W2	10.19
								W3	7.75
	MA.CR.02	F	9	Walking	15	1000	part-time (afternoon)	W1	6.05
								W2	4.63
								W3	4.61
	MA.CR.03	F	12	Vehicle (Minibus)	40	1600	part-time (afternoon)	W1	7.13
								W2	9.49
								W3	7.84
	MA.CR.04	M	13	Walking	12	900	part-time (morning)	W1	14.31
							W2	-	
							W3	-	
MA.CR.05	M	11	Walking	10	750		W1	15.44	

<b>W3: December 14-19, 2019</b>							part-time (morning)	W2	10.42
								W3	30.46
								W1	13.40
	MA.CR.06	F	8	Walking	5	400	part-time (morning)	W2	6.15
								W3	13.57
<b>Campaign 3 (C3)</b>	IT.CR.01	M	9	Walking	1	120	part-time (afternoon)	W1	12.69
	IT.CR.02	M	8	Private vehicle	10	2900	part-time (morning)	W1	12.90
	IT.CR.03	M	9	Vehicle (Minibus)	40	2700	part-time (afternoon)	W1	14.61
	IT.CR.04	M	9	Walking	3	290	part-time (morning)	W1	14.34
	IT.CR.05	M	14	Walking	5	350	part-time (afternoon)	W1	18.69
	IT.CR.06	M	12	Bus	15	1100	part-time (morning)	W1	12.80
	IT.CR.07	M	13	Bus	40	2100	full-time	W1	10.08
	IT.CR.08	M	9	Walking	1	110	part-time (morning)	W1	15.08
	IT.CR.09	F	12	Walking	10	650	part-time (morning)	W1	11.69



Table 5. Summary of the experimental campaigns of the ASMA-Vix project.

	<b>Campaign 1</b>	<b>Campaign 2</b>	<b>Campaign 3</b>
<b>Sample size (n)</b>	6 (2 boys, 4 girls)	6 (3 boys, 3 girls)	9 (8 boys, 1 girl)
<b>District</b>	Andorinhas	Maruípe	Itararé
<b>Sampling period</b>	November 2-17, 2019	December 4-19, 2019	February 12-19, 2020
<b>Filters change every</b>	5 days	5 days	7 days
<b>Mean weight [kg ± (SD)]</b>	42.0±10.4	43.0±16.4	42.8±16.8
<b>Passive samplers NO<sub>2</sub> [µg/m<sup>3</sup>]</b>			
<b>Mean</b>	13.0	10.8	13.7
<b>SD</b>	4.7	6.1	2.3
<b>Min</b>	6.7	4.6	10.2
<b>Median</b>	12.2	9.8	12.9
<b>Máx</b>	22.5	30.5	18.8

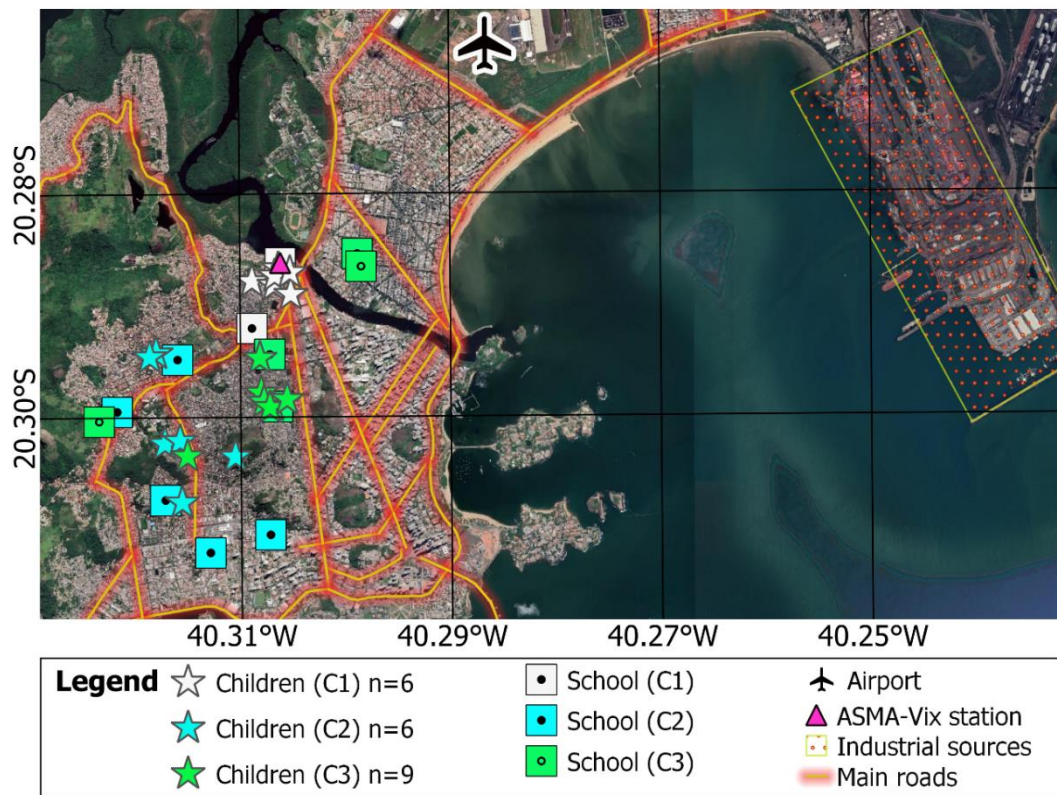


Figure 10. Location of the selected children of the ASMA-Vix project and the location of their schools, main roads, and industries in the city of Vitória.

## 4.2 THE CLIMATOLOGICAL AND METEOROLOGICAL DESCRIPTION OF THE STUDY AREA

As mentioned, the MRV region is located in a coastal area, making the region continuously affected by sea breezes that usually penetrate the inland regions (Salvador *et al.*, 2016). The well-defined atmospheric circulation over the MRV is also influenced by the South Atlantic Subtropical High (SASH) over the Atlantic Ocean, because of which the winds predominantly flow from the north and northeast during part of the dry season (August and September) and during the wet season (October to March). The climatological dry season corresponds to the months between April and September, whereas the wet season is usually between October and March. From April to July, because of the autumn and winter seasons, the availability of solar radiation decreases over the Southern Hemisphere; also, the displacement of SASH closer to the continent, favours the south-southwest winds in the MRV (Cavalcanti *et al.*, 2009, Salvador *et al.*, 2016). Moreover, the observed wind speed is higher when the wind is flowing from the north and northeast, with an annual average of 4.2 m/s according to the climatological normal of the Brazilian Institute of Meteorology (INMET CN 1981–2010, corresponding to the INMET station in Figure 9). The location of all meteorological and air quality monitoring stations used in this study is displayed in Figure 9. The geographic coordinates and the amount of paired data points used to compare observed and simulated data are presented in Table 5. The climatological normals also indicate that the average temperature varies between 23 °C and 28 °C, with a maximum of 32 °C during summer (Dec-Jan-Feb) and a minimum of 20°C during winter (Jun-Jul-Aug). The relative humidity remains almost constant over the year, varying between 70-80%, and the rainfall season occurs during the spring and summer times due to the effect of the South Atlantic Convergence Zone (SACZ) that brings humidity from the Amazon region. The lowest rainfall values are recorded during winter (June-July-August (INMET CN 1981–2010), and according to Köppen-Geiger’s climate classification, the RMV is classified as coastal tropical climate (Af).

Table 6. The location of the meteorological and air quality station in the MRV. The amount of paired data points used to compare observed and simulated data is also presented. M1 and M2 are exclusively meteorological stations.

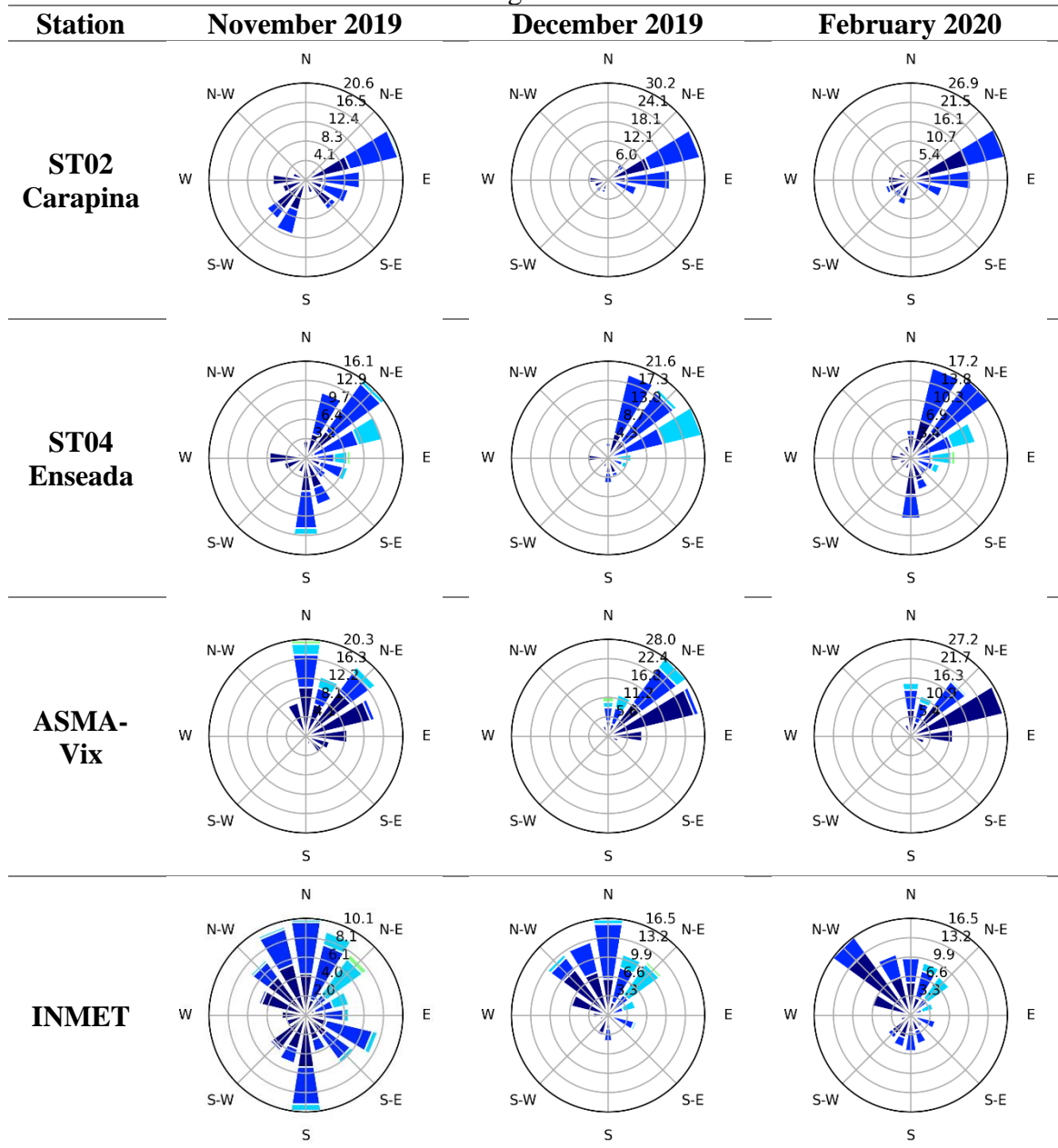
ST	Station name	City	Latitude (°)	Longitude (°)	Altitude (m)	T2 (°C)	RH (%)	WS10 (m/s)	WD10 (°)	PREC (mm)	PM <sub>10</sub>	PM <sub>2.5</sub>	NO <sub>2</sub>	SO <sub>2</sub>	O <sub>3</sub>	CO
01	Laranjeiras	Serra	-20.196	-40.245	27.0	-	-	-	-	-	-	-	2160 (100%)	1638 (75.8%)	1375 (63.7%)	2160 (100%)
02	Carapina		-20.232	-40.255	23.0	2154 (99.7%)	2154 (99.7%)	2154 (99.7%)	2153 (99.7%)	2148 (99.4%)	2154 (99.7%)	-	-	-	-	-
03	Jardim Camburi (JC)	Vitória	-20.255	-40.270	5.0	-	-	-	-	-	1943 (90%)	-	1119 (51.8%)	1400 (64.8%)	-	-
04	Enseada		-20.313	-40.291	3.0	-	-	2160 (100%)	2160 (100%)	-	1754 (81.2%)	2100 (97.2%)	2093 (96.9%)	2011 (93.1%)	1473 (68.2%)	2160 (100%)
05	Centro-Vix		-20.321	-40.333	2.0	-	-	-	-	-	2160 (100%)	-	1927 (89.2%)	1177 (54.5%)	-	2160 (100%)
	ASMA-Vix		-20.288	-40.308	11.0	2103 (97.4%)	2103 (97.4%)	2103 (97.4%)	2099 (97.2%)	-	2027 (93.8%)	1981 (91.7%)	2101 (97.3%)	2100 (97.2%)	2096 (97%)	-
M1	INMET-Vix		-20.271	-40.306	1.0	2119 (98.1%)	2119 (98.1%)	2119 (98.1%)	2085 (96.5%)	2087 (96.6%)	-	-	-	-	-	-
M2	Airport		-20.251	-40.285	3.0	2135 (98.8%)	-	2131 (98.7%)	2096 (97%)	-	-	-	-	-	-	-
06	IBES	Vila Velha	-20.349	-40.317	5.0	-	-	2095 (97%)	2094 (96.9%)	-	2151 (99.6%)	-	2093 (96.9%)	1939 (89.8%)	1439 (66.6%)	2160 (100%)
07	Centro-VV		-20.337	-40.290	6.0	-	-	-	-	-	2128 (98.5%)	-	-	-	-	-
08	Cariacica	Cariacica	-20.342	-40.402	18.0	2160 (100%)	2112 (97.8%)	2160 (100%)	2159 (100%)	1078 (49.9%)	-	-	2097 (97.1%)	2087 (96.6%)	1399 (64.8%)	2160 (100%)

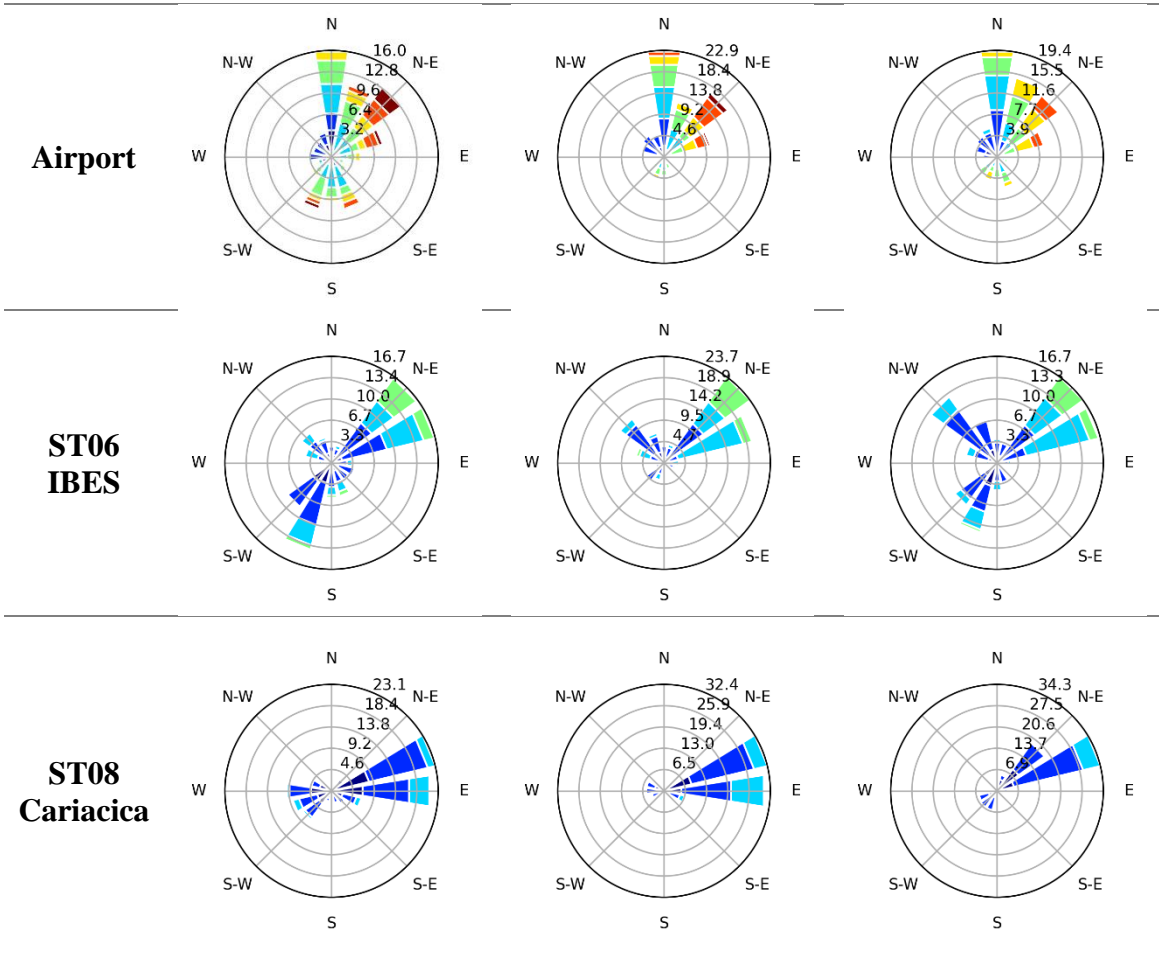
\*The geographical coordinates were extracted from the Google Earth program.



The present study was performed in November and December 2019 and February 2020, and according to the observations across the meteorological stations located in the MRV, the wind direction predominantly flowed from the north, northeast, and east sectors over these three months, agreeing with the climatological data, except for the INMET station where winds from the south and northwest were also registered in November and February (Table 7).

Table 7. Observed wind roses at meteorological stations in the MRV.





The hourly wind speed at 10 meters (WS10) observed at the surface meteorological stations over the period under analysis in the MRV is shown in Figure 11 as well as the boxplots in Figure 12. The Airport station recorded the highest values of WS10 (maximum of 10.81 m/s), with a mean (median) of  $3.97$  ( $3.60$ )  $\pm$   $2.22$  m/s. The second-highest wind speed values were registered at the ST06 (IBES station) with a mean (median) of  $2.57$  ( $2.41$ )  $\pm$   $1.24$  m/s. The other stations in the MRV registered an average wind speed lower than 2 m/s, which varied between  $1.16$  ( $0.75$ )  $\pm$   $1.07$  m/s at the ASMA-Vix station and  $1.86$  ( $1.78$ )  $\pm$   $0.88$  m/s at ST08 (Cariacica station). These differences seen in observed WS10 data were due to the fact that the Airport is the only station located at an open site and it is not highly influenced by the presence of buildings and vegetation; or any other obstacle, that can slow down the wind speed.

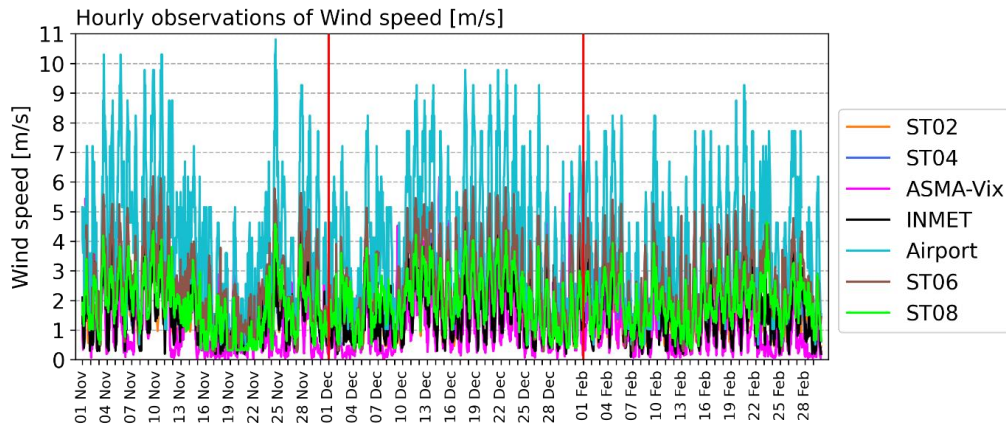


Figure 11. Hourly time series of observed WS10 in November/December 2019 and February 2020 at the surface meteorological stations in the MRV.

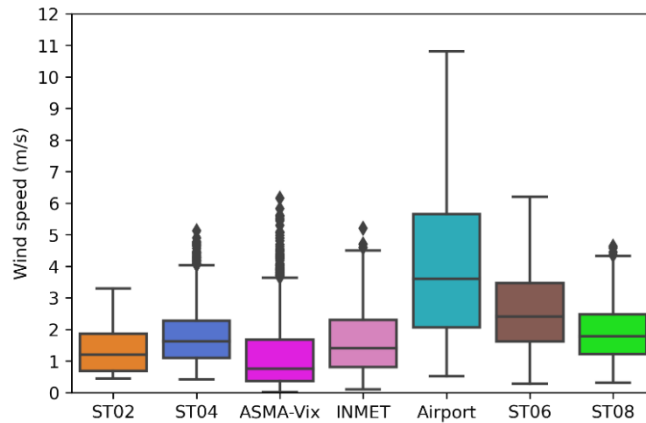


Figure 12. Boxplots of observed WS10 in November/December 2019 and February 2020 at the surface meteorological stations in the MRV. The diamonds represent the outliers, the bars represent the minimum and maximum values, and the lines represent the mean values.

In contrast to WS10, the observed temperature (Figure 13), relative humidity (Figure 14), and precipitation (Figure 15) had much more similar behaviour among the surface monitoring stations in the MRV. Over the study time period, the lowest and highest temperatures occurred both in November 2019, with minima between 14.77 °C (at ST02 – Carapina station) and 19.44 °C (at ASMA-Vix station) and maxima between 34.41 °C (at ST02 – Carapina station) and 40.56 °C (at ST07 – Cariacica station). Considering the INMET station, where the climatological normals (CN 1981–2010) are registered, the mean (minimum-maximum) temperature in November 2019 was 24.77 (16.9–37.2) °C, 25.90 (20.2–34.9) °C in December 2019, and 26.73 (22.0–35.4) °C in February 2020. The observations in 2019/2020 indicated that the monthly extreme temperatures were higher (lower) compared with the CN 1981–2010, in

which the CN 1981–2010 maxima were 28.5 °C, 30.0 °C, and 31.7 °C and the CN 1981–2010 minima were 24.1 °C, 22.1 °C, and 23.10 °C in November, December and February, respectively. Similarly to temperature, relative humidity was similar among the monitoring stations, with the mean (median) varying between 74.04 (77.56) ± 14.27 % at ST08 (Cariacica station) and 80.84 (83.81) ± 13.11 % at ST02 (Carapina station). The mean monthly observed relative humidity at the INMET station (78.9%, 76.8%, and 77.5%) were almost identical to the CN 1981–2010 (79.2%, 78.4%, and 75.8%).

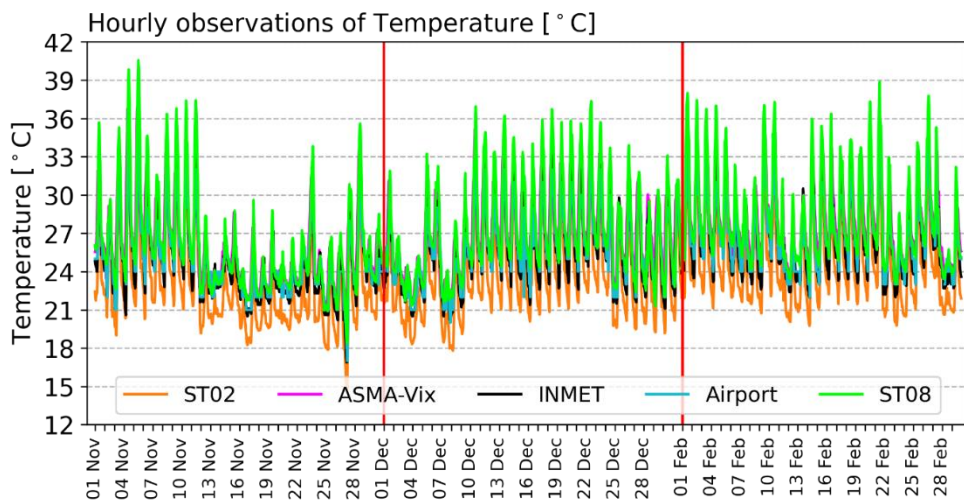


Figure 13. Hourly temperature comparing the observations among the stations in the MRV.

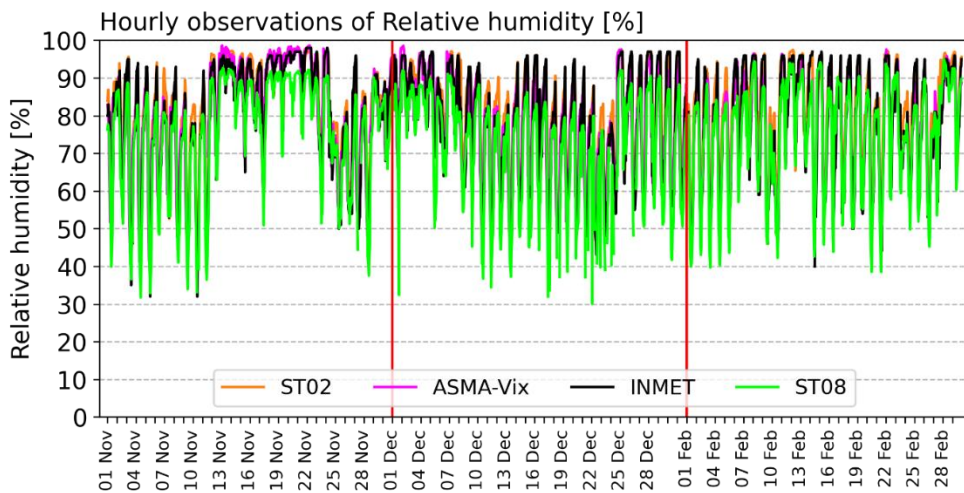


Figure 14. Hourly relative humidity comparing the observations among the stations in the MRV.

With respect to the rainfall, November 2019 was the second wettest November in Vitória since 1992, in which about 200 mm of rain was registered in one single day (November 13, 2019) (Figure 15). According to the synoptic weather charts of CPTEC/INPE, humidity in the lower atmosphere was transported from the ocean to the coastline of Espírito Santo (represented by the yellow line in Figure 16) together with a frontal system (represented by the blue-red lines also in Fig. 16) were responsible for the heavy rainfall in the MRV on this day. The total monthly rainfall recorded at the INMET station in November 2019 was 552.2 mm, which was more than double when compared to the CN 1981–2010/1991–2020 (219.9/233.6 mm). In December 2019 (181.2 mm), the monthly accumulated observations were lower than the CN 1981–2010/1991–2020 (199.7/201 mm), but in February 2020 (128 mm) they were higher than the CN 1981–2010/1991–2020 (79.4/79.4 mm), despite the differences were not excessive as in November 2019.

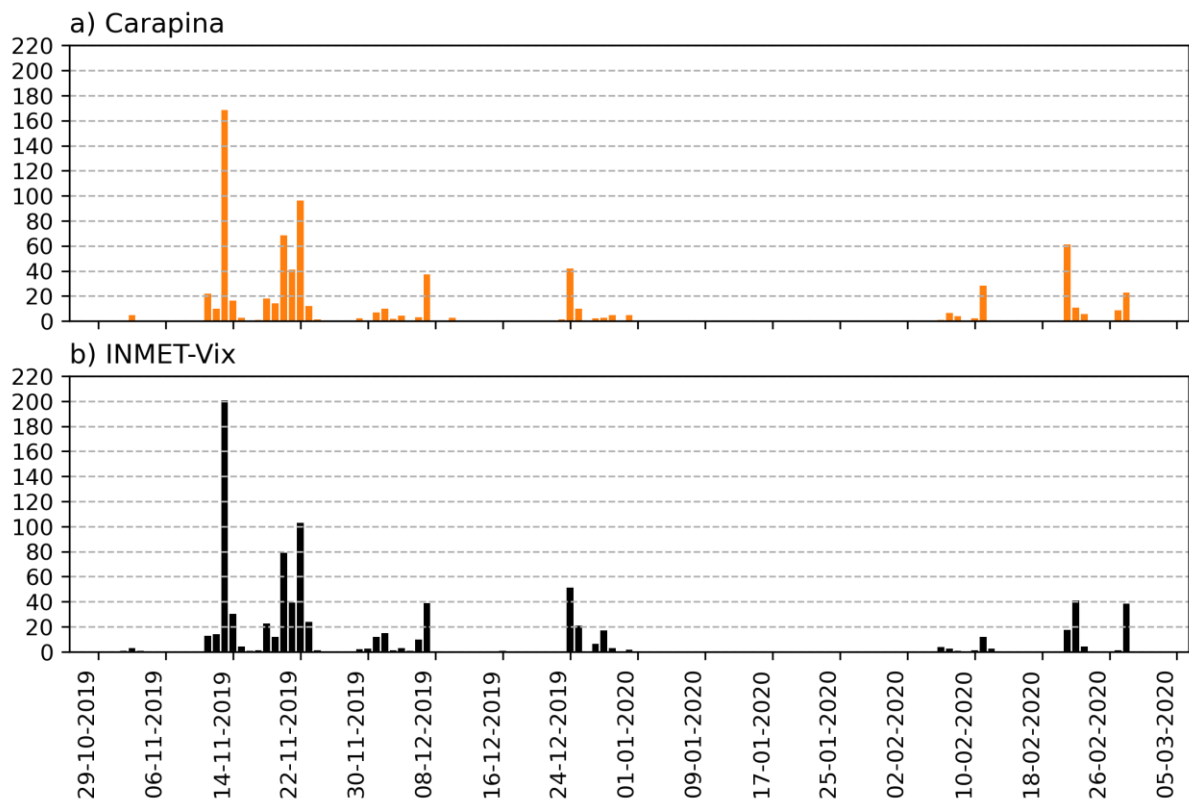


Figure 15. Observed accumulated daily precipitation at ST02 (Carapina) and INMET stations.



Figure 16. The synoptic weather charts of CPTEC/INPE on November 13, 2019.



### 4.3 MODELLING APPROACH

The numerical modelling approach consists of a combination of various models and tools, which mainly includes the Weather Research and Forecasting (WRF-Urban) model (Skamarock *et al.*, 2008, 2021; Powers *et al.*, 2017), the GEOS-Chem global chemical transport model (Bey *et al.*, 2001), and the Community Multiscale Air Quality (CMAQ) model (Byun and Schere, 2006; Appel *et al.*, 2020), among others (Figure 17). The air pollutant concentrations at the home and school postcodes of the selected children and adolescents of the ASMA-Vix study are provided by the CMAQ model version 5.3.2. The choice of this advanced chemistry-transport model is made because it has been successfully used in previous studies in the study area (Pedruzzi *et al.*, 2019). To run the CMAQ model, it is necessary to provide information such as initial conditions (ICON) and boundary conditions (BCON), meteorological fields, and emissions rates of natural and anthropogenic sources. The CMAQ model adopts spatial and temporal configurations that were set up in the simulations using the WRF-Urban model.

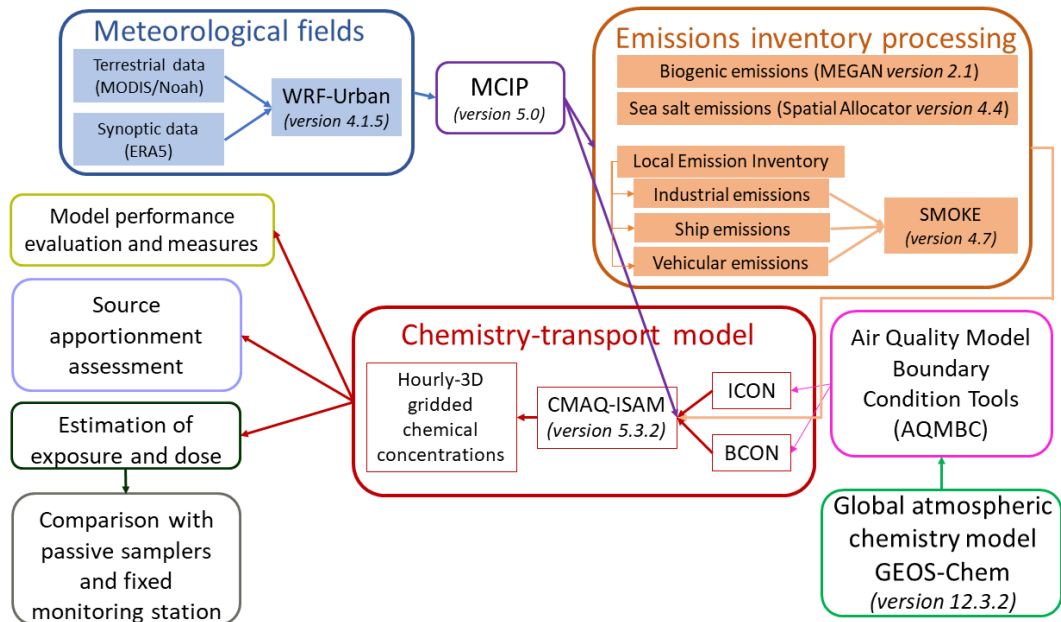


Figure 17. Schematic representation of the various models and methods used in the present work to evaluate the exposure of children that reside in the Metropolitan Region of Vitória (MRV), Brazil.

### 4.3.1 WRF-URBAN MODEL

The WRF-Urban model (Skamarock *et al.*, 2008, 2021), version 4.1.5, was responsible for providing the meteorological conditions in the present study. The initial and boundary conditions for the initialization of the WRF-Urban model came from the ERA5 reanalysis dataset (available at <https://cds.climate.copernicus.eu/cdsapp#!/dataset/reanalysis-era5-pressure-levels>). ERA5 is a global atmospheric reanalysis of the European Centre for Medium-Range Weather Forecasts (ECMWF), with higher spatial and temporal resolutions ( $0.25^\circ \times 0.25^\circ$  at every hour) when compared to its previous generation (ERA-Interim which has a spatial resolution of  $0.75^\circ$  at every 6 hour). The land use and vegetation types categories were derived from the Moderate Resolution Imaging Spectroradiometer (MODIS) sensor aboard the Terra and Aqua satellites. The MODIS data is a default setup of the WRF model, which classifies natural vegetation, urbanized, and water surfaces into 21 land use categories based on the International Geosphere Biosphere Programme (IGBP). The WRF-Urban model was set to run for the entire months in which the monitoring campaigns were performed, that is November and December 2019, and February 2020, instead of the exclusively days that the campaigns occurred. The simulations were split up by month with a spin-up of one day.

Regarding the physics options, several WRF parameterisation tests were performed for the same study area in a previous study (Salvador *et al.*, 2016), in which the planetary boundary layer (PBL) YSU and the land surface model (LSM) Noah schemes showed the most satisfactory performance in determining PBL height in sea breeze conditions and captured the energy balance information from the soil. However, since some parameterisation schemes were updated or added as new options, Kitagawa *et al.* (2022b) performed new tests in order to assess the urban canopy model (UCM) schemes available in the WRF model as well as the lowest model level height. The authors obtained a significant improvement using the building effect parameterisation (BEP) formulation to emulate meteorological variables over urban surfaces, especially for wind speed. Regarding the model's height, the wind speed was found to be sensitive to the lowering of the model height, in which the vertical resolution with model level height at 10 m was associated with the best result for wind speed over urban surfaces. For temperature, relative humidity, and wind direction, no significant differences could be seen by changing the height of the first layer of the model.



The presence of urban structures modifies the surface albedo and roughness length, and consequently, the generation of turbulent eddies that drives vertical mixing. The classical approach in the WRF model accounts for the processes of urban surfaces through the bulk urban parameterisation method in land surface models, and it represents the urban areas as flat surfaces, and therefore, it does not depict the city's heterogeneity (i.e. buildings and roads are treated as the same). The next level of complexity was incorporated into the WRF model to provide a better representation of the physical processes involved in the interaction of the urban environment with the atmosphere using the single-layer urban canopy model (SLUCM), developed by Kusaka *et al.* (2001) and Kusaka and Kimura (2004). The SLUCM represents the effect of the building structures as a model cell value-averaged within a single layer; thus, parameter information within the urban canopy is not available, and the height of the first layer of the model must be higher than the height of the buildings (for which the default value is 7.5 m). SLUCM assumes a two-dimensional geometry of the urban canopy layer, with radiation treated as three-dimensional because it accounts for the solar azimuth angle. Then, to recognise the three-dimensional nature of urban surfaces, the second level of complexity is introduced in the WRF model using the multilayer urban canopy model, also known as building effect parameterisation (BEP), developed by Martilli *et al.* (2002). This new formulation attempts to consider the presence of vertical structures and their effects on heat, moisture, and momentum fluxes. To maximise the advantage of BEP, a high vertical resolution is suggested, which is close to the ground with several layers within the urban canopy. The dissipation term, introduced in momentum and turbulent kinetic energy equations, is computed only based on two PBL options of WRF: the MYJ (Mellor and Yamada, 1982; Janjić, 1994) or BouLac (Bougeault and Lacarrere, 1989) parameterisation schemes, and two land surface models: Noah LSM and Noah-MP (Niu *et al.*, 2011). Experiments using BEP indicate an improvement in the representation of nocturnal urban heat islands that are influenced by the sensible heat fluxes from the vertical structures, in the inversion layer above the urban region, and in the representation of wind fields and temperature surface variables (Kusaka *et al.*, 2001; Martilli *et al.*, 2002; Liu *et al.*, 2006; Lin *et al.*, 2008; Martilli *et al.*, 2009; Chen *et al.*, 2011; La Paz *et al.*, 2016; Sarmiento *et al.*, 2017).

In this sense, in this study, the BEP scheme was chosen to represent the effects of urban structures. However, as pointed out by Salamanca *et al.* (2011), together with a complex urban canopy scheme, it is also necessary to use representative urban morphological parameter values. But, it is sometimes difficult to choose representative UCPs values for a city because of the

need for experimental campaigns. Thus, the simulations of the present study followed the default values of BEP's algorithm, which comprise more than 20 parameters. For instance, urban fraction of 0.90, heat capacity of roof and building wall of  $10^{-6}$ , thermal conductivity of roof and building wall of 0.67, surface albedo of roof, building wall and road of 0.20, surface emissivity of roof and building wall of 0.90, building height of 15 m, building width of 17 m, and street widths of 25 m. Note that the building height in BEP is not fixed, instead, it is classified with different percentages, which the mean building height was 15 m.

A literature review was also performed to assess at which height the WRF model should be set up for air quality assessment. However, many studies have not addressed this height but have only focussed on the number of vertical layers required for simulations (Hu *et al.*, 2016, 2017; Lu *et al.*, 2016; Wang *et al.*, 2017; Mathur *et al.*, 2017; Jiang and Yoo, 2018; Liu *et al.*, 2018, 2020; Nguyen *et al.*, 2019; Feng *et al.*, 2019; Yoo *et al.*, 2019; Lai *et al.*, 2019; Andreão *et al.*, 2020; Souri *et al.*, 2020; Tao *et al.*, 2020; Lin *et al.*, 2020). Shin *et al.* (2012) reported that surface parameters and PBL structures have a high sensitivity when the height is below 12 m in the daytime and below 40 m in the nighttime. However, several studies have adopted different heights, which usually vary among the locations: for instance, 19, 25, and 54 m in China (Liao *et al.*, 2014; Tan *et al.*, 2017; Yang *et al.*, 2019); 39 m in Europe (Schaap *et al.*, 2015); 19 m in France (Lian *et al.*, 2018); 25 m in Italy (Pepe *et al.*, 2016); 36 m in the Iberian Peninsula (Jiménez *et al.*, 2006); 7 and 11 m in Spain (Salamanca *et al.*, 2012; La Paz *et al.*, 2016); 21, 30, and 38 m in the US (Punger and West, 2013; Chen *et al.*, 2014; Sharma *et al.*, 2017); 43 m in South Korea (Han *et al.*, 2019); 50 m in India (Rooney *et al.*, 2019) and 15 m in East Asia (Choi *et al.*, 2019). Because no consensus was found during the literature review about at which height the WRF model should be set up, the heights were chosen based on the formulations of BEP, which assumes several layers within the urban canopy with a high vertical resolution close to the ground. Thus, three different configurations were assessed regarding model height ( $z$ ), which were set up at  $z = 4, 10, \text{ and } 20$  meters. However, the air pollutant concentrations are a scalar variable, which means that the concentrations are calculated in the center of each grid cell, that is at  $z = 2, 5, \text{ and } 10$  meters. As the vertical layer structure configuration in the CMAQ model matches the WRF model, the results were labelled as the WRF configuration.

The other physical parameterisation schemes adopted were Rapid Radiative Transfer Model (RRTMG) for shortwave and longwave radiation, Thompson scheme as microphysics option, Noah-MP as the land surface model, Grell-Freitas as cumulus scheme, Bougeault-Lacarrere

scheme as planetary boundary layer scheme, and Eta similarity as the surface layer. An overview of the spatial configurations and physical parameterization schemes used to run the WRF-Urban model is presented in Table 8. In addition, the model was run with three nested domains with grid resolutions of 9 km, 3 km, and 1 km; being the domain of interest with 162 km<sup>2</sup> (Figure 9). The vertical resolution had 44 layers with the model top set at 50 hPa. Note that the number of the vertical levels did not increase, they remained constant and all configurations were set up with 44 layers from the bottom to the model top. However, with the lowering of the first-level height, the number of layers increased close to the ground and practically remained constant near the top (Figure 18). Within the first 500 m of the atmosphere, if the model is set up to a height equal to 20 m, 10 m, and 4 m, there will be 8, 10, and 14 vertical layers, respectively.

Table 8. The spatial configuration adopted and physical parameterization schemes in the WRF-Urban simulations.

	<b>November, December, and February</b>
<b>Horizontal resolution</b>	9 km, 3 km, and 1 km (domain of interest)
<b>Domains dimensions</b>	73, 121, and 163 cells
<b>Vertical resolution</b>	44 layers
<b>Model height (z)</b>	z = 20 m
	z = 10 m
	z = 4 m
<b>Longwave radiation</b>	RRTMG (option 4)
<b>Shortwave radiation</b>	RRTMG (option 4)
<b>Land surface scheme</b>	Noah-MP (option 4)
<b>Cumulus scheme</b>	Grell-Freitas (option 3)
<b>Microphysics scheme</b>	New Thompson (option 8)
<b>Surface layer scheme</b>	Eta-similarity (option 2)
<b>PBL scheme</b>	BouLac (option 8)
<b>UCM scheme</b>	BEP (option 2)
<b>Meteorological data</b>	ERA5 with 0.25° grid resolution at every hour
<b>Land use data</b>	MODIS_NOAH

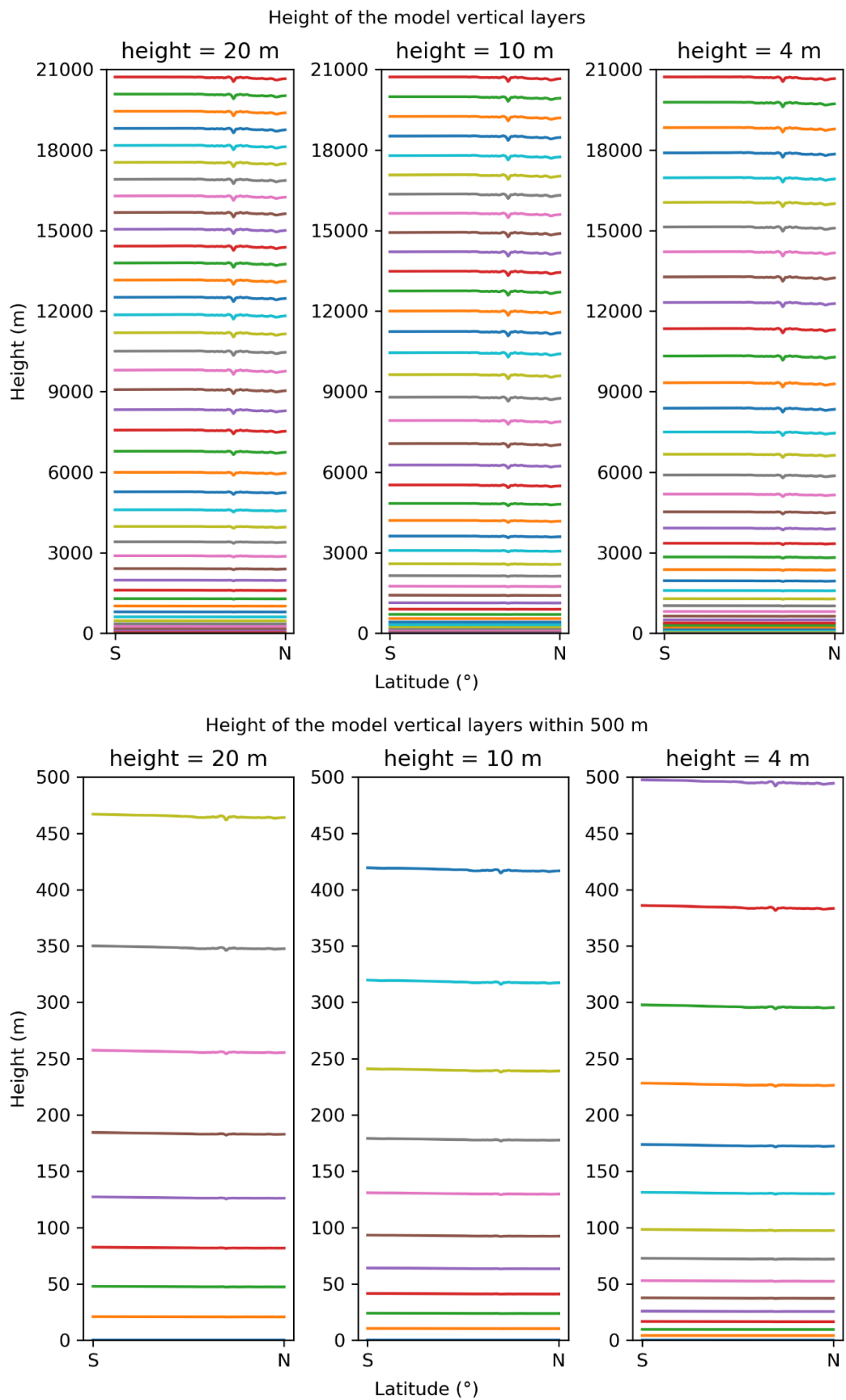


Figure 18. Geopotential height across the D03 domain from the south (S) to north (N) from the bottom to the model top and within the first 500 m.

Finally, the Meteorology-Chemistry Interface Processor (MCIP), version 5.0 (Otte and Pleim, 2010) ingests output from the WRF-Urban model to prepare the meteorology files that are required by the CMAQ model, by the Sparse Matrix Operator Kernel Emission (SMOKE; available at <https://zenodo.org/record/4088945>), by the Model of Emissions of Gases and Aerosols from Nature (MEGAN) (Guenther *et al.*, 2012), and by the Spatial Allocator Vector Tools (available at <https://github.com/CMASCenter/Spatial-Allocator>).

#### **4.3.2 BIOGENIC EMISSIONS**

The biogenic emissions of the present study were estimated by the MEGAN model version 2.1. The MEGAN is an offline model that estimates the flux of biogenic volatile organic compounds (BVOCs) between earth and atmosphere by using meteorological data from CMAQ and provides emissions in a format suitable for input to the CMAQ and CAMx models (Guenther *et al.*, 2012). The MEGAN driving variables, which include meteorology (e.g., temperature, solar radiation, humidity, wind speed, and soil moisture) and land cover data (e.g. leaf area index and plant functional types), were provided by the Meteorology-Chemistry Interface Processor (MCIP) by using the outputs of the WRF model. The final result of MEGAN processing was hourly biogenic emissions ready for the CMAQ model.

The plant functional type (PFT) distribution data were based on MODIS. Figure 19 presents the land use and cover (LULC) input data of MODIS used by the WRF model in the D03 domain. The urban occupation class (category number 13, in red) is mostly concentrated over the MRV and represents only 2.5% of the total amount of land grid cells in D03, that is, not considering the water surfaces that accounted for 50.1% of the D03. MODIS considered most areas as savannas (33.1%, category number 9, in light green), evergreen broadleaf forest (25.3%, category number 2, in dark green), and woody savannas (12.2%, category number 8, in light pink), followed by grasslands (category number 10, in orange, 8.8%) and natural vegetation mosaic (8.2%, category number 14, in purple). The percentages for each land cover class are presented in Table 9.

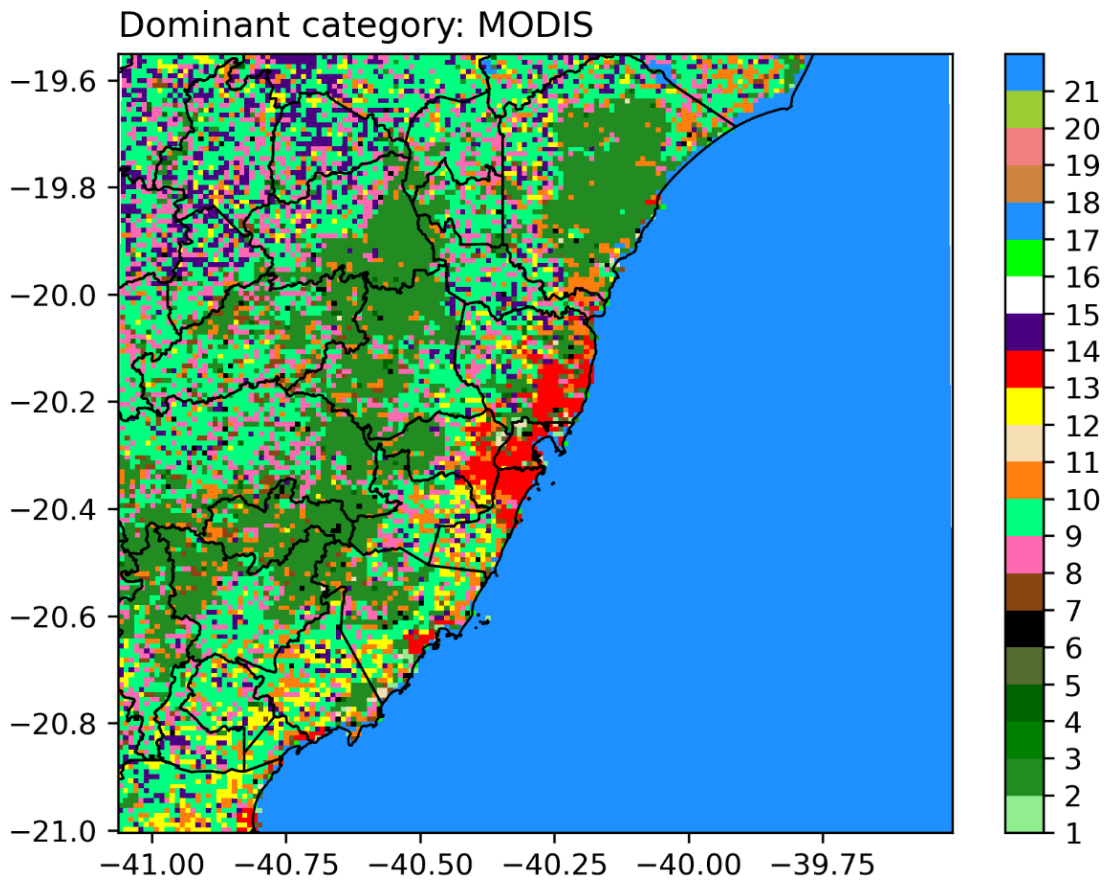


Figure 19. Land use classes of MODIS used as input data for the WRF model and MCIP processor. 2: Evergreen broadleaf forest (dark green), 8: Woody savannas (light pink), 9: Savannas (light green), 10: Grasslands (orange), 12: Croplands (yellow), 13: Urban and Built-up (red), 14: Natural Vegetation Mosaic (purple).

Table 9. Land use classification of MODIS and the occupation (%) of each class in the D03.

Category number	Class MODIS-IBGP	Occupation (%)	
		With water surfaces	Without water surfaces
<b>1</b>	Evergreen Needleleaf Forest	0.1%	0.3%
<b>2</b>	Evergreen Broadleaf Forest	12.6%	25.3%
<b>3</b>	Deciduous Needleleaf Forest	-	-
<b>4</b>	Deciduous Broadleaf Forest	0.4%	0.8%
<b>5</b>	Mixed Forests	0.2%	0.5%
<b>6</b>	Closed Shrublands	0.4%	0.8%
<b>7</b>	Open Shrublands	1.1%	2.2%
<b>8</b>	Woody Savannas	6.1%	12.2%
<b>9</b>	Savannas	16.5%	33.1%
<b>10</b>	Grasslands	4.4%	8.8%
<b>11</b>	Permanent Wetlands	0.1%	0.3%

<b>12</b>	Croplands	2.5%	5.0%
<b>13</b>	Urban and Built-Up	1.2%	2.5%
<b>14</b>	Natural Vegetation Mosaic	4.1%	8.2%
<b>15</b>	Snow and Ice	-	-
<b>16</b>	Barren or Sparsely Vegetated	0.1%	0.2%
<b>17/21</b>	Water surfaces	50.1%	-
<b>18</b>	Wooded Tundra	-	-
<b>19</b>	Mixed Tundra	-	-
<b>20</b>	Barren Tundra	-	-

However, the WRF and MEGAN models use different PFTs classes because WRF is based on MODIS-IGBP (20 categories) while MEGAN uses Community Land Model 4 (CLM4) data, which is composed of 15 categories of plants (Guenther *et al.*, 2012), meaning that the land use input for MEGAN must be coherent with CLM4 vegetation classes and some modification has to be performed. Thus, Gomes (2020) developed an algorithm that crosses both classifications based on climatic and seasonal criteria available in the literature. The dominant PFT classes in the D03 domain considering CLM4 data were PFT 4 (Broadleaf Evergreen Tropical Tree), PFT 9 (Broadleaf Evergreen Temperate Shrub), PFT 13 (Cool C3 Grass), PFT 14 (Warm C4 Grass), and PFT 15 (Crop).

For the leaf area index (LAI) parameter, MEGAN does not assume that LAI is uniformly spread over a grid cell, instead, it assumes that foliage covers only that part of the grid cell containing vegetation. The average LAI for vegetated areas is estimated by dividing the grid average LAI by the fraction of the grid that is covered by vegetation, which is referred to as LAI<sub>v</sub> (the LAI of vegetation covered surfaces) (Guenther *et al.*, 2006). The MCIP does not directly provide the LAI<sub>v</sub> data required by MEGAN. Thus, the calculation of this parameter was done by using the MCIP variables: LAI and VEG, which the latter represents the vegetation coverage that varies from 0 to 1, with 1 indicating that the coverage is 100% vegetal. Figure 20 shows the spatial distribution of the monthly mean LAI during November and December 2019 and February 2020 (the study period) over the D03 domain. The maximum LAI values (in yellow) were attributed to the grid cells in which MODIS LULC has been considered as an evergreen broadleaf forest (category 2).

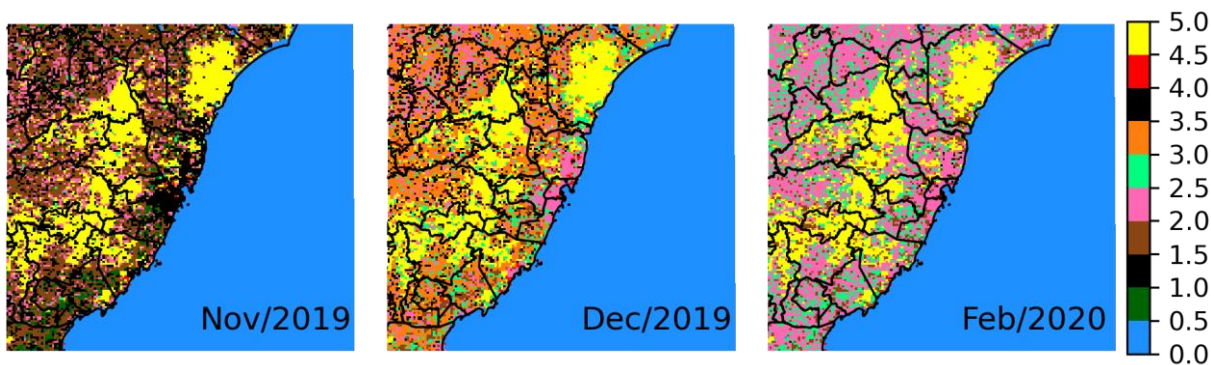


Figure 20. Spatial distribution of the monthly mean leaf area index (LAI) during November and December 2019 and February 2020 over the D03 domain.

MEGAN estimates emissions ( $F_i$ ) of BVOCs chemical species  $i$  (isoprene, methanol, acetone, terpenes, toluene, among others that include 19 compounds) from terrestrial landscapes as the product of emission factors ( $\varepsilon$ , in  $\mu\text{m}^2\cdot\text{h}$ ) available in the literature at standard conditions for vegetation type  $j$  and the coverage fraction of the PFT ( $f_j$ ) of each grid cell (that varies from 1 to 15). The activity factor for each compound class ( $\gamma_i$ ) accounts for emission response to sunlight, temperature, leaf age, soil moisture, LAI, and  $\text{CO}_2$  inhibition (Guenther *et al.*, 2012).

$$F_i = \gamma_i \sum \varepsilon_{i,j} f_j \quad (1)$$

BVOCs emissions estimated by MEGAN indicated that the compounds with the highest emission rate were isoprene and terpenes (Figure 21a,b), which represented an average of 88% and 10% of the total emissions of BVOCs, respectively, for the months under analysis in the present study. The other compounds represented less than 1% of total emissions. Similar results were reported by Gomes (2020) which found that isoprene and terpenes constituted around 74% and 25% of the total emissions of BVOCs in August 2010 in the MRV. In addition, the author reported that the spatial distribution of isoprenes was mostly associated with the distribution of broadleaf forests and shrubs because their PFTs had the highest emission factors for this compound. Meanwhile, the terpenes did not present a specific distribution pattern.



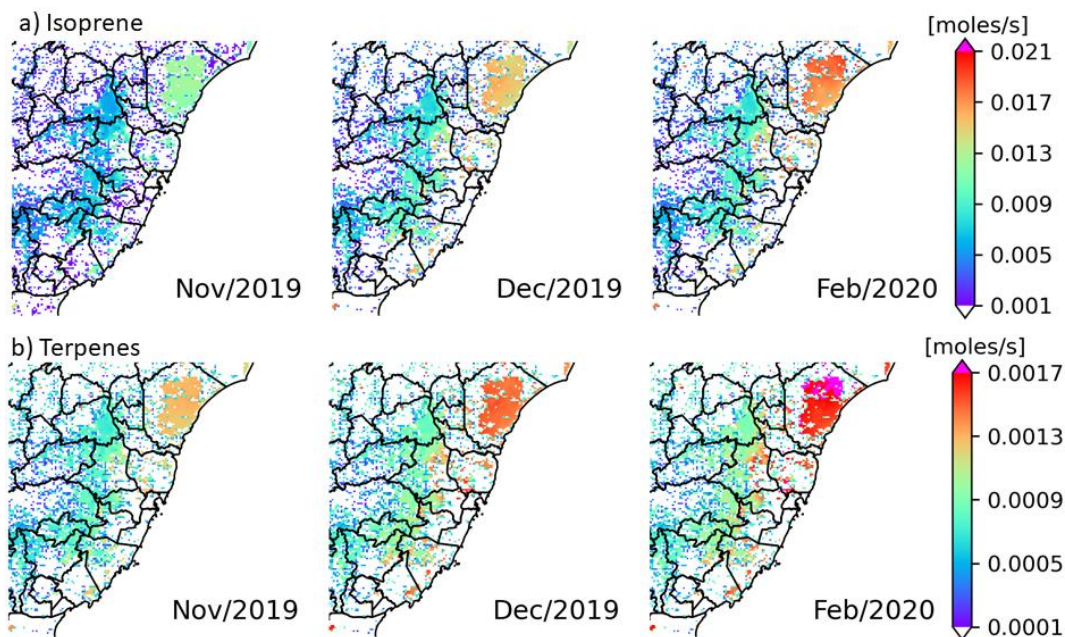


Figure 21. Spatial distribution of the monthly mean of isoprenes and terpenes emissions (moles/s) during November and December 2019 and February 2020 over the D03 domain.

### 4.3.3 SMOKE PROCESSOR

The emissions processed by SMOKE included the data provided by the local environmental agency (the base year of 2015) of the MRV (IEMA, 2019). The official emissions inventory was developed based on emission factors from literature, such as those from American (USEPA) and European (EMEP/EEA) environmental agencies. In addition, the method of the emission inventory followed the Data Attribute Rating System (DARS), which was a method proposed by USEPA (1996). Through this methodology, the emission inventory was developed according to the criteria of the Emission Inventory Improvement Programme (EIIP) for Level II regarding the quality assurance and quality control requirements, which include the following steps: reality check; peer review; sample calculations; sensitivity analysis; and independent audits. Finally, this emission inventory included data for five of the seven municipalities of the MRV (Serra, Cariacica, Viana, Vila Velha, and Vitória). Table 10 summarizes the total annual emissions of PM, PM<sub>10</sub>, PM<sub>2.5</sub>, NO<sub>x</sub>, CO, SO<sub>2</sub>, and VOCs from more than 3,000 sources.

Table 10. The total emission of atmospheric pollutants by source (IEMA, 2019).

Sectors	PM (kg/h)	PM <sub>10</sub> (kg/h)	PM <sub>2.5</sub> (kg/h)	NO <sub>x</sub> (kg/h)	SO <sub>2</sub> (kg/h)	CO (kg/h)	VOC (kg/h)
Landfill	22.6	6.3	1.8	4.8	0.4	4.1	6.5
Civil construction	96.1	31.2	3.4	n.a	n.a	n.a	n.a
Fuel distribution	n.a	n.a	n.a	n.a	n.a	n.a	210.8
Food industry	16.3	11.2	10.3	17.6	2.9	25.6	0.7
Mineral products industry	143.8	84.7	43.8	65.8	24.7	192.7	21.4
Chemical products industry	8.3	6.2	3.8	16.1	3.7	8.9	62.7
Mining-steel industry	887.0	566.9	368.9	4141.1	3971.0	19826.9	323.0
Shipping	72.4	52.9	44.2	364.1	180.8	182.8	30.1
Others of the industrial sector	59.7	46.0	39.4	990.3	315.1	245.5	34.0
Residential and commercial sectors	1.0	1.0	1.0	19.0	0.3	10.5	850.2
Vehicular emissions	55.9	43.1	32.5	1020.8	28.1	1282.8	595.6
Road dust resuspension	6744.7	1294.6	313.2	n.a	n.a	n.a	n.a
Total	8107.8	2144.1	862.3	6639.6	4527.2	21779.8	2135.1

n.a.: not applicable

The aforementioned sectors were treated as point, area, and volume emission sources by SMOKE. The point source sector included industrial stack emissions for all facilities inside the MRV, such as sintering facilities, pelletizing furnaces, coke ovens, blast furnaces, thermoelectric power plants, grain processing, activities chemical and mineral products, among others. The area and volume sources were also represented by industrial sources, but those as piles, material handling, load and unload process, nonroad emissions, landfills, civil construction, wind erosion, and airport, among others. The vehicular emissions were treated as area sources and represent the vehicular hot exhaust, vehicle evaporative emissions, and tires and brake wearing. The shipping sector represents the marine logistics in the region and was treated as a volume source. The spatial allocation was taken from the local emissions inventory (IEMA, 2019).

The local emissions inventory informs the annual emission rates of the sources. Thus, except for the vehicular emissions, all other sectors had their emissions split equally over the months, weeks, and hours. The monthly, weekly, and hourly temporal profiles used in this work are

shown in Figures 22, 23, and 24, respectively. The temporal profiles for vehicular emissions were taken from IEMA (2019).

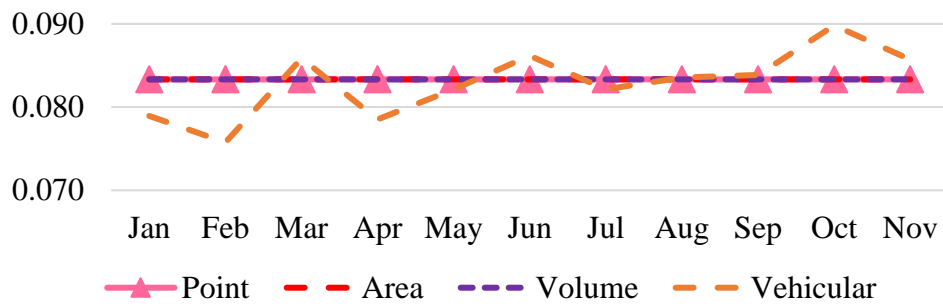


Figure 22. Monthly temporal profile used by the SMOKE.

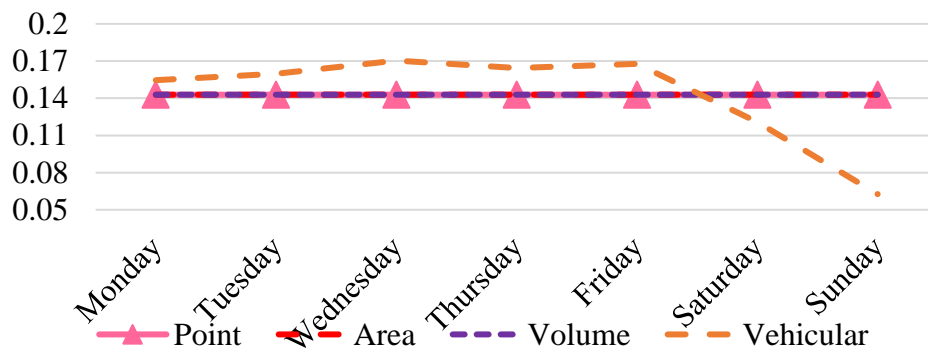


Figure 23. Weekly temporal profile used by the SMOKE.

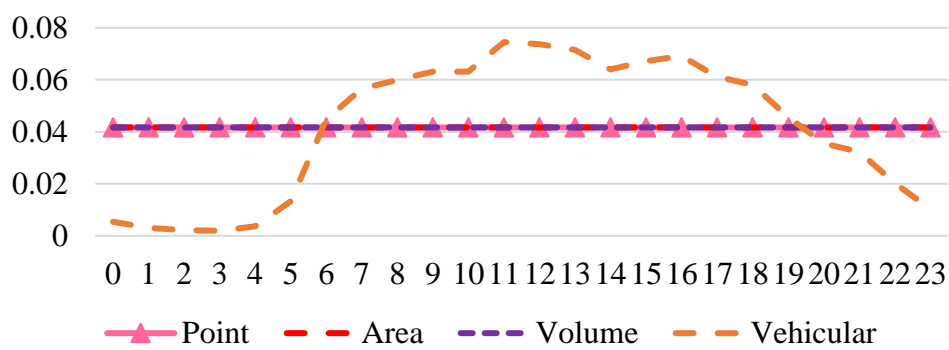


Figure 24. Hourly temporal profile used by the SMOKE.

The emission inventory reports the emission rates for a variety of pollutants, such as CO, NO<sub>x</sub>, VOC, PM<sub>10</sub>, PM<sub>2.5</sub>, and SO<sub>2</sub>. However, the CMAQ model uses chemical mechanisms that require model species to represent atmospheric chemistry. Therefore, emissions processing requires chemical speciation profiles to convert the emissions in terms of pollutant values to the species, especially for NO<sub>x</sub>, VOC, and PM<sub>2.5</sub>. In this study, the chemical profiles were obtained from the literature, specifically, the EPA SPECIATE version 5.0 database (available at <https://www.epa.gov/air-emissions-modeling/speciate>), as there is no observed chemical profile for the emissions sources in the region. The profiles were selected according to the local source characteristics, aiming to capture the most appropriate profiles. Moreover, the chemical speciation was made by considering the chemical mechanism Carbon Bond 06 (CB06) with AERO 07 aerosol module for consistency with the CMAQ model. Figure 25 exhibits, as an example, the chemical profiles adopted by the sources that had the highest annual emissions for PM<sub>2.5</sub> (top 10), which are related to the mining-steel industries and shipping sectors. It exposes that the most significant species for stacks are the unspiciated particulates (PMOTHR), organic carbon (POC), iron (PFE), and sulfate (PSO4). Whereas, for ships emissions, PMOTHR and elemental carbon (PEC) are responsible for most PM<sub>2.5</sub> emissions. In addition, Figure 26 displays their spatial allocation, although it is important to highlight that there are other sources in this area. Five out of six of the primary point source (stacks) emissions are situated in the industrial complex of mining and steel, which represent a thermoelectric power plant, pelletizing furnaces, sintering plant, basic oxygen steelmaking furnace, and coke oven batteries. The shipping sector characterizes the port terminals, but there is also the marine traffic close to the line coast.

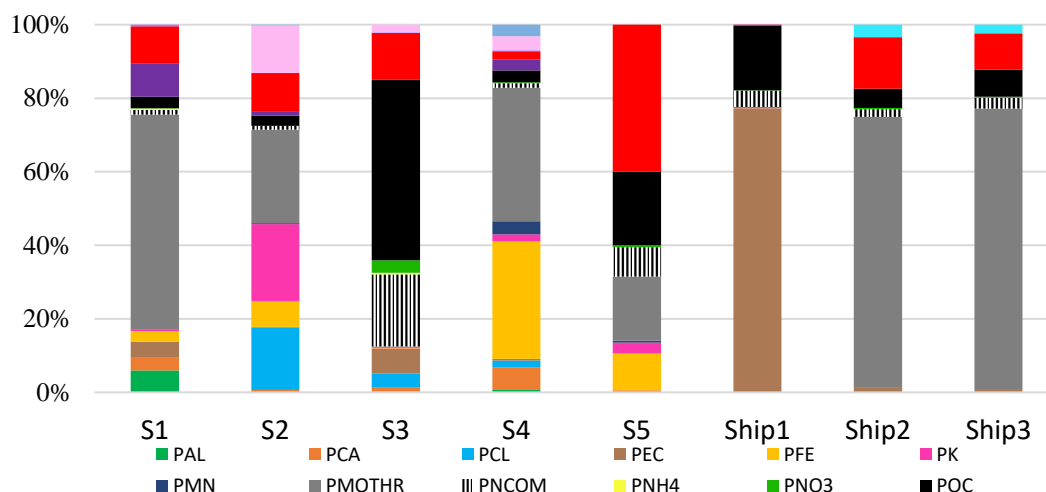


Figure 25. Chemical speciation of the main sources, which *S* represents the stacks labelled as point sources and *Ship* the shipping sector. The names of the species are described as follows, which *P* means particulate: *PAL*: aluminum, *PCA*: calcium, *PCL*: chloride, *PEC*: elemental carbon, *PFE*: iron, *PK*: potassium, *PMN*: manganese, *PMOTHR*: all other unspiciated particulates, *PNCOM*: non-carbon organic matter, *PNH4*: ammonium, *PNO3*: nitrate, *POC*: organic carbon, *PSI*: silica, *PSO4*: sulfate, *PTI*: titanium, *PNA*: sodium, *PMG*: magnesium, *PH2O*: particle-bound water.

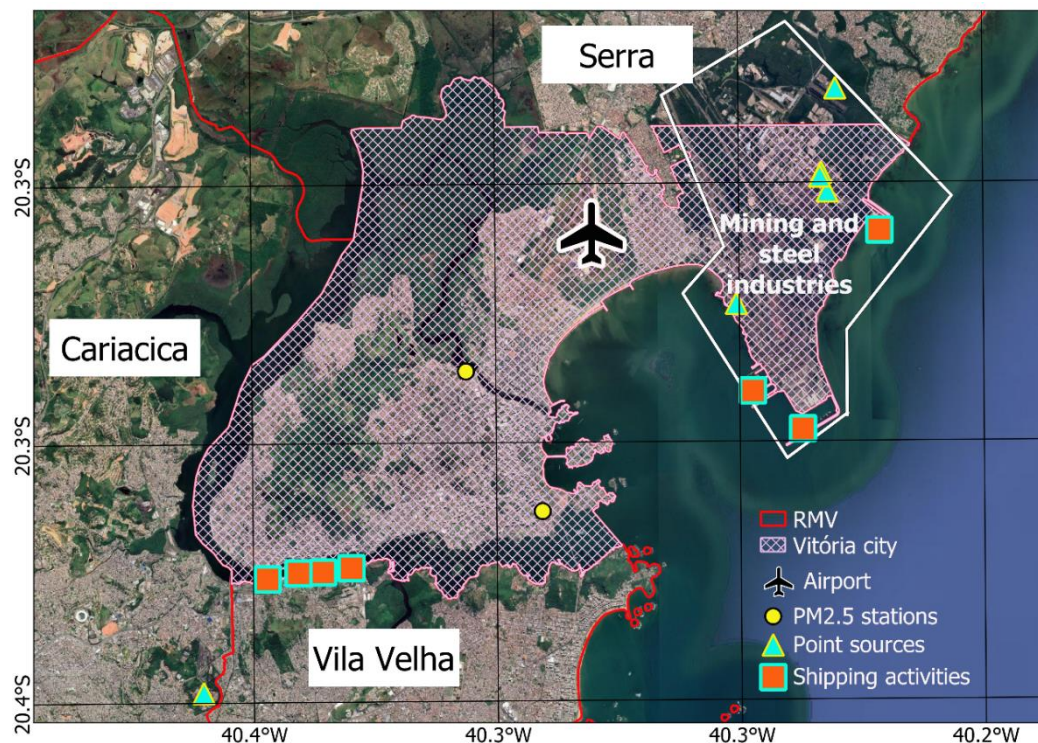


Figure 26. Location of the top ten largest emission sources of  $PM_{2.5}$  according to the local emission inventory (IEMA, 2019), which are represented by the point sources and shipping sector. The yellow dots are the air quality stations.



#### 4.3.4 BOUNDARY AND INITIAL CONDITIONS

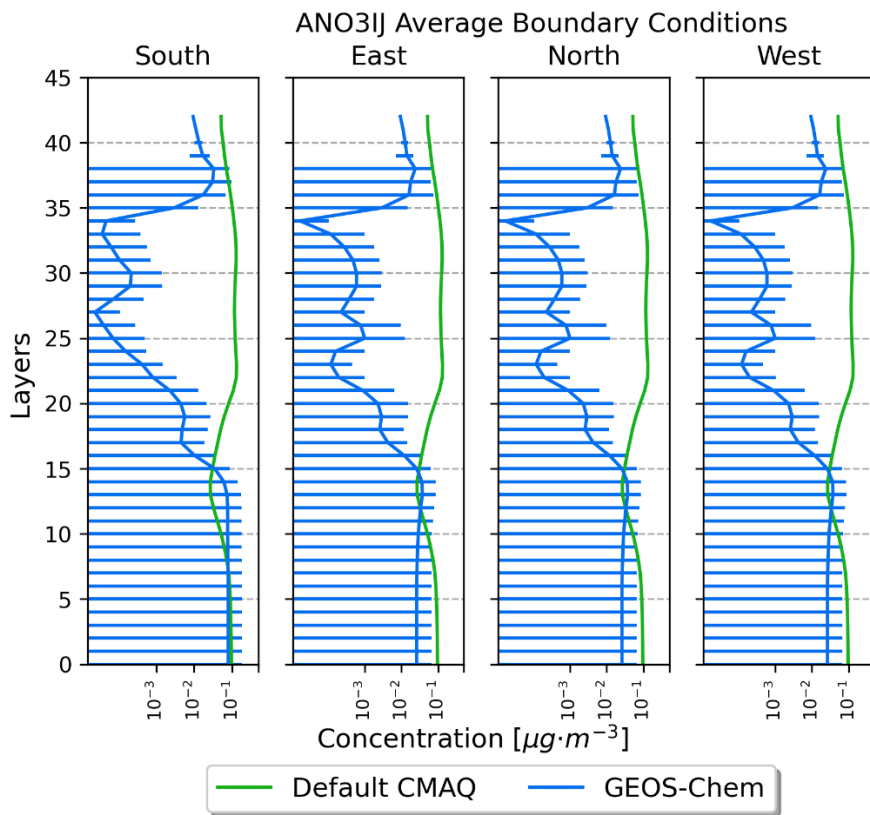
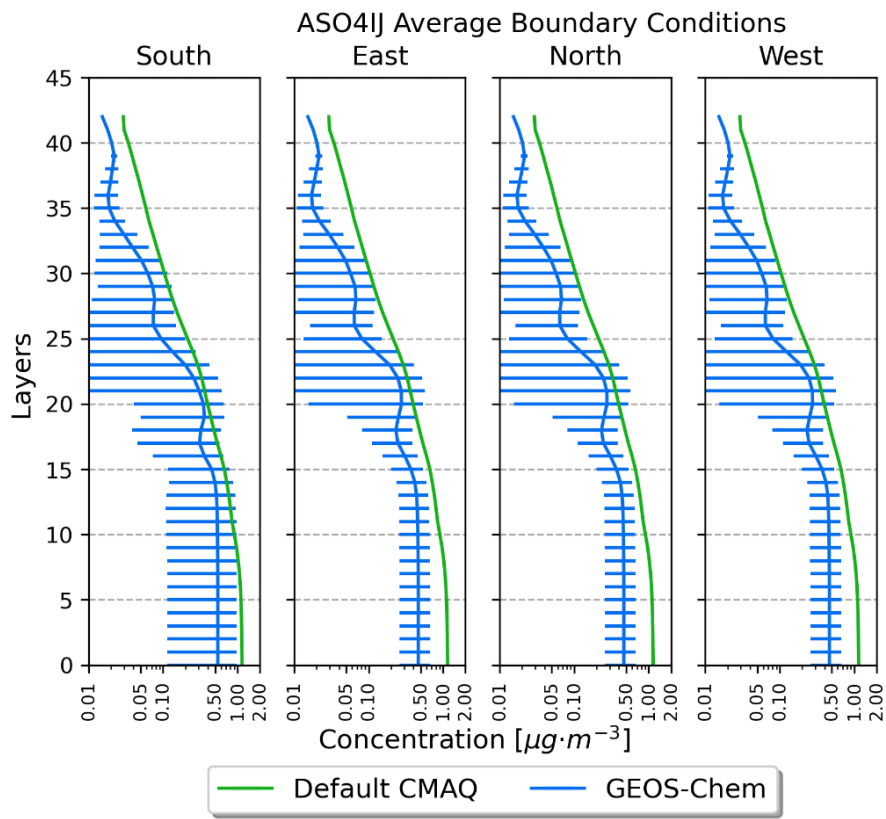
To initialise the CMAQ model, it is also necessary to provide initial conditions (ICON) and boundary conditions (BCON) of the atmospheric pollutants. ICON module generates pollutants concentrations for all grid cells in the modelling domain, that is the background concentration. On the other hand, the BCON module generates pollutants concentrations for all grid cells along the modelling domain's horizontal boundaries, meaning that pollutants are coming through the boundaries every time step. By default, the CMAQ model generates ICON and BCON as spatially uniform and time-independent based on a profile that was developed from an annual average hemispheric modelling run with CMAQ for a marine remote grid cell over the Pacific Ocean (latitude 37N, longitude -157W) for 2016. Thus, to produce a more realistic scenario, in the present study, the GEOS-Chem model version 12.3.2 (Bey *et al.*, 2001) was used to provide ICON and BCON for the CMAQ model. The use of the GEOS-Chem was made based on a previous study over the same study area that evaluated different approaches of the lateral boundary conditions and how they affected air pollutant concentrations (Pedruzzi *et al.*, 2019). The author found out that the dynamic ICON and BCON provided by the GEOS-Chem approach presented the best performance compared to the other methods that are used to provide ICON and BCON.

The GEOS-Chem was set up with meteorological conditions derived from the GEOS-FP, with a spatial resolution of 2° latitude by 2.5° longitude and 47 vertical levels. The simulation adopted the full-chemistry plus secondary organic aerosols (complexSOA), with one year of spin-up and hourly concentration output. The transport and emission options were taken from the default settings of version 12.3.2. Subsequently, the downscaling of the GEOS-Chem for the CMAQ model was performed through the air quality model boundary condition (AQMBC) tool (available at <https://github.com/barronh/aqmbc>), which follows Henderson *et al.* (2014).

In general, for particles, either the CMAQ default and GEOS-Chem profiles had close values, even though with slight differences. Figure 27 shows a comparison between the boundary conditions generated by the CMAQ default and GEOS-Chem models in November 2019. For the other two months under analysis in the present study, the vertical profiles had similar behaviours, minima, maxima, and averages. The CMAQ default had higher concentrations than GEOS-Chem for particles of sulfate (ASO4IJ) and nitrate (ANO3IJ) at the four edges of the D03 domain (south, east, north, and west), whereas the GEOS-Chem had higher concentrations

over the first 17 levels than the CMAQ default for particles of ammonium (ANH4IJ) and elemental carbon (AECIJ). For these species, the concentrations varied between  $8 \times 10^{-4}$  and  $1.2 \mu\text{g}/\text{m}^3$  using the CMAQ default, and between  $2 \times 10^{-5}$  and  $0.5 \mu\text{g}/\text{m}^3$  using the GEOS-Chem.

For the gases (Figure 28), GEOS-Chem had lower concentrations than the CMAQ default for  $\text{O}_3$  throughout the layers. The average concentrations were  $38.8$  and  $52.4 \mu\text{g}/\text{m}^3$  over the first 25 levels using GEOS-Chem and the CMAQ default, respectively, while in the upper layers, the concentrations reached around  $260 \mu\text{g}/\text{m}^3$ . For  $\text{SO}_2$ ,  $\text{NO}_x$ , and  $\text{CO}$ , the concentrations were lower when compared to  $\text{O}_3$ , with averages of the CMAQ default of  $0.05 \mu\text{g}/\text{m}^3$ ,  $0.04 \mu\text{g}/\text{m}^3$ , and  $0.06 \text{ ppm}$  and  $0.11 \mu\text{g}/\text{m}^3$ ,  $0.05 \mu\text{g}/\text{m}^3$ , and  $0.22 \text{ ppm}$  for GEOS-Chem. The CMAQ default assigned lower values for  $\text{SO}_2$  and  $\text{NO}_x$ , and for  $\text{CO}$ , the vertical profiles were similar on the ground, with larger differences in the upper levels.





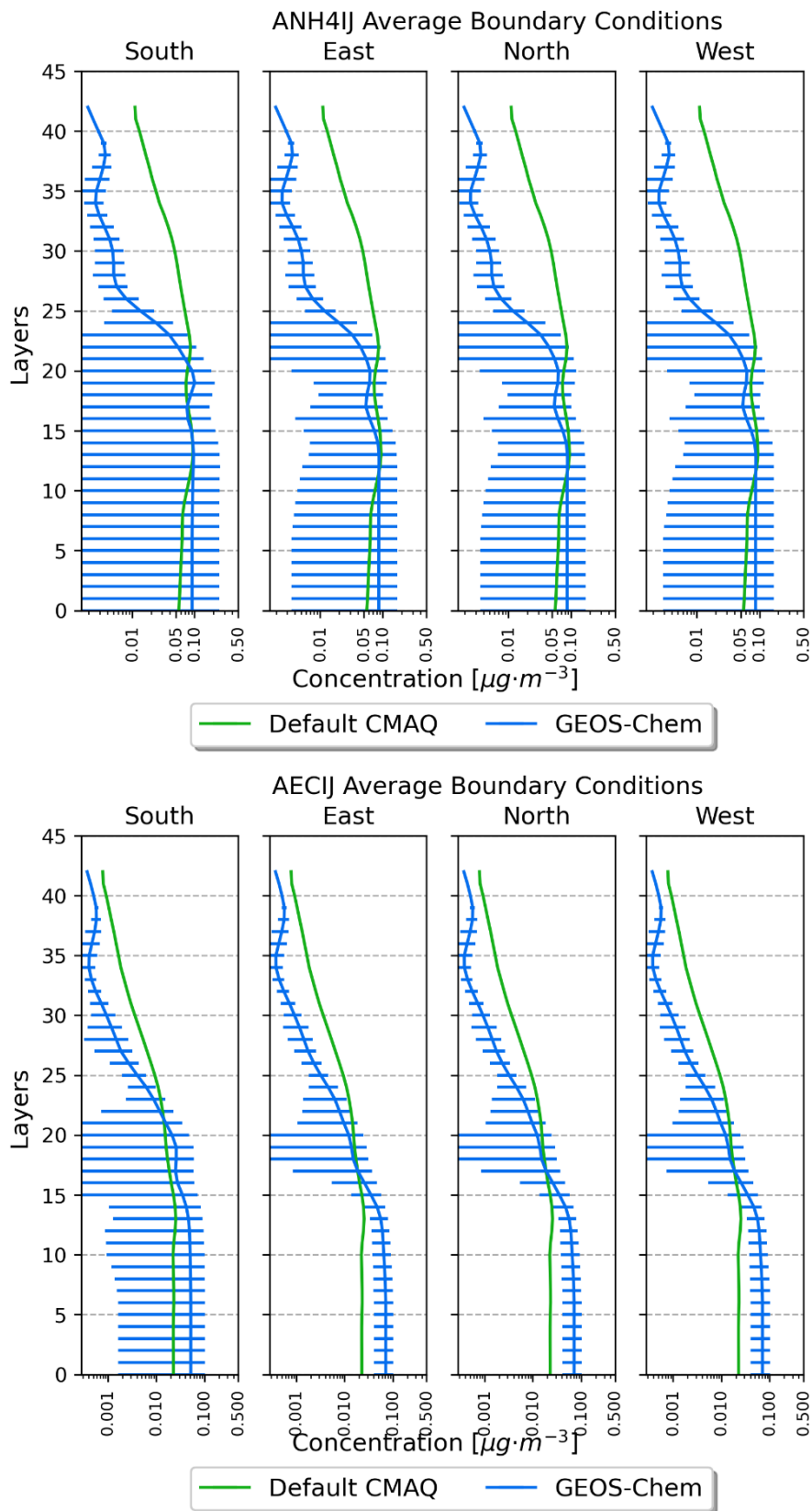
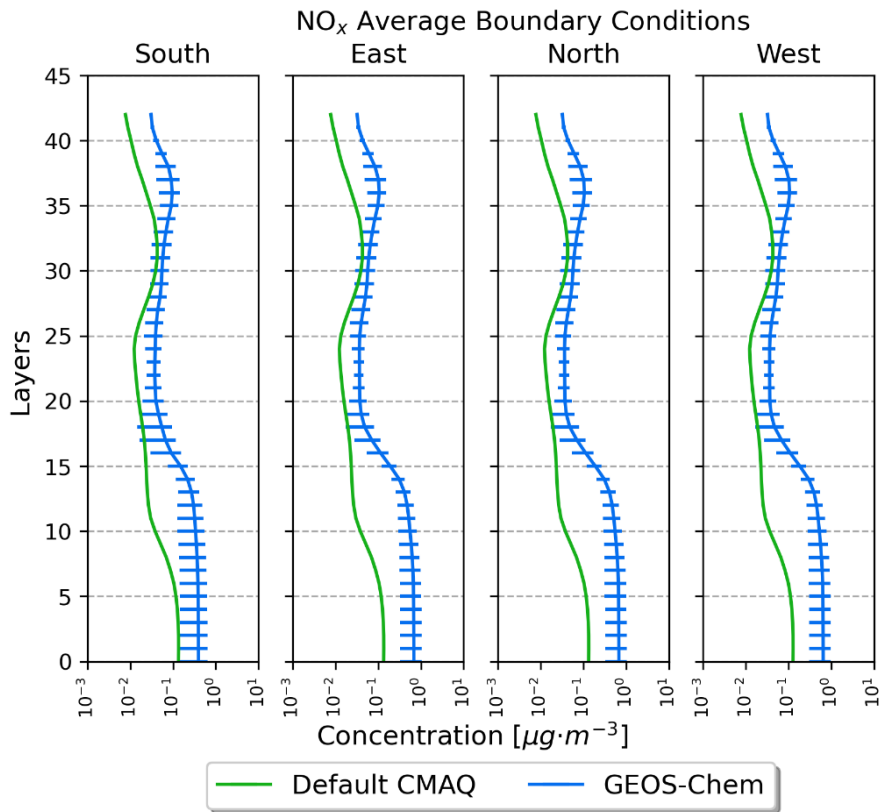
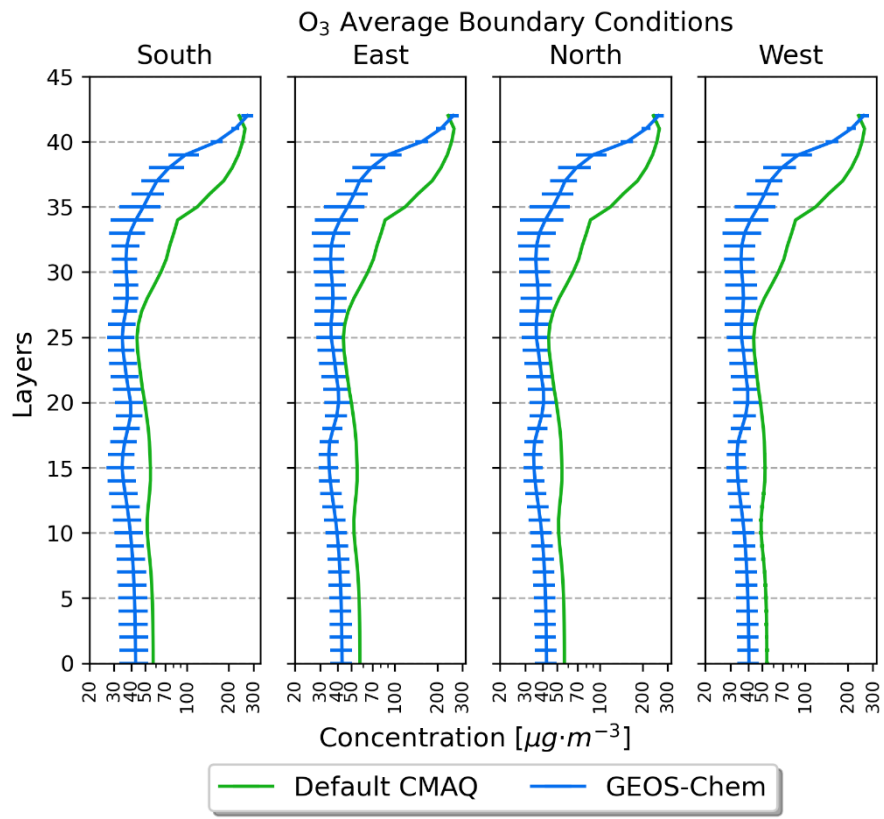


Figure 27. Comparison of average boundary conditions of the particles from the GEOS-Chem simulation in November 2019 and the CMAQ default fixed values available in version 5.3.2. The bars represent minimum and maximum values.



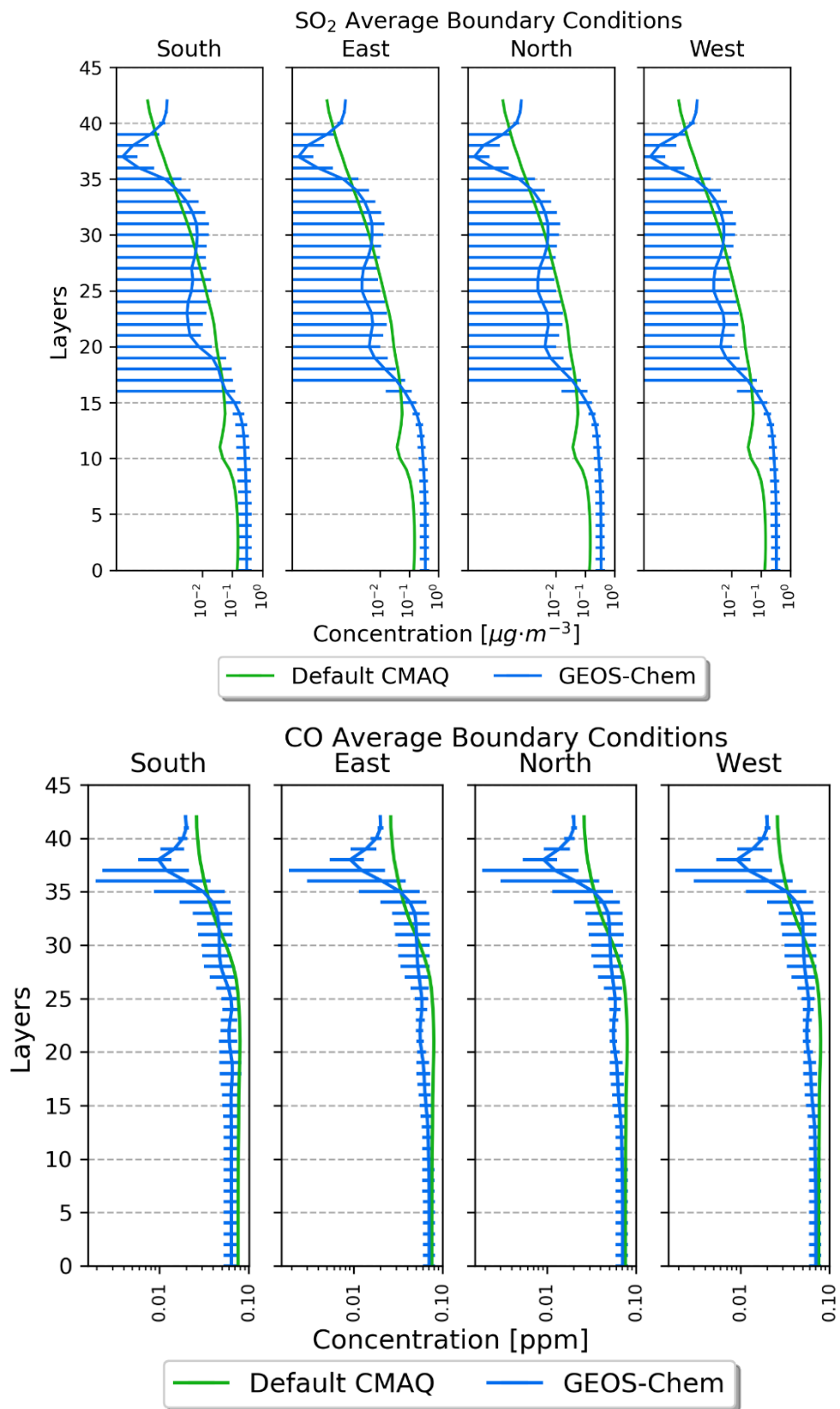


Figure 28. Comparison of average boundary conditions of the gases from GEOS-Chem simulation in November 2019 and the CMAQ default fixed values available in version 5.3.2. The bars represent minimum and maximum values.

The horizontal and vertical patterns of the four edges for O<sub>3</sub> and NO<sub>x</sub> are also displayed in Figure 29. The pattern reveals that the West edge had slightly lower concentrations when compared to the other edges that had similar results. A different pattern is seen for NO<sub>x</sub>, in which the South edge was the one that presented lower concentrations when compared to the other edges.

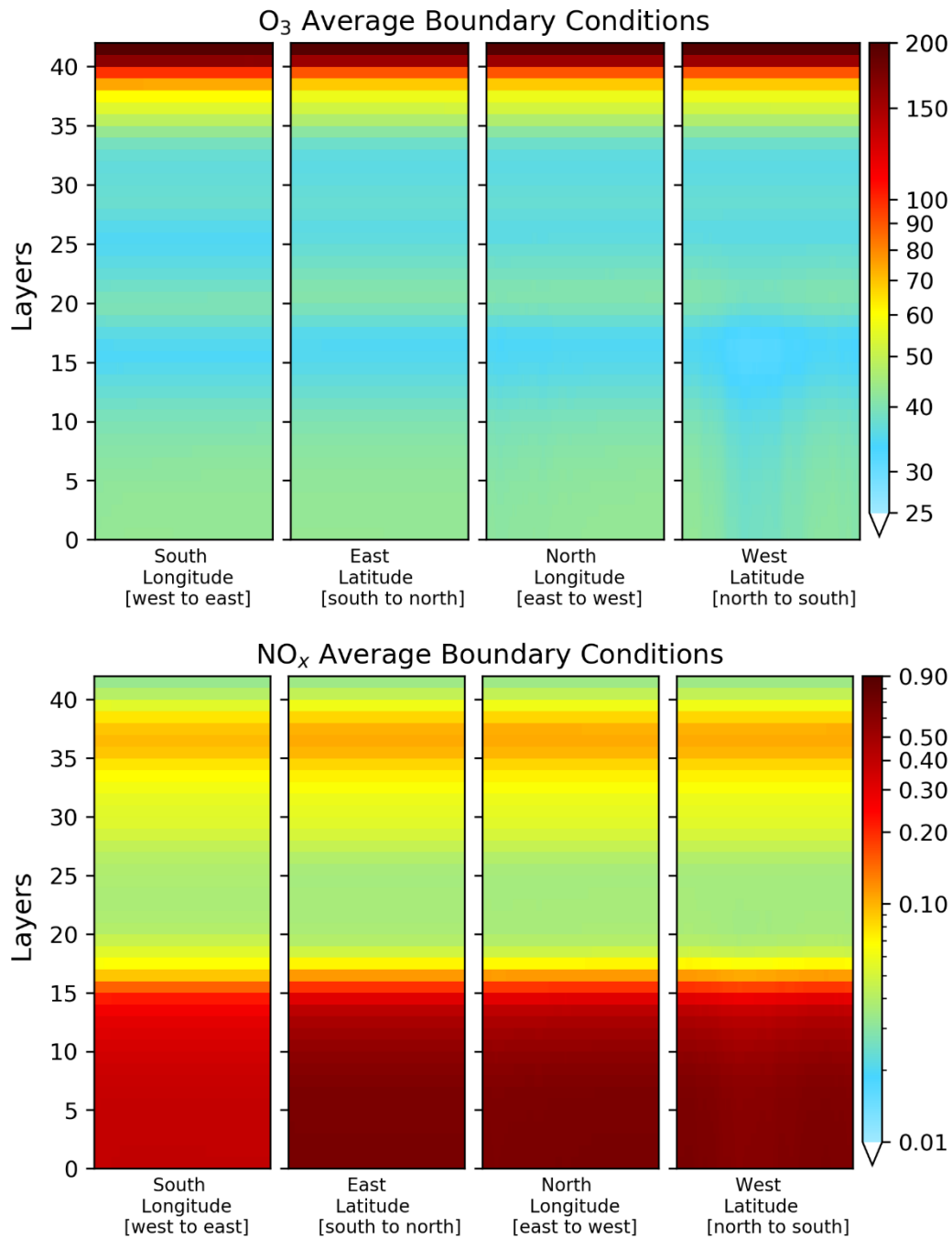


Figure 29. Vertical and horizontal patterns of the four boundary conditions of the D03 domain for O<sub>3</sub> and NO<sub>x</sub> in November 2019.

#### 4.3.5 CMAQ MODEL

The CMAQ model is an active open-source development project of the Environmental Protection Agency of the U.S. (USEPA) that consists of programmes for conducting air quality model simulations. CMAQ is a three-dimensional Eulerian atmospheric chemistry and transport model which uses the governing equations to represent processes such as horizontal advection, vertical advection, horizontal diffusion, vertical diffusion, photolysis, chemical reactions in the gas, aqueous, and cloud phases, aerosol dynamics, particle size distributions, plume effects, and gas and aerosol deposition estimation (Byun and Schere, 2006). Equation 2 mathematically represents the general form of the theoretical basis of CMAQ's formulation which is the conservation of mass for atmospheric chemical species.

$$\frac{\partial C_i}{\partial t} + \frac{\partial(uC_i)}{\partial x} + \frac{\partial(vC_i)}{\partial y} + \frac{\partial(wC_i)}{\partial z} = \frac{\partial}{\partial x} \left( k_H \frac{\partial C_i}{\partial x} \right) + \frac{\partial}{\partial y} \left( k_H \frac{\partial C_i}{\partial y} \right) + \frac{\partial}{\partial z} \left( k_V \frac{\partial C_i}{\partial z} \right) + R + L + S \quad (2)$$

(a)                      (b)                      (c)                      (d)                      (e)                      (f) (g) (h)

- (a) pollutant concentration rate of specie *i*
- (b) horizontal advection
- (c) vertical advection
- (d) horizontal diffusion
- (e) vertical diffusion
- (f) rate of formation of specie *i* by chemical reactions
- (g) net rate of removal of pollutant *i* by surface uptake processes (e.g. wet and dry deposition)
- (h) emission rate of all precursors

Where *C* is the concentration of each chemical specie *i*; *u*, *v*, and *w* are horizontal and vertical wind speed components; and *K<sub>H</sub>* and *K<sub>V</sub>* are horizontal and vertical turbulent diffusion coefficients. The wind components are provided by the WRF model as well as the diffusion coefficients are based on the values for the temperature, wind speed, total liquid water content, specific humidity, surface pressure, friction velocity, and height of the boundary layer which also come from the WRF model.

The CMAQ model provides the concentration of many pollutant species that are usually combinations of different types of primary emissions and secondary formations that have been

physically and chemically transformed in the atmosphere, which makes the CMAQ model be used in different applications with different temporal and spatial resolutions. Some examples are studies that have employed CMAQ to evaluate the anthropogenic emissions, along with the effects of wildfires and marine and vegetative biogenic emissions, on air quality in urban areas (Albuquerque *et al.*, 2018; Nedbor-Gross *et al.*, 2018); on population exposure (Chen *et al.*, 2014; Tao *et al.*, 2020); on human health interpreted as estimations of mortality (Punger and West, 2013; Liu *et al.*, 2018, 2020) and hospital admissions (Jiang and Yoo, 2018); economic losses (Lu *et al.*, 2016), air pollution control strategies (Feng *et al.*, 2019), and future projections of climate change (Nguyen *et al.*, 2020). Previous studies using the CMAQ model in South America characterized the air quality conditions over São Paulo (Brazil) and Bogotá (Colombia) (Albuquerque *et al.*, 2018; Nedbor-Gross *et al.*, 2018), whereas Pedruzzi *et al.* (2019) evaluated different approaches of the lateral boundary conditions and how they affected air pollutant concentrations over the same study area of this study (MRV). However, sometimes it is desirable to know specific source attribution information, for example, how much of the ozone in the urban area was formed due to nitrogen oxides emitted from motor vehicles? Or, which emissions sectors most contribute to air quality problems in a city? In this sense, the new versions of the CMAQ model have been coupled with the Integrated Source Apportionment Method (ISAM) tool.

The studies worldwide using the CMAQ-ISAM approach have been carried out mainly in regions of East Asia, such as China and South Korea, to assess the source apportionment of O<sub>3</sub> and PM<sub>2.5</sub> (Han and Zhang, 2018; Han *et al.*, 2018, 2021; Chang *et al.*, 2019; Li *et al.*, 2019; Liu *et al.*, 2019; Dong *et al.*, 2020; Yang *et al.*, 2021; Zhang *et al.*, 2021). These studies sustained that the surrounding areas had larger contributions against the pollution background and suggested that emission control strategies should be implemented in a coordinated manner by decision-makers at local and regional scales with unified control to specifically targeted sources. The main sources of air pollution in those areas were related to industries, domestic combustion, transportation, and agriculture activities. In addition, despite air pollutant concentrations significantly decreasing due to effective emission reduction measures, meteorological variations also played an important role in regional transport, which can be significant if the region is located in the prevailing wind direction.

These investigations developed in East Asia are examples of how air pollution affects local and regional scales, including other countries. However, this type of assessment, for a continental

dimension, is inexistent in Brazil, even though it is a single country, which, in principle, air pollution controls could be more easily implemented than regions such as Europe, where there are several countries concentrated in a single continent. In Brazil, air pollution controls and emission reduction policies started to be launched from the 80s, e.g., the National Programme for Control of Air Pollution by Automotive Vehicles (PROCONVE) and the National Programme for Control of Air Quality (PRONAR). These programmes were effective in reducing emissions from industrial stationary and vehicular sources, especially for primary atmospheric pollutants such as  $\text{NO}_x$ ,  $\text{PM}_{10}$ ,  $\text{SO}_2$ , and  $\text{CO}$ , and had a positive impact on air quality (Andrade *et al.*, 2017). However, ozone and fine particles are not yet controlled and little has been done from the point of view of political regulations to ensure the air quality regarding these pollutants. Furthermore, Brazil does not have a fully national emission inventory and only 1.7% of Brazilian municipalities have air quality monitoring stations (ISS, 2019), which mostly do not include  $\text{PM}_{2.5}$  and are located only in some cities in the Southeast of Brazil (Peláez *et al.*, 2020).  $\text{PM}_{2.5}$  was included as a criteria pollutant in Brazil only in 2018, and its standard was divided into four stages, but the deadlines for its implementation are not yet defined and the initial standard is still permissive compared to the WHO guidelines (Andreão and Albuquerque, 2021).

In South America, some studies have investigated the main emissions sectors that contribute to air quality problems in urban areas. For instance, East *et al.* (2021) investigated the main emissions sectors that most contributed to  $\text{PM}_{2.5}$  concentrations in Bogotá, Colombia, and reported that resuspended dust from unpaved roads and boundary conditions were the largest contributors. In addition, they also evaluated the potential benefits of emission reductions by 2030 by considering four emission scenarios. Despite the emissions reductions taking into account the likely paving of roads,  $\text{PM}_{2.5}$  increased driven by industrial activity and traffic, reinforcing the need for emissions control policies in Bogotá. Maciel *et al.* (2021) assessed eight emission scenarios in two periods of 7 days to quantify the impact of emission reductions by sector (industry, transport, and both) in Piracicaba city, São Paulo. The emission reduction did not significantly alter  $\text{O}_3$  concentrations ( $< 1\%$ ), or in some scenarios, it resulted in worse ambient concentrations, corroborating the non-linearity behaviour of this pollutant. Similarly, Albuquerque *et al.* (2019) considered seven different emission scenarios to assess the relationship between the emission of precursors ( $\text{SO}_2$ ,  $\text{NO}_x$ ,  $\text{NH}_3$ , and particulates of sulfate and nitrate) and  $\text{PM}_{2.5}$  concentrations in São Paulo city. Their results showed that the reduction ratios applied to precursor emissions were not effective at reducing  $\text{PM}_{2.5}$  concentrations,

mainly due to the contribution of organic and elemental carbon, and other secondary organic aerosol species. The largest reduction was obtained with the scenario that considered a reduction of 50% together of SO<sub>2</sub>, NO<sub>x</sub>, and NH<sub>3</sub> emissions (1 to 2 µg/m<sup>3</sup> on average). However, their study considered only a period of 10 days which can be a drawback for the development of air pollution control programmes that would require a longer time scale (seasonal or annual) to be more effective. They underpinned the need for simulations with longer periods. The aforementioned studies used the brute force method (BFM) approach which required a series of simulations and affected the amount of time considered by their studies.

So far, Pedruzzi (2020) was the single study in South America using the CMAQ-ISAM to evaluate the interaction of air pollutants among the capital cities of each state of Brazilian Southeastern. For that, he used the Emissions Database for Global Atmospheric Research-Hemispheric Transport of Air Pollution (EDGAR) global emission inventory to characterize the anthropogenic emissions over the study area. The use of global scale inventories is useful to consider the emissions of regions without data, however, at the same time, they might not be representative or capture local features. As described by Huneus *et al.* (2020), global emissions datasets have significant discrepancies when compared to local/national city emissions data. Maciel *et al.* (2021) also pointed out the challenge of using global inventory due to the need for spatial allocation (regridding from 0.1 degrees to 1 km resolution), which negatively affected the simulation results. Andreão *et al.* (2020) reported higher PM<sub>2.5</sub> and PM<sub>10</sub> concentrations using the EDGAR inventory in different metropolitan areas in Brazil.

In the present study, the anthropogenic emissions were provided by a local emission inventory in which each source type was considered as a tag in the source apportionment assessment. The point source sector includes industrial stack emissions for all facilities inside the MRV, such as sintering facilities, pelletizing furnaces, coke ovens, blast furnaces, thermoelectric power plants, grain processing, chemical and mineral products, among others. The industrial activities also include area and volume sources, which are represented by piles, material handling, load and unload process, nonroad emissions, landfills, civil construction, wind erosion, airports, among others. The label called vehicles represents the vehicular hot exhaust, vehicle evaporative emissions, and tires and brake wearing. Ship emissions represent marine logistics in the region. The biogenic tag is the emissions emitted by the vegetation. The dust resuspension label is the dust deposited on the road surface that is resuspended by vehicular traffic. Three additional tags to account for boundary conditions (BCON) and initial conditions (ICON) and



any remaining categories that were not explicitly tracked (OTHERS) were also provided by the model.

#### 4.4 PERFORMANCE EVALUATION OF WRF-URBAN/CMAQ MODELS

The performance of the WRF-Urban model was evaluated by comparing the hourly modelled and observed data of meteorological variables of 2-meter surface temperature (T2), 2-meter relative humidity (RH2), 10-meter wind speed (WS10), and 10-meter wind direction (WD10) through land surface stations. For the CMAQ model validation, it was used PM<sub>10</sub>, PM<sub>2.5</sub>, NO<sub>2</sub>, and O<sub>3</sub> parameters available at air quality stations (Figure 9). The meteorological and air quality monitoring data are provided by national and local agencies, except for the ASMA-Vix station, which was set up exclusively for the ASMA-Vix project, within the district and next to the school and the residence of children, between narrow streets and surrounded by buildings and vegetation. The statistical indices considered in this study were mean bias (MB), root mean square error (RMSE), mean absolute gross error (MAGE), normalized mean bias (NMB), normalized mean error (NME), Pearson correlation coefficient ( $r$ ), index of agreement (IOA), and the fraction of predictions within a factor of two of observations (FAC2).

$$MB = \frac{1}{n} \sum_{i=1}^n (M_i - O_i) \quad (3)$$

$$RMSE = \sqrt{\frac{1}{n} \sum_{i=1}^n (M_i - O_i)^2} \quad (4)$$

$$MAGE = \frac{1}{n} \sum_{i=1}^n |M_i - O_i| \quad (5)$$

$$NMB = \frac{\sum_{i=1}^n M_i - O_i}{\sum_{i=1}^n O_i} \times 100 \quad (6)$$

$$NME = \frac{\sum_{i=1}^n |M_i - O_i|}{\sum_{i=1}^n O_i} \times 100 \quad (7)$$

$$r = \frac{\sum_{i=1}^n [(M_i - \bar{M})(O_i - \bar{O})]}{\sqrt{\sum_{i=1}^n (M_i - \bar{M})^2 \sum_{i=1}^n (O_i - \bar{O})^2}} \quad (8)$$

$$IOA = 1 - \left[ \frac{\sum_{i=1}^n (M_i - O_i)^2}{\sum_{i=1}^n (|M_i - \bar{O}| + |O_i - \bar{O}|)^2} \right] \quad (9)$$

$$FAC2 = \text{fraction of data that satisfies the expression } 0.5 < \frac{M}{O} < 2 \quad (10)$$

where  $O_i$  and  $M_i$  are the observed and modelled value;  $\bar{O}$  and  $\bar{M}$  are the mean of the observed and modelled samples; and  $n$  is the total number of observations.

These indices are recommended by various studies to assess the reliability and representativeness of the simulations (e.g. Boylan and Russell, 2006; Kumar *et al.*, 2009; Hanna and Chang, 2012; Zhang *et al.*, 2012; Emery *et al.*, 2001; 2017). MB, RMSE, and MAGE are indices related to errors and deviations of the model. Thus, the best quality of the simulations is associated with values closer to zero. Since wind direction is a circular variable, the errors should consider the shortest angular distance between modelled and observed data (Jiménez and Dudhia, 2013). Therefore, for wind direction, it was considered if the observed or modelled value was more significant than 180 degrees, thus this value is subtracted by 360. NMB and NME report mean paired prediction–observation differences normalized by the mean observation. They are unbounded on the positive end ( $+\infty$ ) but bounded at  $-100\%$  for bias and  $0\%$  for error.  $r$ , IOA, and FAC2 are indices of association and agreement between modelled and observed data, with zero indicating the absence of correlation and strong correlation when closer to 1. Additionally, the non-parametric Kruskal-Wallis test (Kruskal and Wallis, 1952) is used to determine whether there are statistically significant differences in WRF-Urban and CMAQ model performance among the three configurations ( $z = 4, 10, \text{ and } 20 \text{ m}$ ).

After the validation of the WRF-Urban/CMAQ models with data from the air monitoring stations in the MRV, hourly concentrations corresponding to the grid cells where children lived and studied were used to calculate the exposure and dose of the children to  $\text{PM}_{10}$ ,  $\text{PM}_{2.5}$ ,  $\text{PM}_{10}$ ,  $\text{NO}_2$ , and  $\text{O}_3$ . Children's exposure to these air pollutants was also assessed at three different heights and the performance of exposure assessment was performed by comparing the  $\text{NO}_2$  data from the passive personal samplers used by the twenty-one children over their daily activities.

#### **4.5 EXPOSURE AND DOSE ASSESSMENT**

Exposure is often confused with concentration, being the latter the most frequently quantified (Rivas *et al.*, 2016). The traditional approach for assessing human exposure to ambient air pollution was proposed by Ott (1982), which described the exposure as the sum of the product

of time spent by a person in different microenvironments and the time-averaged air pollution concentrations occurring in those microenvironments (Branco *et al.*, 2014; Borghi *et al.*, 2021). The children's exposure to air pollutants was calculated by using Equation 11:

$$E_i = \sum_i^j C_j \times t_{ij} \times \left(\frac{I}{O}\right)_j \quad (11)$$

where  $E_i$  is the exposure of the  $i$ th child,  $C_j$  is the concentration of the pollutant ( $\mu\text{g}/\text{m}^3$ ) in the  $j$ th microenvironment (including home, school, in transit, and outdoor),  $t_{ij}$  is the time spent by the  $i$ th child in the  $j$ th microenvironment, and  $\left(\frac{I}{O}\right)_j$  is the indoor-outdoor ratio in the  $j$ th microenvironment. The concentration values ( $C$ ) were based on the nearby fixed station (ASMA-Vix station), and the CMAQ model results.

For the dose assessment, as reviewed by Borghi *et al.* (2021), different formulas are employed to estimate the inhaled dose of pollutants, and most studies focused on particulate matter and ultrafine particles. In a mathematical form, pollutant inhalation depends on the pollutant concentration, the exposure time, and the pulmonary parameters (which depend on the subject's physical effort, age, gender, etc.). The USEPA (2020) suggested estimating the potential average daily dose (ADD) using Equation 12, which considers the subject inhalation rate (IR) (Faria *et al.*, 2020) and the body weight (BW) (Almeida *et al.*, 2018; Goel *et al.*, 2021).

$$ADD_{pot_i} = \frac{\sum_i^j C_j \times t_{ij} \times \left(\frac{I}{O}\right)_j \times IR_k}{BW} \quad (12)$$

where  $ADD_{pot}$  ( $\mu\text{g}/\text{day}/\text{kg}$ ) corresponds to the potential average daily dose per unit of body weight (BW) of the  $i$ th child, and IR is the inhalation rate ( $\text{m}^3/\text{h}$ ) for the activity  $k$ .

Similarly, the estimation of the inhaled dose could consider other physiological parameters, such as the ventilation rate (VR), the tidal volume (VT), and the breathing frequencies ( $f$ ), as

used by various studies (Kumar and Goel, 2016; Kumar *et al.*, 2017; Segalin *et al.*, 2017) (Equation 13).

$$RDD = VR \times DF_i \times PM_i \quad (13)$$

The respiratory deposition dose (RDD) provides the net influx of the PM into the respiratory system and is the product of children's VR, the deposition fraction (DF), and the PM concentration for fraction *i*. The DF varies according to the particle diameter and hence is usually not directly proportional to the mass concentration (Kumar *et al.*, 2017). In the present study, DFs were calculated with the median particle diameter ( $d_p$ ) of PM<sub>2.5</sub> and PM<sub>1</sub> using Equations 14 and 15, provided by Hinds (1999):

$$DF = IF \times \left( 0.0587 + \frac{0.911}{1 + \exp(4.77 + 1.485 \ln d_p)} + \frac{0.943}{1 + \exp(0.508 - 2.58 \ln d_p)} \right) \quad (14)$$

where IF is the inhalable fraction given by:

$$IF = 1 - 0.5 \left[ 1 - \frac{0.911}{1 + (0.00076 d_p^{2.8})} \right] \quad (15)$$

The  $d_p$  was assumed as 1.25  $\mu\text{m}$  for PM<sub>2.5</sub> and 0.50  $\mu\text{m}$  for PM<sub>1</sub> based on Segalin *et al.* (2017). Thus, the total deposition fraction was 0.551 for PM<sub>2.5</sub> and 0.166 for PM<sub>1</sub>.

In the present work, the inhalation rates were adopted from Yoon *et al.* (2020), which assessed the IR of boys and girls during resting and light activity by age (Table 11). The mean inhalation

rates for boys (girls) adopted in this study were 0.54 (0.47) m<sup>3</sup>/h and 1.00 (0.89) m<sup>3</sup>/h during resting and light exercises, respectively. The inhalation rate for ‘light activities’ was considered the most appropriate for commuting, being at school, and outdoor activities, as they might involve some increment in inhalation rates. For the ‘resting’, it was considered if the children were sleeping or doing other sedentary activities.

Table 11. Inhalation rates (m<sup>3</sup>/h) for children that attended the ASMA-Vix project as a function of their activities and age, based on Yoon *et al.* (2020).

Children’s code	Campaign	Gender	Age (years)	Weight (kg)	IR <sub>resting</sub>	IR <sub>light</sub>
AN.CR.01	C1	F	11	25.6	0.54	0.87
AN.CR.02	C1	F	10	54.8	0.40	0.73
AN.CR.03	C1	F	11	39.1	0.54	0.87
AN.CR.04	C1	F	10	45.8	0.40	0.73
AN.CR.05	C1	M	11	36.8	0.48	0.94
AN.CR.06	C1	M	13	49.6	0.61	1.24
MA.CR.01	C2	M	11	30.1	0.48	0.94
MA.CR.02	C2	F	9	37.5	0.44	0.72
MA.CR.03	C2	F	12	64.4	0.50	0.96
MA.CR.04	C2	M	13	62.5	0.61	1.24
MA.CR.05	C2	M	11	36.6	0.48	0.94
MA.CR.06	C2	F	8	26.8	0.42	0.74
IT.CR.01	C3	M	9	42.4	0.49	0.80
IT.CR.02	C3	M	8	25.3	0.47	0.80
IT.CR.03	C3	M	9	29.7	0.49	0.80
IT.CR.04	C3	M	9	23.9	0.49	0.80
IT.CR.05	C3	M	14	70.9	0.66	1.35
IT.CR.06	C3	M	12	38.7	0.57	1.07
IT.CR.07	C3	M	13	61.5	0.61	1.24
IT.CR.08	C3	M	9	35.2	0.49	0.80
IT.CR.09	C3	F	12	57.5	0.50	0.96

AN, MA, and IT correspond to the neighbours from where children are (AN=Andorinhas, MA=Maruípe, IT=Itararé).

C1, C2, and C3 correspond to the period when campaigns occurred, that is November/2019, December/2019, and February/2020, respectively.

M=Male; F=Female

The inhalation rates of Yoon’s study were comparable to those rates adopted, for example, by the USEPA (2011) for children (0.45 m<sup>3</sup>/h for resting and 0.95 m<sup>3</sup>/h for light activities – these values were aggregated between girls and boys). Rivas *et al.* (2016) selected different inhalation rates based on their activities, such as school indoor (0.42 m<sup>3</sup>/h), school outdoor (1.27 m<sup>3</sup>/h), commuting (0.91 m<sup>3</sup>/h), home non-sleeping time (0.42 m<sup>3</sup>/h), home sleeping time (0.31 m<sup>3</sup>/h), and other (0.91 m<sup>3</sup>/h), but also considering the same rates for boys and girls. In addition, if Yoon’s inhalation rates would be converted to daily rates (the inhalation rates for boys (girls) would be 12.96 (11.28) m<sup>3</sup>/day during resting activities), the values would be comparable to those adopted by Brochu *et al.* (2011; 2014) (see Table 12). Similarly, Allan and Richardson (1998) found breathing rates of 15.09 m<sup>3</sup>/day (boys) and 13.98 m<sup>3</sup>/day (girls), with an average of 14.54 m<sup>3</sup>/day for children between 5 to 11 years old. Overall, boys breathe faster than girls, and overweight and obese individuals usually breathe faster than their normal-weight counterparts. Infants and children have a higher resting metabolic rate and oxygen consumption rate per unit of body weight than adults because of their rapid growth and relatively larger lung surface area per unit of body weight (USEPA, 2011). Such age-related differences, lung structure and function, and breathing patterns affect the inhaled dose and deposition of particles in the lungs; important factors to consider in risk assessments for inhalation exposures (Foos *et al.*, 2008).

Table 12. The mean inhalation rates for males and females by age group and body mass index. Source: (Brochu *et al.*, 2011; Brochu *et al.*, 2014)

Age (years)	Boys/Males				Girls/Females			
	Normal weight		Overweight/obese		Normal weight		Overweight/obese	
	(m <sup>3</sup> /day)	(m <sup>3</sup> /kg.day)	(m <sup>3</sup> /day)	(m <sup>3</sup> /kg.day)	(m <sup>3</sup> /day)	(m <sup>3</sup> /kg.day)	(m <sup>3</sup> /day)	(m <sup>3</sup> /kg.day)
<b>2-5</b>	7.35	0.493	-	-	6.90	0.492	-	-
<b>5-7</b>	9.04	0.463	10.86	0.408	8.59	0.441	10.18	0.372
<b>7-10</b>	11.17	0.428	13.84	0.354	10.71	0.395	12.70	0.335
<b>10-16.5</b>	15.64	0.383	15.02	0.260	13.32	0.306	15.15	0.254
<b>16.5-25</b>	20.39	0.290	23.35	0.228	16.46	0.275	18.18	0.221
<b>25-35</b>	20.00	0.282			15.82	0.273		
<b>35-45</b>	20.12	0.289	26.34	0.269	16.21	0.277	21.57	0.228
<b>45-65</b>	18.41	0.259	21.97	0.228	14.46	0.247	14.63	0.182
<b>65-96</b>	15.25	0.225	17.00	0.199	11.51	0.202	12.32	0.175

Like *IR*, *VR* is also a parameter that depends on personal data and physical activity. Although personal data (i.e., age, weight, physical activity) of the selected children were registered during the experimental campaigns, their pulmonary ventilation rates were not collected due to technical limitations for this personal parameter. In this sense, we assumed the ventilation rate provided by USEPA (2009) for the boys and girls for sleep and light exercises (Table 13).

Table 13. Mean ventilation rate (m<sup>3</sup>/min) for children that attended the ASMA-Vix project as a function of their activities and age, based on USEPA (2009).

Age (years)	Activity	Boys		Girls	
		(m <sup>3</sup> /min)	(m <sup>3</sup> /kg.min)	(m <sup>3</sup> /min)	(m <sup>3</sup> /kg.min)
<b>6 to &lt;11</b>	Sleep	0.00461	0.00015	0.00436	0.00015
<b>6 to &lt;11</b>	Light	0.01164	0.00038	0.01107	0.00038
<b>11 to &lt;16</b>	Sleep	0.00526	0.00010	0.00481	0.00009
<b>11 to &lt;16</b>	Light	0.01322	0.00025	0.01202	0.00023

Because the concentration values (*C*) of the nearby fixed station and the CMAQ model represent ambient concentrations and people spend most of their time indoors, some studies assessed indoor and outdoor concentrations simultaneously to account for how much of the outdoor concentration would be transferred to indoor environments, the so-called indoor/outdoor (I/O) ratio. Chao (2001) evaluated the relationships between indoor and outdoor concentrations of NO ( $0.98 \pm 0.19$ ), NO<sub>2</sub> ( $0.79 \pm 0.30$ ), SO<sub>2</sub> ( $1.01 \pm 0.78$ ), and O<sub>3</sub> ( $0.40 \pm 0.31$ ) in residential buildings in Hong Kong. Similarly, Lee *et al.* (2002) evaluated I/O ratios of NO<sub>2</sub> ( $2.08 \pm 1.69$ ) and O<sub>3</sub> ( $0.24 \pm 0.18$ ) in residential environments in Southern California, USA. Later, Lee *et al.* (2004) conducted O<sub>3</sub> I/O experiments ( $0.10 \pm 1.09$ ) in homes of elementary school children (10-12 years old) living in Nashville, Tennessee, USA. Meanwhile, Blondeau *et al.* (2005) considered experiments for NO<sub>2</sub> (from 0.88 to 1), NO (from 0.5 to 1), and O<sub>3</sub> (from 0 to 0.45) at schools located in La Rochelle, France. Esplugues *et al.* (2010) assessed indoor and outdoor concentrations of NO<sub>2</sub> in homes of 1-year-old children residing in Valencia, Spain. The outdoor NO<sub>2</sub> concentrations were 26.2 µg/m<sup>3</sup> while those measured indoors averaged 18.0 µg/m<sup>3</sup>, being a ratio of 0.69. Pegas *et al.* (2011) found I/O ratios ranging between 0.35 and 1

for NO<sub>2</sub> at primary schools in Lisbon, Portugal. Godoi *et al.* (2013) found I/O ratios varying from 0.62 to 1.38 for SO<sub>2</sub> and from 1.02 to 1.12 for NO<sub>2</sub> in homes and schools in Curitiba, South Brazil. Likewise, Demirel *et al.* (2014) assessed NO<sub>2</sub> (0.67–1.75) and O<sub>3</sub> (0.46–1.08) I/O ratios in primary schools in Eskişehir, Turkey. In Barcelona, Spain, Rivas *et al.* (2014) evaluated NO<sub>2</sub> (0.67–1.75) and PM<sub>2.5</sub> (0.46–1.08) I/O ratios also in primary schools. Dèdelè and Miškinytė (2016) evaluated NO<sub>2</sub> concentrations in various microenvironments (kitchen, living room, bedroom) of houses with gas and electric stoves in Kaunas, Lithuania. The concentration of NO<sub>2</sub> depended on the stove type used in the kitchen, those with gas stoves (I/O = 1.1–1.7) had higher concentrations compared to homes with electric stoves (I/O = 0.6–0.9). Segalin *et al.* (2017) assessed the PM<sub>2.5</sub> (1.89) and PM<sub>10</sub> (1.06) concentrations inside elderly residences in the Metropolitan Region of São Paulo. Meanwhile, Martins *et al.* (2020) examined the relationship between indoor and outdoor size-fractionated particulate matter in homes and schools in Lisbon, Portugal. The I/O ratios varied between 0.5 and 6.4 for PM<sub>1</sub>, 0.7–5.2 for PM<sub>2.5</sub>, and 0.4–6.5 for PM<sub>10</sub>. The I/O ratio greater than unity indicates that either there are significant indoor sources and there can be a transport event from outside towards the inside environment. It can be considered a ‘correction factor’ to represent the difference between concentrations indoors and outdoor (Monticelli *et al.*, 2021).

The ASMA-Vix project has determined the air pollutant I/O ratio in the microenvironments of the schools and homes for PM<sub>2.5</sub>, PM<sub>10</sub>, and NO<sub>2</sub> can be found in Velasco (2020). Thus, in this study, the schools (homes) I/O ratios for PM<sub>2.5</sub> were 4.18 (3.84), PM<sub>10</sub> 2.03 (2.21), and NO<sub>2</sub> 1.52 (Velasco, 2020). The I/O ratio for NO<sub>2</sub> in homes was adopted from the literature (1.40) because of the lack of data during the experimental campaigns for this parameter at homes. In this sense, the study of Dedele and Miskinyte (2016) was considered because homes with gas stoves were considered in their study, which was a characteristic similar to the residences of the selected children in the ASMA-Vix project. In the same way, the I/O ratios for O<sub>3</sub> and PM<sub>1</sub> were also taken from the literature because there were no experimental campaigns for these parameters. Thus, the I/O ratios for O<sub>3</sub> and PM<sub>1</sub> were 0.45 (Blondeau *et al.*, 2005) and 1.44 (Martins *et al.*, 2020) for schools, and 0.40 (Chao, 2001) and 1.34 (Martins *et al.*, 2020) for residences, respectively. Table 14 summarizes the I/O ratios used in the exposure and dose assessments of this study. It is important to highlight that the literature is limited to the I/O values for the microenvironments under analysis. For this reason, a sensitivity test was also performed to assess the impact of the I/O parameter in the exposure and dose assessment, which considered the I/O equal to 1. Similarly, the estimation of personal exposure and inhaled doses



is also highly affected by transport microenvironments (private vehicles, buses, metro), road types, street configuration, and commuting behaviour (Boniardi *et al.*, 2019b; Borghi *et al.*, 2021). However, due to the absence of these types of data related to the subjects and to avoid further possible biases, the time spent in home-to-school commuting (which had an average of 8 minutes) was treated as outdoor concentrations.

Table 14. The I/O ratios adopted in the present study.

<b>Pollutant</b>	<b>School</b>	<b>Home</b>
NO <sub>2</sub>	1.52 (Asma-Vix project)	1.40 (Dédelè and Miškinytė, 2016)
PM <sub>10</sub>	2.03 (Asma-Vix project)	2.21 (Asma-Vix project)
PM <sub>2.5</sub>	4.18 (Asma-Vix project)	3.84 (Asma-Vix project)
PM <sub>1</sub>	1.44 (Martins <i>et al.</i> , 2020)	1.34 (Martins <i>et al.</i> , 2020)
O <sub>3</sub>	0.45 (Blondeau <i>et al.</i> , 2005)	0.40 (Chao <i>et al.</i> , 2001)

## 5. RESULTS AND DISCUSSION

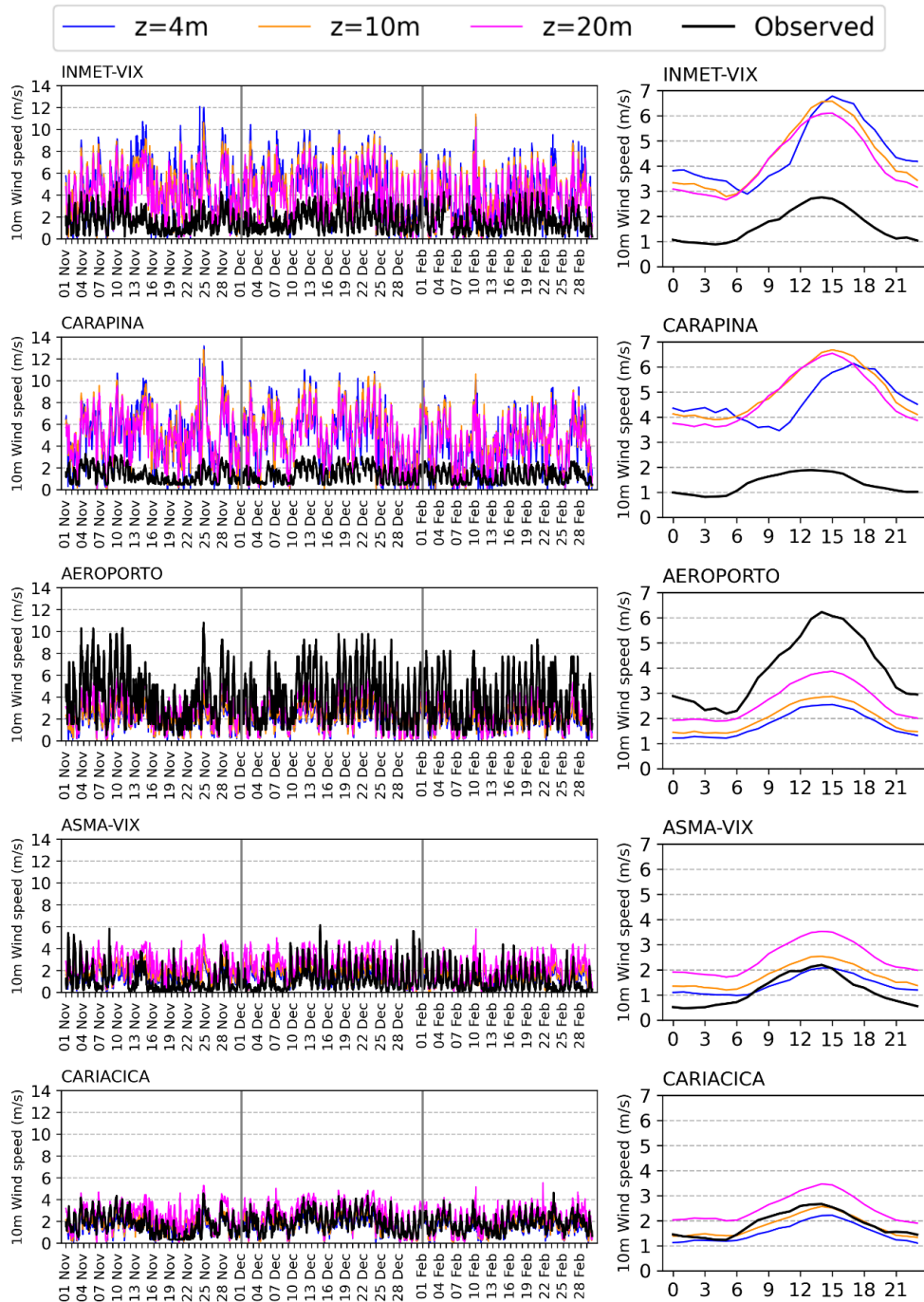
### 5.1 THE WRF-URBAN VALIDATION

In this section, it is presented the performance of the WRF-Urban model because changes in the magnitude of meteorological parameters, especially temperature and wind speed, affect the chemical reactions of secondary pollutants and pollution dispersion, which can induce, for instance, an increase in concentrations of ozone and particulate matter (Liao *et al.*, 2014; La Paz *et al.*, 2016; Franco *et al.*, 2019). Each subsection shows hourly time series and diurnal variation plots for each station that measured the specific meteorological parameter. Tables with the statistical indices of errors and correlation for the variables over the three months (November, December, February) and the three configurations ( $z = 4$  m,  $z = 10$  m,  $z = 20$  m) are displayed in the Appendix. In summary, the results will show that the lowering of the model height was more sensitive to wind speed than the other parameters, despite slight differences also being seen for T2 and RH2. However, the Kruskal-Wallis test revealed that there was no statistical difference in the statistical indices (MB, RMSE, MAGE, r, IOA, FAC2) among the three configurations for any of the meteorological parameters.

#### 5.1.1 WIND SPEED AND DIRECTION

The most significant performance variability with the lowering of the model height was seen for the wind speed parameter. During the experimental campaigns, the hourly mean (median) observed and standard deviation of WS10 over the three months was 4.0 (3.5) $\pm$ 2.2 m/s at Airport, 1.2 (0.8) $\pm$ 1.1 m/s at ASMA-Vix, 1.3 (1.2) $\pm$ 0.7 m/s at Carapina, 1.9 (1.8) $\pm$ 0.9 m/s at Cariacica, 1.8 (1.6) $\pm$ 0.9 m/s at Enseada, 2.6 (2.4) $\pm$ 1.2 m/s at IBES, and 1.6 (1.4) $\pm$ 1.0 m/s at INMET-VIX. As we can see, the Airport site registered the highest wind speed values while the other stations recorded wind speeds lower than 2 m/s, except for the IBES station. This difference seen in observed data is due to the fact that the Airport site is the only station located at an open site and it is not influenced by the presence of buildings and vegetation; or any other obstacle, that can slow down the wind speed. Figure 30 exhibits the comparison of hourly (left) and diurnal variation (right) between modelled WS10 for the three configurations, and the observed data for each station separately. Overall, the configuration with  $z = 4$  m simulated the lowest wind speeds, with a mean (median) observed and standard deviation averaged over the

seven stations of  $2.5 (2.5)\pm 1.3$  m/s, followed by  $z = 10$  m  $2.7 (2.8)\pm 1.3$  m/s, and then,  $z = 20$  m  $3.2 (3.2)\pm 1.4$  m/s.



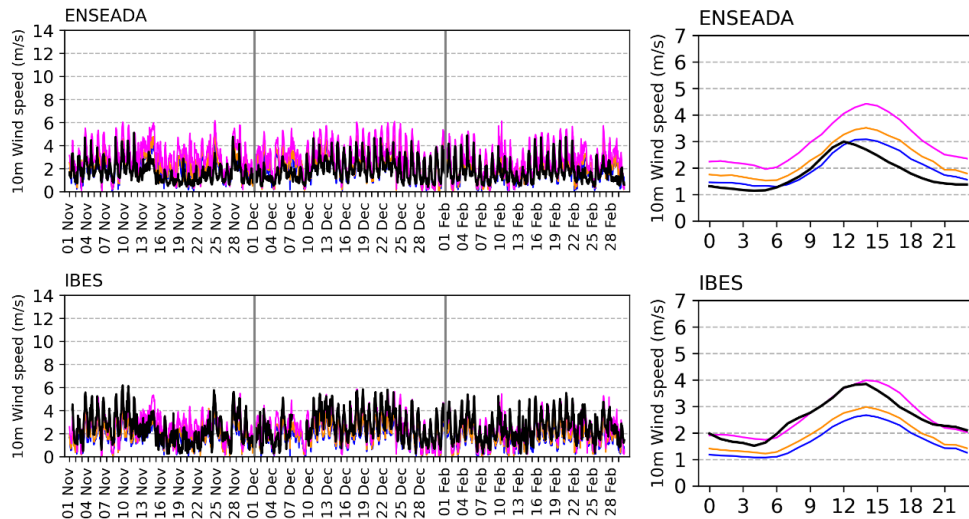


Figure 30. Comparison of WS10 hourly time series (left) and mean hourly variation (right) for observed (black line) and modelled by the WRF-Urban varying the lowest model height for each monitoring site.

The mean hourly variation plots show that as the model height reduced, the magnitude of WS10 also decreased. However, this behaviour was not evident for Carapina and INMET-Vix stations analyses, in which the three configurations had similar results and the WRF model more overestimated WS10 when compared to the other paired values of modelled/observed (RMSE equal to 4.0 m/s for Carapina and 3.2 m/s for INMET-Vix). These differences in results among the stations can be explained by the fact that the WRF-Urban BEP is exclusively activated in the grid cells assigned as ‘Urban and Built-up’ class, which in this study were represented by Airport, ASMA-Vix, Cariacica, Enseada, and IBES stations; whereas the location of Carapina and INMET-Vix stations were seen as vegetated surfaces by the WRF model. For urban surfaces, the BEP parameterization forces WS10 (and T2 as well) to be equal to the values at the lowest model level, in which U and V are prognostic variables computed by the model dynamically following the Navier–Stokes equations. This is mainly for two reasons: (i) The Monin–Obukhov similarity theory is not valid in the urban canopy, thus the 2m and 10m values do not use the log-law, (ii) to use BEP, it is necessary to have a very high vertical resolution close to the ground, thus the differences between the lowest model level value and the 2m and 10m values are expected to be small. On the other hand, over the vegetated/natural surfaces, WS10 is diagnosed in the surface-layer scheme and is calculated from the wind speed in the first level via the logarithmic formula, following the Monin–Obukhov similarity theory. A recent study suggested an unphysical characteristic related to the 10-m wind speed

parameterization based on Monin-Obukhov similarity (Avisar *et al.*, 2021), which can explain why no differences could be seen over vegetated surfaces with the lowering of the model height.

In the bulk schemes, the roughness length and thermal properties, which represent the sink of momentum and heat storage, are fixed values that are not directly dependent on the urban morphology. On the opposite, BEP estimates the sink of momentum with a drag coefficient force that depends on the urban morphology and the density of vertical surfaces (walls) distributed from the ground surface up to the height of the highest building. The sources/sinks of heat due to the heat fluxes from walls, streets, and roofs are estimated by solving an energy budget for each surface which takes into account the shadowing and radiation trapping effects (Martilli *et al.*, 2002; Chen *et al.*, 2011; Salamanca *et al.*, 2011; Liao *et al.*, 2014; La Paz *et al.*, 2016; Huang *et al.*, 2019). The presence of buildings is modelled through two parts: the building heights and their corresponding proportions. This study used building heights of 10 m, 15 m, and 20 m corresponded to a proportion of 20%, 60%, and 20%, respectively, for all the three configurations. As a consequence, the turbulent fluxes are different among the configurations in the urban canopy layer, and the configuration with the model height at  $z=4$  m depicts a higher building density at the first level of the model than the other configurations, which can be conducive to trapping more heat and enhancing the drag force, leading to weaker winds and higher temperatures.

In comparison with observations, the statistical analyses (Figure 31 and Table S1) showed that Carapina and INMET-Vix stations had the greatest errors (e.g. RMSE ranged between 3–4 m/s) and the lowest agreements (e.g. IOA under 0.5) for all configurations, despite the  $r$ -values were at about 0.4 for Carapina and 0.7 for INMET-Vix. The low FAC2 values, which were under 0.30, indicated that the modelled wind speeds at these two locations were not within a factor of 2 of observations. On the other hand, the results over urban surfaces had a better agreement with the observed data, with absolute errors under 2 m/s and IOA-values above 0.6. ASMA-Vix, Cariacica, Enseada, and IBES stations met the criteria suggested by Emery *et al.* (2001) and Hanna and Chang (2012) ( $RMSE \leq 2$  m/s;  $FAC2 \geq 0.50$ ), which are more conservative when compared to those suggested by Kemball-Cook *et al.* (2005) ( $RMSE \leq 2.5$  m/s) for complex terrains. All statistical indices separated by station and month are presented in the Appendix, in which the lowest errors and highest indices of agreements are highlighted in green (conversely, the worst indices are in red). Statistical indices for WS10 are exhibited in Table S1 and showed that, overall, the configuration with the model height at 4 m was the one that

most met the benchmark value of  $MB \leq \pm 0.5$  m/s, in contrast to the reference value of  $RMSE \leq 2$  m/s, in which the model height configured with  $z = 20$  m presented the best performance. However, as mentioned, the Kruskal-Wallis test revealed that there was no statistical difference in the statistical indices (MB, RMSE, MAGE, r, IOA, FAC2) among the three configurations.

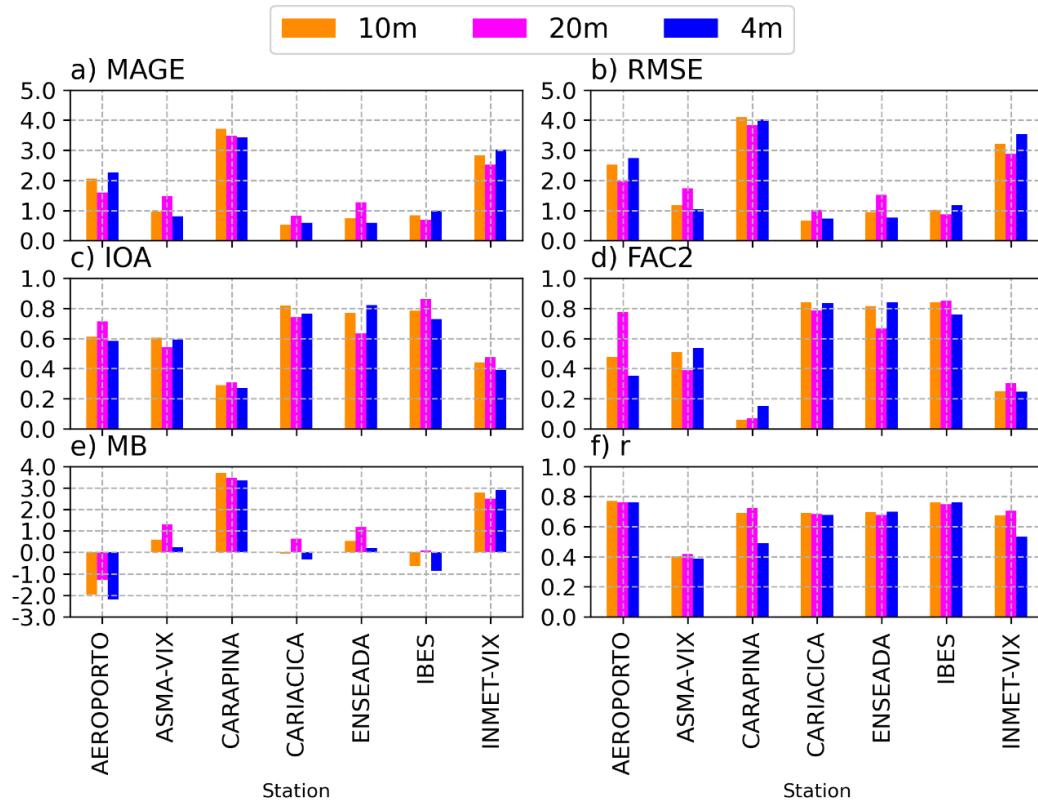


Figure 31. Comparison of the averages of statistical indices for each station and configuration, considering the three months together, for WS10.

The overestimation of wind speed has been reported by several studies using the WRF model (Carvalho *et al.*, 2014; Hariprasad *et al.*, 2014; Banks *et al.*, 2016; Avolio *et al.*, 2017; Siuta *et al.*, 2017; Linaje *et al.*, 2019; Gholami *et al.*, 2021). Potential error sources were related to (i) the initial and boundary conditions dataset used to initialize the model; (ii) the choice of physical parameterisation schemes, which depends on the area under study and the period of the year being analysed; (iii) the ability of the model to simulate topographical features realistically because the model tends to smooth the actual terrain because of the sub-grid scale processes; thus, under the effect of flatter terrains, the friction between surface and atmosphere will be reduced, and thus the model will overestimate the wind speed; (iv) the actual location

of the weather stations which the presence of barriers, such as hills and buildings, slows down the wind speed measured at the stations. The present study sought to minimize these potential error sources by adopting high spatial and temporal resolutions ( $0.25^\circ \times 0.25^\circ$  at every hour) of the initial and boundary conditions with ERA5 and with the use of BEP together with BouLac, which is among the best for the coastal area (Banks *et al.*, 2016) and it is the PBL scheme that has been tested most extensively coupled with BEP (Ribeiro *et al.*, 2021). The results of the present study are consistent with previous studies that evaluated the BEP scheme and generally found a good agreement with wind speed observations (Liao *et al.*, 2014; La Paz *et al.*, 2016; Sarmiento *et al.*, 2017; Franco *et al.*, 2019; Huang *et al.*, 2019; Avisar *et al.*, 2021). A comparison of the statistical indices of errors between this study and the others is presented in Table 15. Sarmiento *et al.* (2017) reported that despite the wind speed exhibiting an overestimation in the model for all configurations tested for summer and winter over Indianapolis, US, the lowest average wind speed error, in both the wintertime (mean error of 1.5 m/s) and summertime (mean error of 2.1 m/s), was with BEP. The use of BEP resolved better heat and momentum balances during the day in Madrid, Spain (La Paz *et al.*, 2016) because the scheme depends on drag coefficients for momentum transfer, and heat exchanges are developed without taking into account thermal stratification. The additional layers in the urban canopy and the fact that wall, street, and roof surfaces particularly act as sources and sinks of heat and momentum lead to the increased production of turbulent kinetic energy, which induced a better representation of the urban boundary-layer height in the city of Lisbon, Portugal (Teixeira *et al.*, 2019). Similarly, Franco *et al.* (2019), which conducted experiments in São Paulo city, affirmed that BEP showed much better 10-m wind speed agreement with the observed data because in BEP's formulation the exchange of momentum on the vertical surfaces of the buildings exerts pressure and viscous drag force on the flow. This force induces an orthogonal movement in the direction of the street canyon with a component against the horizontal wind direction (Martilli *et al.*, 2002), causing a reduction in the wind speed.

Table 15. Comparison of the wind speed performance of the present study with others found in the literature review. The values of this study were averaged among the stations.

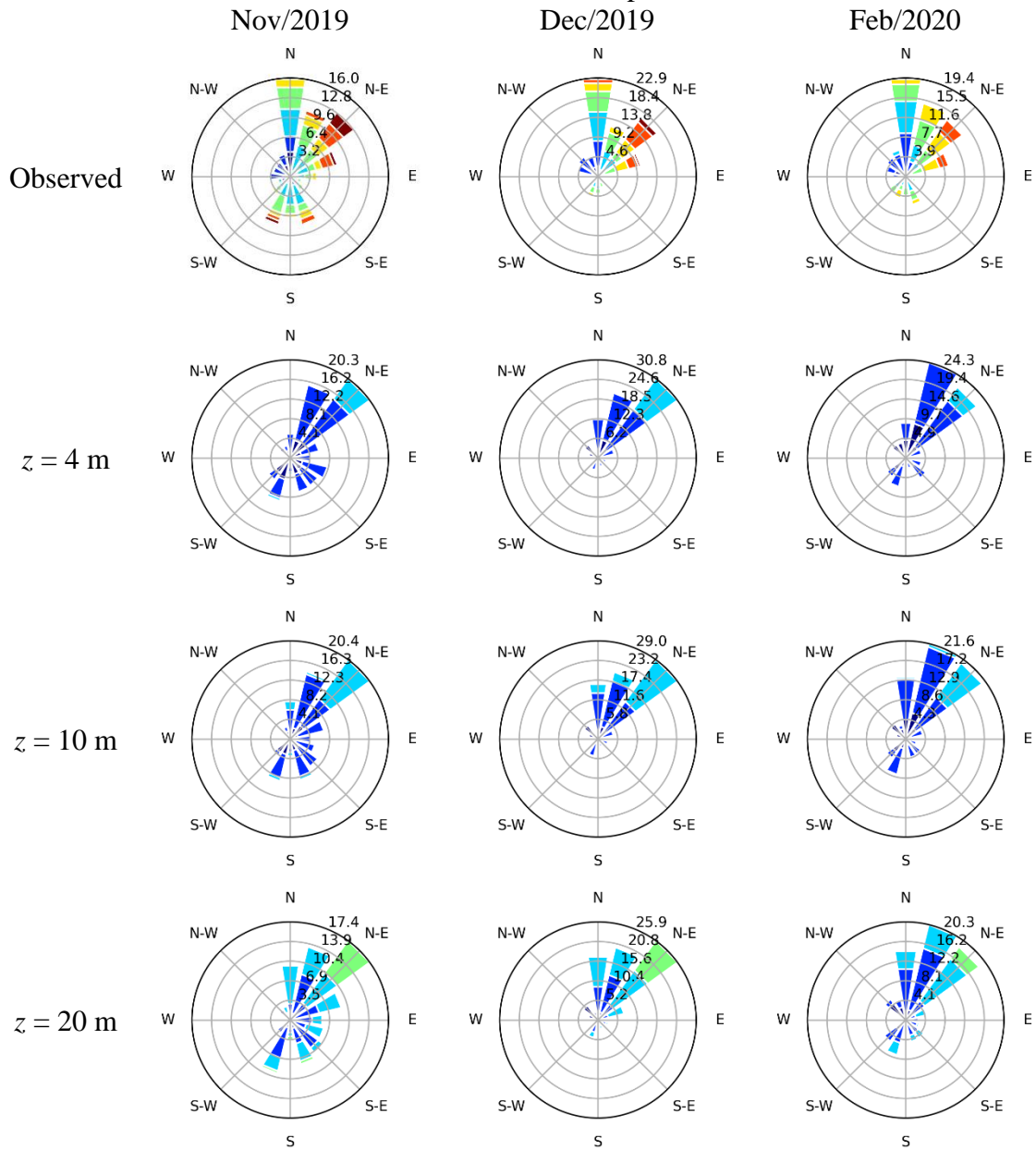
Authors	Study Area	Statistic	Value	Period analysed
Liao <i>et al.</i> (2014)	Yangtze River Delta, China	RMSE	1.20	January, 2010
		RMSE	1.39	July, 2010
		r	0.62	January, 2010
		r	0.39	July, 2010
La Paz <i>et al.</i> (2016)	Madrid, Spain	RMSE	0.90	Annual
		IOA	0.80	
Sarmiento <i>et al.</i> (2017)	Indianapolis, US	MB	2.10	June 15 to July 20, 2013
		MB	1.50	February 15 to March 20, 2013
Franco <i>et al.</i> (2019)	São Paulo, Brazil	MB	-0.19	October 31 to November 4, 2013
		RMSE	1.12	
Huang <i>et al.</i> (2018)	Beijing, China	MB	0.34	5 to 8 July 2015
		RMSE	1.18	
		r	0.32	
Avisar <i>et al.</i> (2021)	Tel-Aviv Metropolitan Area, Israel	MB	-0.68	13 to 14 July 2013
		MAGE	0.71	
		RMSE	0.82	
Present study	MRV, Brazil	RMSE $z=4$ m	2.00	November, December/2019, and February/2020
		RMSE $z=10$ m	1.95	
		RMSE $z=20$ m	1.97	
		$r$ $z=4$ m	0.61	
		$r$ $z=10$ m	0.67	
		$r$ $z=20$ m	0.67	

In contrast to WS10, the results for WD10 had much more similar behaviour among the three configurations. Based on the Airport station measurements (Table 16), wind roses showed that winds predominantly came from the north 16%, 22.9%, and 19.4% of the time, and northeast 12.8%, 18.4%, 15.5% in November, December, and February, respectively. Similar behaviour was depicted by the WRF model, despite the model predicting that the winds mostly came from north-northeast and northeast regardless of the model height configuration. For instance, in November, the configuration  $z = 4$  m,  $z = 10$  m, and  $z = 20$  m indicated that the winds blew from the northeast (north-northeast) 20.3% (16.2%), 20.4% (16.3%), and 17.4% (13.9%) of the time, respectively. This indicates that the model rotated clockwise the winds with respect to the



observed records, also represented by the positive MB (Table S2 and Figure 32) for Airport, IBES, INMET-VIX stations over the three months, and Carapina in November. For Carapina in December and February, ASMA-VIX, Cariacica, and Enseada stations, the statistical analyses showed negative MB which meant that the model counterclockwise shifted the winds. The wind roses for each station and month are displayed in the Appendix (Table S3).

Table 16. Observed and simulated wind roses at the Airport station for each month.



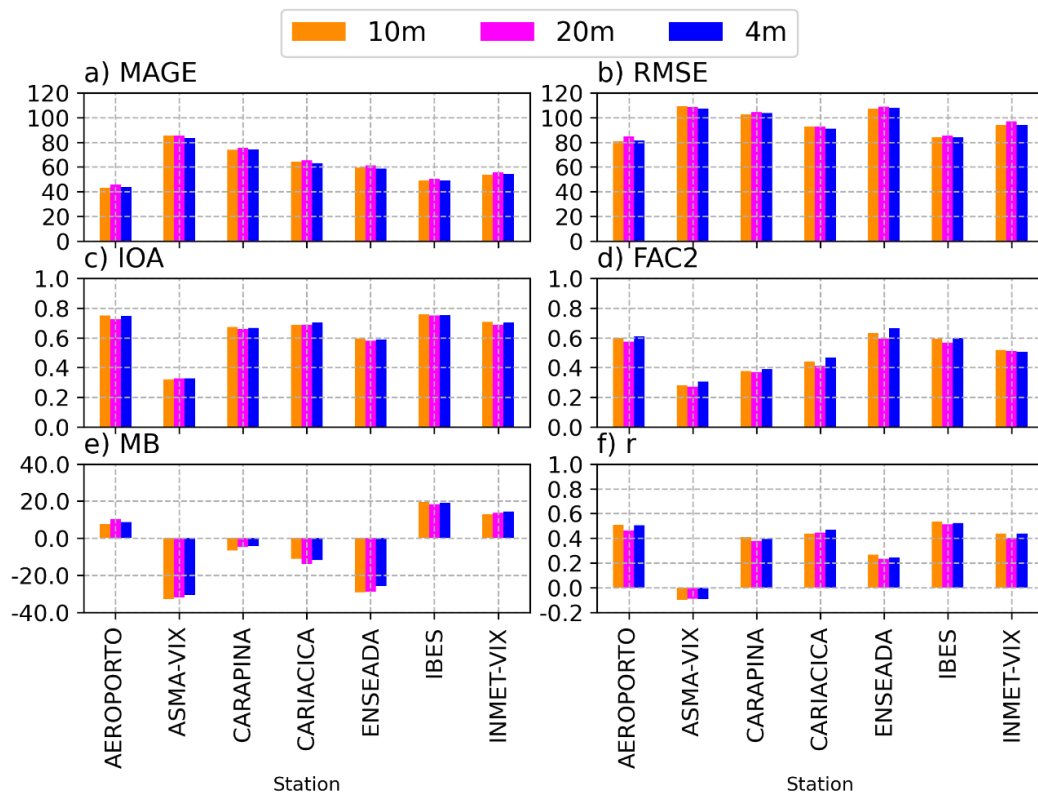


Figure 32. Comparison of the averages of statistical indices for each station and configuration, considering the three months together, for WD10.

The results for WD10 were beyond the benchmark suggested by Emery *et al.* (2001), which indicated  $MB < \pm 10^\circ$  and  $MAGE \leq 30^\circ$ , except for some specific months and stations, but without a clear pattern. Figure 32 shows that the lowest errors were seen for Airport and IBES stations, while the highest errors occurred for ASMA-VIX, Carapina, and Enseada. Since all configurations had similar results, averaged MAGE over the three configurations were  $44^\circ$  for Airport,  $85^\circ$  for ASMA-Vix,  $75^\circ$  for Carapina,  $64^\circ$  for Cariacica,  $60^\circ$  for Enseada,  $49^\circ$  for IBES, and  $54^\circ$  for INMET-Vix. Similar results were found in Franco *et al.* (2019), in which the use of BEP in São Paulo city had MAGE equal to  $56^\circ$ . According to Jiménez and Dudhia (2013), the errors in wind direction usually become larger at low wind speeds, as well as, the errors are also larger over complex terrain than in flatter areas. As shown, observed wind speeds at the Airport (mean of 4.0 m/s) and IBES (mean of 2.6 m/s) stations were greater when compared to the other stations. Figure 32 also presents the indices of agreement in which r-, IOA-, and FAC2-values varied between -0.1–0.6, 0.3–0.8, and 0.3–0.7, respectively. FAC2 was under 0.5 for ASMA-Vix, Carapina and Cariacica stations. The IOA-values were above 0.6, except for the ASMA-Vix station, which also had weak negative correlations between modelled and observed data,

meanwhile, the other stations presented stronger and positive correlations. Regarding the configuration that presented the most suitable results compared to the observations, Table S2 shows that the configuration with the model height of 4 m had the lowest errors and the highest indices of agreements (highlighted in green), followed by the configuration with the model height of 10 m, and then, of 20 m.

### **5.1.2 TEMPERATURE AND RELATIVE HUMIDITY**

During the experimental campaigns, the hourly mean observed and standard deviation of T2 (RH2) at the meteorological stations was  $24.8 \pm 3.2^\circ\text{C}$  ( $79.2 \pm 14.6\%$ ) in November,  $26.0 \pm 3.1^\circ\text{C}$  ( $75.7 \pm 14.8\%$ ) in December, and  $27.0 \pm 3.1^\circ\text{C}$  ( $77.5 \pm 13.5\%$ ) in February. Meanwhile, the WRF model set up at  $z = 4$  m simulated mean values of  $25.4 \pm 3.3^\circ\text{C}$  ( $77.5 \pm 14.4\%$ ),  $26.3 \pm 3.5^\circ\text{C}$  ( $76.5 \pm 14.9\%$ ), and  $27.2 \pm 3.5^\circ\text{C}$  ( $78.4 \pm 15.3\%$ ). The configuration with model height at 10 m had mean values of  $25.3 \pm 3.1^\circ\text{C}$  ( $77.5 \pm 14.2\%$ ),  $26.2 \pm 3.3^\circ\text{C}$  ( $76.6 \pm 14.6\%$ ), and  $26.9 \pm 3.4^\circ\text{C}$  ( $79.1 \pm 15.1\%$ ); and at  $z = 20$  m of  $25.1 \pm 2.9^\circ\text{C}$  ( $78.2 \pm 13.9\%$ ),  $25.8 \pm 3.0^\circ\text{C}$  ( $77.7 \pm 13.9\%$ ), and  $26.7 \pm 3.1^\circ\text{C}$  ( $79.6 \pm 14.6\%$ ) in November, December, and February, respectively. The time-series plots comparing hourly and diurnal variation of simulated T2 and RH2 and observed data separated by station over the three months are shown in Figures 33 and 34. Comparing observed and modelled data, one can see that the WRF model had an acceptable agreement in simulating T2 and RH2 over the MRV regardless of the model height configuration. Usually, the model overestimated T2 during the daytime and underestimated it during the nighttime. The opposite behaviour is seen for RH2 (right side of Figs. 33-34).

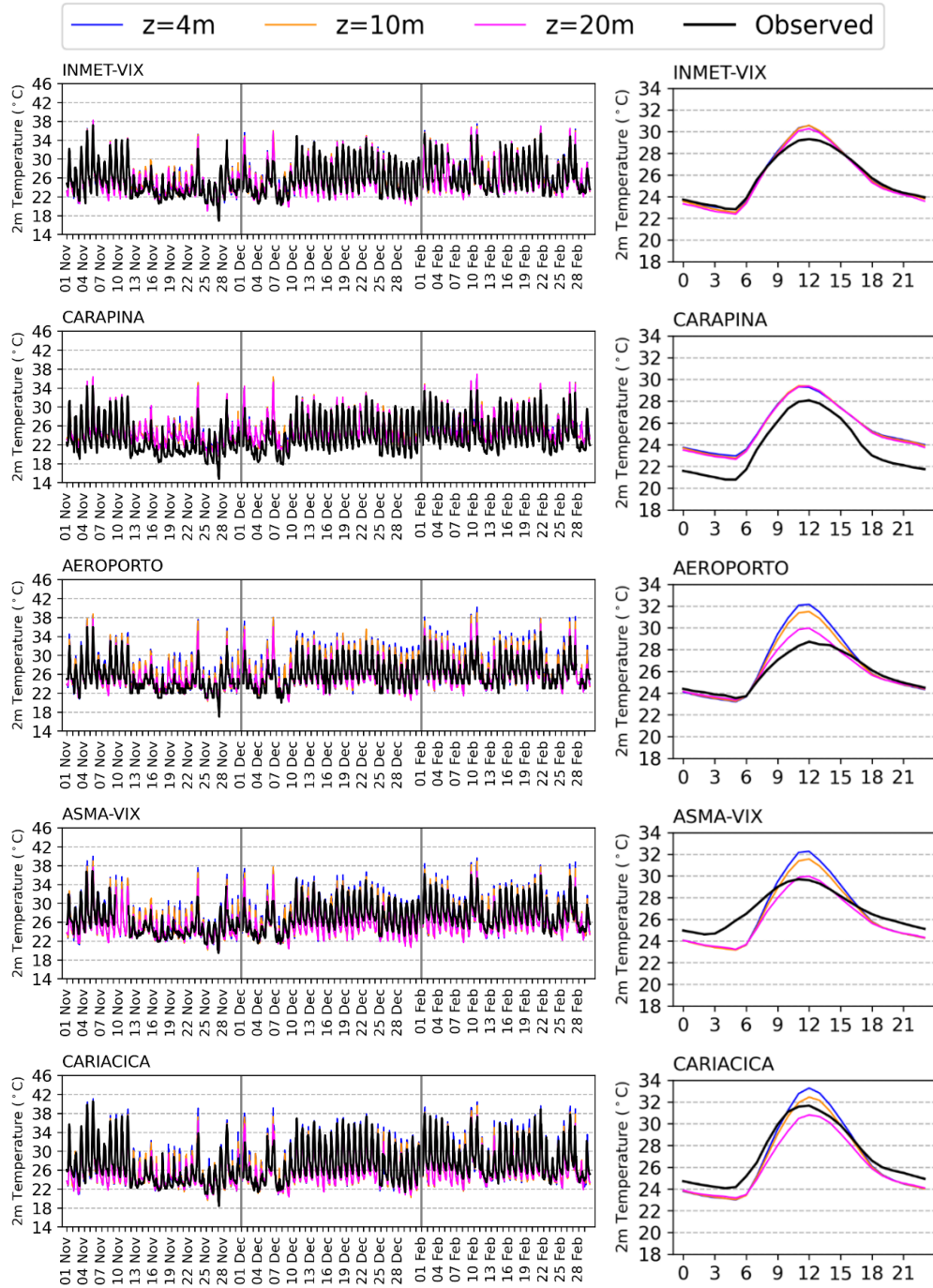


Figure 33. Comparison of T2 hourly time series (left) and mean hourly variation (right) for observed (black line) and modelled by the WRF-Urban varying the lowest model height for each monitoring site.

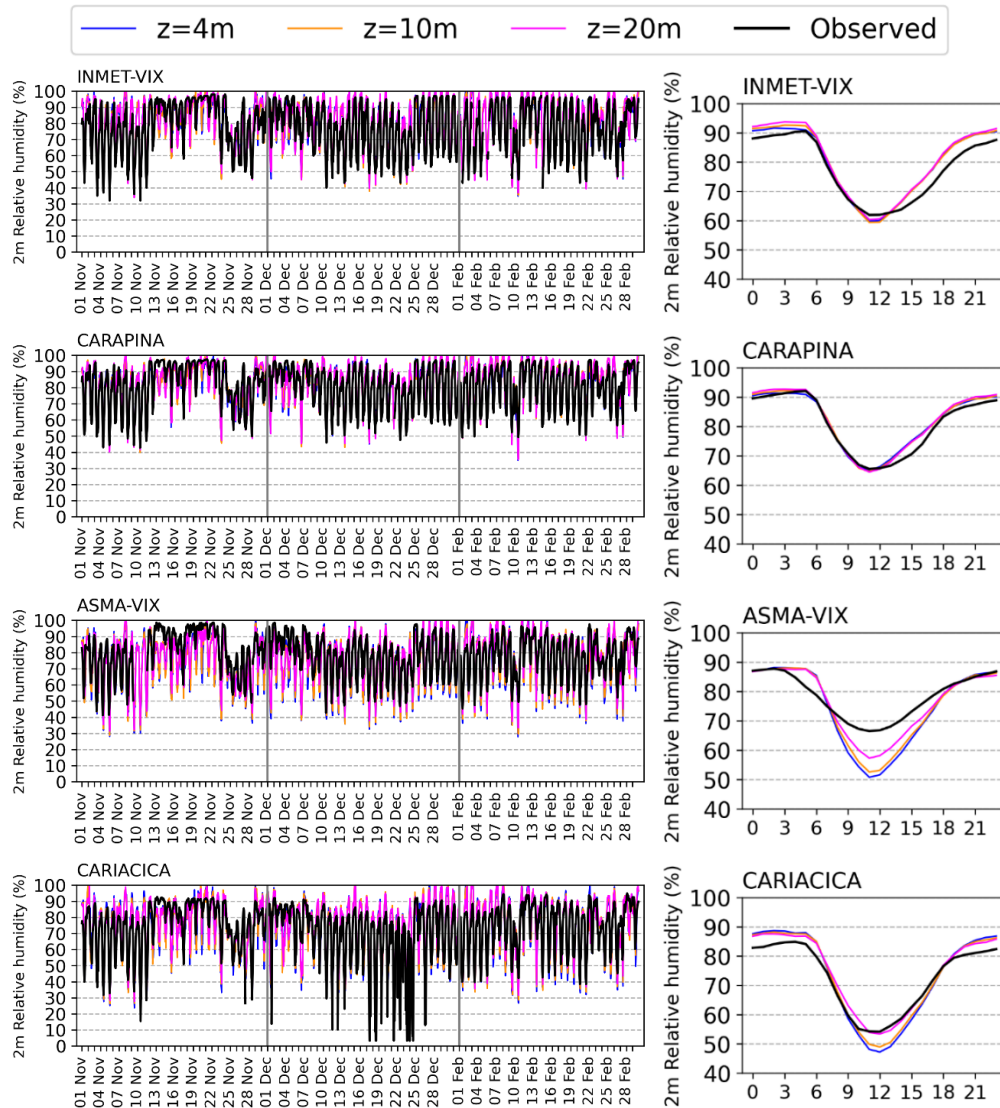


Figure 34. Comparison of RH2 hourly time series (left) and mean hourly variation (right) for observed (black line) and modelled by the WRF-Urban varying the lowest model height for each monitoring site.

The statistical analyses (Figures 35-36 and Tables S4-S5) showed the configuration with the model height of 20 m had lower errors and greater correlations for RH2 at ASMA-Vix station, and for T2 at Airport and Carapina stations throughout the three months. On the other hand, for the Cariacica station, the model height of 10 m had better results when compared to the other two configurations. Despite there being differences among the statistical indices values, they were not remarkable. As mentioned, the Kruskal-Wallis test revealed that there was no statistical difference in the statistical indices (MB, RMSE, MAGE, r, IOA) among the three configurations ( $z = 4$  m, 10 m, 20 m) for temperature and humidity. In fact, all configurations met the criteria for T2 suggested by Emery *et al.* (2001) and Hanna and Chang (2012) ( $MB \pm$

0.50;  $MAGE \leq 2.00$ ;  $IOA \geq 0.80$ ;  $FAC2 \geq 0.50$ ), except for the Carapina station in November, in which  $MAGE$  was equal to  $2.2^{\circ}\text{C}$ . The T2 (RH2) WRF-modelled mean absolute errors ( $MAGE$ ) were around  $1.5^{\circ}\text{C}$  (7.1%),  $1.5^{\circ}\text{C}$  (6.9%), and  $1.4^{\circ}\text{C}$  (6.8%) for  $z=4$  m,  $z=10$  m, and  $z=20$  m configurations, respectively.  $FAC2$  was equal to 1.00 over the entire period for both T2 and RH2. The modelled and observed data presented strong positive correlations, with  $r$ -values varying between 0.77 (ASMA-Vix) and 0.91 for T2, and between 0.72 (ASMA-Vix) and 0.87 for RH2. The  $IOA$ -values were also high, which varied between 0.87 (ASMA-Vix and Carapina) and 0.95 for T2, and between 0.84 (ASMA-Vix) and 0.92 for RH2 (Figure 35-36). The high  $r$ - and  $IOA$ -values point out that the model captures the temporal trends correctly.

Overall, the statistical analyses indicated that the lowering of the model height did not significantly affect the results of T2 and RH2 over urban surfaces (represented by Airport, ASMA-Vix, and Cariacica stations) and natural areas, which were represented by INMET-Vix and Carapina stations. However, as discussed, the WRF-Urban is activated exclusively in the grid cells assigned as ‘Urban and Built-up’ class, in which the BEP algorithm forces T2 to be equal to the values calculated at the lowest model level height, explaining the differences in the results when compared to the vegetated surfaces.

Like WS10 and WD10, the T2 results of the present study are consistent with previous studies that generally found a better statistical indices agreement using BEP (see Table 17) (Liao *et al.*, 2014; La Paz *et al.*, 2016; Sarmiento *et al.*, 2017; Franco *et al.*, 2019; M. Huang *et al.*, 2019; Avisar *et al.*, 2021). The study of Franco *et al.* (2019), which was conducted for São Paulo city, was the single study that evaluated the RH2 performance. The authors reported an MB of 0.9%,  $MAGE$  of 5.8%, and  $IOA$  of 0.95. Similarly, this study found an MB of 0.1%, 0.4%, and 1.2%,  $MAGE$  of 7.1%, 6.9%, and 6.8%, and  $IOA$  of 0.89, 0.90, and 0.90 for  $z = 4$  m,  $z = 10$  m,  $z = 20$  m, respectively.

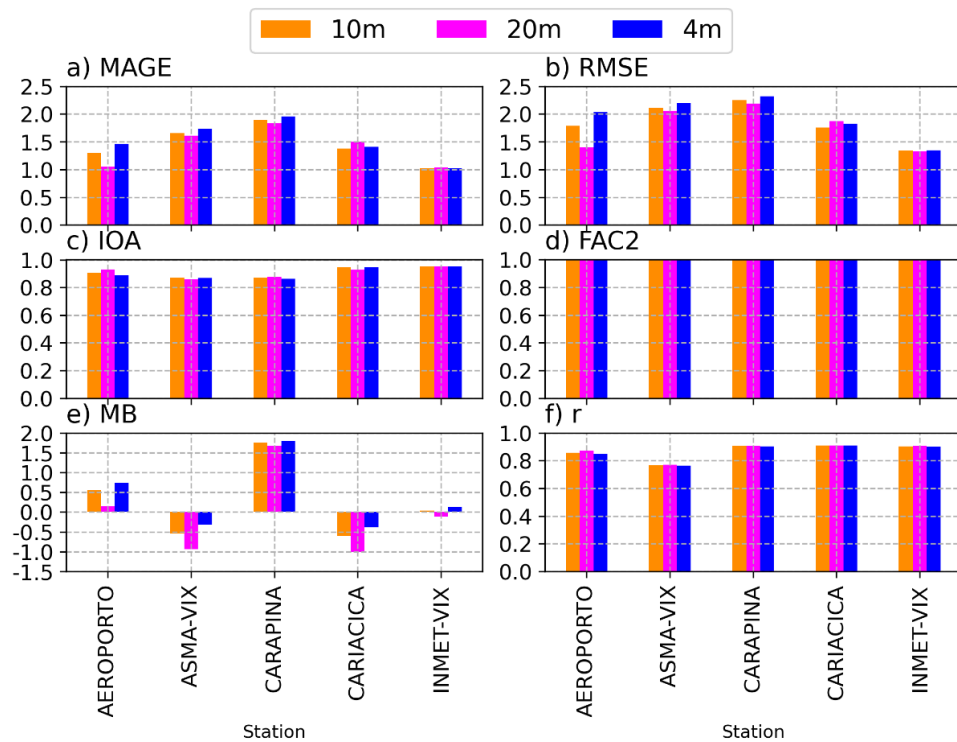


Figure 35. Comparison of the averages of statistical indices for each station and configuration, considering the three months together, for T2.

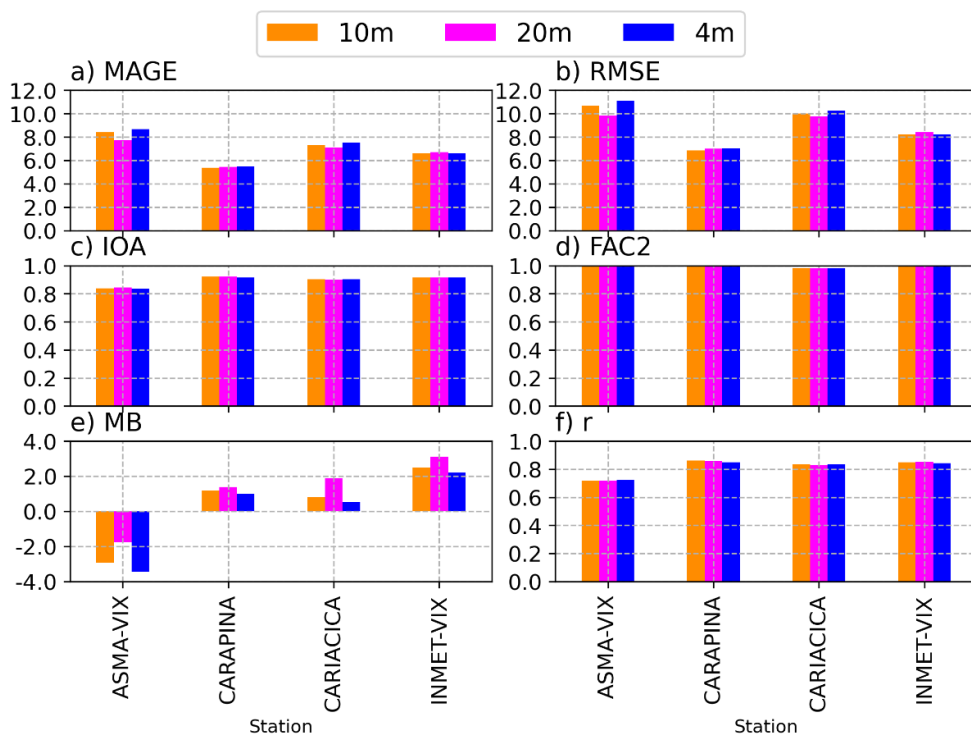


Figure 36. Comparison of the averages of statistical indices for each station and configuration, considering the three months together, for RH2.

Table 17. Comparison of the temperature performance of the present study with others found in the literature review. The values of this study were averaged among the stations.

Authors	Study Area	Statistic	Value	Period analysed
Liao <i>et al.</i> (2014)	Yangtze River Delta, China	RMSE	1.97	January, 2010
		RMSE	2.47	July, 2010
		<i>r</i>	0.91	January, 2010
		<i>r</i>	0.75	July, 2010
La Paz <i>et al.</i> (2016)	Madrid, Spain	RMSE	2.10	Annual
		IOA	0.98	
Sarmiento <i>et al.</i> (2017)	Indianapolis, US	MB	-0.20	June 15 to July 20, 2013
		MB	-0.10	February 15 to March 20, 2013
Franco <i>et al.</i> (2019)	São Paulo, Brazil	MB	0.12	October 31 to November 4, 2013
		MAGE	1.22	
		IOA	0.97	
Huang <i>et al.</i> (2018)	Beijing, China	MB	-0.16	5 to 8 July 2015
		RMSE	1.54	
		<i>r</i>	0.93	
Avisar <i>et al.</i> (2021)	Tel-Aviv Metropolitan Area, Israel	MB	-2.54	13 to 14 July 2013
		MAGE	2.61	
		RMSE	2.79	
Present study	MRV, Brazil	MAGE z=4 m	1.52	November, December/2019 and February/2020
		MAGE z=10 m	1.45	
		MAGE z=20 m	1.41	
		IOA z=4 m	0.90	
		IOA z=10 m	0.91	
		IOA z=20 m	0.91	
		<i>r</i> z=4 m	0.86	
<i>r</i> z=10 m	0.87			
<i>r</i> z=20 m	0.87			

## 5.2 THE CMAQ MODEL EVALUATION

In this section, the performance of the CMAQ model for NO<sub>2</sub>, O<sub>3</sub>, PM<sub>2.5</sub>, and PM<sub>10</sub> is presented considering the three configurations adopted by the WRF model ( $z = 4$  m,  $z = 10$  m,  $z = 20$  m) over the three months. Tables with the statistical indices of errors and correlation separated by



month, configuration, and monitoring station for the pollutants are displayed in the Appendix (Tables S6–S9). Overall, the CMAQ model overpredicted the hourly PM and NO<sub>2</sub> concentrations, and underpredicted ozone when compared to the monitoring data. The results also showed that the lowering of the model height increased the pollutant concentrations, and the most suitable performance was related to the meteorological conditions that came from WRF with the lowest model level height of 20 m. However, the differences in results due to the different configurations did not have a pronounced effect on concentrations as we observed for wind speed, e.g. from  $z = 20$  m to  $z = 4$  m. Again, the Kruskal-Wallis test revealed that there was no statistical difference in the statistical indices (MB, RMSE, MAGE, r, IOA, FAC2) among the three configurations for any of the air pollutants.

Figure 37 displays the boxplots of hourly observed NO<sub>2</sub>, O<sub>3</sub>, PM<sub>2.5</sub>, and PM<sub>10</sub> concentrations for each monitoring station in the MRV for (a) November, (b) December, and (c) February. Note that no observations of NO<sub>2</sub> were available in February at Jardim Camburi (JC) station, nor of O<sub>3</sub> at Cariacica, Enseada, IBES, and Laranjeiras in November, and at ASMA-Vix station in December and February. Similar levels of NO<sub>2</sub> were obtained over the three months in all the stations, except for the ASMA-Vix station which varied substantially compared to the other stations, with the lowest levels and less variability (mean±SD of  $6.7 \pm 3.1$  µg/m<sup>3</sup> and median of  $5.8$  µg/m<sup>3</sup>). The means of PM<sub>2.5</sub> concentrations at the ASMA-Vix station (mean/median less than  $5$  µg/m<sup>3</sup>) also were lower than at Enseada (mean/median around  $10$  µg/m<sup>3</sup>). Note that there were only two stations monitoring PM<sub>2.5</sub> in the MRV during the experimental campaigns. On the other hand, O<sub>3</sub> and PM<sub>10</sub> levels were more comparable among all the stations. O<sub>3</sub> means varied between a minimum of  $27.2 \pm 14.8$  µg/m<sup>3</sup> registered at Cariacica and a maximum of  $42.4 \pm 17.1$  µg/m<sup>3</sup> at IBES, both in February. For PM<sub>10</sub>, the means varied between a minimum of  $12.6 \pm 4.7$  µg/m<sup>3</sup> at Carapina and a maximum of  $29.9 \pm 9.7$  µg/m<sup>3</sup> at Enseada, both in November.

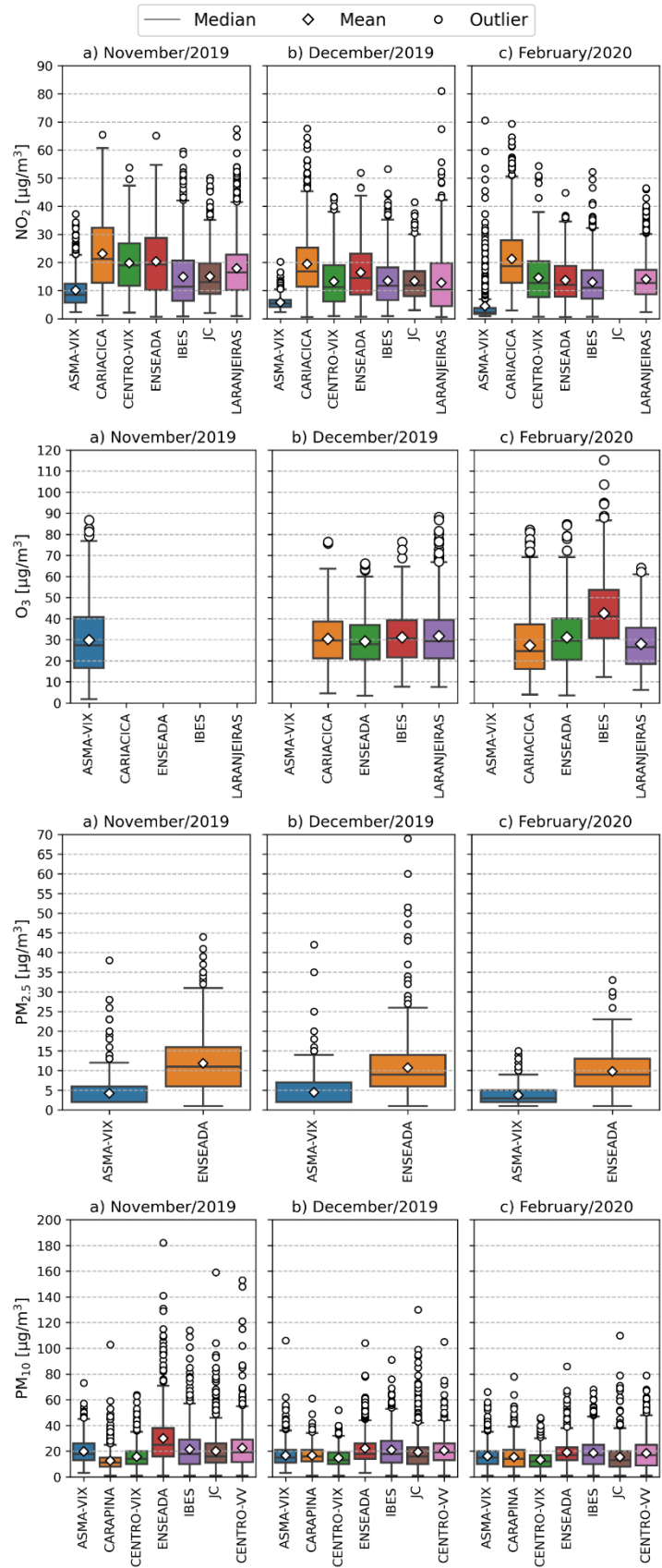


Figure 37. Boxplots of hourly observed NO<sub>2</sub>, O<sub>3</sub>, PM<sub>2.5</sub>, and PM<sub>10</sub> for each station and month.

These differences in concentrations among the stations may be related to a couple of factors, e.g. the distance of emission sources, urban landscapes, and meteorological conditions, that can favour (or not) the process of pollutant dispersion. For instance, Cariacica station is located in the parking lot of Espírito Santo Central Food Supply (CEASA - Central de Abastecimento do Espírito Santo), where there is intense traffic of vehicles, surrounded by trees and obstacles that can hinder the dispersion of pollutants and aid to trap them (Sharma and Kumar, 2018). Enseada station is placed at street level next to a busy road, which is also highly influenced by the traffic of vehicles, apart from the influence of industrial sources due to the proximity to the Tubarão Complex that has pelletizing, steel, and port activities (Galvão *et al.*, 2018). Conversely, the ASMA-Vix station was placed in a playground of a school in low traffic neighbourhood, where the principal circulation of vehicles can be related to the drop-off and pick-up of students at school. Experiments in Canada and England have already affirmed that during the drop-off and pick-up of children at school, local concentrations can significantly increase, regardless of background conditions (Adams and Requia, 2017; Kumar *et al.*, 2017), which can be represented by the outliers displayed in the boxplots.

The mean $\pm$ SD for observed NO<sub>2</sub>, O<sub>3</sub>, PM<sub>2.5</sub>, and PM<sub>10</sub> over the three months were 14.8 $\pm$ 5.4  $\mu\text{g}/\text{m}^3$ , 31.2 $\pm$ 14.2  $\mu\text{g}/\text{m}^3$ , 7.5 $\pm$ 2.1  $\mu\text{g}/\text{m}^3$ , and 18.6 $\pm$ 5  $\mu\text{g}/\text{m}^3$ , respectively. Meanwhile, the modelled mean $\pm$ SD with the configuration at  $z = 20$  m ( $z = 4$  m) were 19.6 $\pm$ 8.3 (23.0 $\pm$ 8.3)  $\mu\text{g}/\text{m}^3$ , 27.8 $\pm$ 16.6 (25.3 $\pm$ 16.9)  $\mu\text{g}/\text{m}^3$ , 9.5 $\pm$ 3.4 (12.0 $\pm$ 4.4)  $\mu\text{g}/\text{m}^3$ , and 20.5 $\pm$ 6.7 (26.1 $\pm$ 8.6)  $\mu\text{g}/\text{m}^3$  for NO<sub>2</sub>, O<sub>3</sub>, PM<sub>2.5</sub>, and PM<sub>10</sub>, respectively. The modelled mean $\pm$ SD for  $z = 10$  m fell between the values of the  $z = 20$  m and  $z = 4$  m configurations, with 20.8 $\pm$ 8  $\mu\text{g}/\text{m}^3$ , 26.5 $\pm$ 16.8  $\mu\text{g}/\text{m}^3$ , 10.6 $\pm$ 9.9  $\mu\text{g}/\text{m}^3$ , and 22.9 $\pm$ 7.2  $\mu\text{g}/\text{m}^3$  for NO<sub>2</sub>, O<sub>3</sub>, PM<sub>2.5</sub>, and PM<sub>10</sub>, respectively. Figures 38, 39, 40, and 41 show time series plots for the air pollutant concentrations together with the mean daily variations. The vertical bars indicate the standard deviation of the pollutants concentrations measured at the air quality stations. NO<sub>2</sub>, PM<sub>2.5</sub>, and PM<sub>10</sub> are displayed as 24-hour averages and the maximum daily 8-hour average (MDA8) for O<sub>3</sub> in order to compare the concentration levels in the MRV with the final standard of WHO (2021) and to evaluate the CMAQ performance through the proposed goals and criteria, which usually are based on 24-hour means (Boylan and Russell, 2006; Emery *et al.*, 2017). The WHO (2021) has lowered by 5  $\mu\text{g}/\text{m}^3$  the limits for PM<sub>2.5</sub> (from 25  $\mu\text{g}/\text{m}^3$  to 15  $\mu\text{g}/\text{m}^3$ ) and PM<sub>10</sub> (from 50  $\mu\text{g}/\text{m}^3$  to 45  $\mu\text{g}/\text{m}^3$ ) when compared to the previous air quality guidelines. The 24-hour guideline for NO<sub>2</sub> (25  $\mu\text{g}/\text{m}^3$ ) has been additionally introduced, and for O<sub>3</sub>, the MDA8 standard remains the same at 100  $\mu\text{g}/\text{m}^3$ .

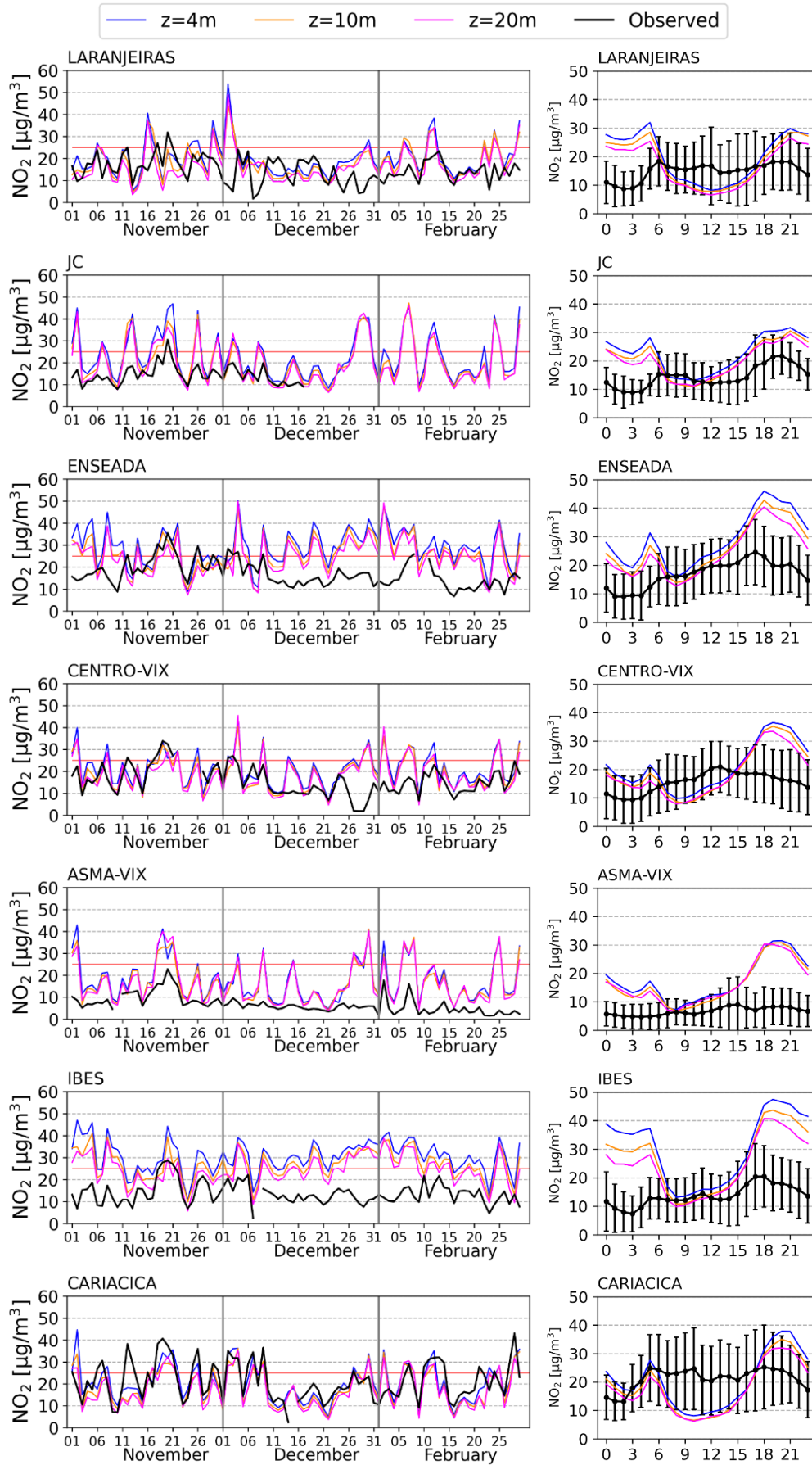


Figure 38. Comparison of observed and modelled 24-h average NO<sub>2</sub> (left) and mean hourly variation (right) for each monitoring station and model's configuration. The red line represents the final standard of WHO 2021 (25 µg/m<sup>3</sup>).

Figure 38 exhibits that observed NO<sub>2</sub> concentrations exceeded the air quality standard established by the WHO (2021) at all monitoring stations, except for the ASMA-Vix station. Cariacica was the place that most exceeded the air quality standard (31 times) over the three months, followed by Enseada (12 times), Centro-Vix (7 times), IBES and Laranjeiras (both 3 times). The modelled results enhanced the number of times that air quality limits were surpassed because NO<sub>2</sub> concentrations were overpredicted by the CMAQ model. On average, NO<sub>2</sub> was overestimated by 9.7 µg/m<sup>3</sup> ( $z = 4$  m), 7.5 µg/m<sup>3</sup> ( $z = 10$  m), and 6.2 µg/m<sup>3</sup> ( $z = 20$  m) by CMAQ model when compared with observations. However, this bias typically was compensated by an underestimation during the day and an overestimation during the night. The daily average profiles of NO<sub>2</sub> observations indicate that concentrations started to increase from 4 a.m. local time (LT) (3 a.m. for Cariacica and 7 a.m. for ASMA-Vix) with the first peak corresponding to the traffic peak between 6–7 a.m. LT. After that, the concentrations remained nearly constant with slight increases and decreases until reaching the second peak which occurred between 6–7 p.m. The concentrations of the second peak usually were greater than the first peak, except for Cariacica and Laranjeiras where both peaks had the same levels. The higher concentrations of the second peak might be a result of continuous NO<sub>x</sub> emission throughout the day together with the reaction between NO and O<sub>3</sub> to form NO<sub>2</sub> at night when the photolysis reaction of NO<sub>2</sub> is stagnant, resulting in its gradual accumulation (Wang *et al.*, 2020). In urban centers, NO<sub>2</sub> is recognized as mainly originating from vehicular emissions (Janssen *et al.*, 2001; Kornartit *et al.*, 2010), a fact that was well-pictured in the first semester of 2020, during the COVID-19 pandemic. The studies showed that due to restricted movements, NO<sub>2</sub> concentrations decreased between 30% and 60% when compared to previous periods (Baldasano, 2020; Dantas *et al.*, 2020; Salma *et al.*, 2020; Jephcote *et al.*, 2021). However, that is not the case of the MRV, which has a peculiar arrangement and NO<sub>2</sub> is not mostly exclusively emitted by vehicular sources. The local emission inventory pointed out that the major contributor of NO<sub>x</sub> emissions in the region is the industrial sources, especially those related to the pelletizing-siderurgy activities, which are located together in the same port complex and relatively near the population residences.

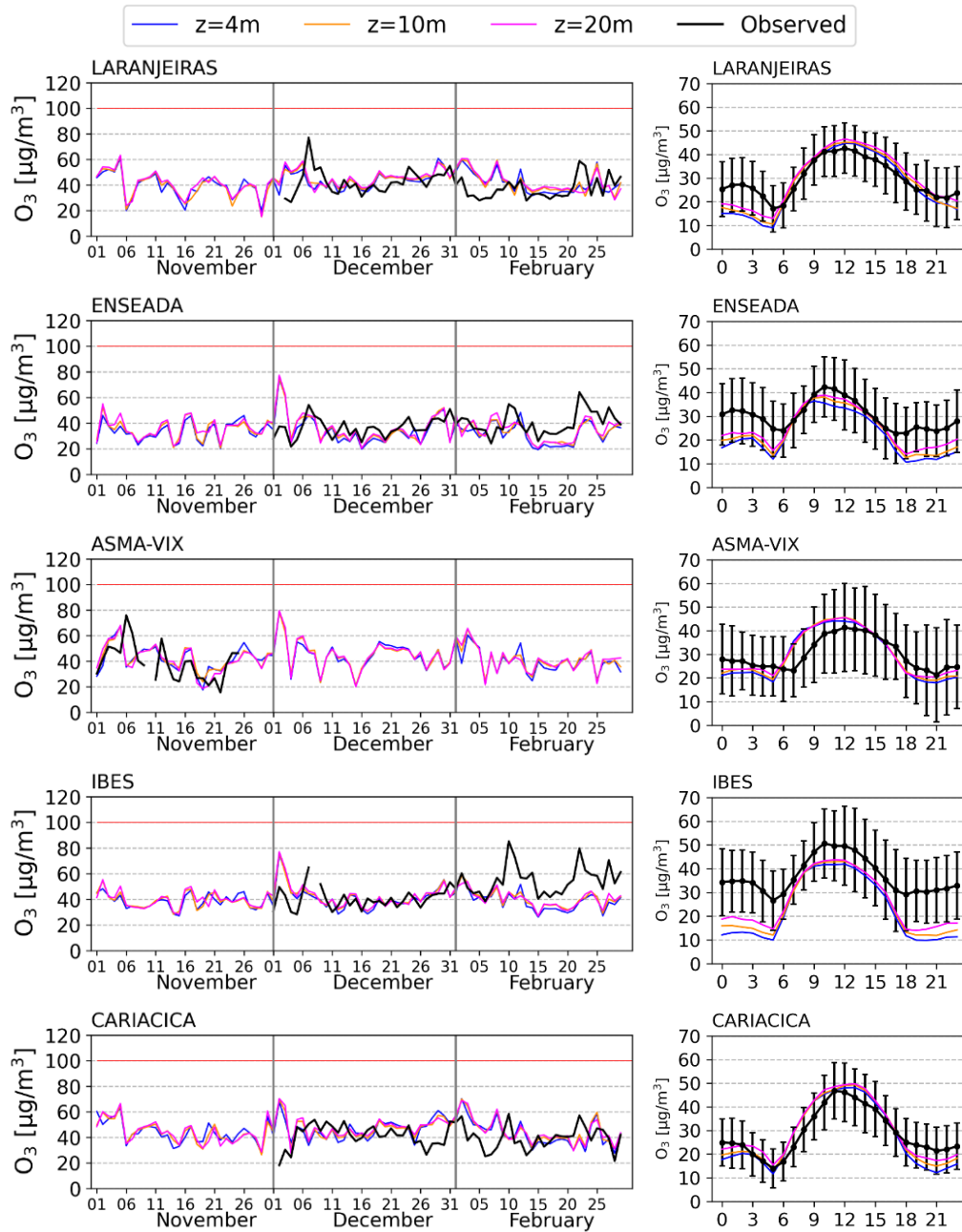


Figure 39. Comparison of observed and modelled MDA8 O<sub>3</sub> (left) and mean hourly variation (right) for each monitoring station and model's configuration. The red line represents the final standard of WHO 2021 (100 µg/m<sup>3</sup>).

Differently from NO<sub>2</sub>, O<sub>3</sub> concentrations (Figure 39) did not exceed the air quality standard of WHO (2021). However, it is important to highlight the quantitative lack of observed O<sub>3</sub> data over the three months, which could indicate opposite results. The model adequately simulated the O<sub>3</sub> variations and concentrations, despite MB indicating that all configurations

overestimated MDA8 O<sub>3</sub> (except for Enseada station and IBES in February), but underestimated hourly O<sub>3</sub> by  $-6.2 \mu\text{g}/\text{m}^3$  ( $z = 4 \text{ m}$ ),  $-4.9 \mu\text{g}/\text{m}^3$  ( $z = 10 \text{ m}$ ), and  $-3.6 \mu\text{g}/\text{m}^3$  ( $z = 20 \text{ m}$ ) when compared to observations. The daily average profiles of O<sub>3</sub> observations indicate that concentrations started to increase from 6 a.m. local time (LT) (7 a.m. for ASMA-Vix) with the maximum peak occurring between 10 a.m. and 12 p.m. L.T. After that, the concentrations slightly started to decrease until reached the minima at late night/dawn. The general trend of O<sub>3</sub> concentrations confirms that the production of ozone is induced by the presence of sunlight, high temperature, low winds, and its precursors. The correlation matrix showed that O<sub>3</sub> strongly correlated ( $r$  higher than 0.8) with temperature, relative humidity, and wind speed at all monitoring stations, except for Enseada ( $r \approx 0.6$ ).

PM<sub>2.5</sub> (Fig. 40) and PM<sub>10</sub> (Fig. 41) levels also exceeded the air quality standard by 10 and 3 times at Enseada, respectively. No exceeding of the limits was observed at the other stations over the three months, despite the modelled data indicating the opposite, especially on 2-7 November, 28-30 December, and 6-7-11 February. On average, PM<sub>2.5</sub> and PM<sub>10</sub> were overestimated by  $4.5$  and  $8.6 \mu\text{g}/\text{m}^3$  ( $z = 4 \text{ m}$ ),  $3.8$  and  $5.6 \mu\text{g}/\text{m}^3$  ( $z = 10 \text{ m}$ ), and  $2.9$  and  $3.7 \mu\text{g}/\text{m}^3$  ( $z = 20 \text{ m}$ ) by CMAQ model, respectively. The modelled daily average variations were similar for both PM, which portrayed two peaks throughout the day, like NO<sub>2</sub>, correlating to the traffic rush hours. However, the observations revealed a different pattern in which the concentrations started to increase from 4 a.m. L.T., remained slightly increasing over the day, until they started to decrease at the beginning of the night, except at JC station where the concentrations kept increasing, with a maximum at 9 p.m. L.T. The vertical bars also indicated a high variability of the hourly data over the days. Intriguingly, the daily average cycle of PM and NO<sub>2</sub> were strongly correlated at all monitoring stations, indicating that these pollutants may have the same source of emission. The correlation coefficient values were 0.98 (CENTRO-Vix), 0.92<sub>PM10</sub> and 0.75<sub>PM2.5</sub> (ASMA-Vix), 0.83<sub>PM10</sub> and 0.94<sub>PM2.5</sub> (Enseada), 0.78 (JC), 0.76 (Laranjeiras), and 0.75 (IBES).

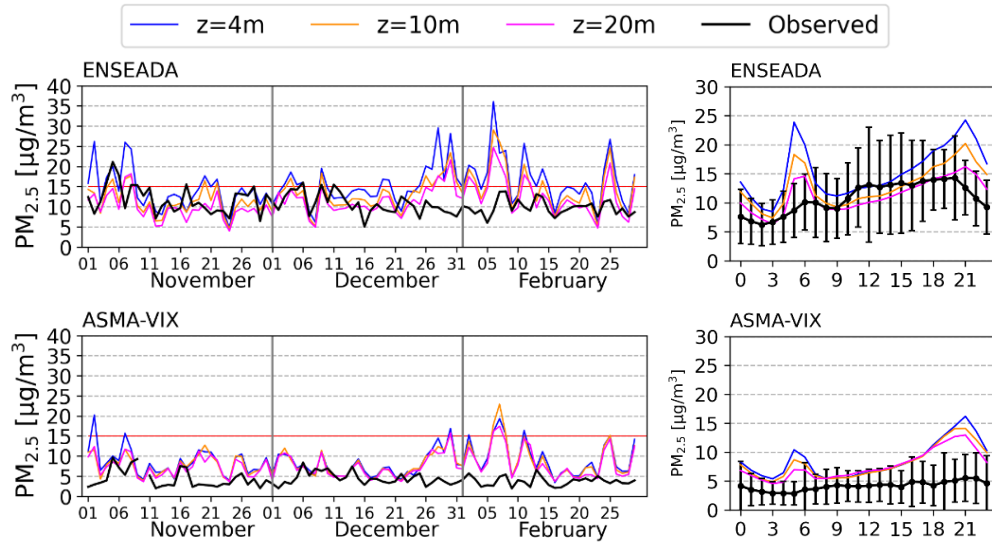
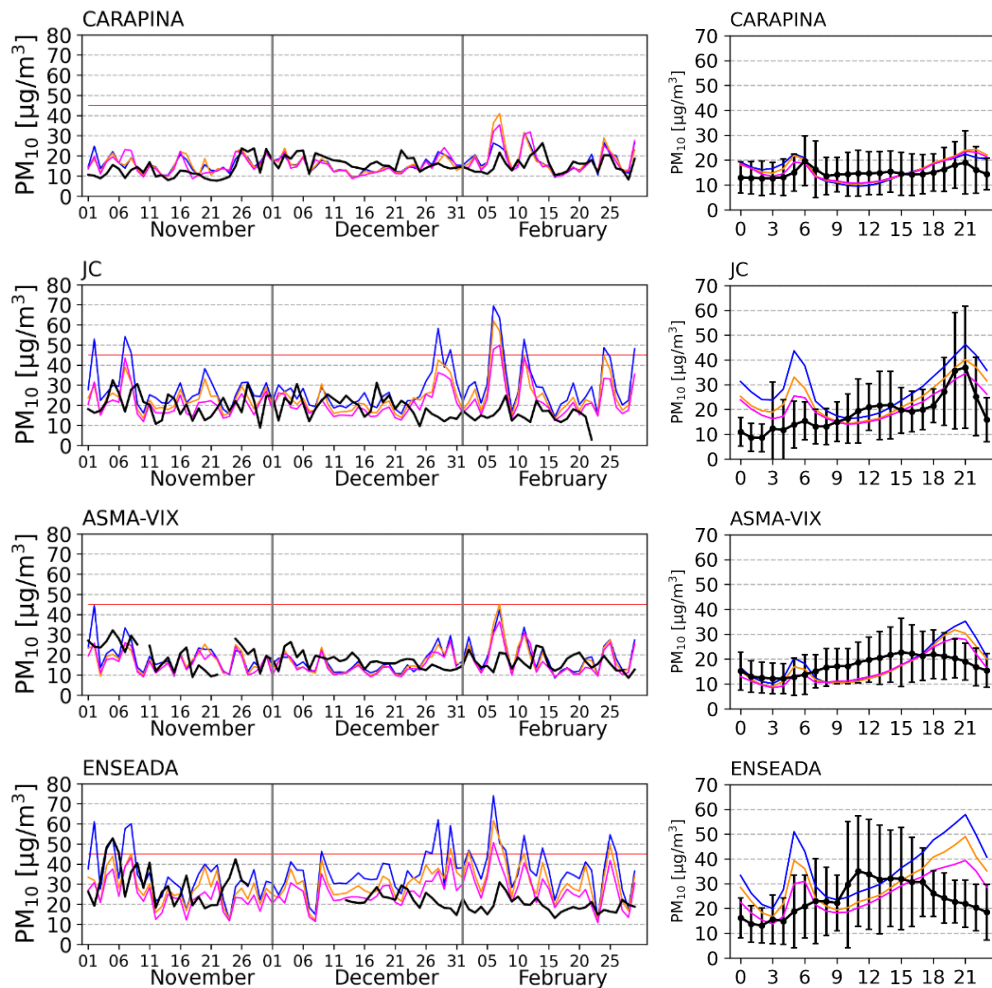


Figure 40. Comparison of observed and modelled 24-h average  $PM_{2.5}$  (left) and mean hourly variation (right) for each monitoring station and model's configuration. The red line represents the final standard of WHO 2021 ( $15 \mu g/m^3$ ).





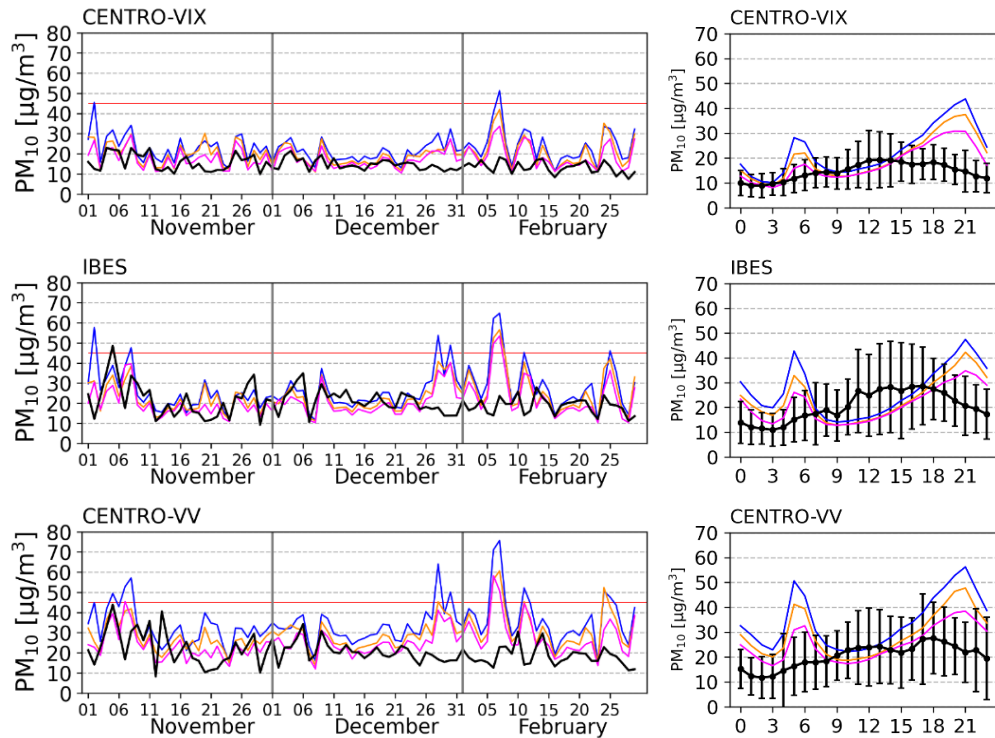


Figure 41. Comparison of observed and modelled 24-h average  $PM_{10}$  for each monitoring station and model's configuration. The red line represents the final standard of WHO 2021 ( $45 \mu\text{g}/\text{m}^3$ ).

The comparison among the three configurations exposed that the lowering of the lowest model level height increased the concentrations and enlarged the overprediction of  $NO_2$ ,  $PM_{2.5}$ , and  $PM_{10}$  when compared to observations, while the opposite behaviour was seen for  $O_3$ . Higher temperature and lower wind speed magnitudes, as emulated by the configuration  $z = 4 \text{ m}$  in comparison with the other two configurations, affected the dispersion of the pollutants and increased their concentrations near-surface. In this sense, the better agreement of modelled WS10 with observations using the model height at  $4 \text{ m}$  did not reflect an improvement in the CMAQ results when compared to air quality observations. Additionally, it is worth mentioning that the use of  $z = 4 \text{ m}$  also implied higher computational costs due to the high vertical resolution close to the ground. The overprediction of air pollutant concentrations not only can be related to low wind speed values ( $<1 \text{ m/s}$ ) simulated by the WRF model, especially during the nighttime, but also it can be attributable to a limitation in the representation of nocturnal PBL and atmospheric chemistry, and inaccuracies in the temporal profiles of the emissions inventory (Shin *et al.*, 2012; Liao *et al.*, 2014; La Paz *et al.*, 2016; Huang *et al.*, 2019). The configuration  $z = 4 \text{ m}$  augmented the mean concentrations of  $PM_{10}$  ( $+5.5 \mu\text{g}/\text{m}^3$ ),  $PM_{2.5}$  ( $+2.6 \mu\text{g}/\text{m}^3$ ) and  $NO_2$  ( $+3.4 \mu\text{g}/\text{m}^3$ ) when compared to the simulations with  $z = 20 \text{ m}$ . This effect was the opposite for

O<sub>3</sub> (−2.5 μg/m<sup>3</sup>). In comparison with  $z = 10$  m, the mean concentrations followed the same trend of  $z = 20$  m, but with fewer differences +3.2, +1.4, +2.2, and −1.3 μg/m<sup>3</sup>, respectively. Together with the lowering of the model height, the use of BEP also can be pointed to as a source of contribution to increasing the concentrations. La Paz *et al.* (2016) reported that the use of BEP increased the simulated NO<sub>2</sub> concentrations in the city of Madrid by 40% (or 10 μg/m<sup>3</sup>), especially during the summer season due to higher simulated temperatures, in comparison with bulk schemes. Similarly, the PM<sub>10</sub> concentrations were 32.7% (or 18.3 μg/m<sup>3</sup>) higher in Hangzhou city during summer (Liao *et al.*, 2014) when compared to the non-use of BEP. According to the authors, the wind speed and the diffusion condition influenced the PM<sub>10</sub> spatial distributions, leading to its accumulation over the urban areas. Similar results also were found in Franco *et al.* (2019) who reported a better representation of the meteorological fields over São Paulo city considering BEP parameterization, but the same was not achieved for the ozone surface concentrations.

Regarding the CMAQ performance, Boylan and Russel (2006) proposed the use of the mean fractional bias (MFB) and the mean fractional error (MFE) as indicators to evaluate the robustness of air quality models. They stated that if the MFB value was between −60% and 60% and the MFE was less than 75%, the model simulation result could be considered to be within an acceptable range. Although, the model performance goal would be to meet the criteria of MFB between −30% and 30% and MFE less than 50%. Recently, Emery *et al.* (2017) suggested a more restrictive range of values through the statistics of normalized mean bias (NMB) and normalized mean error (NME). They proposed that if the NMB value was between ±50% (±35%) and the NME is less than 35% (10%), the simulations could be considered to be within an acceptable (goal) range. MDA8 O<sub>3</sub> adhered to different values which considered NME (NMB) goal of <15% (<±5%) and criteria of < 25% (<±15%). Figure 42 presents the CMAQ statistical metrics for NO<sub>2</sub>, O<sub>3</sub>, PM<sub>2.5</sub>, and PM<sub>10</sub> based on Emery's recommendations which are more conservative when compared to those suggested by Boylan and Russel (2006).

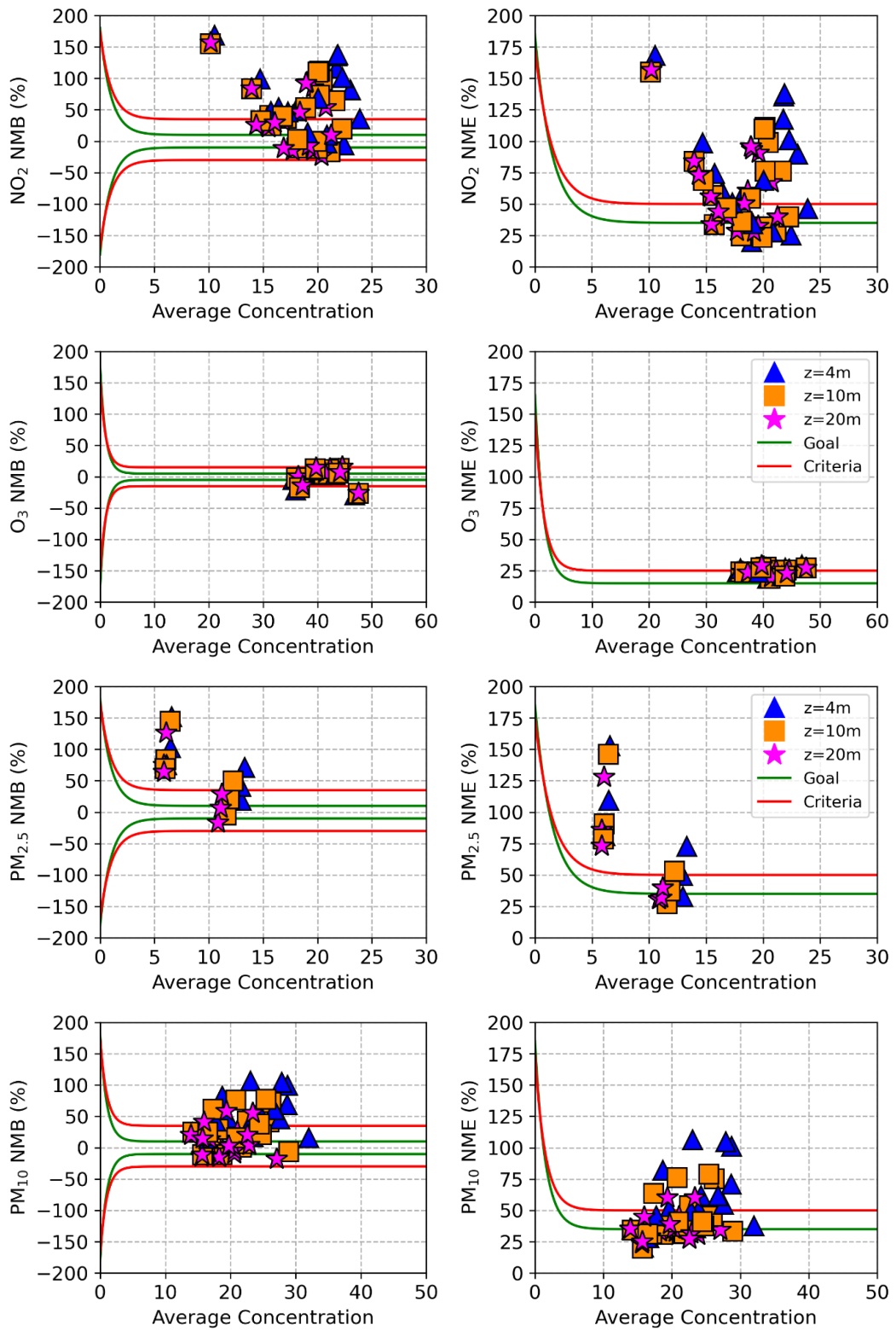


Figure 42. NME and NMB for 24-h averages of NO<sub>2</sub>, PM<sub>2.5</sub>, and PM<sub>10</sub>. The NME (NMB) goal (green line) and criteria (red line) considered <35% (<±10%) and <50% (<±30%), respectively. For MDA8 O<sub>3</sub>, NME (NMB) goals and criteria were <15% (<±5%) and < 25% (<±15%), respectively.

The three configurations had similar results, especially for O<sub>3</sub> which the markers (that varied by station and month) fell close to each other. Even so, overall, the configuration  $z = 20$  m (★ in Fig. 42) was the one that most met Emery's criteria of NMB ( $\pm 35\%$ ) and NME ( $< 35\%$ ). The model predicted well O<sub>3</sub> concentrations with slight underprediction in February at Enseada and IBES stations. Likewise, the model also had a good performance for PM<sub>10</sub> and the NMB goal ( $\pm 35\%$ ) and the NME criteria ( $< 35\%$ ) were met. Positive NMB was found in all months and stations (except for Cariacica), indicating the model overpredicted the NO<sub>2</sub> concentrations. For PM<sub>2.5</sub>, the model performance was completely different between the only two stations available in the region. The PM<sub>2.5</sub> concentrations measured at the ASMA-Vix station ( $4.2 \pm 1.6 \mu\text{g}/\text{m}^3$ ) were lower than Enseada ( $10.8 \pm 2.6 \mu\text{g}/\text{m}^3$ ). The low values were not depicted by the model, which grossly overpredicted PM<sub>2.5</sub> over the three months, with NMB means of 110% ( $z = 4$  m), 99% ( $z = 10$  m), and 88% ( $z = 20$  m). Meanwhile, at Enseada, PM<sub>2.5</sub> was well represented and met the performance NMB goal ( $\pm 35\%$ ), especially using the configuration  $z = 20$  m. Nevertheless, NME and NMB can grow disproportionately for overpredictions scenarios because it gives more weight to them than underpredictions (Zhang *et al.*, 2012). Therefore, it is important to bolster NME and NMB indicators with other types of statistical measure that addresses variability over the entire range of prediction–observation pairs (Emery *et al.*, 2017). Tables S6 (NO<sub>2</sub>), S7 (O<sub>3</sub>), S8 (PM<sub>2.5</sub>), and S9 (PM<sub>10</sub>) present the statistical indices split by station and month. The agreement indices had varied results, with some stations having low  $r$ , IOA, and FAC2-values, while others reached the criteria benchmarks of  $r > 0.5$  for O<sub>3</sub> and  $r > 0.40$  for PM (Emery *et al.*, 2017), and FAC2  $> 0.5$  (Hanna and Chang, 2012). A comparison of the statistical indices between this study and other studies that also evaluated air quality models' performance using BEP is presented in Table 18 (NO<sub>2</sub>). The studies carried out in the city of Madrid, Spain (La Paz *et al.*, 2016; Martilli *et al.*, 2022), had higher errors when compared to the present study, but IOA-value was higher. Wang *et al.* (2021), that performed sensitivity experiments over Chengdu, southwestern China, found MFE= 34.3% and  $r=0.36$  (MFE= 34.4%,  $r=0.31$ ) for NO<sub>2</sub> (PM<sub>2.5</sub>) in winter. However, during the summer, the concentrations were more overestimated, with MFE of 44.6% and  $r=0.36$  for NO<sub>2</sub> (MFE= 44.6%,  $r=0.31$  for PM<sub>2.5</sub>). This study also found similar NO<sub>2</sub> MFE ( $\approx 50 \mu\text{g}/\text{m}^3$ ), but higher PM<sub>2.5</sub> MFE ( $\approx 60 \mu\text{g}/\text{m}^3$ ) than Wang *et al.* (2021). O<sub>3</sub> RMSE was about  $17 \mu\text{g}/\text{m}^3$  while the other studies had higher errors, except for Liao *et al.* (2014) in the winter (Table 19). The IOA-values were close to 0.70 for all configurations, meanwhile, La Paz *et al.* (2016) reported an IOA of 0.60 and Franco *et al.* (2019) of 0.80. In this study, the averages of MFE were 67% for  $z = 4$  m,

62% for  $z = 10$  m, and 58% for  $z = 20$  m, with the  $r$ -values equal to 0.53 for all configurations. Similar results were also found in a previous study in the same study area (Pedruzzi *et al.*, 2019). The authors found MFE of 48%, RMSE of  $19 \mu\text{g}/\text{m}^3$ , and  $r$  of 0.39 for  $\text{O}_3$ , while for  $\text{PM}_{10}$ , MFE was 64%,  $\text{RMSE} = 30 \mu\text{g}/\text{m}^3$ , and  $r = 0.23$ . For  $\text{PM}_{10}$ , the averages of MFE (RMSE) were 41% ( $13 \mu\text{g}/\text{m}^3$ ) for  $z = 4$  m, 36% ( $10 \mu\text{g}/\text{m}^3$ ) for  $z = 10$  m, and 33% ( $9 \mu\text{g}/\text{m}^3$ ) for  $z = 20$  m.

Table 18. Comparison of  $\text{NO}_2$  performance of the present study with others found in the literature review. The values of this study were averaged among the stations.

Study	Study Area	Statistic	Value	Period
La Paz <i>et al.</i> (2016)	Madrid, Spain	MB	1.5	Annual
		RMSE	41.0	
		IOA	0.68	
Jiang <i>et al.</i> (2020)	Paris, France	MB	-5.1	27 <sup>th</sup> November to 4 <sup>th</sup> December 2016
		RMSE	2.9	
		$r$	0.79	
Wang <i>et al.</i> (2021)	Chengdu, China	MFB	37.2	January 2017
		MFE	34.3	
		$r$	0.36	
		MFB	49.7	July 2017
		MFE	44.6	
$r$	0.36			
Martilli <i>et al.</i> (2022)	Madrid, Spain	MB	-12.8	22 <sup>nd</sup> to 30 <sup>th</sup> December 2016
		RMSE	38.0	
		IOA	0.68	
		$r$	0.49	
Present study	MRV, Brazil	MB $z=4$ m	8.2	Nov/2019 Dec/2019 Feb/2020
		MB $z=10$ m	6.0	
		MB $z=20$ m	4.8	
		RMSE $z=4$ m	12.1	
		RMSE $z=10$ m	10.8	
		RMSE $z=20$ m	10.5	
		IOA $z=4$ m	0.47	
		IOA $z=10$ m	0.49	
IOA $z=20$ m	0.49			

Table 19. Comparison of O<sub>3</sub> performance of the present study with others found in the literature review. The values of this study were averaged among the stations.

Study	Study Area	Statistic	Value	Period
Liao <i>et al.</i> (2014)	Yangtze River Delta, China	MB	-1.20	January, 2010
		RMSE	7.50	
		<i>r</i>	0.55	
		MB	-11.00	July, 2010
		RMSE	29.80	
		<i>r</i>	0.52	
La Paz <i>et al.</i> (2016)	Madrid, Spain	MB	25.00	Annual
		RMSE	46.00	
		IOA	0.57	
Franco <i>et al.</i> (2019)	São Paulo, Brazil	MB	-11.28	October 31 to November 4, 2013
		RMSE	33.36	
		IOA	0.80	
		NMB	-21.17	
Present study	MRV, Brazil	MB z=4 m	-6.20	Nov/2019 Dec/2019 Feb/2020
		MB z=10 m	-4.90	
		MB z=20 m	-3.60	
		RMSE z=4 m	17.30	
		RMSE z=10 m	16.80	
		RMSE z=20 m	16.50	
		IOA z=4 m	0.68	
		IOA z=10 m	0.69	
		IOA z=20 m	0.69	
		<i>r</i> z=4 m	0.53	
		<i>r</i> z=10 m	0.53	
<i>r</i> z=20 m	0.52			

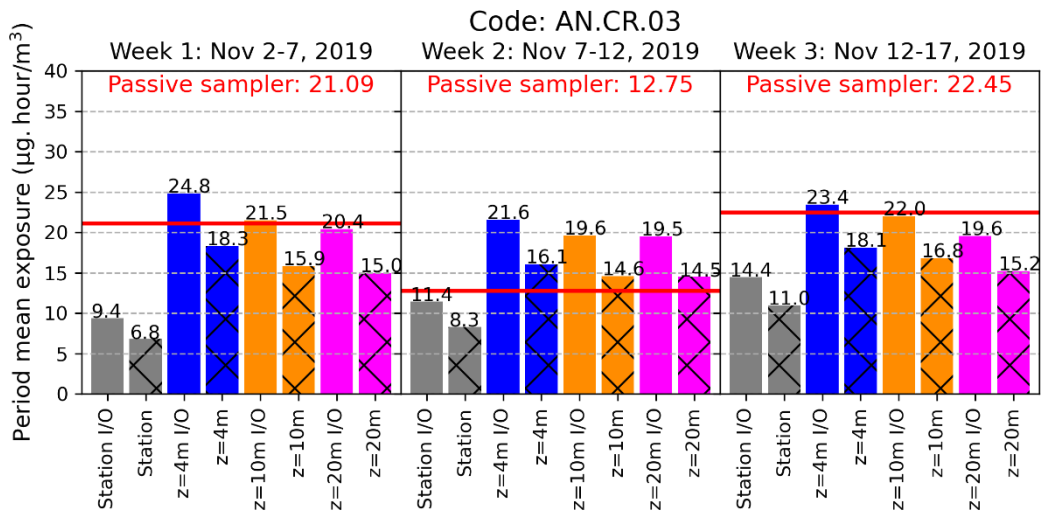
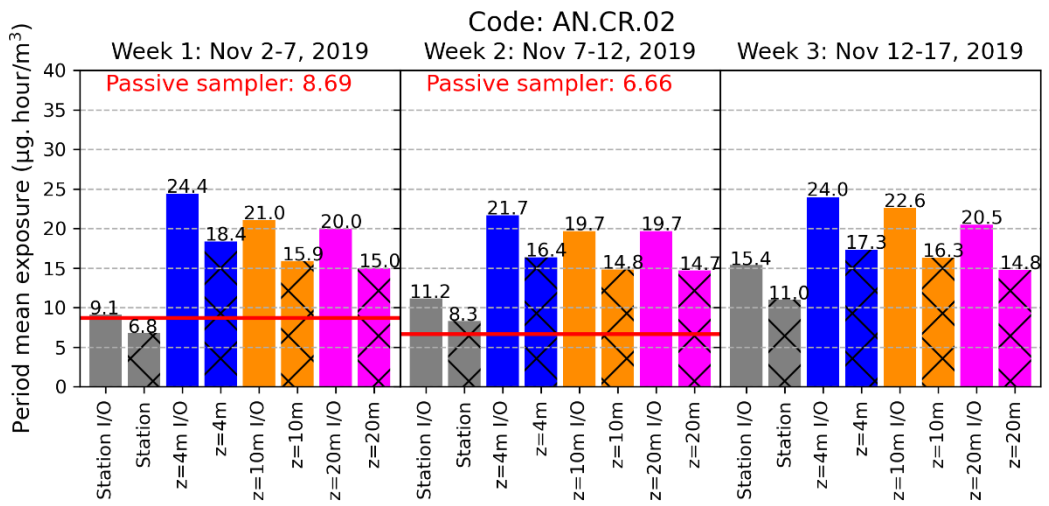
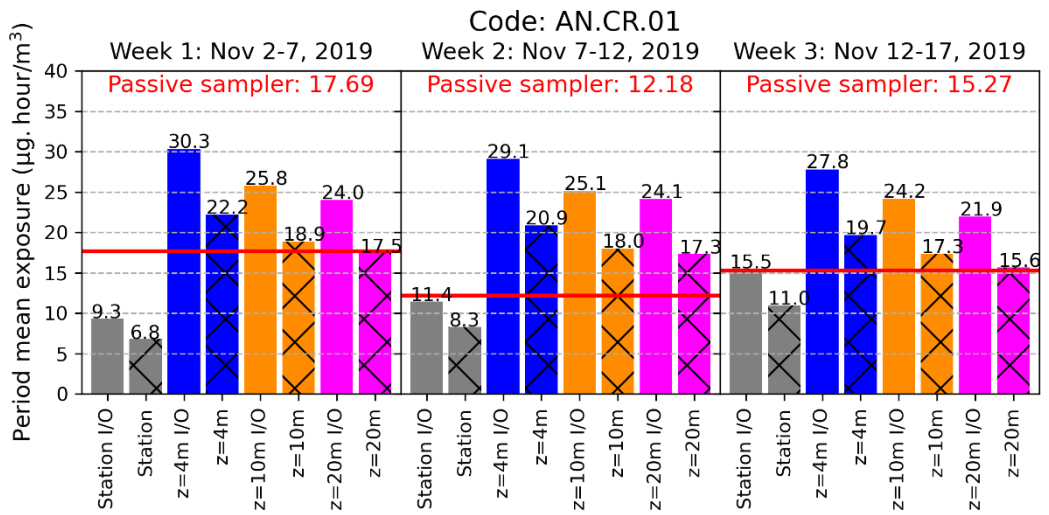
Overall, the CMAQ model overpredicted the PM and NO<sub>2</sub>, and underpredicted ozone when compared to the monitoring data. These results can infer that either the modelling is overestimating concentrations, either the monitoring stations are not placed in the neighbourhoods with higher concentrations, which may contribute to underestimating the city-level concentration; or the combination of both situations. Additionally, other sources of bias in model predictions are related to uncertainties in emission inventory (Hu *et al.*, 2016), chemical mechanisms (Kitayama *et al.*, 2019), and boundary conditions (Pedruzzi *et al.*, 2019). Therefore, it can be assumed that the CMAQ model suitably simulated air pollutant

concentrations over the MRV because the representation of air pollutant concentrations by models without bias is a complex task. After all, modelling cannot capture some local features and there is also a lack/few observed monitoring data (Andreão *et al.*, 2020).

### 5.3 PERSONAL EXPOSURE TO NO<sub>2</sub>: COMPARISON WITH PERSONAL DATA

In this section, it is presented the assessment of personal exposure of twenty-one children to NO<sub>2</sub> based on concentrations estimated by the CMAQ model. The results obtained using the chemical transport model were compared to passive samplers wore by children and also to the monitoring station placed close to their homes and schools. In addition, indoor/outdoor ratios were used to consider the amount of time spent indoors by children in homes and schools. Thus, eight scenarios are evaluated using data from the ASMA-Vix station and the three configurations of the CMAQ model ( $z = 4$  m,  $z = 10$  m,  $z = 20$  m). Each one considered two approaches (i) using I/O equal to 1, that is assuming no indoor correction, and (ii) using I/O values to represent differences between indoor and outdoor concentrations of home and school microenvironments (values were exhibited in Table 13).

Figures 43, 44, and 45 present the exposures calculated for the aforementioned scenarios for six children in Campaign 1 (November 2-17, 2019) in Andorinhas (Code #AN.CR.0\*), six children in Campaign 2 (December 4-19, 2019) in Maruípe (Code #MA.CR.0\*), and nine children in Campaign 3 (February 12-19, 2020) in Itararé (Code #IT.CR.0\*). As mentioned, in C1 and C2, the filters were changed every 5 days over three weeks, while in C3, children used the personal sampler over 7 days of one single week.





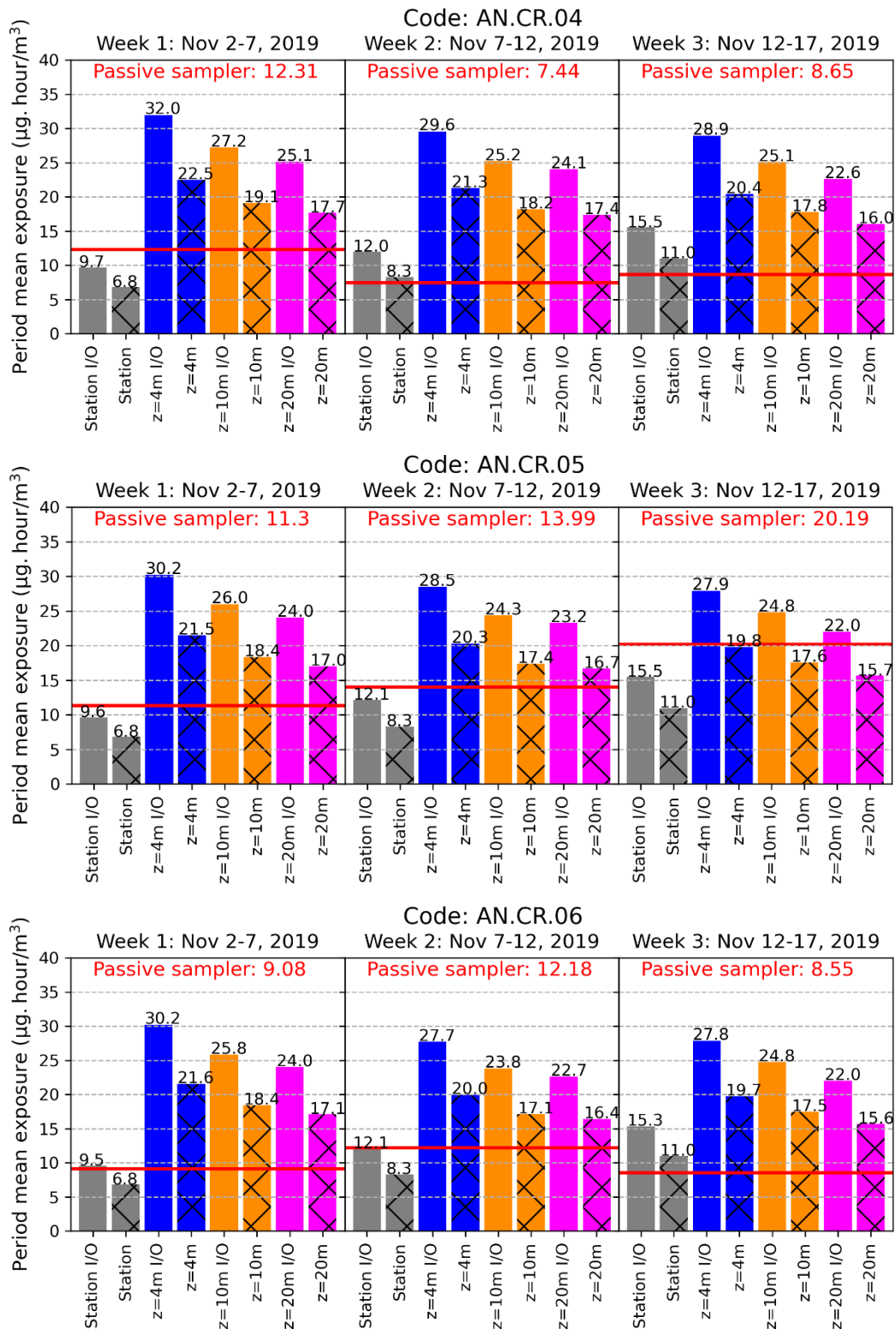
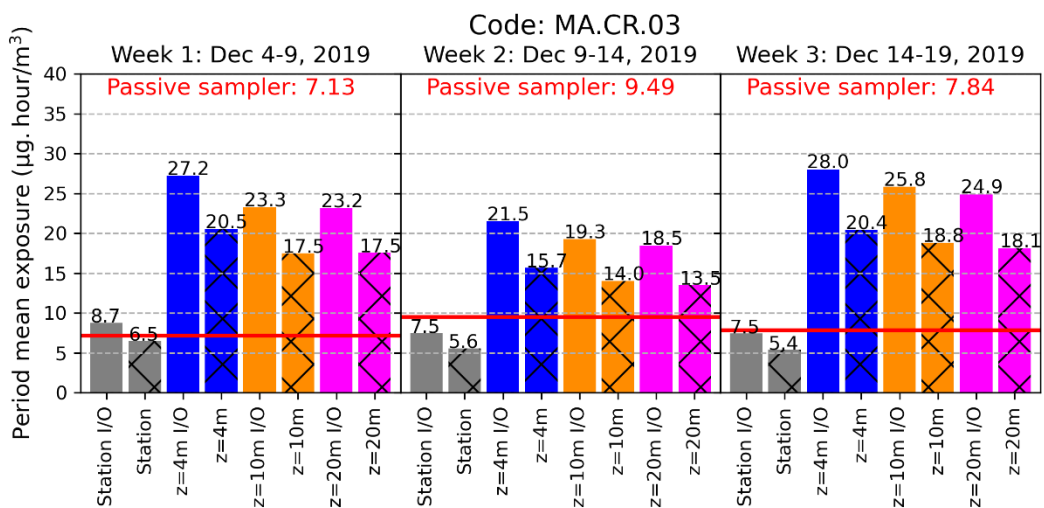
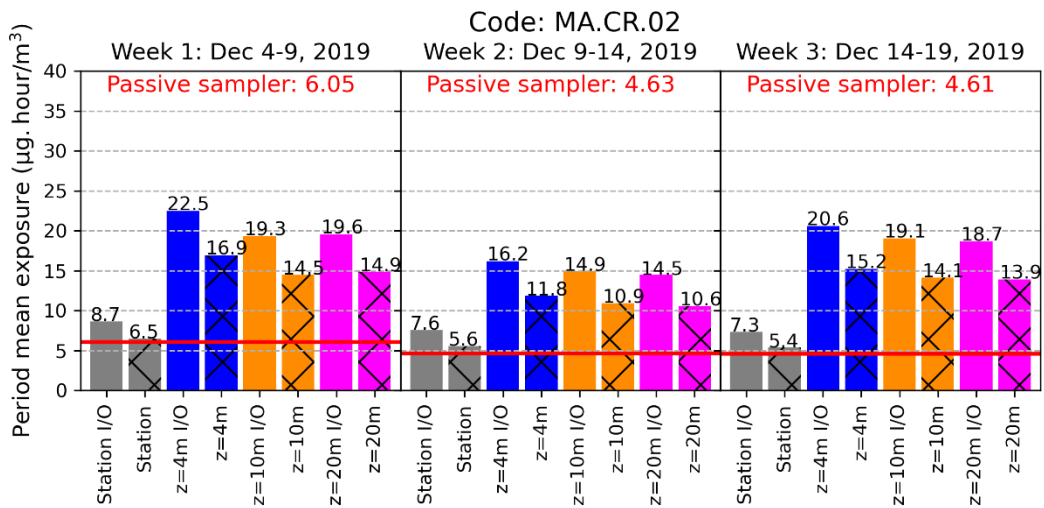
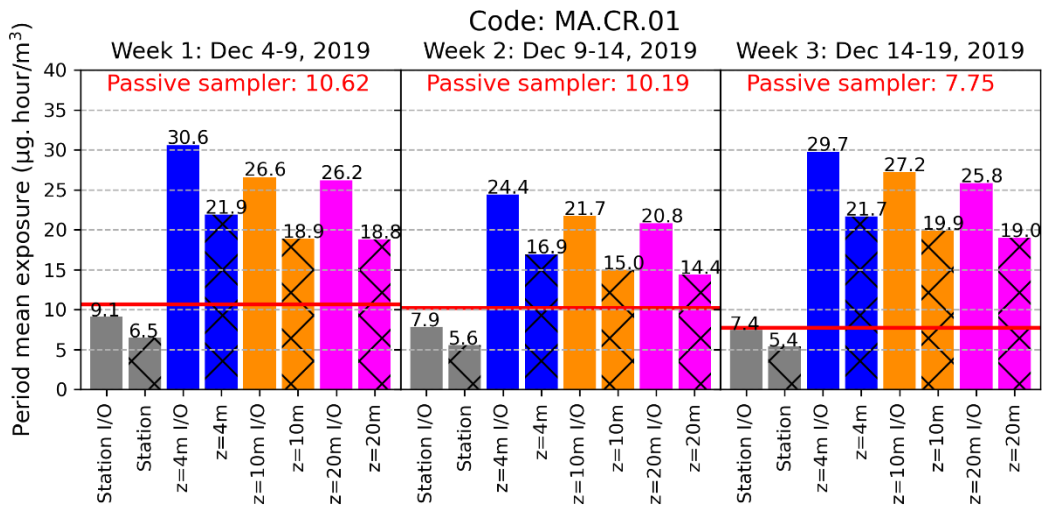


Figure 43. Comparison of children’s hour-mean exposure estimates using data from the ASMA-Vix station and the CMAQ model during Campaign 1 (November 2-17, 2019) in Andorinhas. The red line represents the concentration detected in the passive samplers wore by the children. The suffix I/O indicates that concentrations were adjusted for home and school microenvironments.



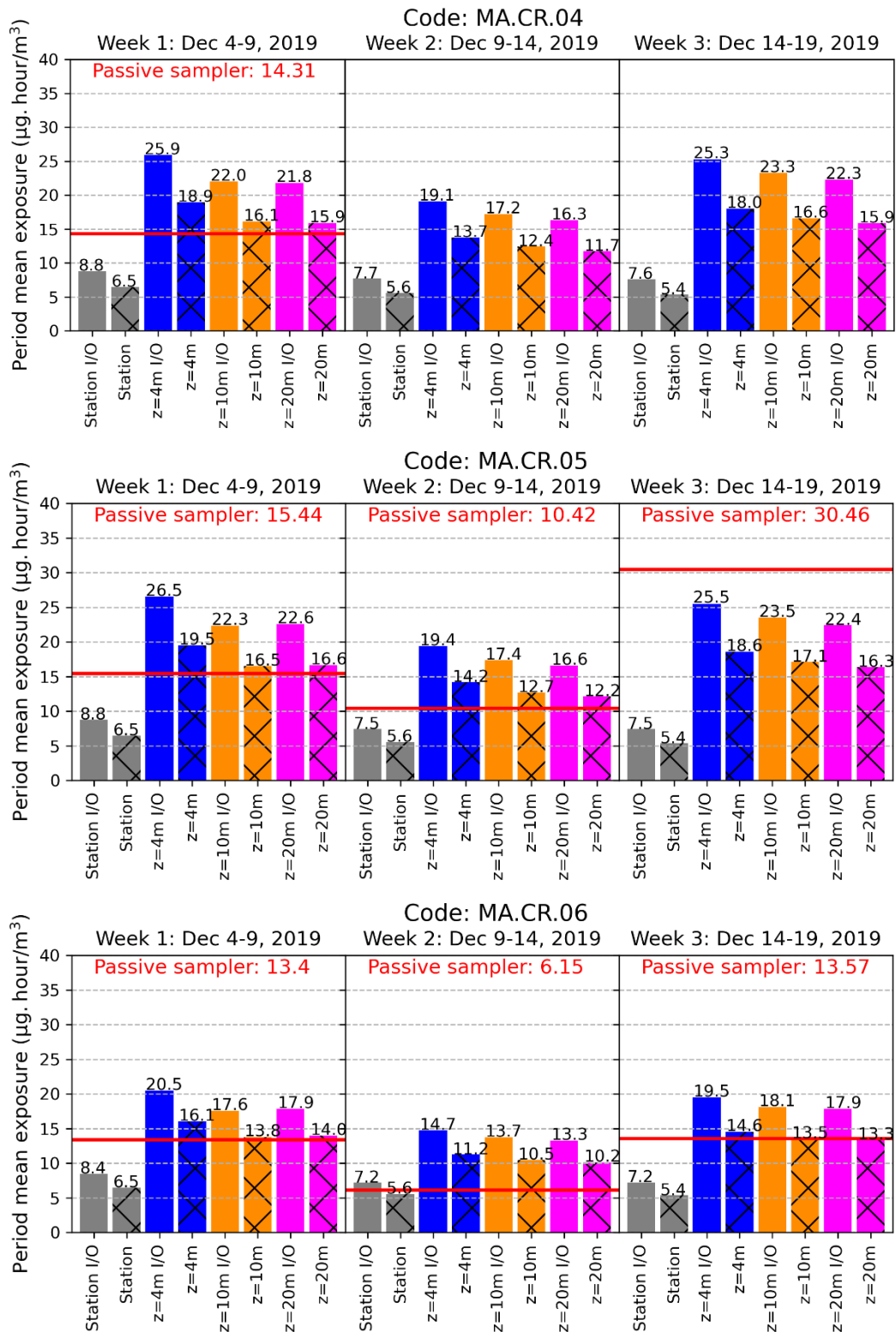


Figure 44. Comparison of children’s hour-mean exposure estimates using data from the ASMA-Vix station and the CMAQ model during Campaign 2 (December 4-19, 2019) in Marúpe. The red line represents the concentration detected in the passive samplers wore by the children. The suffix I/O indicates that concentrations were adjusted for home and school microenvironments.

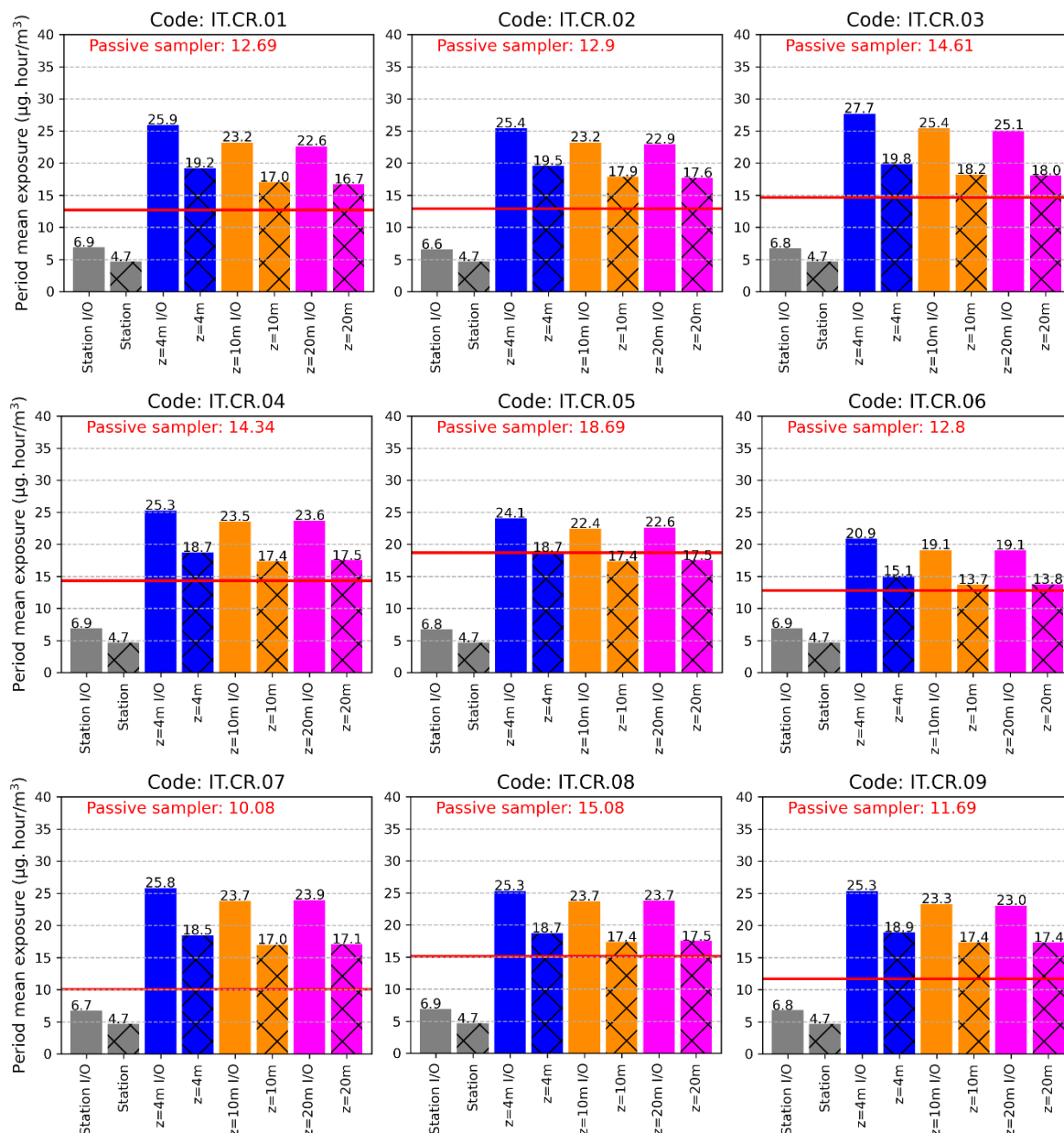


Figure 45. Comparison of children's hour-mean exposure estimates using data from the ASMA-Vix station and the CMAQ model during Campaign 3 (February 12-19, 2020) in Itararé. The red line represents the concentration detected in the passive samplers worn by the children. The suffix I/O indicates that concentrations were adjusted for home and school microenvironments.

Campaigns 1 (Fig. 43) and 2 (Fig. 44) had similar results between them. The mean (median)  $\pm$  standard deviation of the personal monitors in C1 and C2 was  $13.0 \pm 4.7 \mu\text{g}/\text{m}^3$  ( $12.2 \mu\text{g}/\text{m}^3$ ) and  $10.8 \pm 6.1 \mu\text{g}/\text{m}^3$  ( $9.8 \mu\text{g}/\text{m}^3$ ), respectively. The closest results to personal samplers in terms of mean hour exposure were provided by the monitoring station with I/O adjusted ( $C1_{\text{mean}} = 11.9 \pm 2.4 \mu\text{g}/\text{m}^3$ ;  $C2_{\text{mean}} = 7.9 \pm 0.7 \mu\text{g}/\text{m}^3$ ). Meanwhile, the poorest results were provided by the exposure scenario that was estimated using the CMAQ model  $z = 4 \text{ m}$  with I/O adjusted.

Although the largest MB ( $C1 = 14.4 \mu\text{g}/\text{m}^3$ ;  $C2 = 12.5 \mu\text{g}/\text{m}^3$ ), RMSE ( $C1 = 15.6 \mu\text{g}/\text{m}^3$ ;  $C2 = 14.2 \mu\text{g}/\text{m}^3$ ), and MAGE ( $C1 = 14.4 \mu\text{g}/\text{m}^3$ ;  $C2 = 13.2 \mu\text{g}/\text{m}^3$ ); the standard deviation (SD) was better captured by CMAQ model  $z = 4 \text{ m}$  with I/O adjusted ( $C1 = \pm 3 \mu\text{g}/\text{m}^3$ ;  $C2 = \pm 4.5 \mu\text{g}/\text{m}^3$ ) than the monitoring station with I/O adjusted when compared to personal monitors, as well as the maximum values. In C3 (Fig. 45), better results were found using the CMAQ model  $z = 10 \text{ m}$  and  $z = 20 \text{ m}$  without I/O adjusted ( $C3_{\text{mean}+\text{SD}} = 17.0 \pm 1.2 \mu\text{g}/\text{m}^3$ ) when compared to personal monitors ( $C3_{\text{mean}+\text{SD}} = 13.7 \pm 2.3 \mu\text{g}/\text{m}^3$ ). The differences between both configurations regard the statistical indices of  $r$  and IOA, in which  $z = 20 \text{ m}$  had  $r = 0.25$  and  $\text{IOA} = 0.46$  while  $z = 10 \text{ m}$  was equal to  $0.21$  and  $0.45$ , respectively (Table 20).

Figures 43, 44, and 45 also exhibit that there was a better agreement between the monitoring station without I/O correction and the personal samplers when  $\text{NO}_2$  concentrations were lower than  $9 \mu\text{g}/\text{m}^3$  for C1 and  $7 \mu\text{g}/\text{m}^3$  for C2. For the monitoring station with I/O correction, the method well-captured concentrations between  $9\text{--}15 \mu\text{g}/\text{m}^3$  for C1,  $8\text{--}11 \mu\text{g}/\text{m}^3$  for C2, and  $10\text{--}12 \mu\text{g}/\text{m}^3$  for C3. However, this changes for higher concentrations. For instance, the children more exposed according to the personal monitor in C1 ( $22.5 \mu\text{g}/\text{m}^3$  in week 3), C2 ( $30.5 \mu\text{g}/\text{m}^3$  in week 3), and C3 ( $18.7 \mu\text{g}/\text{m}^3$ ) were better depicted by the CTM model. CMAQ had better results when exposures to  $\text{NO}_2$  concentrations were higher than  $17 \mu\text{g}/\text{m}^3$  for C1,  $11 \mu\text{g}/\text{m}^3$  for C2, and  $13 \mu\text{g}/\text{m}^3$  for C3. In this sense, we could assume that for  $\text{NO}_2$  exposures lower than  $15 \mu\text{g}/\text{m}^3$ , the monitoring station with or without I/O correction could be representative to assess the children's personal exposure, otherwise, it is preferable to choose a CTM approach.

Table 20. Statistical analysis of exposure methods

	<b>MB</b>	<b>RSME</b>	<b>MAGE</b>	<b>r</b>	<b>IOA</b>	<b>FAC2</b>
Station	-5.57	7.66	6.02	0.10	0.42	0.60
Station I/O adj.	-2.95	6.23	4.61	0.11	0.45	0.86
$z = 4 \text{ m}$	6.26	8.16	7.18	0.21	0.43	0.69
$z = 4 \text{ m I/O adj.}$	13.06	14.31	13.30	0.17	0.33	0.43
$z = 10 \text{ m}$	4.18	6.51	5.52	0.25	0.47	0.74
$z = 10 \text{ m I/O adj.}$	10.24	11.57	10.59	0.22	0.38	0.52
$z = 20 \text{ m}$	3.60	6.19	5.20	0.22	0.45	0.81
$z = 20 \text{ m I/O adj.}$	9.39	10.81	9.95	0.19	0.38	0.57

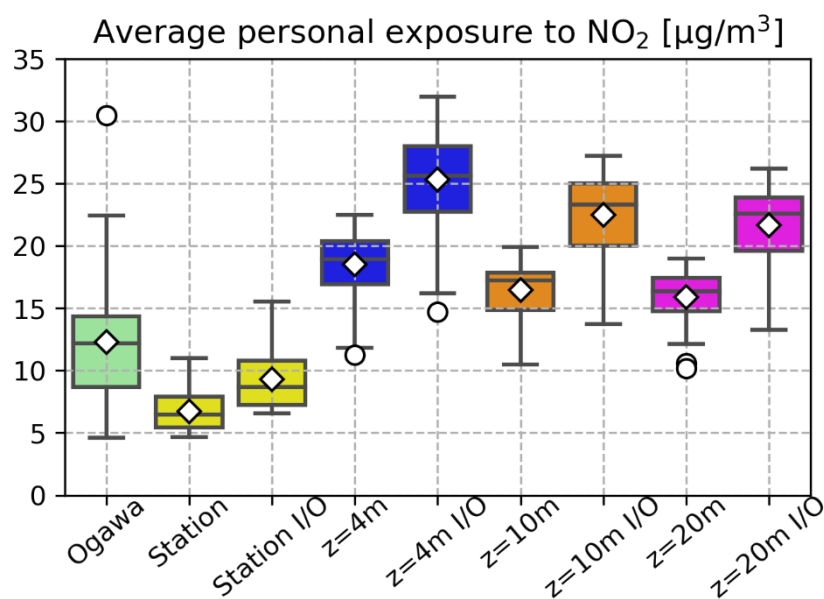


Figure 46. Comparison of the children personal exposure to NO<sub>2</sub> measured by the passive samplers (green), and estimated using data from the ASMA-Vix station (yellow) and the CMAQ model with three different heights. The diamond (lines) represent the mean (median) values, the circles represent the outliers, and the bars represent the minimum and maximum values.

Figure 46 summarizes the average children's personal exposure to NO<sub>2</sub> considering the three experimental campaigns together. The measured children's personal exposure to NO<sub>2</sub> varied between 4.6 and 30.5 µg/m<sup>3</sup>, with a mean and standard deviation of 12.3±5.1 µg/m<sup>3</sup>. The exposures were underestimated using the monitoring station concentrations with or without I/O correction, while the CMAQ model provided higher exposures regardless of the configuration. The results using the monitoring station data without I/O adjusted had lower variability, with a mean personal exposure of 6.7±1.9 µg/m<sup>3</sup>, which varied between 4.7 and 11.0 µg/m<sup>3</sup>. The personal exposure characterized by the nearest air quality station (with an average distance of 2 km between the participants) was less than those measured by the passive samplers. Various studies already reported that the monitoring stations offer a limited spatial resolution, leading to a misclassification of the exposure assessment to air pollution and can be unsuitable for epidemiological studies (Ott, 1982; Mölter *et al.*, 2012; Steinle *et al.*, 2013; Reis *et al.*, 2018; Salonen *et al.*, 2019). However, the use of a fixed I/O ratio has benefitted exposure results using the monitoring station, which provided the results closer to the personal monitors, with an average of 9.3±2.7 µg/m<sup>3</sup> (6.6–15.5 µg/m<sup>3</sup>) and the lowest MB (−3.0 µg/m<sup>3</sup>) and MAGE (4.6 µg/m<sup>3</sup>). On the opposite, the use of a fixed I/O ratio has not improved the exposure results using

the CMAQ model, in which the configuration  $z = 20$  m without I/O adjusted exhibited the closest results to the personal monitors, with an average of  $15.9 \pm 2.0 \mu\text{g}/\text{m}^3$  ( $10.2\text{--}19.0 \mu\text{g}/\text{m}^3$ ) and the lowest RMSE ( $6.2 \mu\text{g}/\text{m}^3$ ). Additionally, the use of fixed I/O ratios enlarged the results estimated with the configuration  $z = 4$  m ( $25.4 \pm 3.9 \mu\text{g}/\text{m}^3$ ), which did not agree well with personal monitoring and had the largest positive bias for all campaigns ( $\text{MB} = 13.1 \mu\text{g}/\text{m}^3$ ). As seen in the previous section, the lowering of the model height (from  $z = 20$  m to  $z = 10$  m, and then, to  $z = 4$  m) enhanced the concentrations, suggesting that children would be exposed to higher levels of air pollution. Similar results were reported in Monticelli *et al.* (2021), in which the I/O correction for the monitoring station made the exposure results closer to personal monitors, but not for dispersion model results with CALPUFF. Table 20 presents the statistical indices between the personal monitors and the eight indirect methods used to evaluate children's personal exposure to  $\text{NO}_2$ . The correlations were better using CMAQ  $z = 10$  m without adjustment ( $r = 0.26$ ,  $\text{IOA} = 0.47$ ).  $\text{FAC2}$  was less than 0.5 only when using the  $z = 4$  m with I/O adjusted.

Few studies have conducted the exposure assessment on a personal level to air pollutants in Brazil, especially with children. Godoi *et al.* (2013) evaluated children's personal exposure to  $\text{NO}_2$  in the south of Brazil. The authors found that the average personal exposure over 2 weeks ( $21 \mu\text{g}/\text{m}^3$ ) in an urban area, in which vehicular traffic played an appreciable role, was almost twice that of our study. However, their study only considered two subjects to carry the passive samplers. Similarly, a study performed in Manchester, UK (Mölter *et al.*, 2012), which also used passive samplers to estimate the exposure of sixty children to  $\text{NO}_2$ , found that the average exposure over 2-weeks ( $20.4 \mu\text{g}/\text{m}^3$ ) was also greater than in this study. In addition, the use of an urban monitoring station ( $28.6 \mu\text{g}/\text{m}^3$ ) to assess children's exposure presented higher concentrations than the use of a land-use regression model ( $19.6 \mu\text{g}/\text{m}^3$ ). The authors concluded that fixed urban monitoring sites are relatively poor predictors of personal exposure which was on average about 4 km away from the child's home, and more than 60% of children were assigned to the same urban monitor. The study conducted by Demirel *et al.* (2014) also found a higher exposure of sixty-five children to  $\text{NO}_2$  in Turkey, with a mean of  $42.8 \mu\text{g}/\text{m}^3$  over 24 hours. In general, the children's exposure to  $\text{NO}_2$  in this study was found to be lower than those reported in the literature, despite the differences in the sample size and the amount of time they used the passive samplers.



Some limitations of our study can be related to the uncertainties in the personal exposure estimates as participants may have sometimes incorrectly filled their diaries, or they may have forgotten to use the passive monitor with them. In addition, this ASMA-Vix project considered only children with asthma symptoms. Studies that only focus on children with asthma have small sample sizes and the extrapolation of the results could be impaired (Xu *et al.*, 2020).

## 5.4 CHILDREN EXPOSURE TO O<sub>3</sub> AND PARTICULATE MATTER

The exposures to PM<sub>10</sub>, PM<sub>2.5</sub>, PM<sub>1</sub>, and O<sub>3</sub> were also estimated through the children’s routines diaries (Figure 47). One downside factor in this analysis was the lack of personal data to compare with the monitoring station and modelled data, making the analysis exclusively qualitative. The modelling approach can be useful to prognosticate air contaminants that are poorly spatially represented and/or are not routinely monitored by environmental agencies because they are not regulated yet, which is the case of ultrafine particles in the MRV, and also in Brazil.

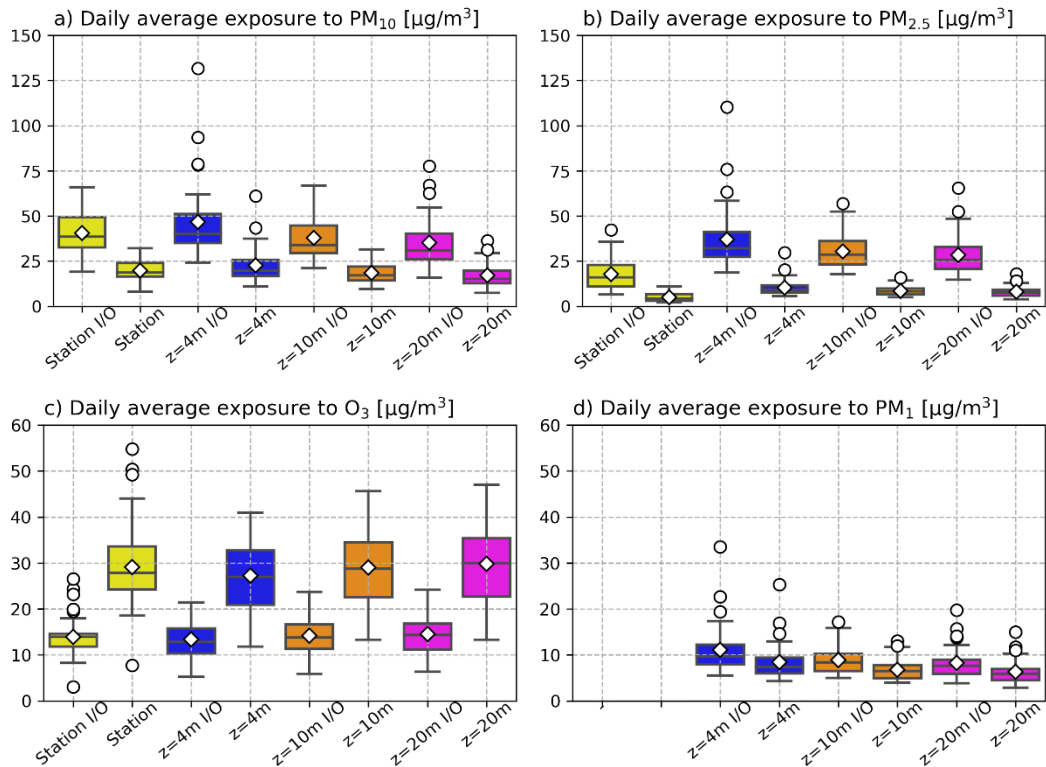




Figure 47. Average daily exposure of children to a) PM<sub>10</sub>, b) PM<sub>2.5</sub>, c) O<sub>3</sub>, and d) PM<sub>1</sub> using the information of their daily routines and data from the ASMA-Vix station and the CMAQ model with three different heights. The diamond (lines) represent the mean (median) values, the circles represent the outliers, and the bars represent the minimum and maximum values.

The sensitivity analyses of the CMAQ model relative to the model height in children's exposure showed the same tendency seen in the performance results presented in the previous section. It means that the configuration with the lowest model height had the highest average daily exposure rates, except for ozone which showed the opposite trend, despite the differences being slight. For the sake of simplicity, from now on, the results will be discussed based on the results of the CMAQ configuration  $z = 20$  m and the monitoring station with and without I/O correction. The choice of these configurations was because they had the most suitable performance when compared to the NO<sub>2</sub> personal monitors.

Overall, the model's results show that the twenty-one children would be exposed on a daily average of  $29.8 \pm 8.7$ ,  $17.2 \pm 6.3$ ,  $8.0 \pm 3.0$ , and  $6.3 \pm 2.6$   $\mu\text{g}/\text{m}^3$  to O<sub>3</sub>, PM<sub>10</sub>, PM<sub>2.5</sub>, and PM<sub>1</sub>, respectively. With the I/O correction, the daily average exposures would increase to  $35.2 \pm 13.1$ ,  $28.5 \pm 10.7$ , and  $8.3 \pm 3.4$   $\mu\text{g}/\text{m}^3$  to PM<sub>10</sub>, PM<sub>2.5</sub>, and PM<sub>1</sub>, respectively, and decrease to  $14.5 \pm 4.4$  for O<sub>3</sub>. For the nearby monitoring station, the daily average exposures were estimated as  $29.1 \pm 9.1$   $\mu\text{g}/\text{m}^3$  for O<sub>3</sub>,  $19.8 \pm 5.9$   $\mu\text{g}/\text{m}^3$  for PM<sub>10</sub>, and  $5.0 \pm 2.3$   $\mu\text{g}/\text{m}^3$  for PM<sub>2.5</sub>. PM<sub>1</sub> data are not presented because it was not subject to monitoring. With the I/O correction, the daily average exposures would be  $13.9 \pm 4.4$ ,  $40.4 \pm 12.1$ , and  $17.8 \pm 8.7$   $\mu\text{g}/\text{m}^3$  for O<sub>3</sub>, PM<sub>10</sub>, and PM<sub>2.5</sub>, respectively. Additionally, the results also revealed that, in terms of daily exposure, children of the first campaign are more exposed to air pollution than children of the C2 and C3. The mean and maximum values were the highest during C1 for O<sub>3</sub>, PM<sub>10</sub>, and PM<sub>2.5</sub> regardless of the method and correction. For instance, the daily means in C1 were  $15 \pm 6.5$  ( $16 \pm 3.6$ )  $\mu\text{g}/\text{m}^3$  for O<sub>3</sub>,  $21 \pm 11.5$  ( $31 \pm 14$ )  $\mu\text{g}/\text{m}^3$  for PM<sub>2.5</sub>, and  $48 \pm 14$  ( $40 \pm 17$ )  $\mu\text{g}/\text{m}^3$  for PM<sub>10</sub> using monitoring station (model) data. For C2, the exposures decreased by  $1-1.5$   $\mu\text{g}/\text{m}^3$  for O<sub>3</sub>,  $3-6$   $\mu\text{g}/\text{m}^3$  for PM<sub>2.5</sub>, and  $10-12$   $\mu\text{g}/\text{m}^3$  for PM<sub>10</sub> when compared to C1 regardless of the method. For C3, the exposures decreased by  $3-5$   $\mu\text{g}/\text{m}^3$  for O<sub>3</sub>, for PM<sub>2.5</sub> and PM<sub>10</sub>, the differences between C1 and C3 depend on the method adopted. The use of the monitoring station exhibited a difference between  $8-12$   $\mu\text{g}/\text{m}^3$ , while the modelled concentrations only showed a difference of  $1-3$   $\mu\text{g}/\text{m}^3$ . For PM<sub>1</sub>, the mean daily exposure was almost the same for children of the first and third campaigns ( $\approx 9$

$\mu\text{g}/\text{m}^3$ ), despite the maximum value being higher in C1 ( $20 \mu\text{g}/\text{m}^3$ ) than C3 ( $14 \mu\text{g}/\text{m}^3$ ). For C2, the daily average exposure to  $\text{PM}_{10}$  was  $7 \mu\text{g}/\text{m}^3$ , varying between  $3.8$  and  $12 \mu\text{g}/\text{m}^3$ .

The use of I/O adjustment has raised the  $\text{PM}_{10}$  daily exposure by twice in comparison to the non-use, for  $\text{PM}_{10}$  the increase was about 30%, and for  $\text{O}_3$  it was half, following the I/O ratios adopted for them. The largest difference regarding the use of I/O correction was seen for  $\text{PM}_{2.5}$ , whose use increased the daily exposure by 250%. By comparing both indirect methods, the exposure to  $\text{O}_3$  and  $\text{PM}_{10}$  showed similar results and practically the same magnitude. Meanwhile, for  $\text{PM}_{2.5}$ , there was a considerable difference between the exposure estimated by the monitoring station and the CTM model. The difference was  $11 \mu\text{g}/\text{m}^3$  using the I/O adjustment scenario and  $3 \mu\text{g}/\text{m}^3$  without it, meaning that the exposure to  $\text{PM}_{2.5}$  can be more than its additional half in the region depending on the type of approach the study relies on. Previous epidemiological studies based on data exclusively from air monitoring stations in the region could be underestimated (Andreão, *et al.*, 2018; Souza *et al.*, 2018). However, it is important to highlight that, although fixed monitoring stations and modelling approaches have been useful to estimate people's exposure to air pollution, these methods cannot replace, in terms of accuracy and representativeness, instrumental personal measures of exposure carried out correctly. The lack of personal monitoring of different PM fractions and  $\text{O}_3$  of the children in the ASMA-Vix study can be pointed out as a drawback of this study.

In this study, ambient modelled  $\text{NO}_2$  ( $19.6 \mu\text{g}/\text{m}^3$ ),  $\text{PM}_{10}$  ( $20.5 \mu\text{g}/\text{m}^3$ ), and  $\text{PM}_{2.5}$  ( $9.5 \mu\text{g}/\text{m}^3$ ) were lower than the exposure levels ( $21.7$ ,  $35.2$ , and  $28.5 \mu\text{g}/\text{m}^3$ , respectively). These results are strictly related to the time spent by children in the indoor environments and the I/O ratios that were greater than 1. The I/O ratios found during the experimental campaigns of this study for  $\text{NO}_2$  and  $\text{PM}_{10}$  were similar to those found in the literature (WHO, 2010; Godoi *et al.*, 2013; Pallarés *et al.*, 2019; Salonen *et al.*, 2019; Shrestha *et al.*, 2019; Faria *et al.*, 2020). However, with respect to  $\text{PM}_{2.5}$ , despite the literature reports that I/O ratios are usually greater than unity, in this study, these ratios were two to four times higher than in other studies which ranged between 1.2 and 2.1 (Rivas *et al.*, 2014; Chen *et al.*, 2020; Faria *et al.*, 2020; Fernandes *et al.*, 2021). According to them, the main factors that caused these differences (in the absence of indoor sources) were a result of ventilation and airtightness of the spaces, the children's activities, and dust resuspension. As mentioned, homes and schools in this project usually used open windows and ceiling fans to allow the entering of fresh and cool air into the indoor environments (Velasco, 2020; Monticelli *et al.*, 2021). In addition, complex urban landscapes,

the distance of pollutant sources, and meteorological conditions within the urban area can hinder the dispersion process, and thus aid in enhancing air pollutants concentrations (Milner *et al.*, 2005).

In this study, the personal exposure of children was comparable to those found in the literature. For example, in Lisbon, Portugal, the average exposure of nine children to PM<sub>1</sub> and PM<sub>2.5</sub> was 14 µg/m<sup>3</sup> and 19 µg/m<sup>3</sup> (Cunha-Lopes *et al.*, 2019), while in this study, these values considering the I/O adjustment were 8.3 µg/m<sup>3</sup> (model) and 17.8 µg/m<sup>3</sup> (monitoring station), respectively. If the model was taken into account for PM<sub>2.5</sub>, the average exposure would be 28.5 µg/m<sup>3</sup> instead of 17.8 µg/m<sup>3</sup> and thus, comparable to studies performed in Asian cities which exposed that the average exposure of children to PM<sub>2.5</sub> was 35 µg/m<sup>3</sup> in Cheonan, Korea (Choi *et al.*, 2020); and 40±17 µg/m<sup>3</sup> in Shanghai, China (Barkjohn *et al.*, 2020). Although higher exposures to PM<sub>2.5</sub> are expected because Eastern Asia is well-known to be more polluted than other parts of the world. The median personal concentration exposure to PM<sub>10</sub> of children living in Australia was 28 µg/m<sup>3</sup>, 48 µg/m<sup>3</sup>, and 45 µg/m<sup>3</sup> in mining, rural, and urban/suburbs areas, respectively (Hinwood *et al.*, 2014). The exposure in the urban area is higher than those found in both methods (monitoring station and model) with or without I/O correction.

Oppositely to PM, ambient modelled MDA8 O<sub>3</sub> concentration (42 µg/m<sup>3</sup>) was about 3 times higher than the daily personal exposure (14 µg/m<sup>3</sup>), being the indoor I/O ratio adopted for O<sub>3</sub> almost half due to its high reactivity. Similarly, Niu *et al.* (2018) found the personal exposure of college students to O<sub>3</sub> to be 1/2 to 1/3 of ambient concentrations in Shanghai, China. In Shanghai, the 48-h personal exposure to O<sub>3</sub> of children was 22±10 µg/m<sup>3</sup> (Barkjohn *et al.*, 2020). In another study performed in Tennessee, USA, children were exposed to O<sub>3</sub> on a weekly average of 7±7.4 µg/m<sup>3</sup>, corresponding to 7 to 31% of outdoor O<sub>3</sub> concentrations (Lee *et al.*, 2004). In addition, children would be more exposed to O<sub>3</sub> during the transit between school to home and vice-versa, or doing outdoor exercises and playing in playgrounds, because they usually do it during the day, when outdoor O<sub>3</sub> concentrations tend to be higher due to its diurnal variation pattern. A comparison of the estimation of the exposure to air pollutants between this study and others is presented in Table 21.

Table 21. Comparison of the exposure to air pollutants of the present study with others found in the literature review. The values are presented in terms of mean  $\pm$  standard deviations. The values of this study were presented with I/O correction.

Study	Study Area	Method	NO <sub>2</sub>	O <sub>3</sub>	PM <sub>10</sub>	PM <sub>2.5</sub>	PM <sub>1</sub>
This study <i>n</i> =21	Vitória, Brazil	passive samplers	12.3 $\pm$ 5.1	-	-	-	-
		monitoring station	9.3 $\pm$ 2.8	13.9 $\pm$ 4.4	40.4 $\pm$ 12.1	17.8 $\pm$ 8.7	-
		CMAQ model <i>z</i> = 20 m	21.7 $\pm$ 2.9	14.5 $\pm$ 4.4	35.2 $\pm$ 13.1	28.5 $\pm$ 10.7	8.3 $\pm$ 3.4
Cunha-Lopes <i>et al.</i> (2019) <i>n</i> =9	Lisbon, Portugal	portable monitoring equipment	-	-	-	19.0	14.0
Choi <i>et al.</i> (2020) <i>n</i> =52	Cheonan, Korea	fixed station	-	-	-	34.6	-
Barkjohn <i>et al.</i> (2020) <i>n</i> =43	Shanghai, China	low-cost monitors	-	21.7 $\pm$ 9.9*	-	40 $\pm$ 17	-
Hinwood <i>et al.</i> (2014) <i>n</i> =70	Perth, Australia	iron ore mining/shipping area ( <i>n</i> =13)	-	-	28.0	-	-
		rural area ( <i>n</i> =15)	-	-	48.4	-	-
		urban area ( <i>n</i> =42)	-	-	44.8	-	-
Lee <i>et al.</i> (2004) <i>n</i> =33	Tennessee, USA	passive samplers	-	7 $\pm$ 7.4*	-	-	-
Godoi <i>et al.</i> (2013) <i>n</i> =2	Curitiba, Brazil	Urban	21.0	-	-	-	-
		Suburban	10.2	-	-	-	-
Molter <i>et al.</i> (2012) <i>n</i> =60	Manchester, UK	passive samplers	20.4 $\pm$ 7.9	-	-	-	-
		fixed station	28.6 $\pm$ 15	-	-	-	-
		microenvironmental exposure model	19.6 $\pm$ 4.7	-	-	-	-
		LUR model	31.2 $\pm$ 5.4	-	-	-	-
Demirel <i>et al.</i> (2014) <i>n</i> =65	Eskişehir, Turkey	passive samplers	42.8 $\pm$ 15	38.4 $\pm$ 10.4	-	-	-

## 5.5 INHALATION DOSE ASSESSMENT OF PARTICULATE MATTER

Inhaled doses of  $PM_{2.5}$  and  $PM_1$  were also evaluated based on the daily activity pattern reported in the time–activity diaries, exposure concentration data in each microenvironment, the inhalation rate ( $m^3/h$ ) and ventilation rate ( $L/min$ ) during resting (sleeping hours) and light exercises using Equations 12 and 13. Figures 48 and 49 show hourly  $PM_{2.5}$  and  $PM_1$  potential inhaled doses (unadjusted for body weight) for children of all campaigns using data from the monitoring station and the CMAQ model with  $z = 20$  m with and without I/O correction. Note that only the simulated data by CMAQ is presented for  $PM_1$ .

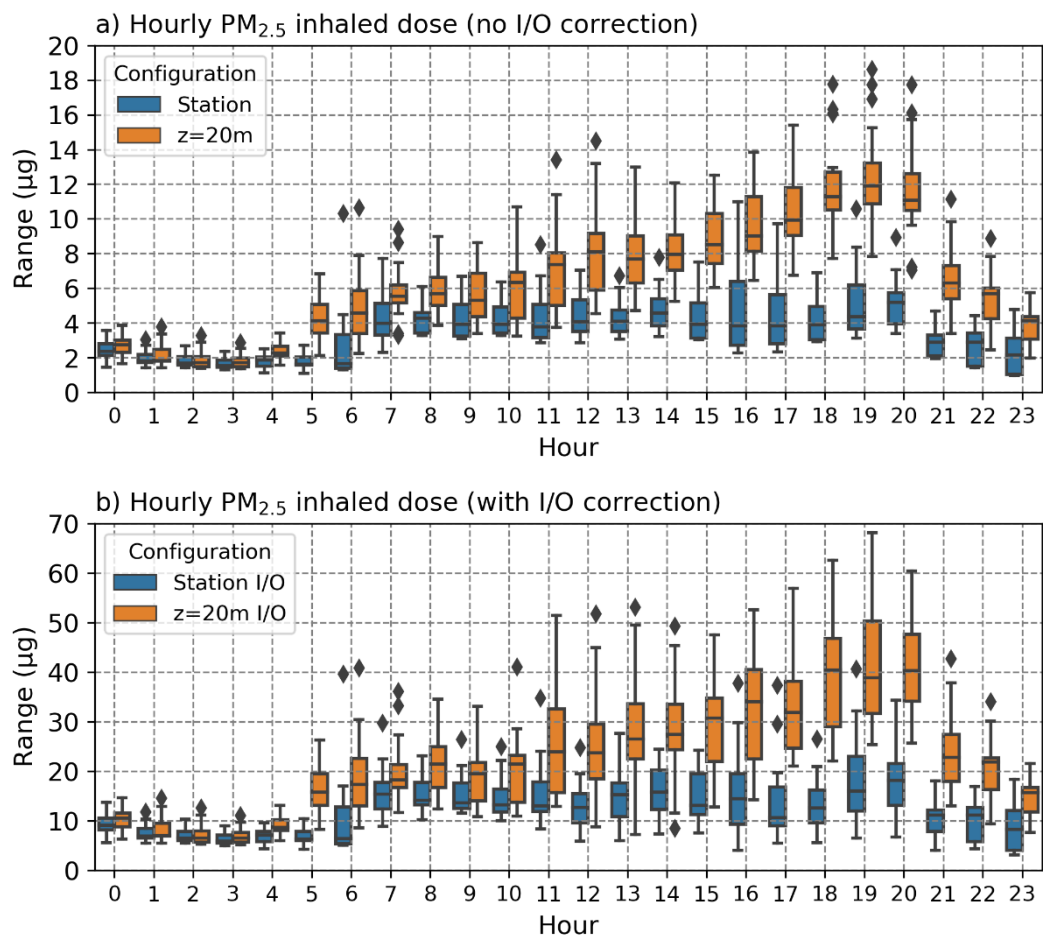


Figure 48. Boxplot of the hourly  $PM_{2.5}$  inhaled dose of children (unadjusted for body weight) considering (a) no I/O correction and (b) with I/O correction using data from the monitoring station and the CMAQ model with  $z = 20$  m.

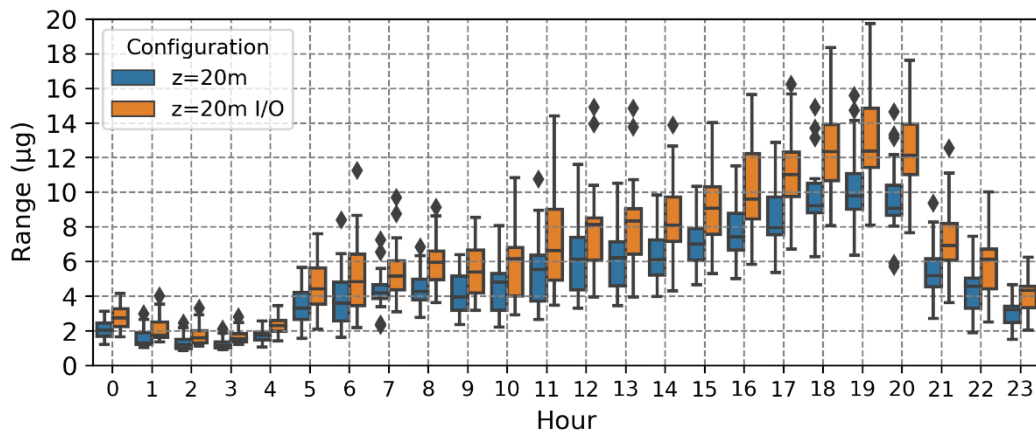


Figure 49. Boxplot of the hourly simulated PM<sub>1</sub> inhaled dose of children (unadjusted for body weight) considering (a) no I/O correction and (b) with I/O correction using data from CMAQ model  $z = 20$  m.

Between 11 p.m. and 5 a.m., when most children were sleeping, the potential inhaled dose was at the lowest level in a day, with a range between 2 and 4  $\mu\text{g}$  for PM<sub>2.5</sub> and 1–3 for PM<sub>1</sub>, with small differences among children. However, considering the I/O correction, the potential inhaled dose increased from a range of 6–16 for PM<sub>2.5</sub>, although these levels were still the lowest in a day. From 6 a.m., children started to have an increase in the potential inhaled dose, with some peaks values (represented by the bar and the outliers), despite the average inhaled dose remaining at a reduced level, with a mean difference of 1–4  $\mu\text{g}$  (monitoring station) and 4–8  $\mu\text{g}$  (model) for PM<sub>2.5</sub> (2  $\mu\text{g}$  for PM<sub>1</sub>) compared to the previous hours. The monitoring station data exhibited that the median potential inhaled dose of children for PM<sub>2.5</sub> tended to be the same between 7 a.m. and 8 p.m., which range between 3.9 (11)  $\mu\text{g}$  and 5.3 (18)  $\mu\text{g}$  considering no (with) I/O correction, with the maximum value occurring at 8 p.m. On the other hand, the modelled data showed more variability and indicated that the potential inhaled dose increased along the day, with the maximum value of 12 (40.8)  $\mu\text{g}$  for PM<sub>2.5</sub> and 10 (12.7)  $\mu\text{g}$  for PM<sub>1</sub> occurring at 7 p.m. As previously discussed, this period is related to the traffic rush hour at the end of a day, indicating the gradual accumulation of particulate matter in the atmosphere. After that, the potential inhaled dose of children dropped and was similar to the other periods of the beginning of the day. Nevertheless, it can be found that the PM inhaled dose was the largest during the late afternoon, the median is 3–4 times the number during sleeping hours.

Figure 50 exhibits the potential accumulated daily dose adjusted for body weight for PM<sub>2.5</sub> and PM<sub>1</sub> for children of all campaigns using data from the monitoring station and the CMAQ model with z = 20 m with and without I/O correction.

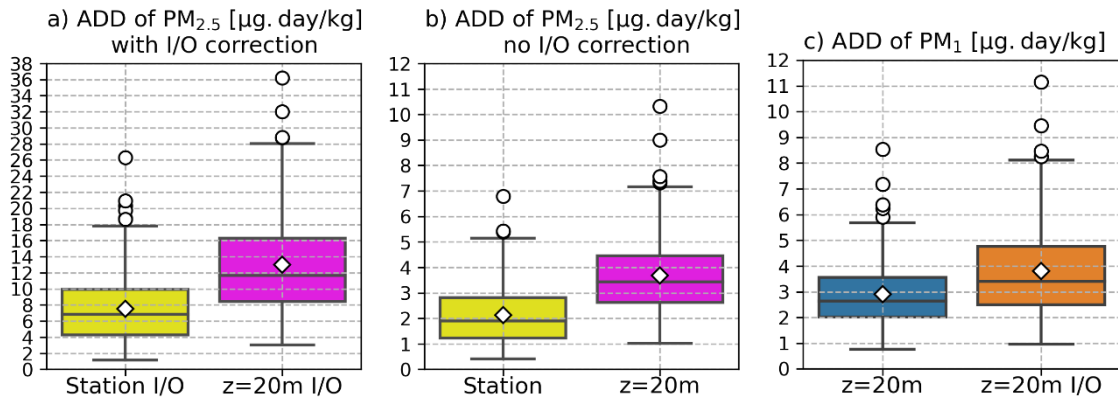


Figure 50. Children's potential average daily dose (ADD<sub>pot</sub>) of a) PM<sub>2.5</sub> with I/O correction, b) PM<sub>2.5</sub> with no I/O correction, and c) PM<sub>1</sub> using data from the monitoring station and the CMAQ model z=20 m. The diamond (lines) represent the mean (median) values, the circles represent the outliers, and the bars represent the minimum and maximum values.

The mean (median) of the potential modelled inhaled daily doses adjusted for body weight was  $13.0 \pm 5.9$  ( $11.7$ )  $\mu\text{g}/\text{kg}$  for PM<sub>2.5</sub> with I/O correction,  $3.7 \pm 1.5$  ( $3.4$ )  $\mu\text{g}/\text{kg}$  for PM<sub>2.5</sub> no I/O correction,  $3.8 \pm 1.7$  ( $3.4$ )  $\mu\text{g}/\text{kg}$  for PM<sub>1</sub> with I/O correction, and  $2.9 \pm 1.2$  ( $2.6$ )  $\mu\text{g}/\text{kg}$  for PM<sub>1</sub> no I/O correction. Correspondingly, considering the nearby urban station, the mean (median) of the potential inhaled daily doses was  $7.5 \pm 4.4$  ( $6.8$ )  $\mu\text{g}/\text{kg}$  for PM<sub>2.5</sub> with I/O correction and  $2.1 \pm 1.2$  ( $1.9$ )  $\mu\text{g}/\text{kg}$  for PM<sub>2.5</sub> no I/O correction. In the toxicological risk assessment, the average daily dose can be used to estimate the risk quotient in relation to a reference dose. If we consider that the reference concentration is  $5 \mu\text{g}/\text{m}^3$  (Oliveira et al., 2012) or  $5.8 \mu\text{g}/\text{m}^3$  (de Souza Silva *et al.*, 2016) for PM<sub>2.5</sub>, the risk quotient using data from the monitoring station or the CMAQ model with I/O correction would be greater than 1, meaning that PM<sub>2.5</sub> causes adverse health effects and is detrimental to public health in the MRV. On the contrary, if no I/O adjustment would be applied, the risk quotient would be less than 1, and thus, the PM<sub>2.5</sub> would not be considered a threat to public health. However, it is important to highlight that these reference concentration values were taken from the literature, in which both studies evaluated the exposure to PM<sub>2.5</sub> of children and adolescents residents in the Brazilian Amazon region during the biomass burning.

By comparing with results found in the literature, our modelled results showed that the children in this study inhaled similar PM doses when compared to the mothers living in Oporto metropolitan area (Portugal), which virtually attended the same microenvironments as newborn children (Madureira *et al.*, 2020). In their study, the PM<sub>2.5</sub> inhalation doses among newborn children were 4-fold higher than their mothers due to their low body weights, with estimated means of 69.8±53.9 µg/kg and 16.7±14.2 µg/kg, respectively. The average body weight of boys (girls) in this study was 41.8±14.4 (43.9±13.3) kg, meaning that the children could inhale daily doses that varied between 155–571 µg for PM<sub>2.5</sub> (model), 88–330 µg for PM<sub>2.5</sub> (monitoring station), and 121–167 µg for PM<sub>1</sub>, according to the different configurations used to estimate the air pollutant concentrations and the use or non-use of I/O ratios. These results show that children residing in the MRV have the potential to inhale more PM when compared to children residing in Lisbon (PM<sub>2.5</sub> = 243.5 µg) (Faria *et al.*, 2020). But does not go beyond the limits found by Song *et al.* (2021) for residents from Guangzhou, China, which revealed that PM<sub>2.5</sub> inhaled dose in a day was about 940±94.5 µg, being higher during the day and low at night (619–1284 µg). In addition, they highlighted that the individual differences in inhaled doses concern the commuting and leisure periods, during the working and sleeping periods, the differences were small.

The estimation of inhaled doses of PM<sub>2.5</sub> and PM<sub>1</sub> in this study considered inhalation rates obtained from the literature (Yoon *et al.*, 2020), which can be pointed out as a limitation of the study, despite the adopted values being consistent with the other studies (Allan and Richardson, 1998; USEPA, 2011; Brochu *et al.*, 2011; 2014; Carvalho *et al.*, 2018). In this sense, since the estimation of the inhaled dose can consider other respiratory parameters (e.g. ventilation rate, tidal volume, breathing frequency) and the values can vary considerably in the literature, we estimated the potential inhaled dose of children also considering the respiratory deposition dose (RDD) approach to putting our results in perspective. Figure 51 presents the results using the RDD equation for PM<sub>2.5</sub> and PM<sub>1</sub> using data from the monitoring station and the CMAQ model with  $z = 20$  m with and without I/O correction, separated for boys and girls.



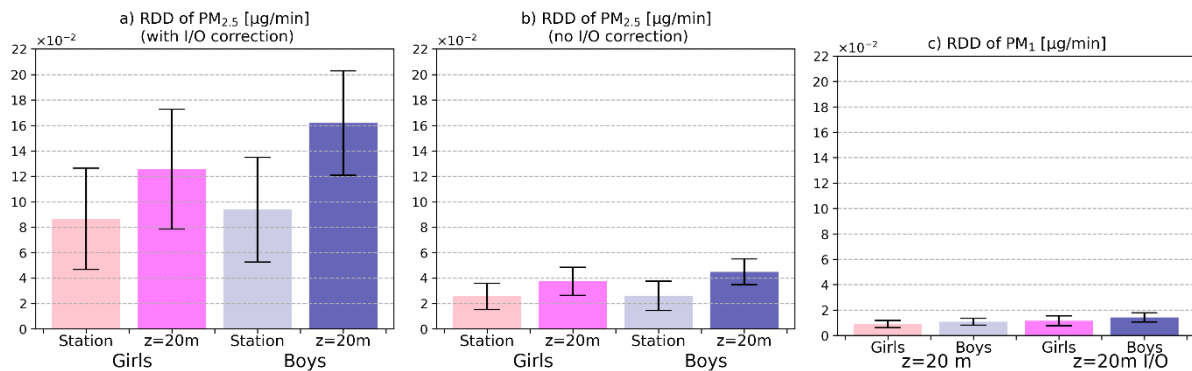


Figure 51. Respiratory deposition doses (RDD) throughout the respiratory tract of boys and girls during sleeping and light exercises for a) PM<sub>2.5</sub> with I/O correction, b) PM<sub>2.5</sub> with no I/O correction, and c) PM<sub>1</sub> using data from the monitoring station and the CMAQ model  $z=20$  m.

The RDD for PM<sub>2.5</sub> and PM<sub>1</sub> was calculated separately for boys and girls considering the sleeping and light exercises. The RDD for girls (boys) varied between  $2.6 \pm 1.0$  ( $2.6 \pm 1.2$ )  $\times 10^{-2}$   $\mu\text{g}/\text{min}$  (station) and  $3.7 \pm 1.1$  ( $4.5 \pm 1.0$ )  $\times 10^{-2}$   $\mu\text{g}/\text{min}$  (model) for PM<sub>2.5</sub> and  $0.9 \pm 0.3$  ( $1.1 \pm 0.3$ )  $\times 10^{-2}$   $\mu\text{g}/\text{min}$  for PM<sub>1</sub>. By considering the I/O correction, the RDD for girls (boys) varied between  $8.7 \pm 4.0$  ( $9.4 \pm 4.1$ )  $\times 10^{-2}$   $\mu\text{g}/\text{min}$  (station) and  $12.6 \pm 4.7$  ( $16.2 \pm 4.1$ )  $\times 10^{-2}$   $\mu\text{g}/\text{min}$  (model) for PM<sub>2.5</sub> and  $1.1 \pm 0.4$  ( $1.4 \pm 0.4$ )  $\times 10^{-2}$   $\mu\text{g}/\text{min}$  for PM<sub>1</sub>. Slight higher RDD was found for boys than girls. That was expected because the respiratory parameters of males usually are greater than females, and thus, males would inhale more PM (Hinds, 1999). Similar results were found in Segalin *et al.* (2017), which evaluated the RDD of elderly residents of São Paulo and reported a mean RDD of  $5.7$  ( $4.3$ )  $\times 10^{-2}$   $\mu\text{g}/\text{min}$  and  $15.8$  ( $14$ )  $\times 10^{-2}$   $\mu\text{g}/\text{min}$  for males (females) during seated position and light exercises. In the same way, Kumar *et al.* (2017) estimated the RDD for babies (< 1 year) in a sedentary condition and found values between  $1.2$ – $20.4$   $\mu\text{g}/\text{h}$  for female babies, with an RDD ratio of 1.06 for male babies.

By integrating the RDD over a day, the respiratory deposition dose assessment presents smaller inhaled doses ( $37$ – $233$   $\mu\text{g}/\text{day}$ ) than the  $\text{ADD}_{\text{pot}}$  ( $88$ – $571$   $\mu\text{g}/\text{day}$ ). That occurred because while the  $\text{ADD}_{\text{pot}}$  equation uses the inhalation rate (IR) parameter, which is given by  $\text{m}^3$  per hour, the RDD alternatively employs the ventilation rate (VR), which usually is measured as the volume of air exhaled per minute. Thus, if the VR values from USEPA (2009) would be converted to hourly rates, the inhalation rates for boys (girls) between 11–16 years old would be  $0.32$  ( $0.29$ )  $\text{m}^3/\text{h}$  and  $0.79$  ( $0.72$ )  $\text{m}^3/\text{h}$  during sleeping and light activities, which are smaller than those adopted from Yoon's study (2020). In addition, the RDD equation considers the deposition fraction (DF) parameter that takes into account the particle diameter and therefore is usually

not directly proportional to the mass concentration (Kumar *et al.*, 2017). This paradigm has been discussed by Borghi *et al.* (2021) and reported that the literature concerning the estimation of the inhaled dose of pollutants is few compared with the exposure assessment studies because the latter considers the external dose (exposure) and not the potential dose (the amount of contaminant inhaled, not all of which is actually absorbed). Furthermore, the estimation of the internal dose (the amount of contaminant that passes the exchange boundary and into the blood, or the amount of the contaminant that can interact with organs and tissues to cause biological effects) is highly sensitive to the physiological parameters (e.g. age, gender, body, weight, intensity of physical activity), especially those related to the mode of a subject breath.

A further important implication is, in the present study, both approaches (ADD or RDD) used respiratory parameters that assumed that children are non-asthmatic. Asthmatic children have higher inhalation rates, and thus, the potential inhaled doses could be higher for asthmatic children (USEPA, 2011). The breathing rates are also higher during heavy activities than the light activities and resting positions (Hinds, 1999). Physical education and other exercises (i.e., walking, running, and cycling) increase the pulmonary ventilation rates, and thereby, increase the risk associated with exposure to air pollution due to higher doses of pollutants that may penetrate the human body. Coarse and ultrafine particles are primarily deposited in the head airways region (nose, mouth, pharynx, and larynx) due to inertial impaction and diffusion (Hinds, 1999). However, fine and ultrafine particles can be efficiently deposited in the pulmonary region, and their sizes can favour the deposition of toxic elements in pulmonary alveoli (Oberdörster *et al.*, 2005; Kumar *et al.*, 2014; Han *et al.*, 2016; Madureira *et al.*, 2020).

## **5.6 SOURCES CONTRIBUTIONS TO THE CHILDREN'S PERSONAL EXPOSURE**

The MRV is a complex urban and industrialized area in southeastern Brazil with significant air pollution problems caused by a peculiar arrangement of pelletizing-siderurgy activities and marine and vehicular traffic within the urban zone. The main sources of emissions are practically located in the same areas, which aids in enhancing the pollutant concentrations in certain regions. Figures 52, 53, and 54 quantify the averaged percentage contribution of each emission sector to NO<sub>2</sub>, O<sub>3</sub>, and PM<sub>2.5</sub> mass concentration, respectively. The results are presented based on the simulations configured with CMAQ  $z = 20$  m without I/O correction.

The influence of source contributions was split into weekdays and weekends and per hour of the day for each campaign. For that, a fixed time activity profile for children was assumed, in which the label ‘Home’ corresponds to the hours between 6 p.m. and 6 a.m. The label ‘Outdoor’ assigns to the hours that usually children are in transit/commuting between microenvironments (7 a.m., 12 p.m., and 5 p.m.). The labels ‘Morning’ and ‘Afternoon’ were assumed to be the hours that children would be at school or doing any other activities, and thus, it was divided from 8 a.m. to 11 a.m. and from 1 p.m. and 4 p.m., respectively.

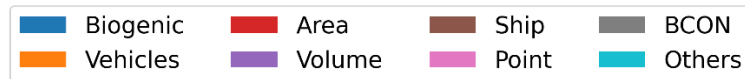
Overall, BCON was the major contributor to NO<sub>2</sub> and O<sub>3</sub> concentrations, corresponding to 42% ( $\approx 5.8 \mu\text{g}/\text{m}^3$ ) and 74% ( $\approx 27 \mu\text{g}/\text{m}^3$ ) of the total mass respectively. The broad influence of BCON on pollutant concentrations, especially ozone, can be related to the fact that BCON was provided by a global model with a dynamic hourly process, making the pollutants constantly transported into the domain. Another factor is the size of the domain, which despite having been increased from a previous study in the same region (Pedruzzi *et al.*, 2019) may still not be adequate. Nonetheless, Pedruzzi *et al.* (2019) exhibited that the non-use of a dynamic process for lateral boundary conditions generates poor results for O<sub>3</sub> simulation, and thus, they highly recommended this scenario for air quality modelling.

The second greatest contributor to NO<sub>2</sub> and O<sub>3</sub> concentrations was the vehicular sources, with an average of 30% ( $3.2 \mu\text{g}/\text{m}^3$ ) and 8% ( $3.2 \mu\text{g}/\text{m}^3$ ), respectively. In comparison among the four categories of time, the vehicles category had its broadest influence during the *Morning* hours (8 a.m. – 11 a.m.) on both NO<sub>2</sub> (39%) and O<sub>3</sub> (10%). In the meantime, BCON had its greatest contribution during the *Home* hours (6 p.m. – 6 a.m.) on both NO<sub>2</sub> (44%) and O<sub>3</sub> (97%). In addition to BCON, the shipping sector also contributed to NO<sub>2</sub> concentrations during *Home* hours, with a mean of 10% ( $1.6 \mu\text{g}/\text{m}^3$ ). The ISAM tool also indicated that point sources also played an important role in NO<sub>2</sub> and O<sub>3</sub> mass concentrations in the campaign areas, especially during the *Afternoon* hours (1 p.m. – 4 p.m.), when its emissions represented an average of 20% ( $4.4 \mu\text{g}/\text{m}^3$ ) and 16% ( $5.1 \mu\text{g}/\text{m}^3$ ) of NO<sub>2</sub> and O<sub>3</sub> total concentrations, respectively.

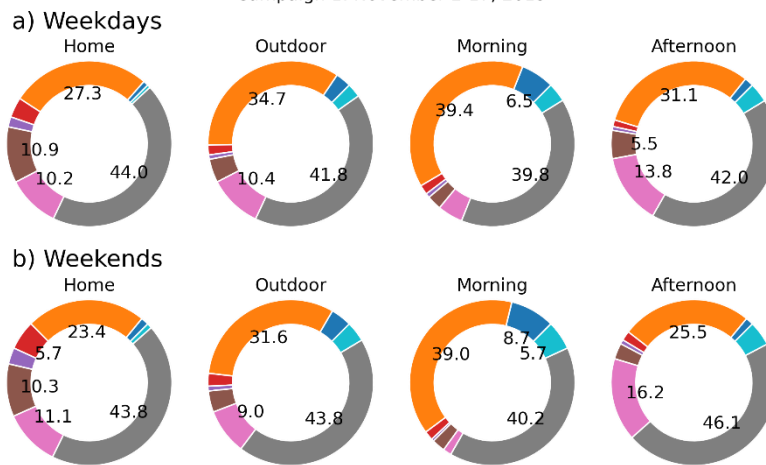
Although BCON influenced 30% ( $1.6 \mu\text{g}/\text{m}^3$ ) of the total PM<sub>2.5</sub> mass, road dust resuspension was its major contributor, with an average of 43% ( $2.9 \mu\text{g}/\text{m}^3$ ), followed by the point (13%,  $1.0 \mu\text{g}/\text{m}^3$ ), vehicles (5%,  $0.3 \mu\text{g}/\text{m}^3$ ), and shipping (4%,  $0.2 \mu\text{g}/\text{m}^3$ ) sources. The road dust resuspension is directly linked to the influence of vehicular traffic movement; however, at the same time, the origin of the PM<sub>2.5</sub> deposited on the road should be attributed to miscellaneous

sources in the region, including industrial (mining, steel, quarries, civil construction, maritime ports, etc.), vehicular, and natural sources such as biogenic, crustal, and sea salt. The transport contribution from sources outside of the domain was also described by Li *et al.* (2019), which evaluated the PM<sub>2.5</sub> contributors over 15 provinces in China and found a proportion of approximately 20%, but it can exceed 50% during some seasons. East *et al.* (2021) also found similar results in Bogotá, Colombia, to those found in this study. The authors identified that dust resuspension of roads was the largest local source of PM<sub>2.5</sub> (37% and 45% during dry and rainy seasons), whereas the BCON also had a great contribution (33% and 18% during dry and rainy seasons).

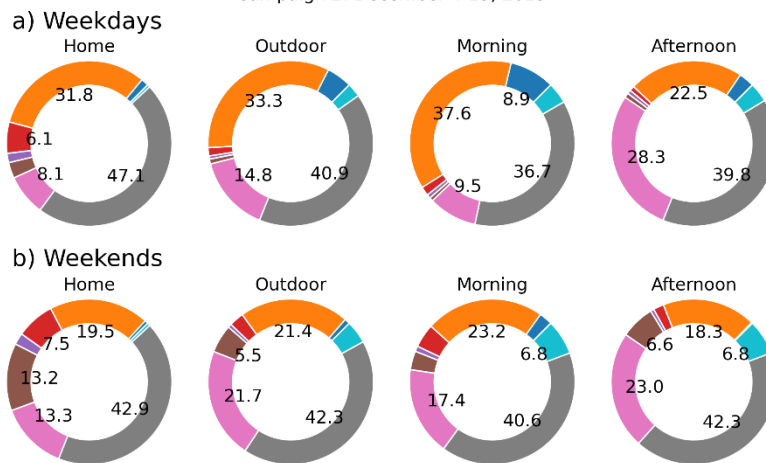
Biogenic emissions notably affected NO<sub>2</sub> concentrations during the *Morning* hours. Little differences could be seen between weekdays and weekends, but the major contributors remained the same. In the same way, despite the main contributors being also the same, the slight differences seen between the campaigns can be attributable to meteorological conditions during the three months in transforming and transporting the air pollutants (Dong *et al.*, 2020; Zhang *et al.*, 2021). The category *Others* represents any remaining that were not explicitly tracked. BCON highly dominated *Home* hours (97%), however over the day, it could be noticed the influence of the local emissions, which make BCON contribution decrease to almost 50%. The emissions from the volume and area sources, which also represent industrial activities, little affected the pollutant concentrations (0.5% – 3%). Although the analyses of Figures 49–51 showed that most of the time BCON was the major contributor, the hourly peaks were caused by the local emission sectors, meaning that their contributions are relevant to the exposure to air pollution in the region.



Campaign 1: November 2-17, 2019



Campaign 2: December 4-19, 2019



Campaign 3: February 12-19, 2020

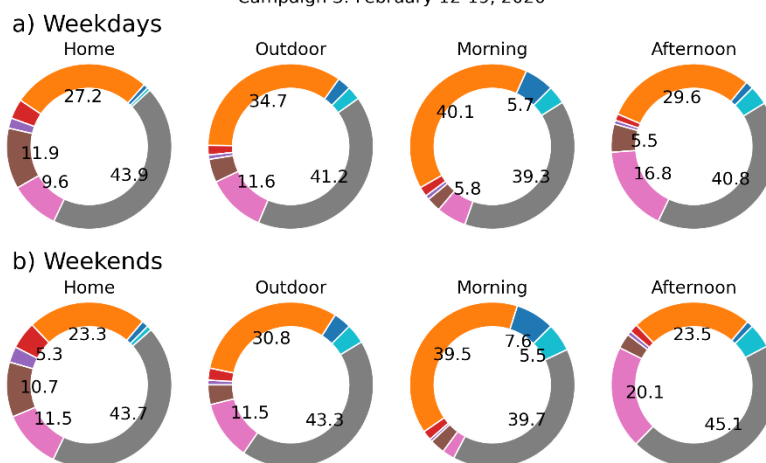
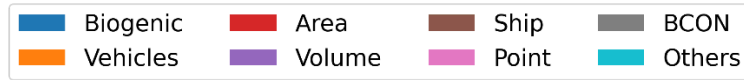
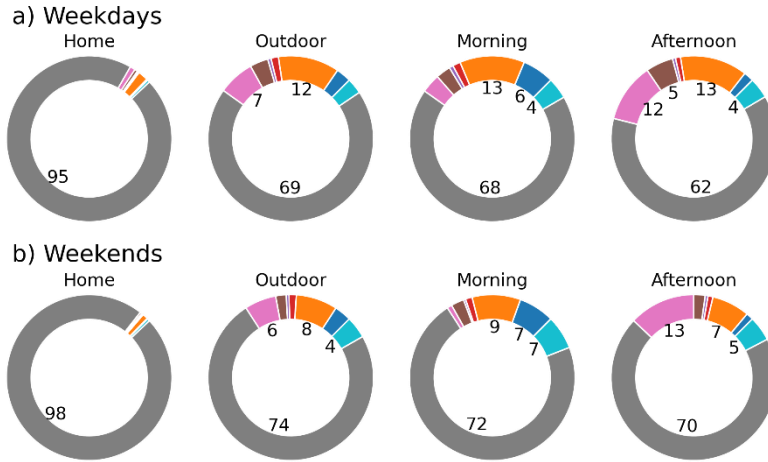


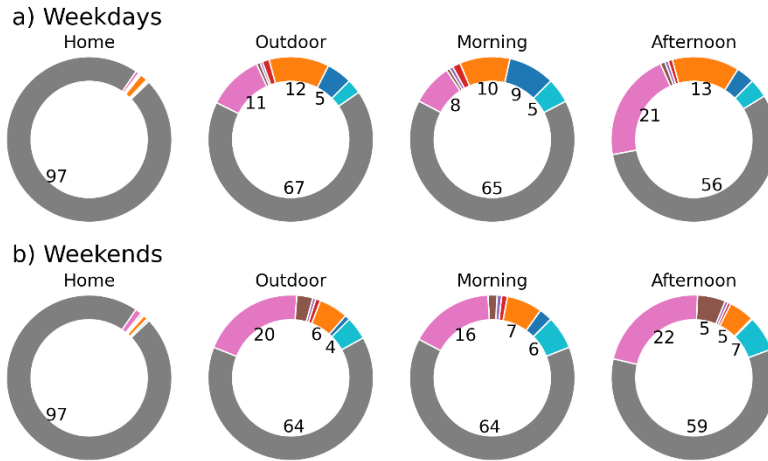
Figure 52. Contributions of different sectors to NO<sub>2</sub> concentrations for each campaign during a) weekdays and b) weekends. The numbers in the pie chart indicate the percentage of the most relevant sectors.



Campaign 1: November 2-17, 2019



Campaign 2: December 4-19, 2019



Campaign 3: February 12-19, 2020

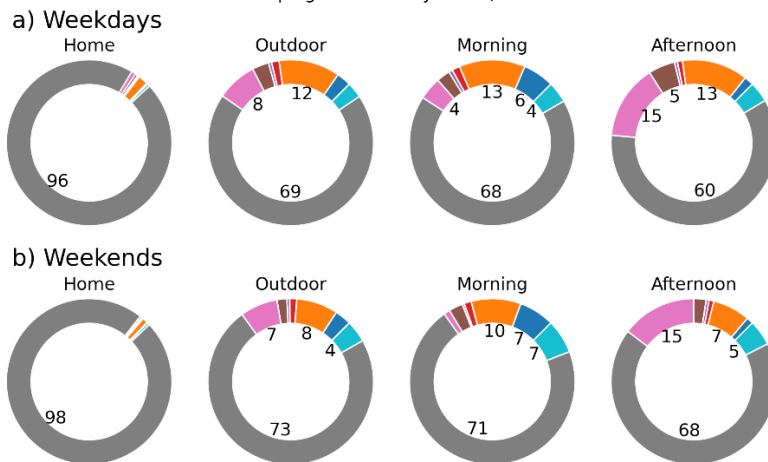


Figure 53. Contributions of different sectors to O<sub>3</sub> concentrations for each campaign during a) weekdays and b) weekends. The numbers in the pie chart indicate the percentage of the most relevant sectors.

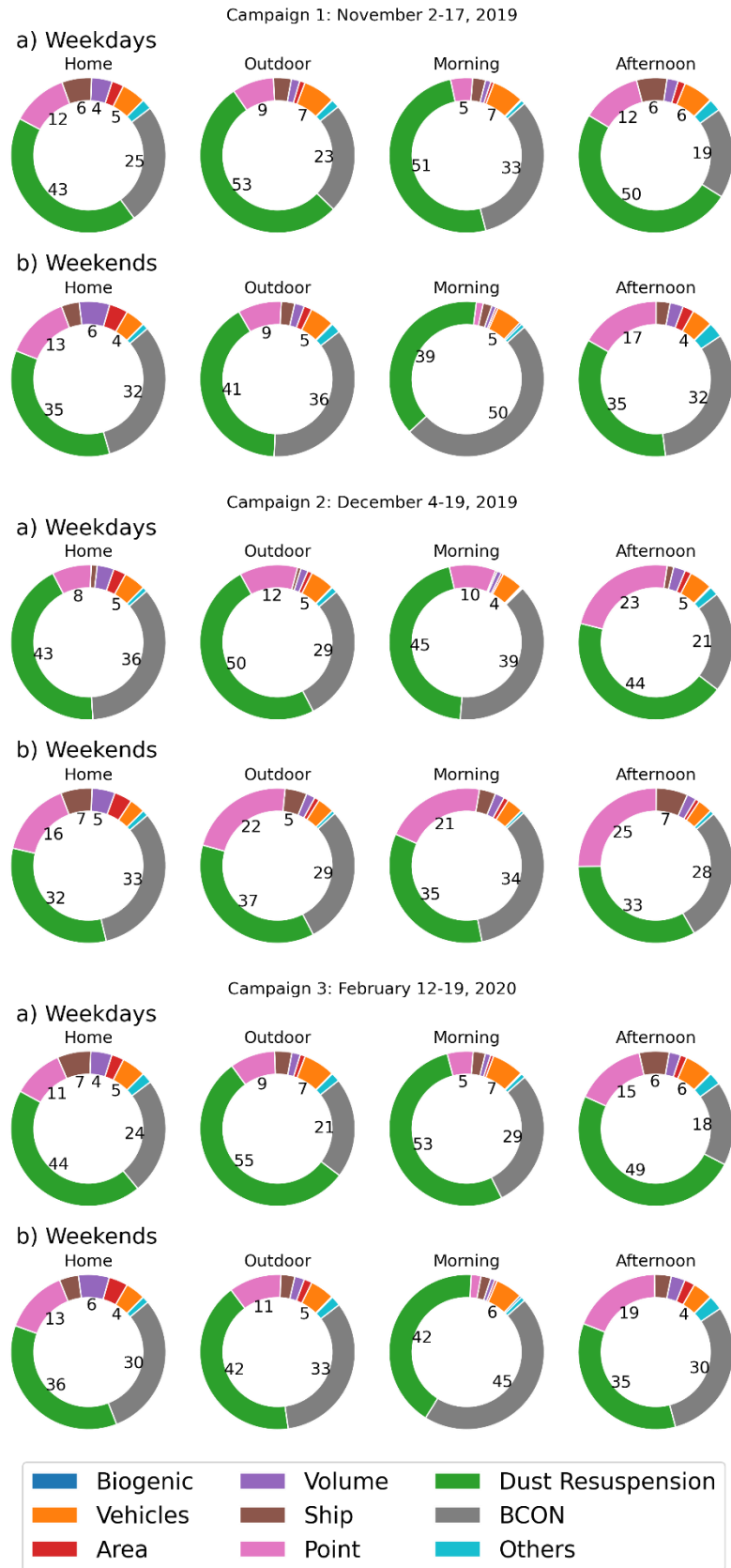


Figure 54. Contributions of different sectors to PM<sub>2.5</sub> concentrations for each campaign during a) weekdays and b) weekends. The numbers in the pie chart indicate the percentage of the most relevant sectors.

## 6. CONCLUSIONS

There are different methods to evaluate exposure to air pollution. In this study, the exposure of children to NO<sub>2</sub>, O<sub>3</sub>, PM<sub>10</sub>, PM<sub>2.5</sub>, and PM<sub>1</sub> was estimated using data from a numerical modelling system combining information from WRF-Urban and CMAQ-ISAM models. In addition, sensitivity tests were conducted to investigate the relationship between the configuration of the lowest model height and air pollutant concentrations over the Metropolitan Region of Vitória, Brazil, in November and December 2019, and February 2020. This period represents the months when experimental campaigns occurred in the region and NO<sub>2</sub> personal exposure data of twenty-one children were collected through passive samplers worn by them.

First, the modelled hourly meteorological parameters (temperature, relative humidity, and wind field) and hourly mass concentrations of NO<sub>2</sub>, O<sub>3</sub>, PM<sub>10</sub>, and PM<sub>2.5</sub> were compared with ground-based observation data to evaluate the accuracy and reliability of the models. The simulation results were generally good and able to broadly capture the values of and variation trends in the observation data. The results exhibited differences when the lowest model level height was changed, although slightly. A great advance was obtained using the BEP formulation together with the model height of 4 meters for wind speed. However, overall, the most suitable results for T2, RH2, NO<sub>2</sub>, O<sub>3</sub>, PM<sub>10</sub>, and PM<sub>2.5</sub>, when compared to observed data, were acquired with the model height set up at 20 meters. The better agreement of WS10 in simulations using the model height at 4 m did not improve the CMAQ performance. In fact, the lowering of the model height together with the use of BEP parameterization increased the concentrations and enhanced the overprediction and exposure to the air pollutants. Despite meteorological conditions playing an important role, the accuracy of the CMAQ model is also highly dependent on the quality of emissions inventory used as model input. For instance, for the majority of emissions sources (excluding the vehicular sector), the quantity of pollutants emitted was provided as a total per year, so they were equally distributed across the year in the model, impacting the hourly, daily, and monthly modelled concentrations.

Once the air pollutant concentrations were estimated by the numerical modelling system, the personal exposure was calculated using the time-activities diaries of the children, and *I/O* ratios were also used to consider the amount of time they spent indoors. In total, eight scenarios were considered to assess the children's exposure, one was using data from the fixed monitoring station and the three came from the CMAQ model that adopted different configurations ( $z = 4$



m,  $z = 10$  m,  $z = 20$  m). Additionally, each one considered two approaches (i) using I/O equal to 1, that is assuming no indoor correction, and (ii) using I/O values to represent differences between indoor and outdoor concentrations of home and school microenvironments. In general, the exposures were underestimated using the monitoring station concentrations with or without I/O correction, while the CMAQ model provided higher exposures regardless of the model height configuration. In comparison with NO<sub>2</sub> personal monitors ( $12.3 \pm 5.1 \mu\text{g}/\text{m}^3$ ), the use of I/O correction benefitted exposure results using the monitoring station ( $9.3 \pm 2.7 \mu\text{g}/\text{m}^3$ ). On the other hand, it has not benefitted exposure results using the CMAQ model, in which the most suitable performance was found with the configuration  $z = 20$  m without I/O adjustment ( $15.9 \pm 2.0 \mu\text{g}/\text{m}^3$ ). It is important to mention that applying constant I/O ratios (some derived from other study sites) could lead to uncertainties and errors in the exposure estimates.

The exposures to O<sub>3</sub>, PM<sub>10</sub>, PM<sub>2.5</sub>, and PM<sub>1</sub> were qualitatively estimated since there were no personal observations. Nevertheless, the results were presented comparing both indirect methods (monitoring station and model), which showed that the exposure to O<sub>3</sub> and PM<sub>10</sub> practically had the same magnitude. Meanwhile, for PM<sub>2.5</sub>, there was a considerable difference between the exposure estimated by the monitoring station and the CMAQ model, suggesting that studies concerning PM<sub>2.5</sub> that rely exclusively on monitoring stations in the region could be underestimated. In any case, the exposures of children to these air pollutants were comparable to other studies found in the literature. The results also revealed that, in terms of daily exposure, children of the first campaign are more exposed to O<sub>3</sub>, PM<sub>10</sub>, and PM<sub>2.5</sub> than children of the second and third campaigns. A potential inhaled dose assessment was performed considering two approaches (ADD and RDD) for PM<sub>2.5</sub> and PM<sub>1</sub>. The results showed that the potential PM inhaled dose can be about 3–4 times higher during daily activities than during sleeping hours, and the highest inhaled doses would occur between 7 p.m. and 8 p.m, with boys intaking greater doses than girls. This difference in intake doses is because the respiratory parameters for the boys were assumed to be higher than for the girls, indicating that dose assessment is highly dependent on the respiratory parameters (e.g. ventilation rate, tidal volume, breathing frequency). Additionally, the use of I/O ratios presented two directions regarding the potential of PM<sub>2.5</sub> to be favourable to cause adverse health effects. That is because if air pollutant concentrations data considered I/O correction, it indicated that PM<sub>2.5</sub> could cause adverse health effects. Otherwise, the result would be the opposite.

The source apportionment assessment revealed that the greatest contributors to children's exposure to NO<sub>2</sub> were the boundary conditions, the vehicular exhausts, the industrial point sources, and the emission from the shipping sector. For PM<sub>2.5</sub> mass concentration, the main sources were the road dust resuspension, boundary conditions, and industrial point sources. Despite the influence of BCON on both pollutant concentrations, the hourly peaks were caused by the local emissions, suggesting that local policies can play an important role in reducing the risk of children being exposed to PM<sub>2.5</sub> and NO<sub>2</sub>. On the other hand, the ISAM tool demonstrated that ozone concentrations predominantly came from the boundary conditions. In other words, outside of our study domain, it means that to reduce the health risk caused by, for instance, O<sub>3</sub>, it should also consider regional and national authorities. Slight differences in the values of source contributors were seen between the campaigns, which can be attributable to meteorological conditions since the emission quantities are almost the same.

Some of the novel aspects of this study were the use of the WRF-Urban model at a high spatial resolution in a tropical Brazilian coastal-urban area. Additionally, the use of the multi-layer urban canopy model BEP together with different model heights ( $z = 4$  m,  $z = 10$  m,  $z = 20$  m) was evaluated in modelling urban meteorological and air pollution conditions. The numerical modelling system also accounted for the source apportionment method using a local emission inventory aiming at investigating the sources that mostly contributed to the increase in children's exposure to air pollutants. This modelled approach, which is an indirect method to estimate air pollutant exposure, was compared with a direct method, which was the data collected from wearable passive samplers during experimental campaigns and are scarce in the literature, especially considering Brazilian children, in which their daily routines and habits may differ from European, American and Chinese children where most studies were carried out. To date, the present work is the first study using the aforementioned combinations.

For future investigation, it is suggested:

- Sensitivity analysis regarding the urban canopy parameters (e.g. building height, street width, building width, among others) in the BEP algorithm could be performed in order to evaluate their influence on meteorological parameters and consequently, on the concentrations of air pollutants.
- Vertical profile measurements of PBL height, ozone, PM concentrations would aid to validate the models' performance.

- Increase the domain size in order to evaluate the influence of BCON on pollutant concentrations, especially ozone.
- Sensitivity analysis of the chemical speciation profiles of the sources should be considered since the present study used those provided by the USEPA dataset and may not accurately represent the local air pollutant species.
- Some parameters adopted values found in the literature (e.g. inhalation rates, I/O ratios, ventilation rates). For future studies, these parameters could be replaced by measured values directly from the children that attend the experimental campaigns.
- The passive samplers represented the accumulative personal exposure over a week. It would be interesting to make further investigation focuses on the microenvironments that children attend, such as the transit/commuting environments (walking, bicycle, car, bus) since the literature points out that despite children spending little time in this microenvironment, the exposure generally results in higher inhaled doses.
- The use of a Global Positioning System (GPS) device to track the children's routines and routes would aid to reduce the uncertainties related to the filling of the diaries.

## 7. REFERENCES

- Adams, M. D. and Requia, W. J. (2017) 'How private vehicle use increases ambient air pollution concentrations at schools during the morning drop-off of children', *Atmospheric Environment*, 165, pp. 264–273. doi: 10.1016/j.atmosenv.2017.06.046.
- Adrees, M. *et al.* (2016) 'Gaseous pollutants from brick kiln industry decreased the growth, photosynthesis, and yield of wheat (*Triticum aestivum* L.)', *Environmental Monitoring and Assessment*, 188(5). doi: 10.1007/s10661-016-5273-8.
- Albuquerque, T. T. A. *et al.* (2019) 'Analysis of PM<sub>2.5</sub> concentrations under pollutant emission control strategies in the metropolitan area of São Paulo, Brazil', *Environmental Science and Pollution Research*, 26(32), pp. 33216–33227. doi: 10.1007/s11356-019-06447-6.
- Albuquerque, T. T. de A. *et al.* (2018) 'WRF-SMOKE-CMAQ modeling system for air quality evaluation in São Paulo megacity with a 2008 experimental campaign data', *Environmental Science and Pollution Research*, 25(36), pp. 36555–36569. doi: 10.1007/s11356-018-3583-9.
- Alimissis, A. *et al.* (2018) 'Spatial estimation of urban air pollution with the use of artificial neural network models', *Atmospheric Environment*, 191(July), pp. 205–213. doi: 10.1016/j.atmosenv.2018.07.058.
- Allan, M., Richardson, G.M., 1998. Probability density functions describing 24-hour inhalation rates for use in human health risk assessments. *Hum Ecol Risk Assess* 4:379–408. <https://doi.org/10.1080/10807039891284389>
- Almeida, D. S. *et al.* (2018) 'Genotoxic effects of daily personal exposure to particle mass and number concentrations on buccal cells', *Atmospheric Environment*, 176(June 2017), pp. 148–157. doi: 10.1016/j.atmosenv.2017.12.021.
- Alonso, M. F. *et al.* (2010) 'An urban emissions inventory for South America and its application in numerical modeling of atmospheric chemical composition at local and regional scales', *Atmospheric Environment*, 44(39), pp. 5072–5083. doi: 10.1016/j.atmosenv.2010.09.013.
- Alvarado, M. J. *et al.* (2019) 'Evaluating the use of satellite observations to supplement ground-level air quality data in selected cities in low- and middle-income countries', *Atmospheric Environment*, 218(September), p. 117016. doi: 10.1016/j.atmosenv.2019.117016.
- Amato, F. *et al.* (2014) 'Sources of indoor and outdoor PM<sub>2.5</sub> concentrations in primary schools', *Science of the Total Environment*, 490, pp. 757–765. doi: 10.1016/j.scitotenv.2014.05.051.
- Andersen, Z. J. (2020) 'Air pollution epidemiology', *Traffic-Related Air Pollution*, pp. 163–182. doi: 10.1016/B978-0-12-818122-5.00007-7.
- Anderson, H. R. *et al.* (2012) 'Satellite-based estimates of ambient air pollution and global variations in childhood asthma prevalence', *Environmental Health Perspectives*, 120(9), pp. 1333–1339. doi: 10.1289/ehp.1104724.

Andrade, M. de F. *et al.* (2017) ‘Air quality in the megacity of São Paulo: Evolution over the last 30 years and future perspectives’, *Atmospheric Environment*, 159, pp. 66–82. doi: 10.1016/j.atmosenv.2017.03.051.

Andreão, W. L., Pinto, J. A., *et al.* (2020) ‘Quantifying the impact of particle matter on mortality and hospitalizations in four Brazilian metropolitan areas’, *Journal of Environmental Management*, 270(January). doi: 10.1016/j.jenvman.2020.110840.

Andreão, W. L., Alonso, M. F., *et al.* (2020) ‘Top-down vehicle emission inventory for spatial distribution and dispersion modeling of particulate matter’, *Environmental Science and Pollution Research*. doi: 10.1007/s11356-020-08476-y.

Andreão, W. L., Albuquerque, T. T. A. and Kumar, P. (2018) ‘Excess deaths associated with fine particulate matter in Brazilian cities’, *Atmospheric Environment*, 194(September), pp. 71–81. doi: 10.1016/j.atmosenv.2018.09.034.

Andreão, W. L. and Albuquerque, T. T. de A. (2021) ‘Avoidable mortality by implementing more restrictive fine particles standards in Brazil: An estimation using satellite surface data’, *Environmental Research*, 192(September 2020). doi: 10.1016/j.envres.2020.110288.

Andries, A. *et al.* (2019) ‘Translation of Earth observation data into sustainable development indicators: An analytical framework’, *Sustainable Development*, 27(3), pp. 366–376. doi: 10.1002/sd.1908.

Ang, C., Ghosh, I. and Schell, H. (2020) *Zooming In: Visualizing the Relative Size of Particles*. Available at: <https://www.visualcapitalist.com/visualizing-relative-size-of-particles/> (Accessed: 30 September 2021).

Appel, K. W. *et al.* (2020) ‘The Community Multiscale Air Quality (CMAQ) Model Versions 5.3 and 5.3.1: System Updates and Evaluation’, *Geoscientific Model Development Discussions*, pp. 1–41. doi: 10.5194/gmd-2020-345.

Arjomandi, M. *et al.* (2015) ‘Exposure to medium and high ambient levels of ozone causes adverse systemic inflammatory and cardiac autonomic effects’, *American Journal of Physiology - Heart and Circulatory Physiology*, 308(12), pp. H1499–H1509. doi: 10.1152/ajpheart.00849.2014.

Avisar, D. *et al.* (2021) ‘High Resolution WRF Simulations for the Tel-Aviv Metropolitan Area Reveal the Urban Fingerprint in the Sea-Breeze Hodograph’, *Journal of Geophysical Research: Atmospheres*, 126(5), pp. 1–23. doi: 10.1029/2020JD033691.

Avolio, E. *et al.* (2017) ‘Sensitivity analysis of WRF model PBL schemes in simulating boundary-layer variables in southern Italy: An experimental campaign’, *Atmospheric Research*, 192(April), pp. 58–71. doi: 10.1016/j.atmosres.2017.04.003.

Baek, J. O., Cho, J. and Roh, J. Y. (2021) ‘Associations between ambient air pollution and medical care visits for atopic dermatitis’, *Environmental Research*, 195(May 2020), p. 110153. doi: 10.1016/j.envres.2020.110153.

Baklanov, A. and Zhang, Y. (2020) ‘Advances in air quality modeling and forecasting’, *Global*

*Transitions*, 2, pp. 261–270. doi: 10.1016/j.glt.2020.11.001.

Baldasano, J. M. (2020) ‘COVID-19 lockdown effects on air quality by NO<sub>2</sub> in the cities of Barcelona and Madrid (Spain)’, *Science of the Total Environment*, 741(2). doi: 10.1016/j.scitotenv.2020.140353.

Banks, R. F. *et al.* (2016) ‘Sensitivity of boundary-layer variables to PBL schemes in the WRF model based on surface meteorological observations, lidar, and radiosondes during the HygrA-CD campaign’, *Atmospheric Research*, 176–177, pp. 185–201. doi: 10.1016/j.atmosres.2016.02.024.

Barck, C. *et al.* (2005) ‘Brief exposures to NO<sub>2</sub> augment the allergic inflammation in asthmatics’, *Environmental Research*, 97(1), pp. 58–66. doi: 10.1016/j.envres.2004.02.009.

Barkjohn, K. K. *et al.* (2020) ‘Children’s microenvironmental exposure to PM<sub>2.5</sub> and ozone and the impact of indoor air filtration’, *Journal of Exposure Science and Environmental Epidemiology*, 30(6), pp. 971–980. doi: 10.1038/s41370-020-00266-5.

Bey, I. *et al.* (2001) ‘Global modeling of tropospheric chemistry with assimilated meteorology: Model description and evaluation’, *Journal of Geophysical Research Atmospheres*, 106(D19), pp. 23073–23095. doi: 10.1029/2001JD000807.

Blondeau, P. *et al.* (2005) ‘Relationship between outdoor and indoor air quality in eight French schools’, *Indoor Air*, 15(1), pp. 2–12. doi: 10.1111/j.1600-0668.2004.00263.x.

Boniardi, L. *et al.* (2019a) ‘Annual, seasonal, and morning rush hour Land Use Regression models for black carbon in a school catchment area of Milan, Italy’, *Environmental Research*, 176(June), p. 108520. doi: 10.1016/j.envres.2019.06.001.

Boniardi, L. *et al.* (2019b) ‘Is a land use regression model capable of predicting the cleanest route to school?’, *Environments - MDPI*, 6(8), pp. 1–12. doi: 10.3390/environments6080090.

Boniardi, L. *et al.* (2021) ‘Personal exposure to equivalent black carbon in children in Milan, Italy: Time-activity patterns and predictors by season’, *Environmental Pollution*, 274. doi: 10.1016/j.envpol.2021.116530.

Bont, J. *et al.* (2019) ‘Ambient air pollution and overweight and obesity in school-aged children in Barcelona, Spain’, *Environment International*, 125(September 2018), pp. 58–64. doi: 10.1016/j.envint.2019.01.048.

Borghi, F. *et al.* (2021) ‘Estimation of the inhaled dose of pollutants in different micro-environments: A systematic review of the literature’, *Toxics*, 9(6). doi: 10.3390/toxics9060140.

Boucher, O. *et al.* (2013) ‘Clouds and aerosols’, *Climate Change 2013 the Physical Science Basis: Working Group I Contribution to the Fifth Assessment Report of the Intergovernmental Panel on Climate Change*, 9781107057, pp. 571–658. doi: 10.1017/CBO9781107415324.016.

Bougeault, P., and Lacarrere P., 1989. Parameterisation of orography-induced turbulence in a mesobeta-scale model. *Monthly Weather Review*, 117, 1872–1890. [https://doi.org/10.1175/1520-0493\(1989\)117<1872:POOITI>2.0.CO;2](https://doi.org/10.1175/1520-0493(1989)117<1872:POOITI>2.0.CO;2)

Boylan, J. W. and Russell, A. G. (2006) 'PM and light extinction model performance metrics, goals, and criteria for three-dimensional air quality models', *Atmospheric Environment*, 40(26), pp. 4946–4959. doi: 10.1016/j.atmosenv.2005.09.087.

Branco, P. T. B. S. *et al.* (2014) 'The microenvironmental modelling approach to assess children's exposure to air pollution - A review', *Environmental Research*, 135, pp. 317–332. doi: 10.1016/j.envres.2014.10.002.

Brand, V. S. *et al.* (2019) 'Impact of route choice and period of the day on cyclists' exposure to black carbon in London, Rotterdam and São Paulo', *Journal of Transport Geography*, 76(February), pp. 153–165. doi: 10.1016/j.jtrangeo.2019.03.007.

Bravo, M. A. *et al.* (2012) 'Comparison of exposure estimation methods for air pollutants: Ambient monitoring data and regional air quality simulation', *Environmental Research*, 116, pp. 1–10. doi: 10.1016/j.envres.2012.04.008.

Brochu, P., Bouchard, M. and Haddad, S. (2014) 'Physiological daily inhalation rates for health risk assessment in overweight/obese children, adults, and elderly', *Risk Analysis*, 34(3), pp. 567–582. doi: 10.1111/risa.12125.

Brochu, P., Brodeur, J. and Krishnan, K. (2011) 'Derivation of physiological inhalation rates in children, adults, and elderly based on nighttime and daytime respiratory parameters', *Inhalation Toxicology*, 23(2), pp. 74–94. doi: 10.3109/08958378.2010.543439.

Brunekreef, B. *et al.* (1997) 'Air Pollution from Truck Traffic and Lung Function in Children Living near Motorways', *Epidemiology*, 8(3), pp. 298–303.

Bruyn, S. and Vries, J. (2020) 'Health costs of air pollution in European cities and the linkage with transport', p. 86. Available at: <https://ec.europa.eu/transport/sites/transport/files/studies/internalisation-handbook-isbn-978-92-79-96917-1.pdf>.

Buonanno, G. *et al.* (2012) 'Individual dose and exposure of Italian children to ultrafine particles', *Science of the Total Environment*, 438, pp. 271–277. doi: 10.1016/j.scitotenv.2012.08.074.

Buonanno, G. *et al.* (2013) 'Children exposure assessment to ultrafine particles and black carbon: The role of transport and cooking activities', *Atmospheric Environment*, 79, pp. 53–58. doi: 10.1016/j.atmosenv.2013.06.041.

Buonanno, G., Marks, G. B. and Morawska, L. (2013) 'Health effects of daily airborne particle dose in children: Direct association between personal dose and respiratory health effects', *Environmental Pollution*, 180, pp. 246–250. doi: 10.1016/j.envpol.2013.05.039.

Burr, M. J. and Zhang, Y. (2011) 'Source apportionment of fine particulate matter over the Eastern U.S. Part I: Source sensitivity simulations using CMAQ with the Brute Force method', *Atmospheric Pollution Research*, 2(3), pp. 300–317. doi: 10.5094/APR.2011.036.

Byun, D. and Schere, K. L. (2006) 'Review of the Governing Equations, Computational Algorithms, and Other Components of the Models-3 Community Multiscale Air Quality

"CMAQ... Modeling System'. doi: 10.1115/1.2128636.

Cavalcanti, I.F.A., Ferreira, N.J., Dias, M.A.F., Justi, M.G.A., 2009. Tempo e Clima no Brasil. São Paulo, Oficina de Textos.

Carvalho, A. M., Krecl, P. and Targino, A. C. (2018) 'Variations in individuals' exposure to black carbon particles during their daily activities: a screening study in Brazil', *Environmental Science and Pollution Research*, 25(19), pp. 18412–18423. doi: 10.1007/s11356-018-2045-8.

Carvalho, D. *et al.* (2014) 'WRF wind simulation and wind energy production estimates forced by different reanalyses: Comparison with observed data for Portugal', *Applied Energy*, 117, pp. 116–126. doi: 10.1016/j.apenergy.2013.12.001.

CDC, C. for D. C. and P. (2012) *Principles of Epidemiology in Public Health Practice: An Introduction to Applied Epidemiology and Biostatistics*. Atlanta, GA. Available at: <https://www.cdc.gov/csels/dsepd/ss1978/SS1978.pdf>.

Cerza, F. *et al.* (2019) 'Long-term exposure to air pollution and hospitalization for dementia in the Rome longitudinal study', *Environmental Health: A Global Access Science Source*, 18(1), pp. 1–12. doi: 10.1186/s12940-019-0511-5.

Cesaroni, G. *et al.* (2013) 'Long-term exposure to urban air pollution and mortality in a cohort of more than a million adults in Rome', *Environmental Health Perspectives*, 121(3), pp. 324–331. doi: 10.1289/ehp.1205862.

Chang, X. *et al.* (2019) 'Contributions of inter-city and regional transport to PM 2.5 concentrations in the Beijing-Tianjin-Hebei region and its implications on regional joint air pollution control', *Science of the Total Environment*, 660, pp. 1191–1200. doi: 10.1016/j.scitotenv.2018.12.474.

Chao, C. Y. H. (2001) 'Comparison between indoor and outdoor air contaminant levels in residential buildings from passive sampler study', *Building and Environment*, 36(9), pp. 999–1007. doi: 10.1016/S0360-1323(00)00057-3.

Chen, F. *et al.* (2011) 'The integrated WRF/urban modelling system: Development, evaluation, and applications to urban environmental problems', *International Journal of Climatology*, 31(2), pp. 273–288. doi: 10.1002/joc.2158.

Chen, G. *et al.* (2014) 'Evaluation of observation-fused regional air quality model results for population air pollution exposure estimation', *Science of the Total Environment*, 485–486(1), pp. 563–574. doi: 10.1016/j.scitotenv.2014.03.107.

Chen, L. A. *et al.* (2020) 'Schoolchildren ' s exposure to PM 2 . 5 : a student club – based air quality monitoring campaign using low-cost sensors', 2, pp. 543–551.

Choi, K. H. *et al.* (2020) 'Indoor and outdoor PM2.5 exposure, and anxiety among schoolchildren in Korea: a panel study', *Environmental Science and Pollution Research*, 27(22), pp. 27984–27994. doi: 10.1007/s11356-020-08900-3.

Choi, M. W. *et al.* (2019) 'Comparison of PM2.5 chemical components over East Asia



simulated by the WRF-Chem and WRF/CMAQ models: On the models' prediction inconsistency', *Atmosphere*, 10(10). doi: 10.3390/atmos10100618.

Clappier, A. *et al.* (2017) 'Source apportionment and sensitivity analysis: Two methodologies with two different purposes', *Geoscientific Model Development*, 10(11), pp. 4245–4256. doi: 10.5194/gmd-10-4245-2017.

Clench-Aas, J. *et al.* (1999) 'Air pollution exposure monitoring and estimating Part I. Integrated air quality monitoring system', *Journal of Environmental Monitoring*, 1(4), pp. 313–319. doi: 10.1039/a902775k.

Clifford, S. *et al.* (2018) 'Effects of exposure to ambient ultrafine particles on respiratory health and systemic inflammation in children', *Environment International*, 114(March), pp. 167–180. doi: 10.1016/j.envint.2018.02.019.

Cohan, D. S. and Sergey, N. L. (2011) 'Air quality response modeling for decision support', *Atmosphere*, 2(3), pp. 407–425. doi: 10.3390/atmos2030407.

Collet, S. *et al.* (2018) 'Future year ozone source attribution modeling study using CMAQ-ISAM', *Journal of the Air and Waste Management Association*, 68(11), pp. 1239–1247. doi: 10.1080/10962247.2018.1496954.

Crouse, D. L. *et al.* (2012) 'Risk of nonaccidental and cardiovascular mortality in relation to long-term exposure to low concentrations of fine particulate matter: A canadian national-level cohort study', *Environmental Health Perspectives*, 120(5), pp. 708–714. doi: 10.1289/ehp.1104049.

Cunha-Lopes, I. *et al.* (2019) 'Children's exposure to sized-fractioned particulate matter and black carbon in an urban environment', *Building and Environment*, 155(February), pp. 187–194. doi: 10.1016/j.buildenv.2019.03.045.

Dantas, G. *et al.* (2020) 'The impact of COVID-19 partial lockdown on the air quality of the city of Rio de Janeiro, Brazil', *Science of the Total Environment*, 729, p. 139085. doi: 10.1016/j.scitotenv.2020.139085.

Demirel, G. *et al.* (2014) 'Personal exposure of primary school children to BTEX, NO<sub>2</sub> and ozone in Eskişehir, Turkey: Relationship with indoor/outdoor concentrations and risk assessment', *Science of the Total Environment*, 473–474(2), pp. 537–548. doi: 10.1016/j.scitotenv.2013.12.034.

Dedele, A., Miskinyte, A., 2016. Seasonal variation of indoor and outdoor air quality of nitrogen dioxide in homes with gas and electric stoves. *Environ Sci Pollut Res* 23, 17784–17792. <https://doi.org/10.1007/s11356-016-6978-5>

Deng, Q. *et al.* (2016) 'Exposure to outdoor air pollution during trimesters of pregnancy and childhood asthma, allergic rhinitis, and eczema', *Environmental Research*, 150, pp. 119–127. doi: 10.1016/j.envres.2016.05.050.

Deygas, F. *et al.* (2021) 'Long-term atmospheric exposure to PCB153 and breast cancer risk in a case-control study nested in the French E3N cohort from 1990 to 2011', *Environmental*

*Research*, 195(September 2020). doi: 10.1016/j.envres.2021.110743.

Dimakopoulou, K. *et al.* (2020) ‘Long-term exposure to ozone and children’s respiratory health: Results from the RESPOZE study’, *Environmental Research*, 182, p. 109002. doi: 10.1016/j.envres.2019.109002.

Dockery, D. W. *et al.* (1993) ‘An association between air pollution and mortality in six U.S. cities’, *Journal of Occupational and Environmental Medicine*, p. 136. doi: 10.1097/00043764-199502000-00008.

Dong, Z. *et al.* (2020) ‘Regional transport in Beijing-Tianjin-Hebei region and its changes during 2014–2017: The impacts of meteorology and emission reduction’, *Science of the Total Environment*, 737, p. 139792. doi: 10.1016/j.scitotenv.2020.139792.

East, J. *et al.* (2021) ‘Air quality modeling to inform pollution mitigation strategies in a Latin American megacity’, *Science of the Total Environment*, 776, p. 145894. doi: 10.1016/j.scitotenv.2021.145894.

EEA, E. E. A. (2019) *Healthy environment, healthy lives: how the environment influences health and well-being in Europe — European Environment Agency*. doi: <https://doi.org/10.2800/53670>.

Elten, M. *et al.* (2020) ‘Ambient air pollution and the risk of pediatric-onset inflammatory bowel disease: A population-based cohort study’, *Environment International*, 138(January), p. 105676. doi: 10.1016/j.envint.2020.105676.

Emery, C. *et al.* (2017) ‘Recommendations on statistics and benchmarks to assess photochemical model performance’, *Journal of the Air and Waste Management Association*, 67(5), pp. 582–598. doi: 10.1080/10962247.2016.1265027.

Emery, C., Tai, E. and Yarwood, G. (2001) ‘Enhanced Meteorological Modeling and Performance Evaluation for Two Texas Ozone Episodes’, *Environ International Corporation*, p. 235.

Faria, T. *et al.* (2020) ‘Children’s exposure and dose assessment to particulate matter in Lisbon’, *Building and Environment*, 171(January), p. 106666. doi: 10.1016/j.buildenv.2020.106666.

Feng, J. *et al.* (2019) ‘The influence of spatiality on shipping emissions, air quality and potential human exposure in the Yangtze River Delta/Shanghai, China’, *Atmospheric Chemistry and Physics*, 19(9), pp. 6167–6183. doi: 10.5194/acp-19-6167-2019.

Feng, R. *et al.* (2019) ‘Investigation on air pollution control strategy in Hangzhou for post-G20/pre-Asian-games period (2018–2020)’, *Atmospheric Pollution Research*, 10(1), pp. 197–208. doi: 10.1016/j.apr.2018.07.006.

Feng, Z. *et al.* (2019) ‘Economic losses due to ozone impacts on human health, forest productivity and crop yield across China’, *Environment International*, 131(February), p. 104966. doi: 10.1016/j.envint.2019.104966.

Fernandes, K. S. *et al.* (2021) ‘Characterization, source apportionment and health risk

assessment of PM<sub>2.5</sub> for a rural classroom in the amazon: A case study', *Journal of the Brazilian Chemical Society*, 32(2), pp. 363–375. doi: 10.21577/0103-5053.20200188.

Fernandes, M. A. de O. *et al.* (2020) 'Avoiding hospital admissions for respiratory system diseases by complying to the final Brazilian air quality standard: an estimate for Brazilian southeast capitals', *Environmental Science and Pollution Research*. doi: 10.1007/s11356-020-07772-x.

Finlayson-Pitts, B. J. and Pitts, J. N. (2000) *Chemistry of the Upper and Lower Atmosphere: Theory, Experiments, and Applications*. San Diego: Academic Press.

Fino, A. (2018) *Air quality legislation*. 2nd edn, *Encyclopedia of Environmental Health*. 2nd edn. Elsevier Inc. doi: 10.1016/B978-0-12-409548-9.11045-0.

Flanders, W. D. and Kleinbaum, D. G. (1995) 'Basic models for disease occurrence in epidemiology', *International Journal of Epidemiology*, 24(1), pp. 1–7. doi: 10.1093/ije/24.1.1.

Foos, B. *et al.* (2008) 'Focusing on children's inhalation dosimetry and health effects for risk assessment: An introduction', *Journal of Toxicology and Environmental Health - Part A: Current Issues*, 71(3), pp. 149–165. doi: 10.1080/15287390701597871.

Franco, D. M. P. *et al.* (2019) 'Effect of Local Climate Zone (LCZ) classification on ozone chemical transport model simulations in Sao Paulo, Brazil', *Urban Climate*, 27(December 2018), pp. 293–313. doi: 10.1016/j.uclim.2018.12.007.

Freitas, C. U. *et al.* (2016) 'Air pollution and its impacts on health in Vitoria, Espirito Santo, Brazil', *Revista de saude publica*, 50, p. 4. doi: 10.1590/S1518-8787.2016050005909.

Fulk, F. *et al.* (2016) 'Comparison of stationary and personal air sampling with an air dispersion model for children's ambient exposure to manganese', *Journal of Exposure Science and Environmental Epidemiology*, 26(5), pp. 494–502. doi: 10.1038/jes.2016.30.

Furtaw, E. J. (2001) 'An overview of human exposure modeling activities at the USEPA's National Exposure Research Laboratory', *Toxicology and Industrial Health*, 17(10), pp. 302–314. doi: 10.1191/0748233701th107oa.

Galvão, E. S. *et al.* (2018) 'Resonant Synchrotron X-ray Diffraction determines markers for iron-rich atmospheric particulate matter in urban region', *Chemosphere*, 212, pp. 418–428. doi: 10.1016/j.chemosphere.2018.08.111.

Galvão, E. S. *et al.* (2019) 'Use of inorganic and organic markers associated with their directionality for the apportionment of highly correlated sources of particulate matter', *Science of the Total Environment*, 651, pp. 1332–1343. doi: 10.1016/j.scitotenv.2018.09.263.

Galvão, E. S., Reis, N. C. and Santos, J. M. (2020) 'The role of receptor models as tools for air quality management: a case study of an industrialized urban region', *Environmental Science and Pollution Research*, 27(29), pp. 35918–35929. doi: 10.1007/s11356-020-07848-8.

Gariazzo, C. *et al.* (2021) 'Impact of different exposure models and spatial resolution on the long-term effects of air pollution', *Environmental Research*, 192. doi:

10.1016/j.envres.2020.110351.

Gauderman, W. J. *et al.* (2004) ‘The Effect of Air Pollution on Lung Development from 10 to 18 Years of Age’, *New England Journal of Medicine*, 351(11), pp. 1057–1067. doi: 10.1056/NEJMoa040610.

George, A., Stead, T. S. and Ganti, L. (2020) ‘What’s the Risk: Differentiating Risk Ratios, Odds Ratios, and Hazard Ratios?’, *Cureus*, 12(8), pp. 6–13. doi: 10.7759/cureus.10047.

George, S. *et al.* (2020) ‘Personal level exposure and hazard potential of particulate matter during haze and non-haze periods in Singapore’, *Chemosphere*, 243, p. 125401. doi: 10.1016/j.chemosphere.2019.125401.

Géron, A. (2019) *Hands-on Machine Learning with Scikit-Learn, Keras & TensorFlow*. 2nd edn. Edited by R. Roumeliotis and N. Tache. Sebastopol, Canada: O’Reilly. Available at: <https://www.oreilly.com/library/view/hands-on-machine-learning/9781492032632/>.

Gholami, S. *et al.* (2021) ‘Sensitivity of WRF-simulated 10 m wind over the Persian Gulf to different boundary conditions and PBL parameterization schemes’, *Atmospheric Research*, 247(June 2020), p. 105147. doi: 10.1016/j.atmosres.2020.105147.

Godoi, R. H. M. *et al.* (2013) ‘Healthy environment - indoor air quality of Brazilian elementary schools nearby petrochemical industry’, *Science of the Total Environment*, 463–464, pp. 639–646. doi: 10.1016/j.scitotenv.2013.06.043.

Goel, S. *et al.* (2015) ‘Investigation of particulate matter performances in relation to chalk selection in classroom environment’, *Indoor and Built Environment*, 26(1), pp. 119–131. doi: 10.1177/1420326X15607951.

Goel, S. G. *et al.* (2021) ‘Characteristics of indoor air pollutants and estimation of their exposure dose’, *Air Quality, Atmosphere and Health*, 14(7), pp. 1033–1047. doi: 10.1007/s11869-021-00996-x.

Gomes, T. V. (2020). Avaliação da influência das emissões biogênicas na qualidade do ar: Estudo de caso para um região tropical urbanizada. Universidade Federal de Minas Gerais (UFMG). Available at <https://www.smarh.eng.ufmg.br/defesas/1386M.PDF>

Grøntoft, T. (2018) ‘Maintenance costs for European zinc and Portland limestone surfaces due to air pollution since the 1980s’, *Sustainable Cities and Society*, 39(January), pp. 1–15. doi: 10.1016/j.scs.2018.01.054.

Guarnieri, M. and Balmes, J. R. (2014) ‘Outdoor air pollution and asthma’, *The Lancet*, 383(9928), pp. 1581–1592. doi: 10.1016/S0140-6736(14)60617-6.

Guenther, A. *et al.* (2006) ‘Edinburgh Research Explorer Estimates of global terrestrial isoprene emissions using MEGAN ( Model of Emissions of Gases and Aerosols from Nature ) and Physics Estimates of global terrestrial isoprene emissions using MEGAN ( Model of Emissions of Gases an’, *Atmospheric Chemistry and Physics*, (6), pp. 3181–3210.

Guenther, A. B. *et al.* (2012) ‘The model of emissions of gases and aerosols from nature version

2.1 (MEGAN2.1): An extended and updated framework for modeling biogenic emissions’, *Geoscientific Model Development*, 5(6), pp. 1471–1492. doi: 10.5194/gmd-5-1471-2012.

Guo, M. *et al.* (2021) ‘Exposure to ambient air pollution during trimesters of pregnancy and childhood allergic diseases in Wuhan, China’, *International Journal of Environmental Health Research*, 00(00), pp. 1–11. doi: 10.1080/09603123.2021.1929873.

Habre, R. *et al.* (2018) ‘Short-term effects of airport-associated ultrafine particle exposure on lung function and inflammation in adults with asthma’, *Environment International*, 118(April), pp. 48–59. doi: 10.1016/j.envint.2018.05.031.

Han, B. S., Baik, J. J. and Kwak, K. H. (2019) ‘A preliminary study of turbulent coherent structures and ozone air quality in Seoul using the WRF-CMAQ model at a 50 m grid spacing’, *Atmospheric Environment*, 218(September). doi: 10.1016/j.atmosenv.2019.117012.

Han, X. *et al.* (2018) ‘Modeling study of impacts on surface ozone of regional transport and emissions reductions over North China Plain in summer 2015’, *Atmospheric Chemistry and Physics*, 18(16), pp. 12207–12221. doi: 10.5194/acp-18-12207-2018.

Han, X. *et al.* (2021) ‘Numerical simulation of interannual variation in transboundary contributions from Chinese emissions to PM<sub>2.5</sub> mass burden in South Korea’, *Atmospheric Environment*, 256, p. 118440. doi: 10.1016/j.atmosenv.2021.118440.

Han, X. and Zhang, M. G. (2018) ‘Assessment of the regional source contributions to PM<sub>2.5</sub> mass concentration in Beijing’, *Atmospheric and Oceanic Science Letters*, 11(2), pp. 143–149. doi: 10.1080/16742834.2018.1412796.

Han, Y. *et al.* (2016) ‘Association between size-segregated particles in ambient air and acute respiratory inflammation’, *Science of the Total Environment*, 565, pp. 412–419. doi: 10.1016/j.scitotenv.2016.04.196.

Hanna, S. and Chang, J. (2012) ‘Acceptance criteria for urban dispersion model evaluation’, *Meteorology and Atmospheric Physics*, 116(3–4), pp. 133–146. doi: 10.1007/s00703-011-0177-1.

Hannam, K. *et al.* (2013) ‘A comparison of population air pollution exposure estimation techniques with personal exposure estimates in a pregnant cohort’, *Environmental Sciences: Processes and Impacts*, 15(8), pp. 1562–1572. doi: 10.1039/c3em00112a.

Hänninen, O. *et al.* (2011) ‘Seasonal patterns of outdoor PM infiltration into indoor environments: Review and meta-analysis of available studies from different climatological zones in Europe’, *Air Quality, Atmosphere and Health*, 4(3), pp. 221–233. doi: 10.1007/s11869-010-0076-5.

Hariprasad, K. B. R. R. *et al.* (2014) ‘Numerical simulation and intercomparison of boundary layer structure with different PBL schemes in WRF using experimental observations at a tropical site’, *Atmospheric Research*, 145–146, pp. 27–44. doi: 10.1016/j.atmosres.2014.03.023.

Haynes, E. N. *et al.* (2012) ‘Assessment of personal exposure to manganese in children living

near a ferromanganese refinery’, *Science of the Total Environment*, 427–428, pp. 19–25. doi: 10.1016/j.scitotenv.2012.03.037.

Heal, M. R., Kumar, P. and Harrison, R. M. (2012) ‘Particles, air quality, policy and health’, *Chemical Society Reviews*, 41(19), pp. 6606–6630. doi: 10.1039/c2cs35076a.

Hernández-Cadena, L. *et al.* (2009) ‘Increased levels of outdoor air pollutants are associated with reduced bronchodilation in children with asthma’, *Chest*, 136(6), pp. 1529–1536. doi: 10.1378/chest.08-1463.

Herting, M. M. *et al.* (2019) ‘Outdoor Air Pollution and Brain Structure and Function From Across Childhood to Young Adulthood: A Methodological Review of Brain MRI Studies’, *Frontiers in Public Health*, 7(December). doi: 10.3389/fpubh.2019.00332.

Hesterberg, T. W. *et al.* (2009) ‘Critical review of the human data on short-term nitrogen dioxide (NO<sub>2</sub>) exposures: Evidence for NO<sub>2</sub> no-effect levels’, *Critical Reviews in Toxicology*, 39(9), pp. 743–781. doi: 10.3109/10408440903294945.

Hettfleisch, K. *et al.* (2021) ‘Individual exposure to urban air pollution and its correlation with placental angiogenic markers in the first trimester of pregnancy, in São Paulo, Brazil’, *Environmental Science and Pollution Research*, 28(22), pp. 28658–28665. doi: 10.1007/s11356-021-12353-7.

Hinds, W. C. (1999) *Aerosol Technology: Properties, Behavior, and Measurement of Airborne Particles*. Second Edi. Los Angeles: John Wiley & Sons, Inc.

Hinwood, A. *et al.* (2014) ‘Children’s personal exposure to PM<sub>10</sub> and associated metals in urban, rural and mining activity areas’, *Chemosphere*, 108, pp. 125–133. doi: 10.1016/j.chemosphere.2014.02.071.

Hoek, G. *et al.* (2008) ‘A review of land-use regression models to assess spatial variation of outdoor air pollution’, *Atmospheric Environment*, 42(33), pp. 7561–7578. doi: 10.1016/j.atmosenv.2008.05.057.

Hoek, G. (2017) ‘Methods for Assessing Long-Term Exposures to Outdoor Air Pollutants’, *Current environmental health reports*, 4(4), pp. 450–462. doi: 10.1007/s40572-017-0169-5.

Horie, Y. and Stern, A. C. (1976) *Analysis of Population Exposure to Air Pollution in the New York-New Jersey-Connecticut Tri-State Region*.

Hou, D. *et al.* (2020) ‘Associations of long-term exposure to ambient fine particulate matter and nitrogen dioxide with lung function: A cross-sectional study in China’, *Environment International*, 144(December 2019). doi: 10.1016/j.envint.2020.105977.

Hu, J. *et al.* (2016) ‘One-year simulation of ozone and particulate matter in China using WRF/CMAQ modeling system’, *Atmospheric Chemistry and Physics*, 16(16), pp. 10333–10350. doi: 10.5194/acp-16-10333-2016.

Hu, J. *et al.* (2017) ‘Ensemble prediction of air quality using the WRF/CMAQ model system for health effect studies in China’, *Atmospheric Chemistry and Physics*, 17(21), pp. 13103–

13118. doi: 10.5194/acp-17-13103-2017.

Hu, X. *et al.* (2020) ‘Inflammatory and oxidative stress responses of healthy adults to changes in personal air pollutant exposure’, *Environmental Pollution*, 263, p. 114503. doi: 10.1016/j.envpol.2020.114503.

Huang, J. *et al.* (2019) ‘Cardiorespiratory responses to low-level ozone exposure: The inDoor Ozone Study in childrEn (DOSE)’, *Environment International*, 131(April), p. 105021. doi: 10.1016/j.envint.2019.105021.

Huang, M. *et al.* (2019) ‘Sensitivity of urban boundary layer simulation to urban canopy models and PBL schemes in Beijing’, *Meteorology and Atmospheric Physics*, 131(5), pp. 1235–1248. doi: 10.1007/s00703-018-0634-1.

Huneus, N. *et al.* (2020) ‘Evaluation of anthropogenic air pollutant emission inventories for South America at national and city scale’, *Atmospheric Environment*, 235(July 2019). doi: 10.1016/j.atmosenv.2020.117606.

IBGE, (Brazilian Institute of Geography and Statistics) (2020). Available at <https://cidades.ibge.gov.br/brasil/es/vitoria/panorama>.

IEMA, (Instituto Estadual de Meio Ambiente e Recursos Hídricos) (2019). Inventário de Emissões Atmosféricas Região da Grande Vitória - Ano base 2015. Available at: <https://iema.es.gov.br/qualidadedoar/inventariodefuentes/2015>

INMET (Brazilian Institute of Meteorology). Brazilian Climatology Normal 1981-2010. Available at: <https://portal.inmet.gov.br/normais>

Isakov, V. *et al.* (2009) ‘Combining Regional- and Local-Scale Air Quality Models with Exposure Models for Use in Environmental Health Studies’, *Journal of the Air & Waste Management Association*, 59(4), pp. 461–472. doi: 10.3155/1047-3289.59.4.461.

Isakov, V., Irwin, J. S. and Ching, J. (2007) ‘Using CMAQ for exposure modeling and characterizing the subgrid variability exposure estimates’, *Journal of Applied Meteorology and Climatology*, 46(9), pp. 1354–1371. doi: 10.1175/JAM2538.1.

ISS, I. S. e S. (2019) ‘Análise do monitoramento da qualidade do ar no Brasil’, p. 20. Available at: <http://www.saudeesustentabilidade.org.br/>.

Janjić, Z.I., 1994. The step-mountain eta coordinate model: further developments of the convection, viscous sublayer, and turbulence closure schemes. *Monthly Weather Review*, 122, 927–945. [https://doi.org/10.1175/1520-0493\(1994\)122<0927:TSMECM>2.0.CO;2](https://doi.org/10.1175/1520-0493(1994)122<0927:TSMECM>2.0.CO;2)

Janssen, N. A. H. *et al.* (2001) ‘Assessment of exposure to traffic related air pollution of children attending schools near motorways’, *Atmospheric Environment*, 35(22), pp. 3875–3884. doi: 10.1016/S1352-2310(01)00144-3.

Jephcote, C. *et al.* (2021) ‘Changes in air quality during COVID-19 “lockdown” in the United Kingdom’, *Environmental Pollution*, 272, p. 116011. doi: 10.1016/j.envpol.2020.116011.

- Jerrett, M. *et al.* (2005) ‘A review and evaluation of intraurban air pollution exposure models’, *Journal of Exposure Analysis and Environmental Epidemiology*, 15(2), pp. 185–204. doi: 10.1038/sj.jea.7500388.
- Jerrett, M. *et al.* (2008) ‘Traffic-related air pollution and asthma onset in children: A prospective cohort study with individual exposure measurement’, *Environmental Health Perspectives*, 116(10), pp. 1433–1438. doi: 10.1289/ehp.10968.
- Jiang, X. and Yoo, E. hye (2018) ‘The importance of spatial resolutions of Community Multiscale Air Quality (CMAQ) models on health impact assessment’, *Science of the Total Environment*, 627, pp. 1528–1543. doi: 10.1016/j.scitotenv.2018.01.228.
- Jiménez, P. *et al.* (2006) ‘Evaluation of MM5-EMICAT2000-CMAQ performance and sensitivity in complex terrain: High-resolution application to the northeastern Iberian Peninsula’, *Atmospheric Environment*, 40(26), pp. 5056–5072. doi: 10.1016/j.atmosenv.2005.12.060.
- Jiménez, P. A. and Dudhia, J. (2013) ‘On the ability of the WRF model to reproduce the surface wind direction over complex terrain’, *Journal of Applied Meteorology and Climatology*, 52(7), pp. 1610–1617. doi: 10.1175/JAMC-D-12-0266.1.
- Jung, K. H. *et al.* (2021) ‘Personal exposure to black carbon at school and levels of fractional exhaled nitric oxide in new york city’, *Environmental Health Perspectives*, 129(9), pp. 1–10. doi: 10.1289/EHP8985.
- Karakatsani, A. *et al.* (2017) ‘Weekly personal ozone exposure and respiratory health in a panel of Greek schoolchildren’, *Environmental Health Perspectives*, 125(7), pp. 1–7. doi: 10.1289/EHP635.
- Kesmodel, U. S. (2018) ‘Cross-sectional studies – what are they good for?’, *Acta Obstetricia et Gynecologica Scandinavica*, 97(4), pp. 388–393. doi: 10.1111/aogs.13331.
- Khreis, H., de Hoogh, K. and Nieuwenhuijsen, M. J. (2018) ‘Full-chain health impact assessment of traffic-related air pollution and childhood asthma’, *Environment International*, 114(November 2017), pp. 365–375. doi: 10.1016/j.envint.2018.03.008.
- Kim, K. H., Jahan, S. A. and Kabir, E. (2013) ‘A review on human health perspective of air pollution with respect to allergies and asthma’, *Environment International*, 59, pp. 41–52. doi: 10.1016/j.envint.2013.05.007.
- Kitagawa, Y. K. L. *et al.* (2021) ‘Source apportionment modelling of PM<sub>2.5</sub> using CMAQ-ISAM over a tropical coastal-urban area’, *Atmospheric Pollution Research*, 12(12), p. 101250. doi: 10.1016/j.apr.2021.101250.
- Kitagawa, Y. K. L. *et al.* (2022a) ‘Exposure and dose assessment of school children to air pollutants in a tropical coastal-urban area’, *Science of The Total Environment*, 803(2), p. 149747. doi: 10.1016/j.scitotenv.2021.149747.
- Kitagawa, Y. K. L. *et al.* (2022b) ‘Coastal-urban meteorology: A sensitivity study using the WRF-urban model’, *Urban Climate*, 44, p. 101185. doi: 10.1016/j.uclim.2022.101185.



Kitayama, K. *et al.* (2019) ‘Uncertainties in O<sub>3</sub> concentrations simulated by CMAQ over Japan using four chemical mechanisms’, *Atmospheric Environment*, 198(November 2018), pp. 448–462. doi: 10.1016/j.atmosenv.2018.11.003.

Klepeis, N. E. *et al.* (2001) ‘The National Human Activity Pattern Survey (NHAPS): A resource for assessing exposure to environmental pollutants’, *Journal of Exposure Analysis and Environmental Epidemiology*, 11(3), pp. 231–252. doi: 10.1038/sj.jea.7500165.

Klompaker, J. O. *et al.* (2021) ‘Comparison of associations between mortality and air pollution exposure estimated with a hybrid, a land-use regression and a dispersion model’, *Environment International*, 146, p. 106306. doi: 10.1016/j.envint.2020.106306.

Knol, M. J., Algra, A. and Groenwold, R. H. H. (2012) ‘How to deal with measures of association: A short guide for the clinician’, *Cerebrovascular Diseases*, 33(2), pp. 98–103. doi: 10.1159/000334180.

Koenig, J. Q. *et al.* (1981) ‘Effects of SO<sub>2</sub> plus NaCl aerosol combined with moderate exercise on pulmonary function in asthmatic adolescents’, *Environmental Research*, 25(2), pp. 340–348. doi: 10.1016/0013-9351(81)90036-0.

Koenig, J. Q. (1999) ‘Air pollution and asthma’, *Journal of Allergy and Clinical Immunology*, 104(4 I), pp. 717–722. doi: 10.1016/S0091-6749(99)70280-0.

Kornartit, C. *et al.* (2010) ‘Activity pattern and personal exposure to nitrogen dioxide in indoor and outdoor microenvironments’, *Environment International*, 36(1), pp. 36–45. doi: 10.1016/j.envint.2009.09.004.

Kousa, A. *et al.* (2002) ‘A model for evaluating the population exposure to ambient air pollution in an urban area’, *Atmospheric Environment*, 36(13), pp. 2109–2119. doi: 10.1016/S1352-2310(02)00228-5.

Kreit, J. W. *et al.* (1989) ‘Ozone-induced changes in pulmonary function and bronchial responsiveness in asthmatics’, *Journal of Applied Physiology*, 66(1), pp. 217–222. doi: 10.1152/jappl.1989.66.1.217.

Kruskal, W. H. and Wallis, W. A. (1952) ‘Use of Ranks in One-Criterion Variance Analysis’, *Journal of the American Statistical Association*, 47(260), p. 583. doi: 10.2307/2280779.

Kubesch, N. *et al.* (2015) ‘Arterial blood pressure responses to short-term exposure to low and high traffic-related air pollution with and without moderate physical activity’, *European Journal of Preventive Cardiology*, 22(5), pp. 548–557. doi: 10.1177/2047487314555602.

Kumar, P. *et al.* (2009) ‘Comparative study of measured and modelled number concentrations of nanoparticles in an urban street canyon’, *Atmospheric Environment*, 43(4), pp. 949–958. doi: 10.1016/j.atmosenv.2008.10.025.

Kumar, P. *et al.* (2014) ‘Ultrafine particles in cities’, *Environment International*, 66, pp. 1–10. doi: 10.1016/j.envint.2014.01.013.

Kumar, P. and Goel, A. (2016) ‘Concentration dynamics of coarse and fine particulate matter

at and around signalised traffic intersections’, *Environmental Science: Processes and Impacts*, 18(9), pp. 1220–1235. doi: 10.1039/c6em00215c.

Kumar, P. and Morawska, L. (2019) ‘Could fighting airborne transmission be the next line of defence against COVID-19 spread?’, *City and Environment Interactions*, 4, p. 100033. doi: 10.1016/j.cacint.2020.100033.

Kumar, P., Rivas, I. and Sachdeva, L. (2017) ‘Exposure of in-pram babies to airborne particles during morning drop-in and afternoon pick-up of school children’, *Environmental Pollution*, 224, pp. 407–420. doi: 10.1016/j.envpol.2017.02.021.

Kusaka, H. *et al.* (2001) ‘A Simple Single-Layer Urban Canopy Model For Atmospheric Models: Comparison With Multi-Layer And Slab Models’, *Boundary-Layer Meteorology*, 101(3), pp. 329–358. doi: 10.1023/A:1019207923078.

Kusaka, H. and Kimura, F. (2004) ‘Thermal effects of urban canyon structure on the nocturnal heat island: Numerical experiment using a mesoscale model coupled with an urban canopy model’, *Journal of Applied Meteorology*, 43(12), pp. 1899–1910. doi: 10.1175/JAM2169.1.

Kwok, R. H. F. *et al.* (2015) ‘Photochemical grid model implementation and application of VOC, NO<sub>x</sub>, and O<sub>3</sub> source apportionment’, *Geoscientific Model Development*, 8(1), pp. 99–114. doi: 10.5194/gmd-8-99-2015.

Kwok, R. H. F., Napelenok, S. L. and Baker, K. R. (2013) ‘Implementation and evaluation of PM<sub>2.5</sub> source contribution analysis in a photochemical model’, *Atmospheric Environment*, 80, pp. 398–407. doi: 10.1016/j.atmosenv.2013.08.017.

La Paz, D., Borge, R. and Martilli, A. (2016) ‘Assessment of a high resolution annual WRF-BEP/CMAQ simulation for the urban area of Madrid (Spain)’, *Atmospheric Environment*, 144, pp. 282–296. doi: 10.1016/j.atmosenv.2016.08.082.

Lai, H. C. *et al.* (2019) ‘Design and application of a hybrid assessment of air quality models for the source apportionment of PM<sub>2.5</sub>’, *Atmospheric Environment*, 212(April), pp. 116–127. doi: 10.1016/j.atmosenv.2019.05.038.

Lee, J. Y., Lee, S. B. and Bae, G. N. (2014) ‘A review of the association between air pollutant exposure and allergic diseases in children’, *Atmospheric Pollution Research*, 5(4), pp. 616–629. doi: 10.5094/APR.2014.071.

Lee, K. *et al.* (2004) ‘Outdoor/indoor/personal ozone exposures of children in nashville, tennessee’, *Journal of the Air and Waste Management Association*, 54(3), pp. 352–359. doi: 10.1080/10473289.2004.10470904.

Lei, X. *et al.* (2020) ‘Necessity of personal sampling for exposure assessment on specific constituents of PM<sub>2.5</sub>: Results of a panel study in Shanghai, China’, *Environment International*, 141(April), p. 105786. doi: 10.1016/j.envint.2020.105786.

Li, R. *et al.* (2019) ‘Study on the contribution of transport to PM<sub>2.5</sub> in typical regions of China using the regional air quality model RAMS-CMAQ’, *Atmospheric Environment*, 214, p. 116856. doi: 10.1016/j.atmosenv.2019.116856.

Lian, J. *et al.* (2018) ‘Evaluation of the WRF-UCM mesoscale model and ECMWF global operational forecasts over the Paris region in the prospect of tracer atmospheric transport modeling’, *Elementa*, 6. doi: 10.1525/elementa.319.

Liao, J. *et al.* (2014) ‘Impacts of different urban canopy schemes in WRF/Chem on regional climate and air quality in Yangtze River Delta, China’, *Atmospheric Research*, 145–146, pp. 226–243. doi: 10.1016/j.atmosres.2014.04.005.

Liao, K. *et al.* (2021) ‘Statistical Approaches for Forecasting Primary Air Pollutants: A Review’, *Atmosphere*, 12(6), p. 686. doi: 10.3390/atmos12060686.

Lim, S. S. *et al.* (2012) ‘A comparative risk assessment of burden of disease and injury attributable to 67 risk factors and risk factor clusters in 21 regions, 1990–2010: A systematic analysis for the Global Burden of Disease Study 2010’, *The Lancet*, 380(9859), pp. 2224–2260. doi: 10.1016/S0140-6736(12)61766-8.

Lin, C. Y. *et al.* (2008) ‘Urban heat island effect and its impact on boundary layer development and land-sea circulation over northern Taiwan’, *Atmospheric Environment*, 42(22), pp. 5635–5649. doi: 10.1016/j.atmosenv.2008.03.015.

Lin, W. Y. *et al.* (2020) ‘Analysis of air quality and health co-benefits regarding electric vehicle promotion coupled with power plant emissions’, *Journal of Cleaner Production*, 247, p. 119152. doi: 10.1016/j.jclepro.2019.119152.

Linaje, N. G.-A. de, Mattar, C. and Borvarán, D. (2019) ‘Quantifying the wind energy potential differences using different WRF initial conditions on Mediterranean coast of Chile’, *Energy*, 188. doi: 10.1016/j.energy.2019.116027.

Liu, F. H. *et al.* (2021) ‘Maternal exposure to sulfur dioxide and the risk of oral clefts in Liaoning Province, China: a population-based case-control study’, *Environmental Science and Pollution Research*, 28(29), pp. 39101–39109. doi: 10.1007/s11356-021-13461-0.

Liu, H. *et al.* (2018) ‘Ground-level ozone pollution and its health impacts in China’, *Atmospheric Environment*, 173(July 2017), pp. 223–230. doi: 10.1016/j.atmosenv.2017.11.014.

Liu, H. *et al.* (2019) ‘Episode analysis of regional contributions to tropospheric ozone in Beijing using a regional air quality model’, *Atmospheric Environment*, 199, pp. 299–312. doi: 10.1016/j.atmosenv.2018.11.044.

Liu, T. *et al.* (2020) ‘Impacts of model resolution on predictions of air quality and associated health exposure in Nanjing, China’, *Chemosphere*, 249, p. 126515. doi: 10.1016/j.chemosphere.2020.126515.

Liu, Y. *et al.* (2006) ‘Verification of a mesoscale data-assimilation and forecasting system for the Oklahoma City area during the joint urban 2003 field project’, *Journal of Applied Meteorology and Climatology*, 45(7), pp. 912–929. doi: 10.1175/JAM2383.1.

Lu, X. *et al.* (2016) ‘Estimation of health and economic costs of air pollution over the Pearl River Delta region in China’, *Science of the Total Environment*, 566–567, pp. 134–143. doi:

10.1016/j.scitotenv.2016.05.060.

Lung, S. C. C. *et al.* (2020) ‘Concurrent assessment of personal, indoor, and outdoor PM<sub>2.5</sub> and PM<sub>1</sub> levels and source contributions using novel low-cost sensing devices’, *Indoor Air*, (June 2020), pp. 755–768. doi: 10.1111/ina.12763.

Ly, L. *et al.* (2021) ‘Application of machine learning algorithms to improve numerical simulation prediction of PM<sub>2.5</sub> and chemical components’, *Atmospheric Pollution Research*, 12(11), p. 101211. doi: 10.1016/j.apr.2021.101211.

Machado, M. *et al.* (2015) ‘Annoyance Caused by Air Pollution: A Comparative Study of Two Industrialized Regions’, *World Academy of Science, Engineering and Technology, International Journal of Environmental and Ecological Engineering*, 2(2), pp. 182–187. Available at: <https://www.waset.org/abstracts/15305>.

Maciel, F. M. *et al.* (2021) ‘Impact of emission control strategies on air quality: a case study in Piracicaba, São Paulo—Brazil’, *International Journal of Environmental Science and Technology*, (0123456789). doi: 10.1007/s13762-021-03441-9.

Madureira, J. *et al.* (2020) ‘Assessment of indoor air exposure at residential homes: Inhalation dose and lung deposition of PM<sub>10</sub>, PM<sub>2.5</sub> and ultrafine particles among newborn children and their mothers’, *Science of the Total Environment*, 717. doi: 10.1016/j.scitotenv.2020.137293.

Maji, K. J. *et al.* (2019) ‘Ozone pollution in Chinese cities: Assessment of seasonal variation, health effects and economic burden’, *Environmental Pollution*, 247(x), pp. 792–801. doi: 10.1016/j.envpol.2019.01.049.

Marcon, A. *et al.* (2021) ‘Spatial variability of nitrogen dioxide and formaldehyde and residential exposure of children in the industrial area of Viadana, Northern Italy’, *Environmental Science and Pollution Research*, 28(22), pp. 28096–28106. doi: 10.1007/s11356-020-12015-0.

Martilli, A. *et al.* (2009) ‘Description of the modifications made in WRF.3.1 and short user’s manual of BEP’, *Ncar*, pp. 1–24. Available at: [http://www.ral.ucar.edu/research/land/technology/urban/Multi\\_layer\\_UCM.pdf](http://www.ral.ucar.edu/research/land/technology/urban/Multi_layer_UCM.pdf).

Martilli, A. *et al.* (2022) ‘Simulating the pollutant dispersion during persistent Wintertime thermal Inversions over urban areas. The case of Madrid’, *Atmospheric Research*, 270(January). doi: 10.1016/j.atmosres.2022.106058.

Martilli, A., Clappier, A. and Rotach, M. W. (2002) ‘An urban surface exchange parameterisation for mesoscale models’, *Boundary-Layer Meteorology*, 104(2), pp. 261–304. doi: 10.1023/A:1016099921195.

Martins, V. *et al.* (2020) ‘Relationship between indoor and outdoor size-fractionated particulate matter in urban microenvironments: Levels, chemical composition and sources’, *Environmental Research*, 183(January), p. 109203. doi: 10.1016/j.envres.2020.109203.

Mathur, R. *et al.* (2017) ‘Extending the Community Multiscale Air Quality (CMAQ) modeling system to hemispheric scales: overview of process considerations and initial applications’,

*Atmospheric Chemistry and Physics*, 17(20), pp. 12449–12474. doi: 10.5194/acp-17-12449-2017.

Mazaheri, M. *et al.* (2014) ‘School children’s personal exposure to ultrafine particles in the urban environment’, *Environmental Science and Technology*, 48(1), pp. 113–120. doi: 10.1021/es403721w.

Mazaheri, M. *et al.* (2019) ‘Characteristics of school children’s personal exposure to ultrafine particles in Heshan, Pearl River Delta, China – A pilot study’, *Environment International*, 132(April), p. 105134. doi: 10.1016/j.envint.2019.105134.

Mellor, G.L., and Yamada, T., 1982. Development of a turbulence closure model for geophysical fluid problems. *Rev. Geophys.*, 20, 851–875. <https://doi.org/10.1029/RG020i004p00851>.

Michael, R. *et al.* (2018) ‘Application of geostatistical approaches to predict the spatio-temporal distribution of summer ozone in Houston, Texas’, *Journal of Exposure Science and Environmental Epidemiology*, 29(6), pp. 806–820. doi: 10.1038/s41370-018-0091-4.

Miller, M. R. and Newby, D. E. (2020) ‘Air pollution and cardiovascular disease: Car sick’, *Cardiovascular Research*, 116(2), pp. 279–294. doi: 10.1093/cvr/cvz228.

Milner, J., Dimitroulopoulou, C. and Apsimon, H. (2005) ‘Indoor concentrations in buildings from sources outdoors’, (*ADMLC Annual Report 2004-05 ADMLC/*), (ADMLC/).

Mircea, M. *et al.* (2020) *European guide on air pollution source apportionment for particulate matter with source oriented models and their combined use with receptor models*. Publications Office of the European Union, Luxembourg. doi: 10.2760/470628.

Mölter, A. *et al.* (2012) ‘Performance of a microenvironmental model for estimating personal NO<sub>2</sub> exposure in children’, *Atmospheric Environment*, 51(2), pp. 225–233. doi: 10.1016/j.atmosenv.2012.01.030.

Mölter, A. N. (2012) *Air Pollution Exposure and Respiratory Health in Childhood*. The University of Manchester.

Monticelli, D. de F., Santos, J. M., Goulart, E. V., Mill, J. G., Kumar, P., *et al.* (2021) ‘A review on the role of dispersion and receptor models in asthma research’, *Environmental Pollution*, 287(May). doi: 10.1016/j.envpol.2021.117529.

Monticelli, D. de F., Santos, J. M., Goulart, E. V., Mill, J. G., da Silva Corrêa, J., *et al.* (2021) ‘Comparison of methods for assessment of children exposure to air pollution: dispersion model, ambient monitoring, and personal samplers’, *Air Quality, Atmosphere & Health*, (0123456789). doi: 10.1007/s11869-021-01123-6.

Monticelli, D. de F. (2020). Estimating asthmatic children exposure and dose to air pollutants in an urban industrialized area. Universidade Federal do Espírito Santo (UFES). Available at <https://engenhariaambiental.ufes.br/pt-br/pos-graduacao/PPGEA/detalhes-da-tese?id=14631>

Mudway, I. S. *et al.* (2019) ‘Impact of London’s low emission zone on air quality and children’s

respiratory health: a sequential annual cross-sectional study', *The Lancet Public Health*, 4(1), pp. e28–e40. doi: 10.1016/S2468-2667(18)30202-0.

Nakashima, Y. *et al.* (2014) 'Near-surface vertical profiles of urban roadside NO<sub>x</sub> and fine particles', *Aerosol and Air Quality Research*, 14(6), pp. 1763–1768. doi: 10.4209/aaqr.2013.08.0278.

Nascimento, A. P. *et al.* (2017) 'Association between the concentration of fine particles in the atmosphere and acute respiratory diseases in children', *Revista de Saude Publica*, 51(1), pp. 1–10. doi: 10.1590/S1518-8787.2017051006523.

Nascimento, A. P. *et al.* (2020) 'Association between the incidence of acute respiratory diseases in children and ambient concentrations of SO<sub>2</sub>, PM<sub>10</sub> and chemical elements in fine particles', *Environmental Research*, 188(January), p. 109619. doi: 10.1016/j.envres.2020.109619.

Nascimento, L. R. do *et al.* (2020) 'Performance assessment of solar photovoltaic technologies under different climatic conditions in Brazil', *Renewable Energy*, 146, pp. 1070–1082. doi: 10.1016/j.renene.2019.06.160.

National Research Council, N. (2002) *Estimating the Public Health Benefits of Proposed Air Pollution Regulations*, *Estimating the Public Health Benefits of Proposed Air Pollution Regulations*. doi: 10.17226/10511.

Nedbor-Gross, R. *et al.* (2018) 'Air quality modeling in Bogotá Colombia using local emissions and natural mitigation factor adjustment for re-suspended particulate matter', *Atmospheric Pollution Research*, 9(1), pp. 95–104. doi: 10.1016/j.apr.2017.07.004.

Nguyen, G. T. H. *et al.* (2019) 'Numerical assessment of PM<sub>2.5</sub> and O<sub>3</sub> air quality in continental Southeast Asia: Baseline simulation and aerosol direct effects investigation', *Atmospheric Environment*, 219(March), p. 117054. doi: 10.1016/j.atmosenv.2019.117054.

Nguyen, G. T. H. *et al.* (2020) 'Numerical assessment of PM<sub>2.5</sub> and O<sub>3</sub> air quality in Continental Southeast Asia: Impacts of future projected anthropogenic emission change and its impacts in combination with potential future climate change impacts', *Atmospheric Environment*, 226(September 2019), p. 117398. doi: 10.1016/j.atmosenv.2020.117398.

Nieuwenhuijsen, M. (2015). 'Exposure Assessment in Environmental Epidemiology', 2nd ed., *Exposure Assessment in Environmental Epidemiology*. Oxford University Press. doi: 10.1093/med/9780199378784.001.0001

Niu, G. Y. *et al.* (2011) 'The community Noah land surface model with multiparameterization options (Noah-MP): 1. Model description and evaluation with local-scale measurements', *Journal of Geophysical Research Atmospheres*, 116(12), pp. 1–19. doi: 10.1029/2010JD015139.

Niu, Y. *et al.* (2018) 'Estimation of personal ozone exposure using ambient concentrations and influencing factors', *Environment International*, 117(May), pp. 237–242. doi: 10.1016/j.envint.2018.05.017.

Nyarku, M. *et al.* (2019) 'Schoolchildren's personal exposure to ultrafine particles in and near

Accra, Ghana’, *Environment International*, 133(September), p. 105223. doi: 10.1016/j.envint.2019.105223.

Oberdörster, G., Oberdörster, E. and Oberdörster, J. (2005) ‘Nanotoxicology: An emerging discipline evolving from studies of ultrafine particles’, *Environmental Health Perspectives*, 113(7), pp. 823–839. doi: 10.1289/ehp.7339.

Olaniyan, T. *et al.* (2020) ‘The association between ambient NO<sub>2</sub> and PM<sub>2.5</sub> with the respiratory health of school children residing in informal settlements: A prospective cohort study’, *Environmental Research*, 186(2), p. 109606. doi: 10.1016/j.envres.2020.109606.

Ott, W. R. (1982) ‘Concepts of human exposure to air pollution’, *Environment International*, 7(3), pp. 179–196. doi: 10.1016/0160-4120(82)90104-0.

Otte, T. L. and Pleim, J. E. (2010) ‘The Meteorology-Chemistry Interface Processor (MCIP) for the CMAQ modeling system: Updates through MCIPv3.4.1’, *Geoscientific Model Development*, 3(1), pp. 243–256. doi: 10.5194/gmd-3-243-2010.

Pacitto, A. *et al.* (2021) ‘Daily submicron particle doses received by populations living in different low- and middle-income countries’, *Environmental Pollution*, 269, p. 116229. doi: 10.1016/j.envpol.2020.116229.

Palazzi, P., Hardy, E. M. and Appenzeller, B. M. R. (2019) ‘Biomonitoring of children exposure to urban pollution and environmental tobacco smoke with hair analysis – A pilot study on children living in Paris and Yeu Island, France’, *Science of the Total Environment*, 665, pp. 864–872. doi: 10.1016/j.scitotenv.2019.02.177.

Pallarés, S. *et al.* (2019) ‘The relationship between indoor and outdoor levels of PM<sub>10</sub> and its chemical composition at schools in a coastal region in Spain’, *Heliyon*, 5(8). doi: 10.1016/j.heliyon.2019.e02270.

Pañella, P. *et al.* (2017) ‘Ultrafine particles and black carbon personal exposures in asthmatic and non-asthmatic children at school age’, *Indoor Air*, 27(5), pp. 891–899. doi: 10.1111/ina.12382.

Paunescu, A. C. *et al.* (2017) ‘Personal measurement of exposure to black carbon and ultrafine particles in schoolchildren from PARIS cohort (Paris, France)’, *Indoor Air*, 27(4), pp. 766–779. doi: 10.1111/ina.12358.

Pedruzzi, R. *et al.* (2019) ‘Performance evaluation of a photochemical model using different boundary conditions over the urban and industrialized metropolitan area of Vitória, Brazil’, *Environmental Science and Pollution Research*, 26(16), pp. 16125–16144. doi: 10.1007/s11356-019-04953-1.

Peláez, L. M. G. *et al.* (2020) ‘Air quality status and trends over large cities in South America’, *Environmental Science and Policy*, 114(April), pp. 422–435. doi: 10.1016/j.envsci.2020.09.009.

Pepe, N. *et al.* (2016) ‘Development and application of a high resolution hybrid modelling system for the evaluation of urban air quality’, *Atmospheric Environment*, 141, pp. 297–311.

doi: 10.1016/j.atmosenv.2016.06.071.

Physick, W. *et al.* (2011) ‘Measurements of personal exposure to NO<sub>2</sub> and modelling using ambient concentrations and activity data’, *Atmospheric Environment*, 45(12), pp. 2095–2102. doi: 10.1016/j.atmosenv.2011.01.063.

Pope, C. A. *et al.* (2002) ‘Lung Cancer, Cardiopulmonary Mortality, and Long-term Exposure to Fine Particulate Air Pollution’, *The Journal of the American Medical Association*, 287(9), pp. 1132–1141. Available at: <http://jama.jamanetwork.com/article.aspx?doi=10.1001/jama.287.9.1132>.

Pope, C. A. and Dockery, D. W. (2006) ‘Health effects of fine particulate air pollution: Lines that connect’, *Journal of the Air and Waste Management Association*, 56(6), pp. 709–742. doi: 10.1080/10473289.2006.10464485.

Powers, J. G. *et al.* (2017) ‘The weather research and forecasting model: Overview, system efforts, and future directions’, *Bulletin of the American Meteorological Society*, 98(8), pp. 1717–1737. doi: 10.1175/BAMS-D-15-00308.1.

Prüss-Ustün, A. *et al.* (2016) ‘Preventing disease through healthy environments: A global assessment of the environmental burden of disease’, *Toxicology Letters*, 259, p. S1. doi: 10.1016/j.toxlet.2016.07.028.

Pu, X. *et al.* (2021) ‘Differential effects of size-specific particulate matter on lower respiratory infections in children: A multi-city time-series analysis in Sichuan, China’, *Environmental Research*, 193(October 2020), p. 110581. doi: 10.1016/j.envres.2020.110581.

Punger, E. M. and West, J. J. (2013) ‘The effect of grid resolution on estimates of the burden of ozone and fine particulate matter on premature mortality in the USA’, *Air Quality, Atmosphere and Health*, 6(3), pp. 563–573. doi: 10.1007/s11869-013-0197-8.

Reis, S. *et al.* (2018) ‘The influence of residential and workday population mobility on exposure to air pollution in the UK’, *Environment International*, 121, pp. 803–813. doi: 10.1016/j.envint.2018.10.005.

Ren, X., Mi, Z. and Georgopoulos, P. G. (2020) ‘Comparison of Machine Learning and Land Use Regression for fine scale spatiotemporal estimation of ambient air pollution: Modeling ozone concentrations across the contiguous United States’, *Environment International*, 142(June), p. 105827. doi: 10.1016/j.envint.2020.105827.

Ribeiro, I. *et al.* (2021) ‘Highly resolved WRF-BEP/BEM simulations over Barcelona urban area with LCZ’, *Atmospheric Research*, 248(July 2020), p. 105220. doi: 10.1016/j.atmosres.2020.105220.

Rivas, I. *et al.* (2014) ‘Child exposure to indoor and outdoor air pollutants in schools in Barcelona, Spain’, *Environment International*, 69, pp. 200–212. doi: 10.1016/j.envint.2014.04.009.

Rivas, I. *et al.* (2016) ‘Spatiotemporally resolved black carbon concentration, schoolchildren’s exposure and dose in Barcelona’, *Indoor Air*, 26(3), pp. 391–402. doi: 10.1111/ina.12214.



Rivas, I. *et al.* (2017) ‘Determinants of black carbon, particle mass and number concentrations in London transport microenvironments’, *Atmospheric Environment*, 161, pp. 247–262. doi: 10.1016/j.atmosenv.2017.05.004.

Rodrigues, M., Natário, I. and Martins, M. do R. de O. (2021) ‘Estimate the effects of environmental determining factors on childhood asthma hospital admissions in Lisbon, Portugal: a time series modelling study’, *Theoretical and Applied Climatology*, 143(1–2), pp. 809–821. doi: 10.1007/s00704-020-03415-w.

Rooney, B. *et al.* (2019) ‘Impacts of household sources on air pollution at village and regional scales in India’, *Atmospheric Chemistry and Physics*, 19(11), pp. 7719–7742. doi: 10.5194/acp-19-7719-2019.

Salamanca, F. *et al.* (2011) ‘A study of the urban boundary layer using different urban parameterizations and high-resolution urban canopy parameters with WRF’, *Journal of Applied Meteorology and Climatology*, 50(5), pp. 1107–1128. doi: 10.1175/2010JAMC2538.1.

Salamanca, F., Martilli, A. and Yagüe, C. (2012) ‘A numerical study of the Urban Heat Island over Madrid during the DESIREX (2008) campaign with WRF and an evaluation of simple mitigation strategies’, *International Journal of Climatology*, 32(15), pp. 2372–2386. doi: 10.1002/joc.3398.

Salma, I. *et al.* (2020) ‘What can we learn about urban air quality with regard to the first outbreak of the COVID-19 pandemic? A case study from central Europe’, *Atmospheric Chemistry and Physics*, 20(24), pp. 15725–15742. doi: 10.5194/acp-20-15725-2020.

Salonen, H., Salthammer, T. and Morawska, L. (2019) ‘Human exposure to NO<sub>2</sub> in school and office indoor environments’, *Environment International*, 130(March), p. 104887. doi: 10.1016/j.envint.2019.05.081.

Salvador, N. *et al.* (2016) ‘Estudo da camada limite interna térmica em condições de brisa do mar, utilizando diferentes parametrizações: Aplicação do modelo wrf na região da grande vitória’, *Revista Brasileira de Meteorologia*, 31(4), pp. 593–609. doi: 10.1590/0102-7786312314b20150093.

Salvador, P. (2018) *Ozone, SO<sub>x</sub> and NO<sub>x</sub>, particulate matter, and urban air*, *Encyclopedia of the Anthropocene*. Elsevier Inc. doi: 10.1016/B978-0-12-809665-9.09975-4.

Santos, J. M. *et al.* (2017) ‘Source apportionment of settleable particles in an impacted urban and industrialized region in Brazil’, *Environmental Science and Pollution Research*, 24(27), pp. 22026–22039. doi: 10.1007/s11356-017-9677-y.

Santos, U. P. *et al.* (2016) ‘Association between traffic air pollution and reduced forced vital capacity: A study using personal monitors for outdoor workers’, *PLoS ONE*, 11(10), pp. 1–12. doi: 10.1371/journal.pone.0163225.

Sarmiento, D. P. *et al.* (2017) ‘A comprehensive assessment of land surface-atmosphere interactions in a WRF/Urban modeling system for Indianapolis, IN’, *Elementa*, 5(1), pp. 1–22. doi: 10.1525/elementa.132.

- Schaap, M. *et al.* (2015) ‘Performance of European chemistry transport models as function of horizontal resolution’, *Atmospheric Environment*, 112, pp. 90–105. doi: 10.1016/j.atmosenv.2015.04.003.
- Schultz, E. S. *et al.* (2012) ‘Traffic-related air pollution and lung function in children at 8 years of age: A birth cohort study’, *American Journal of Respiratory and Critical Care Medicine*, 186(12), pp. 1286–1291. doi: 10.1164/rccm.201206-1045OC.
- Schultz, E. S., Litonjua, A. A. and Melén, E. (2017) ‘Effects of Long-Term Exposure to Traffic-Related Air Pollution on Lung Function in Children’, *Current Allergy and Asthma Reports*, 17(6). doi: 10.1007/s11882-017-0709-y.
- Schwartz, J. (2004) ‘Air Pollution and Children’s Health’, 113(4).
- Schwartz, J. and Marcus, A. (1990) ‘Mortality and air pollution in London: A time series analysis’, *American Journal of Epidemiology*, 133(6), pp. 631–632. doi: 10.1093/oxfordjournals.aje.a115937.
- Seinfeld, J. H., and Pandis, S. N. (2006). ‘Atmospheric Chemistry and Physics from Air Pollution to Climate Change’, 2<sup>nd</sup> ed. John Wiley & Sons, Inc., New Jersey.
- Segalin, B. *et al.* (2017) ‘Size-segregated particulate matter inside residences of elderly in the Metropolitan Area of São Paulo, Brazil’, *Atmospheric Environment*, 148, pp. 139–151. doi: 10.1016/j.atmosenv.2016.10.004.
- Seinfeld, J. H. and Pandis, S. N. (2006) *Atmospheric Chemistry and Physics: From Air Pollution to Climate Change*, *Physics Today*. doi: 10.1063/1.882420.
- Serpa, F. S. *et al.* (2014) ‘Prevalência de asma, rinite e eczema atópico em escolares do município de Vitória, Espírito Santo, Brasil’, *Revista Brasileira de Pesquisa em Saúde/Brazilian Journal of Health Research*, (June 2014). doi: 10.21722/rbps.v16i3.10144.
- Sharma, A. *et al.* (2017) ‘Urban meteorological modeling using WRF: a sensitivity study’, *International Journal of Climatology*, 37(4), pp. 1885–1900. doi: 10.1002/joc.4819.
- Sharma, A. and Kumar, P. (2018) ‘A review of factors surrounding the air pollution exposure to in-pram babies and mitigation strategies’, *Environment International*, 120(August), pp. 262–278. doi: 10.1016/j.envint.2018.07.038.
- Sharma, A. and Kumar, P. (2020) ‘Quantification of air pollution exposure to in-pram babies and mitigation strategies’, *Environment International*, 139(December 2019), p. 105671. doi: 10.1016/j.envint.2020.105671.
- Shin, H. H., Hong, S. Y. and Dudhia, J. (2012) ‘Impacts of the lowest model level height on the performance of planetary boundary layer parameterizations’, *Monthly Weather Review*, 140(2), pp. 664–682. doi: 10.1175/MWR-D-11-00027.1.
- Shrestha, P. M. *et al.* (2019) ‘Impact of outdoor air pollution on indoor air quality in low-income homes during wildfire seasons’, *International Journal of Environmental Research and Public Health*, 16(19), pp. 1–8. doi: 10.3390/ijerph16193535.

Silva, A. M. C. *et al.* (2014) ‘Low birth weight at term and the presence of fine particulate matter and carbon monoxide in the Brazilian Amazon: A population-based retrospective cohort study’, *BMC Pregnancy and Childbirth*, 14(1), pp. 1–8. doi: 10.1186/1471-2393-14-309.

Sinharay, R. *et al.* (2018) ‘Respiratory and cardiovascular responses to walking down a traffic-polluted road compared with walking in a traffic-free area in participants aged 60 years and older with chronic lung or heart disease and age-matched healthy controls: a randomised, crossover’, *The Lancet*, 391(10118), pp. 339–349. doi: 10.1016/S0140-6736(17)32643-0.

Siuta, D., West, G. and Stull, R. (2017) ‘WRF hub-height wind forecast sensitivity to PBL scheme, grid length, and initial condition choice in complex terrain’, *Weather and Forecasting*, 32(2), pp. 493–509. doi: 10.1175/WAF-D-16-0120.1.

Skamarock, W. C. *et al.* (2008) *A Description of the Advanced Research WRF Version 3, Technical Report*. doi: 10.5065/D6DZ069T.

Skamarock, W. C. *et al.* (2021) ‘A Description of the Advanced Research WRF Model Version 4.3’, *NCAR Technical Note*, (July), pp. 1–165. doi: <http://dx.doi.org/10.5065/1dfh-6p97>.

Smith, J. D. *et al.* (2016) ‘London Hybrid Exposure Model: Improving Human Exposure Estimates to NO<sub>2</sub> and PM<sub>2.5</sub> in an Urban Setting’, *Environmental Science and Technology*, 50(21), pp. 11760–11768. doi: 10.1021/acs.est.6b01817.

Song, J. *et al.* (2021) ‘From PM<sub>2.5</sub> exposure to PM<sub>2.5</sub> risks of inhaled dose in daily activities: Empirical evidence during workdays from guangzhou, China’, *Atmospheric Environment*, 249(135), p. 118224. doi: 10.1016/j.atmosenv.2021.118224.

Sorek-Hamer, M., Chatfield, R. and Liu, Y. (2020) ‘Review: Strategies for using satellite-based products in modeling PM<sub>2.5</sub> and short-term pollution episodes’, *Environment International*, 144(June), p. 106057. doi: 10.1016/j.envint.2020.106057.

Souri, A. H. *et al.* (2020) ‘An Inversion of NO<sub>x</sub> and NMVOC Emissions using Satellite Observations during the KORUS-AQ Campaign and Implications for Surface Ozone over East Asia’, *Acpd*, (March). doi: 10.5194/acp-2020-220.

Souza, J. B. *et al.* (2014) ‘Principal components and generalized linear modeling in the correlation between hospital admissions and air pollution’, *Revista de Saude Publica*, 48(3), pp. 451–458. doi: 10.1590/S0034-8910.2014048005078.

Souza, J. B. *et al.* (2018) ‘Generalized additive models with principal component analysis: an application to time series of respiratory disease and air pollution data’, *Journal of the Royal Statistical Society. Series C: Applied Statistics*, 67(2), pp. 453–480. doi: 10.1111/rssc.12239.

Souza Silva, P. R. *et al.* (2016) ‘High risk of respiratory diseases in children in the fire period in Western Amazon’, *Revista de Saude Publica*, 50, pp. 1–11. doi: 10.1590/S1518-8787.2016050005667.

Spix, C. *et al.* (1998) ‘Short-term effects of air pollution on hospital admissions of respiratory diseases in europe: A quantitative summary of apeha study results’, *Archives of Environmental Health*, 53(1), pp. 54–64. doi: 10.1080/00039899809605689.

Stare, J. and Maucort-Boulch, D. (2016) ‘Odds Ratio, Hazard Ratio and Relative Risk’, *Advances in Methodology & Statistics*, 13(1), pp. 59–67. Available at: [https://www.researchgate.net/publication/316515598\\_Odds\\_Ratio\\_Hazard\\_Ratio\\_and\\_Relative\\_Risk](https://www.researchgate.net/publication/316515598_Odds_Ratio_Hazard_Ratio_and_Relative_Risk).

Steinle, S., Reis, S. and Sabel, C. E. (2013) ‘Quantifying human exposure to air pollution-Moving from static monitoring to spatio-temporally resolved personal exposure assessment’, *Science of the Total Environment*, 443, pp. 184–193. doi: 10.1016/j.scitotenv.2012.10.098.

Tan, J. *et al.* (2017) ‘Evaluation and potential improvements of WRF/CMAQ in simulating multi-levels air pollution in megacity Shanghai, China’, *Stochastic Environmental Research and Risk Assessment*, 31(10), pp. 2513–2526. doi: 10.1007/s00477-016-1342-3.

Tao, H. *et al.* (2020) ‘Impacts of improved modeling resolution on the simulation of meteorology, air quality, and human exposure to PM<sub>2.5</sub>, O<sub>3</sub> in Beijing, China’, *Journal of Cleaner Production*, 243, p. 118574. doi: 10.1016/j.jclepro.2019.118574.

Thomas, D. C. (2009) *Statistical Methods in Environmental Epidemiology*. New York, NY, USA: Oxford University Press.

Thunis, P. *et al.* (2019) ‘Source apportionment to support air quality planning: Strengths and weaknesses of existing approaches’, *Environment International*, 130(June), p. 104825. doi: 10.1016/j.envint.2019.05.019.

Tran, P. T. M. *et al.* (2020) ‘Cyclists’ personal exposure to traffic-related air pollution and its influence on bikeability’, *Transportation Research Part D: Transport and Environment*, 88(October). doi: 10.1016/j.trd.2020.102563.

Tu, Y. *et al.* (2021) ‘A national cross-sectional study of exposure to outdoor nitrogen dioxide and aeroallergen sensitization in Australian children aged 7–11 years’, *Environmental Pollution*, 271, p. 116330. doi: 10.1016/j.envpol.2020.116330.

USEPA, (United States Environmental Protection Agency) (1996). Quality Assurance Procedures and DARS Software. United States of America. Available at: <https://www.epa.gov/air-emissions-inventories/volume-6-quality-assurance-procedures-and-dars-software>.

USEPA, (United States Environmental Protection Agency) (2009). Metabolically Derived Human Ventilation Rates: A Revised Approach Based Upon Oxygen Consumption Rates (Final Report, 2009). U.S. Environmental Protection Agency, Washington, DC, EPA/600/R-06/129F.

USEPA, (United States Environmental Protection Agency) (2011) *Exposure Factors Handbook: 2011 Edition., Highlights of the Chinese Exposure Factors Handbook*. Edited by U. S. E. P. A. Office of Research and Development. Washington. doi: 10.1016/b978-0-12-803125-4.00012-2.

USEPA, (United States Environmental Protection Agency) (2020). Exposure Assessment Tools by Routes – Inhalation. Disponível em <<https://www.epa.gov/expobox/exposure-assessment-tools-routes-inhalation>>.

Vallero, D. (2014a) 'Air Pollutant Hazards', *Fundamentals of Air Pollution*, pp. 197–214. doi: 10.1016/b978-0-12-401733-7.00007-4.

Vallero, D. (2014b) *Air Pollutant Kinetics and Equilibrium, Fundamentals of Air Pollution*. doi: 10.1016/b978-0-12-401733-7.00018-9.

Vallero, D. (2014c) *The Science of Air Pollution, Fundamentals of Air Pollution*. doi: 10.1016/b978-0-12-401733-7.00003-7.

Velasco, M. L. Z. (2020). Estudo exploratório da qualidade do ar interior em escolas públicas de ensino fundamental. Universidade Federal do Espírito Santo (UFES). Available at <https://engenhariaambiental.ufes.br/pt-br/pos-graduacao/PPGEA/detalhes-da-tese?id=14689>

Viana, M., Díez, S. and Reche, C. (2011) 'Indoor and outdoor sources and infiltration processes of PM1 and black carbon in an urban environment', *Atmospheric Environment*, 45(35), pp. 6359–6367. doi: 10.1016/j.atmosenv.2011.08.044.

Vinceti, M. *et al.* (2016) 'Does maternal exposure to benzene and PM10 during pregnancy increase the risk of congenital anomalies? A population-based case-control study', *Science of the Total Environment*, 541, pp. 444–450. doi: 10.1016/j.scitotenv.2015.09.051.

Vlasenko, A., Matthias, V. and Callies, U. (2021) 'Simulation of chemical transport model estimates by means of a neural network using meteorological data', *Atmospheric Environment*, 254(October 2020), p. 118236. doi: 10.1016/j.atmosenv.2021.118236.

Wang, C. M. *et al.* (2020) 'Exposure to fine particulate matter (PM2.5) and pediatric rheumatic diseases', *Environment International*, 138(August 2019), p. 105602. doi: 10.1016/j.envint.2020.105602.

Wang, H. *et al.* (2021) 'Impact of different urban canopy models on air quality simulation in Chengdu, southwestern China', *Atmospheric Environment*, 267(September), p. 118775. doi: 10.1016/j.atmosenv.2021.118775.

Wang, J. *et al.* (2017) 'Historical Trends in PM 2.5 -Related Premature Mortality during 1990–2010 across the Northern Hemisphere', *Environmental Health Perspectives*, 125(3), pp. 400–408. doi: 10.1289/EHP298.

Wang, L. *et al.* (2020) 'Analysis of NOx pollution characteristics in the atmospheric environment in Changchun city', *Atmosphere*, 11(1). doi: 10.3390/ATMOS11010030.

Wang, S.-W. *et al.* (2009) 'Modeling of Personal Exposures to Ambient Air Toxics in Camden, New Jersey: An Evaluation Study', *Journal of the Air & Waste Management Association*, 59(6), pp. 733–746. doi: 10.3155/1047-3289.59.6.733.

Wang, X. and Cheng, Z. (2020) 'Cross-Sectional Studies: Strengths, Weaknesses, and Recommendations', *Chest*, 158(1), pp. S65–S71. doi: 10.1016/j.chest.2020.03.012.

WHO (1991) *Investigating environmental disease outbreaks : a training manual*. Available at: <https://apps.who.int/iris/handle/10665/58374>.

WHO (2010). World Health Organization European Centre for Environment and Health. Guidelines for indoor air quality - selected pollutants. Available at <[https://www.euro.who.int/\\_\\_data/assets/pdf\\_file/0009/128169/e94535.pdf](https://www.euro.who.int/__data/assets/pdf_file/0009/128169/e94535.pdf)>

WHO (2018) 'Air Pollution and Child Health', *Who*, 113, p. 32. Available at: [http://pediatrics.aappublications.org/content/113/Supplement\\_3/1037.full.html](http://pediatrics.aappublications.org/content/113/Supplement_3/1037.full.html).

WHO (2021) *WHO global air quality guidelines: particulate matter (PM<sub>2.5</sub> and PM<sub>10</sub>), ozone, nitrogen dioxide, sulfur dioxide and carbon monoxide*. World Health Organization. Available at: <https://apps.who.int/iris/handle/10665/345329>.

Wong, P. Y. *et al.* (2021) 'Using land-use machine learning models to estimate daily NO<sub>2</sub> concentration variations in Taiwan', *Journal of Cleaner Production*, 317(2), p. 128411. doi: 10.1016/j.jclepro.2021.128411.

Xie, X. *et al.* (2017) 'A review of urban air pollution monitoring and exposure assessment methods', *ISPRS International Journal of Geo-Information*, 6(12), pp. 1–21. doi: 10.3390/ijgi6120389.

Xu, D. *et al.* (2020) 'Acute effects of ambient PM<sub>2.5</sub> on lung function among schoolchildren', *Scientific Reports*, 10(1), pp. 1–8. doi: 10.1038/s41598-020-61003-4.

Yang, X. *et al.* (2019) 'New method for evaluating winter air quality: PM<sub>2.5</sub> assessment using Community Multi-Scale Air Quality Modeling (CMAQ) in Xi'an', *Atmospheric Environment*, 211(19), pp. 18–28. doi: 10.1016/j.atmosenv.2019.04.019.

Yang, X. *et al.* (2021) 'Origin of regional springtime ozone episodes in the Sichuan Basin, China: Role of synoptic forcing and regional transport', *Environmental Pollution*, 278, p. 116845. doi: 10.1016/j.envpol.2021.116845.

Yoo, J. W. *et al.* (2019) 'Investigating the regional difference of aerosol feedback effects over South Korea using the WRF-CMAQ two-way coupled modeling system', *Atmospheric Environment*, 218(September), p. 116968. doi: 10.1016/j.atmosenv.2019.116968.

Yoon, H. *et al.* (2020) 'Development of General Exposure Factors for Risk Assessment in Korean Children', *International journal of environmental research and public health*, 17(6), pp. 1–14. doi: 10.3390/ijerph17061988.

Zhang, L. *et al.* (2018) 'Personal exposure measurements of school-children to fine particulate matter (PM<sub>2.5</sub>) in winter of 2013, Shanghai, China', *PLoS ONE*, 13(4), pp. 1–16. doi: 10.1371/journal.pone.0193586.

Zhang, Y. *et al.* (2012) 'Real-time air quality forecasting, part I: History, techniques, and current status', *Atmospheric Environment*, 60, pp. 632–655. doi: 10.1016/j.atmosenv.2012.06.031.

Zhang, Y. *et al.* (2021) 'City-level air quality improvement in the Beijing-Tianjin-Hebei region from 2016/17 to 2017/18 heating seasons: Attributions and process analysis', *Environmental Pollution*, 274, p. 116523. doi: 10.1016/j.envpol.2021.116523.

Zhao, H. *et al.* (2013) ‘Characteristics of visibility and particulate matter (PM) in an urban area of Northeast China’, *Atmospheric Pollution Research*, 4(4), pp. 427–434. doi: 10.5094/APR.2013.049.

Zheng, H. *et al.* (2021) ‘Long-term exposure to ambient air pollution and obesity in school-aged children and adolescents in Jiangsu province of China’, *Environmental Research*, 195(January), p. 110804. doi: 10.1016/j.envres.2021.110804.

Zhou, L., Chen, X. and Tian, X. (2018) ‘The impact of fine particulate matter (PM<sub>2.5</sub>) on China’s agricultural production from 2001 to 2010’, *Journal of Cleaner Production*, 178, pp. 133–141. doi: 10.1016/j.jclepro.2017.12.204.

Zou, Q. Y. *et al.* (2018) ‘Exposure to air pollution and risk of prevalence of childhood allergic rhinitis: A meta-analysis’, *International Journal of Pediatric Otorhinolaryngology*, 112(June), pp. 82–90. doi: 10.1016/j.ijporl.2018.06.039.

## Appendix



Table S1. Statistical metrics for WS10.

Month	Station	Mean <sub>Obs</sub>	Media <sub>Obs</sub>	SD <sub>Obs</sub>	Height	Mean <sub>Mod</sub>	Media <sub>Mod</sub>	SD <sub>Mod</sub>	MB	RSME	MAGE	r	IOA	FAC2
Nov	AERO PORT O	4.10	3.60	2.30	4m	1.77	1.78	0.82	-2.32	2.94	2.40	0.70	0.56	0.36
					10m	2.03	2.05	0.92	-2.05	2.69	2.17	0.72	0.58	0.48
					20m	2.79	2.85	1.20	-1.29	2.12	1.68	0.70	0.67	0.76
Dec		4.05	3.60	2.26	4m	1.90	1.93	0.89	-2.15	2.71	2.22	0.80	0.60	0.36
					10m	2.14	2.21	1.00	-1.91	2.47	2.02	0.81	0.63	0.50
					20m	2.79	2.90	1.33	-1.26	1.91	1.55	0.80	0.75	0.81
Feb		3.74	3.35	2.06	4m	1.62	1.67	0.82	-2.12	2.60	2.16	0.78	0.59	0.33
					10m	1.84	1.88	0.89	-1.90	2.40	1.97	0.78	0.61	0.45
					20m	2.45	2.48	1.17	-1.28	1.86	1.52	0.78	0.72	0.76
Nov	ASMA- VIX	1.08	0.67	1.07	4m	1.45	1.43	0.64	0.35	1.15	0.93	0.24	0.51	0.47
					10m	1.81	1.81	0.76	0.69	1.31	1.08	0.28	0.53	0.46
					20m	2.57	2.57	1.05	1.44	1.91	1.63	0.28	0.48	0.36
Dec		1.33	0.91	1.17	4m	1.49	1.53	0.64	0.16	1.10	0.85	0.39	0.58	0.56
					10m	1.88	1.99	0.80	0.55	1.22	0.97	0.43	0.63	0.55
					20m	2.61	2.75	1.12	1.28	1.75	1.49	0.45	0.58	0.42
Feb		1.05	0.71	0.94	4m	1.29	1.29	0.62	0.24	0.85	0.66	0.52	0.69	0.58
					10m	1.60	1.64	0.73	0.55	1.02	0.83	0.50	0.66	0.51
					20m	2.24	2.32	1.01	1.20	1.54	1.28	0.51	0.58	0.39
Nov	CARA PINA	1.33	1.15	0.71	4m	4.89	4.92	2.56	3.56	4.27	3.65	0.41	0.25	0.15
					10m	5.14	5.17	2.28	3.82	4.26	3.84	0.64	0.28	0.05
					20m	4.99	5.01	2.07	3.67	4.03	3.67	0.68	0.29	0.06
Dec		1.41	1.32	0.74	4m	4.93	5.08	2.57	3.54	4.19	3.60	0.57	0.29	0.15
					10m	5.27	5.42	2.34	3.86	4.30	3.89	0.72	0.30	0.06
					20m	4.98	5.19	2.20	3.57	3.96	3.59	0.76	0.32	0.07
Feb		1.24	1.16	0.63	4m	4.19	4.11	2.32	2.95	3.61	3.06	0.49	0.28	0.16
					10m	4.62	4.63	2.00	3.39	3.75	3.40	0.71	0.29	0.07
					20m	4.39	4.47	1.91	3.15	3.49	3.16	0.74	0.31	0.08
Nov	CARIA CICA	1.72	1.65	0.96	4m	1.49	1.55	0.68	-0.23	0.82	0.67	0.58	0.72	0.76
					10m	1.77	1.81	0.76	0.05	0.79	0.63	0.61	0.77	0.77
					20m	2.48	2.58	1.06	0.76	1.19	0.95	0.60	0.69	0.69

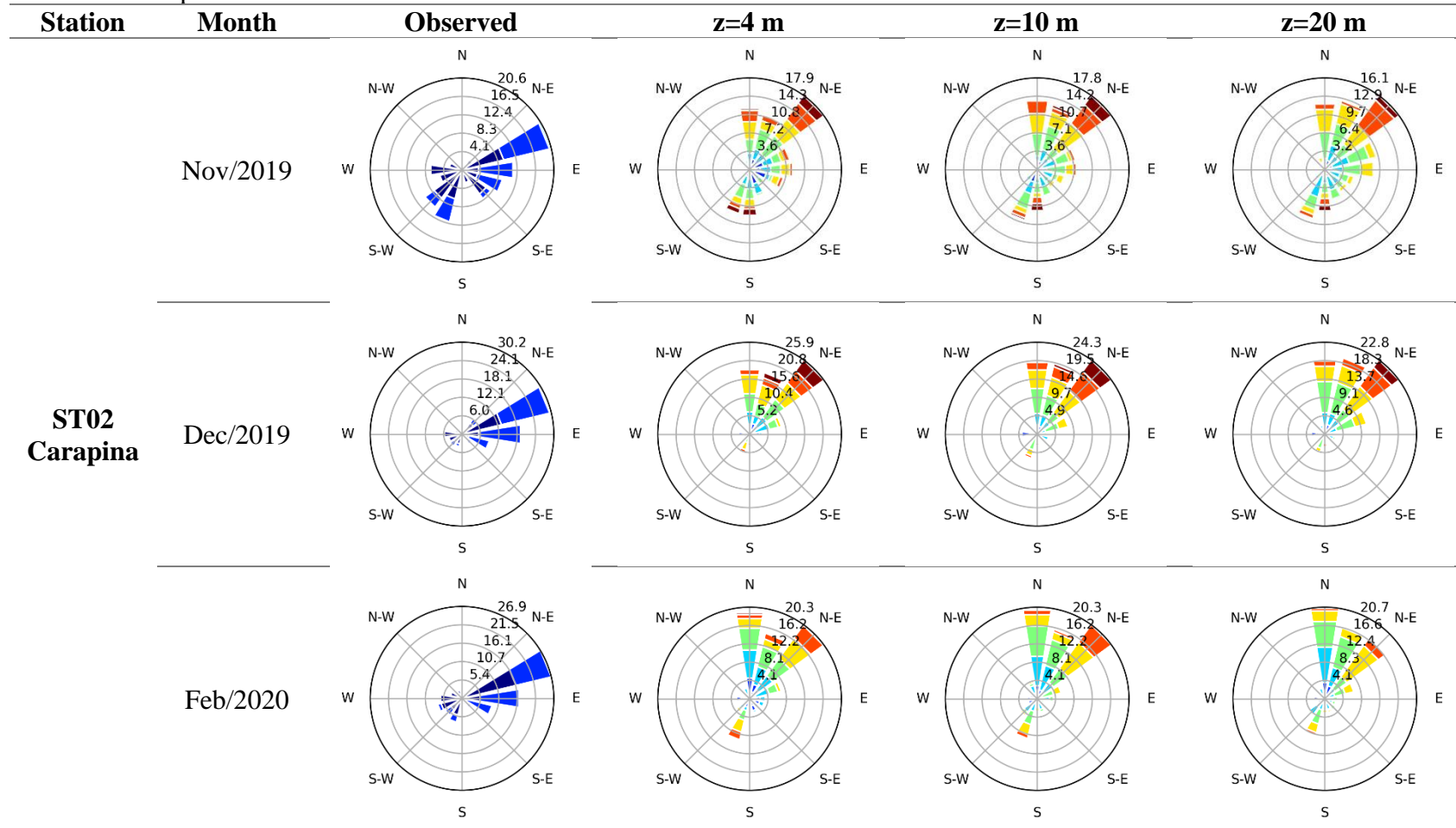
<b>Dec</b>		1.99	1.90	0.91	4m	1.67	1.74	0.71	-0.33	0.67	0.54	0.76	0.82	0.91
					10m	1.94	2.04	0.82	-0.06	0.59	0.46	0.77	0.87	0.90
					20m	2.70	2.85	1.13	0.71	1.02	0.82	0.76	0.78	0.82
<b>Feb</b>		1.85	1.78	0.74	4m	1.44	1.50	0.66	-0.42	0.70	0.55	0.69	0.76	0.83
					10m	1.67	1.73	0.73	-0.19	0.61	0.47	0.69	0.81	0.85
					20m	2.32	2.44	1.00	0.47	0.86	0.70	0.69	0.76	0.85
<b>Nov</b>		1.72	1.55	0.87	4m	2.05	1.96	0.95	0.33	0.83	0.66	0.65	0.78	0.82
					10m	2.41	2.38	1.03	0.69	1.06	0.86	0.66	0.72	0.76
					20m	3.10	3.04	1.27	1.38	1.70	1.47	0.62	0.57	0.56
<b>Dec</b>	ENSEA DA	1.94	1.81	0.91	4m	2.12	2.13	1.02	0.19	0.75	0.60	0.72	0.84	0.86
					10m	2.46	2.50	1.13	0.52	0.94	0.75	0.72	0.79	0.84
					20m	3.10	3.20	1.38	1.17	1.51	1.26	0.72	0.65	0.71
<b>Feb</b>		1.71	1.54	0.86	4m	1.81	1.80	0.96	0.10	0.69	0.53	0.73	0.84	0.84
					10m	2.10	2.08	1.03	0.39	0.83	0.65	0.71	0.80	0.84
					20m	2.68	2.70	1.28	0.97	1.34	1.10	0.69	0.67	0.72
<b>Nov</b>		2.44	2.23	1.29	4m	1.72	1.65	0.81	-0.71	1.17	0.96	0.70	0.71	0.76
					10m	1.97	1.91	0.88	-0.46	1.03	0.84	0.70	0.77	0.83
					20m	2.74	2.69	1.18	0.31	1.04	0.83	0.68	0.81	0.80
<b>Dec</b>	IBES	2.75	2.59	1.29	4m	1.83	1.84	0.88	-0.89	1.17	1.00	0.79	0.76	0.81
					10m	2.07	2.08	0.96	-0.65	0.99	0.83	0.80	0.82	0.89
					20m	2.82	2.88	1.29	0.12	0.81	0.62	0.79	0.90	0.88
<b>Feb</b>		2.53	2.45	1.11	4m	1.55	1.54	0.82	-0.97	1.19	1.02	0.79	0.71	0.71
					10m	1.75	1.72	0.89	-0.78	1.04	0.86	0.79	0.77	0.80
					20m	2.41	2.39	1.19	-0.12	0.77	0.59	0.78	0.88	0.87
<b>Nov</b>		1.61	1.40	0.97	4m	4.81	4.68	2.48	3.20	3.90	3.31	0.45	0.34	0.20
					10m	4.59	4.56	2.12	2.98	3.43	3.02	0.61	0.40	0.22
					20m	4.32	4.30	1.92	2.71	3.10	2.73	0.63	0.43	0.25
<b>Dec</b>	INMET -VIX	1.70	1.50	1.01	4m	4.76	4.95	2.33	3.06	3.61	3.13	0.59	0.40	0.23
					10m	4.70	4.95	2.18	3.00	3.41	3.03	0.71	0.44	0.21
					20m	4.36	4.61	2.04	2.66	3.03	2.68	0.74	0.48	0.28
<b>Feb</b>		1.55	1.30	0.96	4m	3.97	3.92	2.27	2.47	3.11	2.62	0.56	0.43	0.31
					10m	3.90	3.99	2.01	2.38	2.82	2.44	0.70	0.48	0.32
					20m	3.68	3.78	1.85	2.15	2.52	2.18	0.74	0.52	0.38

Table S2. Statistical metrics for WD10.

Month	Station	Mean <sub>BS</sub>	Median <sub>OBS</sub>	SD <sub>OBS</sub>	Height	Mean <sub>MOD</sub>	Median <sub>MOD</sub>	SD <sub>MOD</sub>	MB	RSME	MAGE	r	IOA	FAC2	
Nov	AEROP ORTO	11.49	20.00	96.29	4m	22.69	38.59	96.61	<b>11.83</b>	95.97	52.94	0.49	0.74	0.63	
					10m	24.01	37.66	95.12	<b>13.34</b>	96.48	53.10	0.48	0.73	0.63	
					20m	28.08	39.89	94.00	<b>18.42</b>	101.46	56.60	0.43	0.70	0.60	
Dec		4m	5.95	10.00	74.69	4m	15.62	28.34	68.74	<b>9.67</b>	72.23	37.70	0.50	0.73	0.58
		10m				14.60	25.46	69.52	<b>8.68</b>	74.36	38.58	0.47	0.72	0.55	
		20m				14.58	23.51	69.20	<b>8.96</b>	75.33	39.05	0.46	0.71	0.53	
Feb		4m	11.45	20.00	82.94	4m	11.80	22.36	81.94	<b>4.93</b>	75.40	40.45	0.53	0.77	0.61
		10m				7.13	18.43	83.07	<b>0.99</b>	72.08	37.41	0.57	0.80	0.61	
		20m				9.94	18.48	83.10	<b>3.24</b>	77.60	40.96	0.51	0.76	0.59	
Nov	ASMA- VIX	38.87	38.78	55.36	4m	20.45	39.13	98.25	<b>-19.59</b>	122.55	98.83	-0.10	0.31	0.30	
					10m	20.56	36.24	98.20	<b>-19.08</b>	123.83	99.88	-0.13	0.29	0.29	
					20m	24.83	39.23	97.06	<b>-14.31</b>	121.47	97.60	-0.11	0.30	0.30	
Dec		4m	45.87	50.35	40.45	4m	14.39	28.20	71.40	<b>-31.48</b>	90.93	66.36	-0.09	0.32	0.36
		10m				11.05	23.54	72.00	<b>-34.82</b>	91.24	67.10	-0.05	0.34	0.33	
		20m				7.58	18.19	72.58	<b>-38.30</b>	93.51	69.25	-0.06	0.34	0.29	
Feb		4m	46.79	52.74	45.91	4m	6.22	24.35	86.04	<b>-40.87</b>	108.83	85.74	-0.08	0.34	0.25
		10m				2.88	17.44	87.20	<b>-44.23</b>	112.47	89.37	-0.12	0.32	0.22	
		20m				4.44	14.82	87.03	<b>-42.74</b>	110.55	88.98	-0.09	0.34	0.22	
Nov	CARA PINA	4.11	63.76	109.72	4m	22.07	37.63	98.03	<b>17.87</b>	123.93	86.00	0.31	0.63	0.41	
					10m	20.58	35.09	97.55	<b>16.39</b>	124.78	87.47	0.29	0.62	0.38	
					20m	21.61	37.98	96.45	<b>17.36</b>	124.71	87.90	0.29	0.62	0.39	
Dec		4m	31.85	66.82	86.54	4m	9.58	27.39	72.83	<b>-22.39</b>	81.05	60.40	0.53	0.73	0.40
		10m				9.85	26.49	72.90	<b>-22.09</b>	82.75	61.89	0.51	0.72	0.39	
		20m				10.77	24.03	71.91	<b>-21.16</b>	82.83	61.91	0.50	0.71	0.38	
Feb		4m	14.68	66.76	98.23	4m	6.55	19.37	83.82	<b>-8.14</b>	105.17	76.27	0.34	0.64	0.36
		10m				0.89	15.84	84.05	<b>-13.79</b>	100.04	72.80	0.42	0.68	0.36	
		20m				4.41	15.51	84.68	<b>-10.27</b>	105.27	76.29	0.35	0.64	0.35	
Nov	CARIA CICA	17.48	69.69	97.30	4m	16.02	35.08	97.70	<b>-1.46</b>	112.77	79.26	0.33	0.64	0.47	
					10m	15.00	34.42	96.51	<b>-2.48</b>	109.03	76.84	0.37	0.66	0.45	
					20m	12.49	30.34	97.49	<b>-5.00</b>	109.64	78.60	0.37	0.66	0.43	

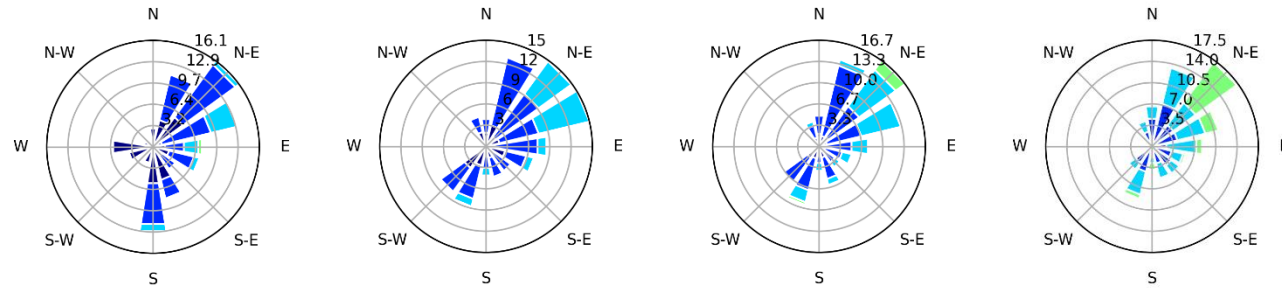
<b>Dec</b>	46.15	75.32	74.33	4m	12.44	29.30	69.52	-33.76	77.60	60.36	0.53	0.71	0.38	
				10m	13.14	26.80	68.10	-33.07	78.83	62.13	0.50	0.70	0.35	
				20m	10.61	22.72	68.52	-35.59	79.15	63.79	0.51	0.70	0.32	
<b>Feb</b>	6.86	52.24	89.13	4m	6.40	24.47	83.98	-0.45	82.96	49.83	0.54	0.76	0.54	
				10m	9.18	23.74	83.46	2.32	90.92	54.25	0.45	0.71	0.52	
				20m	6.29	19.03	82.70	-0.57	90.00	54.14	0.45	0.71	0.48	
<b>Nov</b>	47.50	56.22	94.71	4m	19.65	44.64	97.01	-27.85	125.04	70.25	0.19	0.56	0.65	
				10m	22.23	42.78	96.04	-25.27	124.80	71.11	0.18	0.55	0.63	
				20m	25.31	44.11	93.44	-22.19	123.01	70.94	0.17	0.55	0.61	
<b>Dec</b>	ENSEA DA	39.95	46.43	75.01	4m	20.03	34.81	70.13	-19.93	87.75	44.73	0.31	0.62	0.69
					10m	13.88	29.58	71.82	-26.08	90.23	47.59	0.31	0.62	0.64
					20m	13.07	24.42	70.44	-26.89	92.58	50.49	0.26	0.59	0.60
<b>Feb</b>	42.50	48.34	87.54	4m	13.63	32.31	84.30	-28.87	110.06	61.49	0.24	0.58	0.65	
				10m	6.76	23.43	85.44	-35.74	107.10	59.46	0.32	0.62	0.62	
				20m	5.26	19.22	84.93	-37.24	110.45	62.71	0.27	0.60	0.58	
<b>Nov</b>	-7.08	40.29	105.61	4m	15.76	39.37	96.21	22.71	97.98	55.83	0.56	0.76	0.62	
				10m	21.63	41.53	95.05	28.72	100.62	57.69	0.54	0.75	0.62	
				20m	22.67	42.13	93.58	29.78	105.12	61.18	0.50	0.73	0.59	
<b>Dec</b>	IBES	5.78	45.04	76.21	4m	17.84	32.13	69.22	17.08	73.60	43.26	0.40	0.70	0.58
					10m	12.67	29.76	70.36	12.30	68.93	41.42	0.45	0.74	0.58
					20m	11.37	25.20	69.95	11.07	68.35	41.78	0.45	0.74	0.56
<b>Feb</b>	-11.27	-4.97	94.95	4m	6.21	28.25	83.46	17.48	80.61	47.59	0.62	0.79	0.59	
				10m	6.53	25.92	84.47	17.81	82.29	47.90	0.60	0.79	0.58	
				20m	2.79	20.77	83.82	14.06	82.95	48.17	0.59	0.78	0.56	
<b>Nov</b>	6.91	8.00	100.21	4m	21.48	38.70	99.67	14.61	114.22	65.31	0.35	0.66	0.53	
				10m	21.12	37.44	98.87	14.26	115.52	66.00	0.33	0.65	0.54	
				20m	25.79	41.45	97.49	19.33	119.21	69.15	0.29	0.63	0.52	
<b>Dec</b>	INMET -VIX	-5.44	-5.00	74.32	4m	12.27	21.73	72.06	17.66	77.88	44.44	0.46	0.71	0.44
					10m	10.77	19.56	73.06	16.17	78.03	44.61	0.46	0.71	0.46
					20m	6.09	16.09	73.58	11.49	75.28	43.12	0.49	0.73	0.48
<b>Feb</b>	-5.98	-13.00	89.13	4m	6.63	18.35	87.29	10.76	90.00	52.47	0.49	0.74	0.55	
				10m	3.92	15.43	88.15	8.16	87.75	50.52	0.52	0.75	0.55	
				20m	5.42	14.38	88.05	10.26	96.62	54.67	0.42	0.70	0.54	

Table S3. Comparison of observed and modelled wind roses.

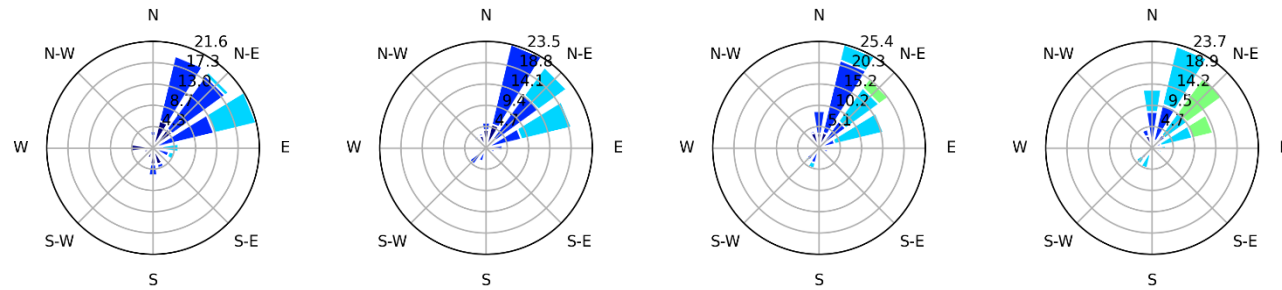


**ST04  
Enseada**

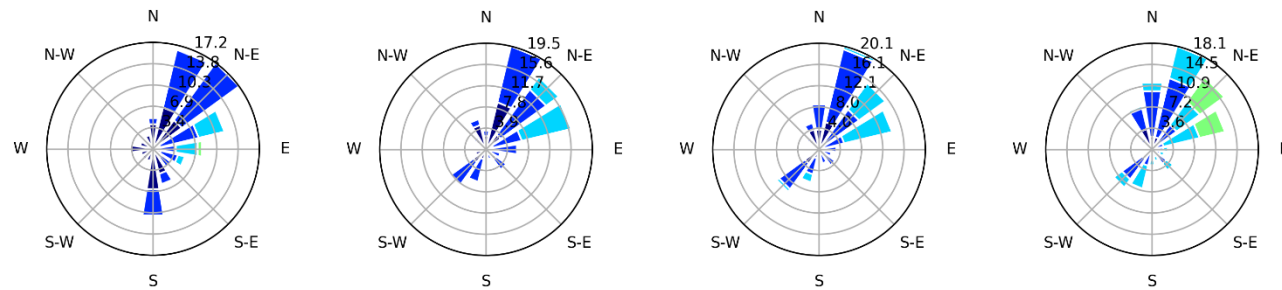
Nov/2019



Dec/2019

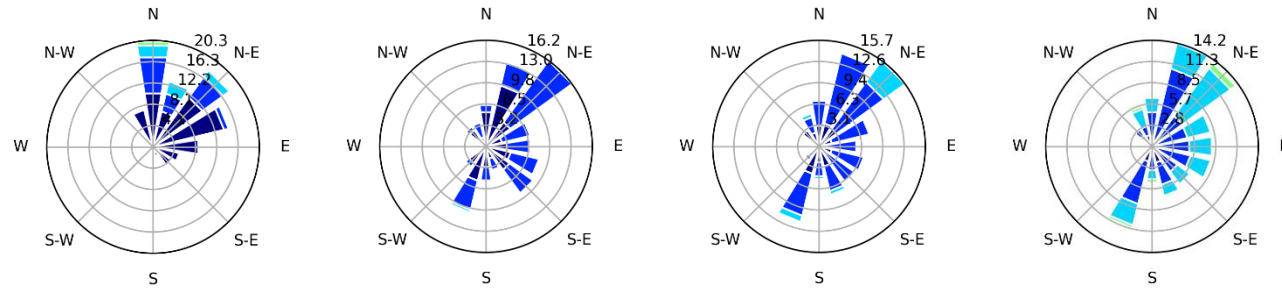


Feb/2020

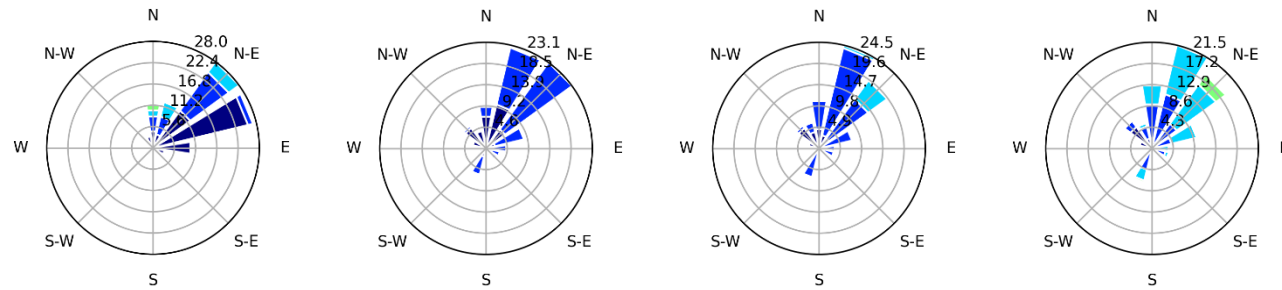


**ASMA-Vix**

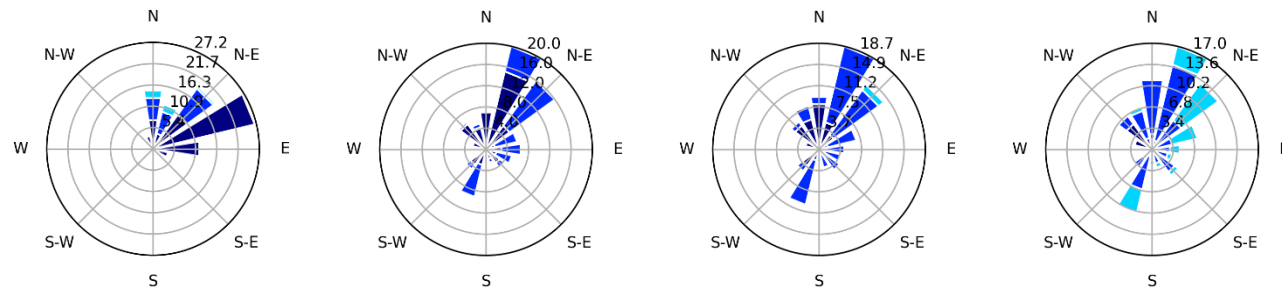
Nov/2019



Dec/2019

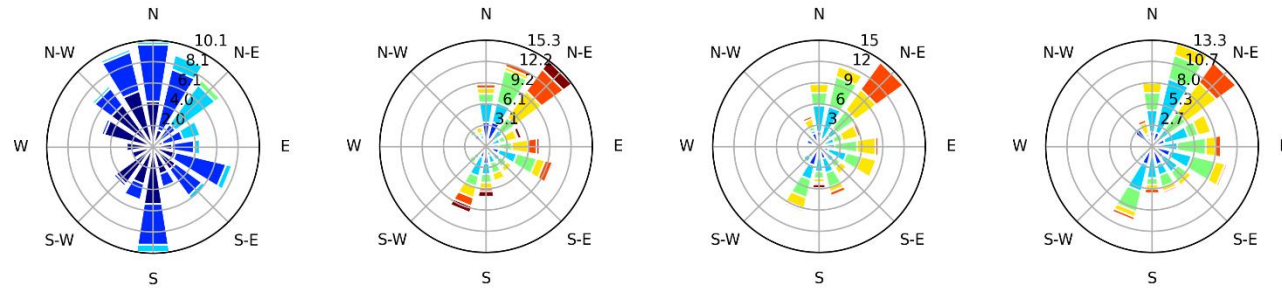


Feb/2020

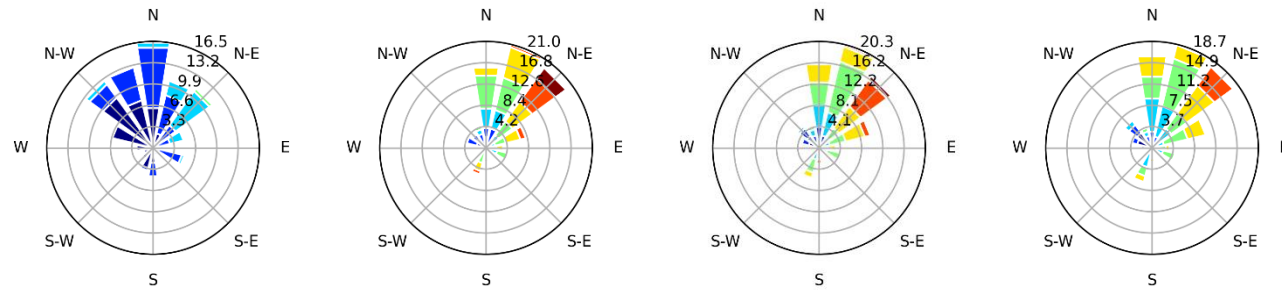


**INMET-  
Vix**

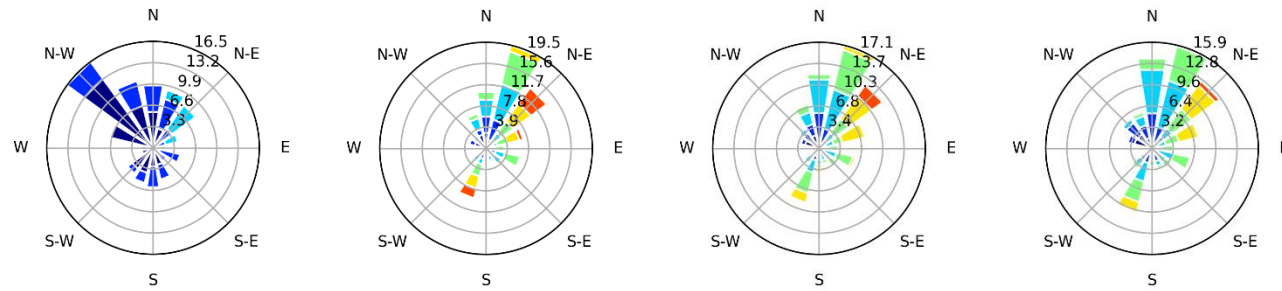
Nov/2019



Dec/2019



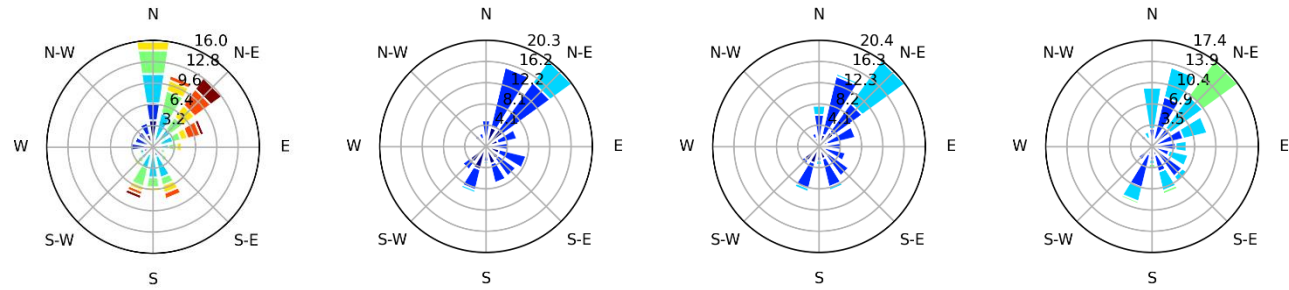
Feb/2020



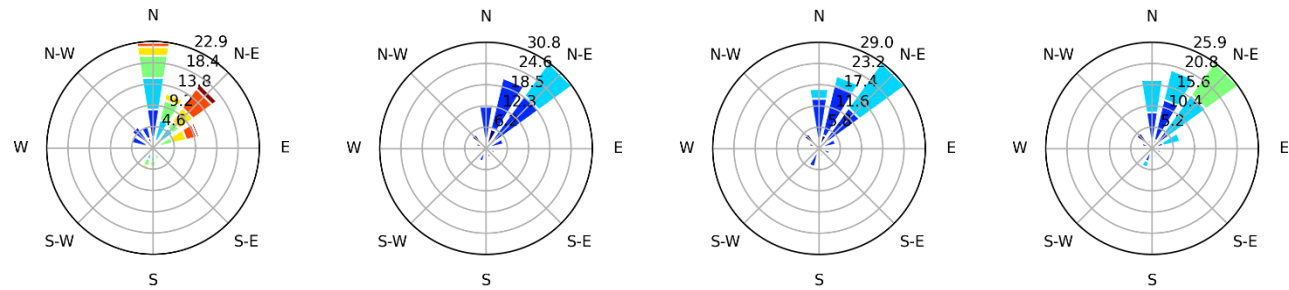


**Airport**

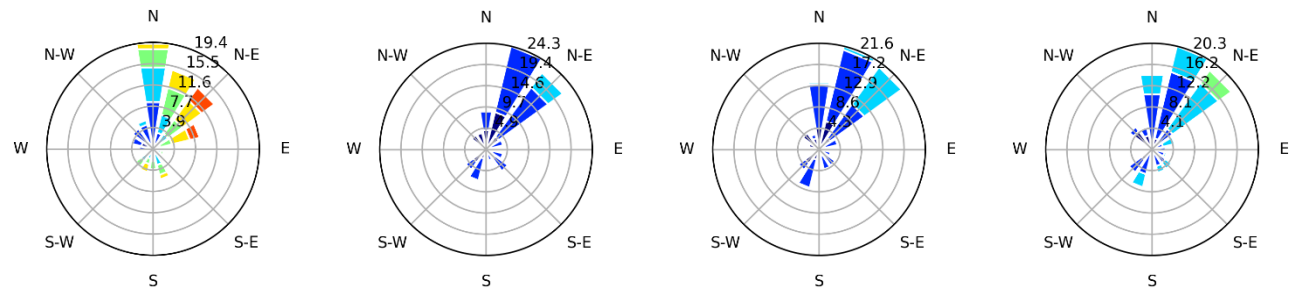
Nov/2019



Dec/2019

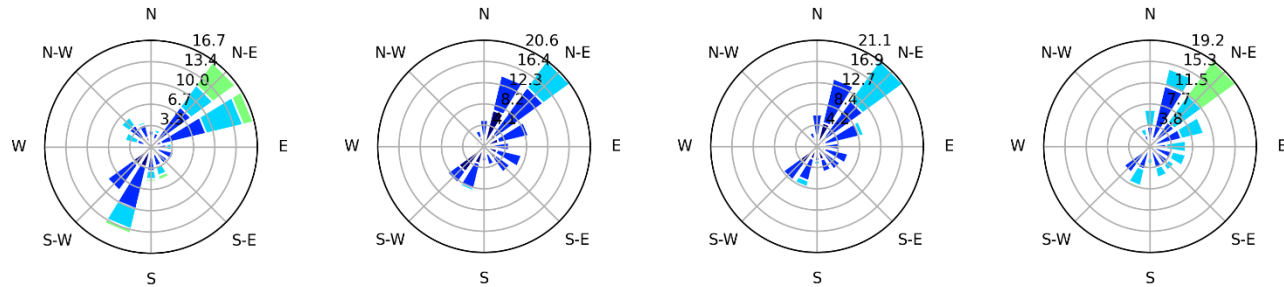


Feb/2020

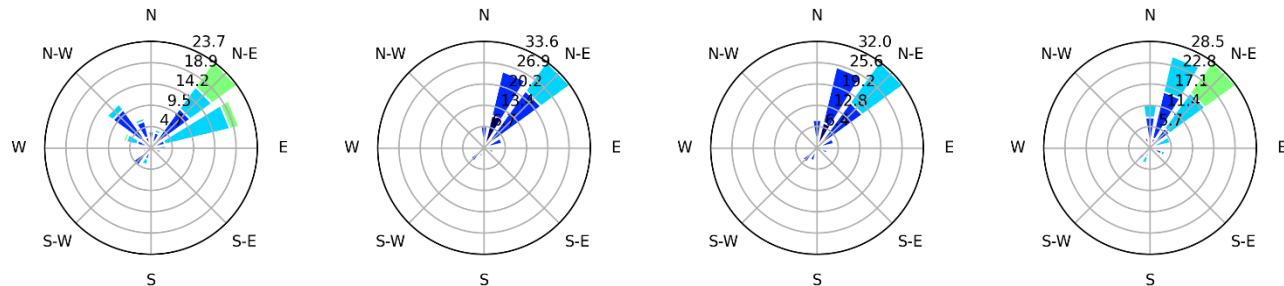


**ST06  
IBES**

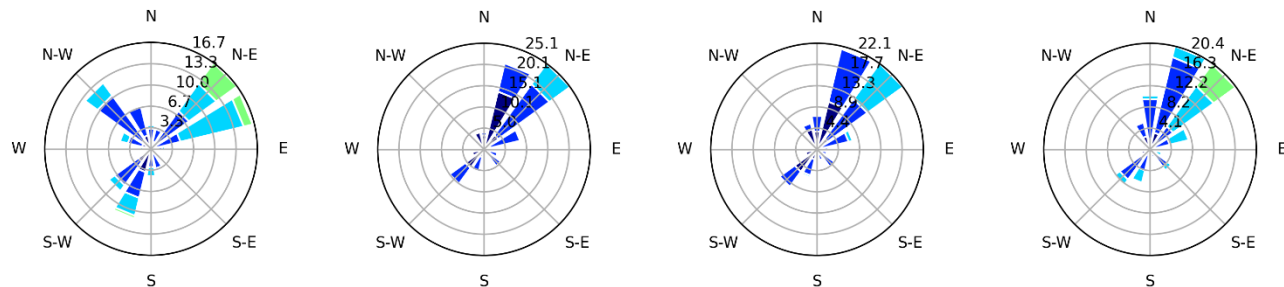
Nov/2019



Dec/2019

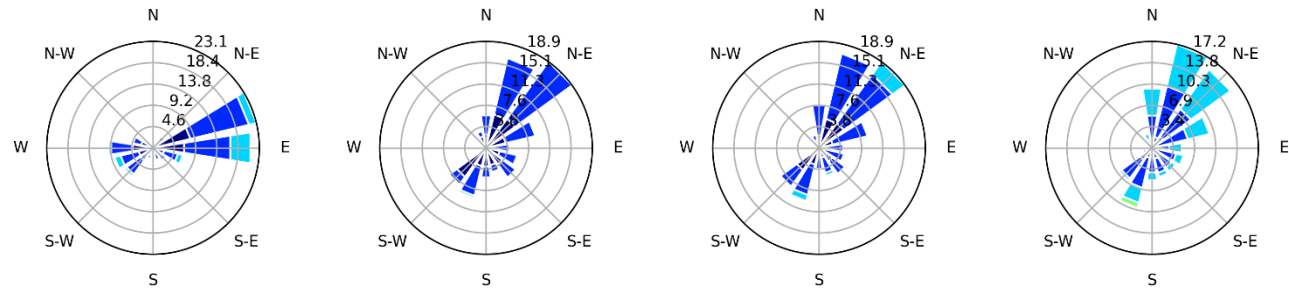


Feb/2020

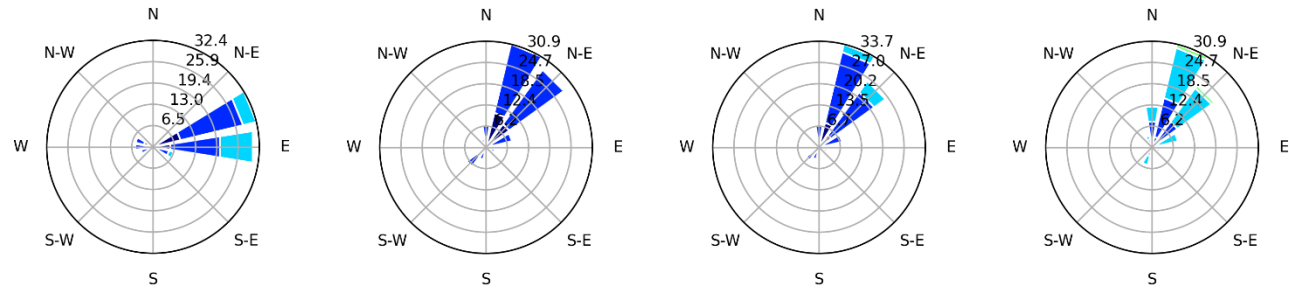


**ST08  
Cariacica**

Nov/2019



Dec/2019



Feb/2020

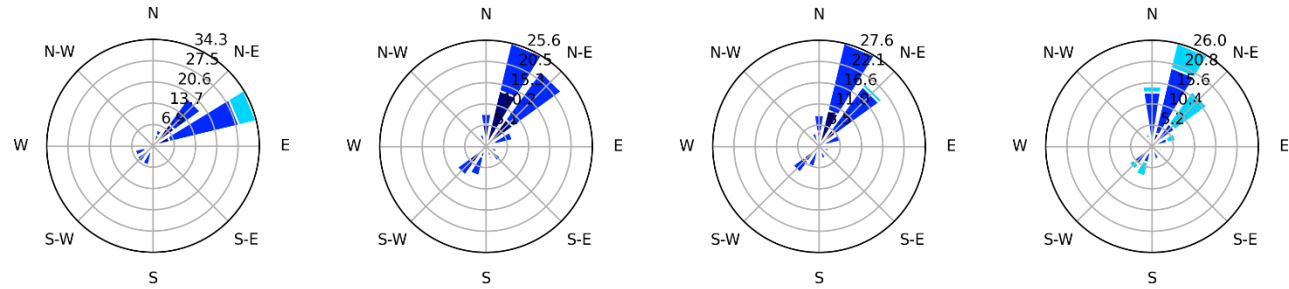


Table S4. Statistical metrics for T2.

Month	Station	Mean <sub>OBS</sub>	Median <sub>OBS</sub>	SD <sub>OBS</sub>	Height	Mean <sub>MOD</sub>	Median <sub>MOD</sub>	SD <sub>MOD</sub>	MB	RSME	MAGE	r	IOA	FAC2
Nov	AEROPORTO	24.84	24.00	2.76	4m	25.74	24.74	3.30	<b>0.94</b>	2.02	1.46	0.84	0.89	1.00
					10m	25.60	24.67	3.08	<b>0.80</b>	1.81	1.32	0.85	0.90	1.00
					20m	25.25	24.65	2.65	0.44	1.45	1.10	0.87	0.93	1.00
Dec		25.93	26.00	2.65	4m	26.58	25.35	3.57	<b>0.65</b>	2.10	1.47	0.83	0.88	1.00
					10m	26.41	25.35	3.34	0.48	1.89	1.33	0.84	0.89	1.00
					20m	25.95	25.21	2.83	0.02	1.48	1.07	0.85	0.92	1.00
Feb		26.88	26.00	2.60	4m	27.44	26.19	3.68	<b>0.63</b>	1.99	1.46	0.87	0.90	1.00
					10m	27.20	26.02	3.40	0.38	1.67	1.25	0.88	0.92	1.00
					20m	26.81	26.07	2.89	-0.02	1.26	0.98	0.89	0.95	1.00
Nov	ASMA-VIX	25.46	24.94	2.83	4m	25.76	24.67	3.43	0.08	2.31	1.74	0.65	0.84	1.00
					10m	25.60	24.59	3.22	-0.07	2.20	1.64	0.65	0.85	1.00
					20m	25.23	24.51	2.78	-0.43	2.04	1.51	0.66	0.85	1.00
Dec		27.03	26.66	2.86	4m	26.60	25.41	3.64	-0.43	2.42	1.85	0.76	0.85	1.00
					10m	26.36	25.29	3.38	-0.67	2.35	1.80	0.75	0.85	1.00
					20m	25.90	25.19	2.89	-1.13	2.35	1.80	0.74	0.83	1.00
Feb		28.04	27.43	2.84	4m	27.43	26.12	3.73	-0.61	1.87	1.61	0.89	0.92	1.00
					10m	27.17	25.97	3.46	-0.87	1.78	1.52	0.90	0.92	1.00
					20m	26.79	25.97	2.96	-1.25	1.78	1.53	0.90	0.91	1.00
Nov	CARAPINA	22.75	21.94	3.33	4m	24.79	24.18	2.55	<b>2.04</b>	2.59	2.21	0.89	0.83	1.00
					10m	24.76	24.17	2.65	<b>2.00</b>	2.53	2.16	0.89	0.84	1.00
					20m	24.71	24.08	2.73	<b>1.96</b>	2.49	2.12	0.89	0.85	1.00
Dec		23.78	22.99	3.31	4m	25.56	24.92	2.69	<b>1.76</b>	2.29	1.90	0.89	0.86	1.00
					10m	25.58	24.93	2.77	<b>1.78</b>	2.29	1.89	0.90	0.87	1.00
					20m	25.46	24.79	2.79	<b>1.66</b>	2.20	1.81	0.89	0.88	1.00
Feb		24.82	23.82	3.34	4m	26.44	25.77	2.71	<b>1.62</b>	2.08	1.78	0.93	0.89	1.00
					10m	26.30	25.58	2.78	<b>1.48</b>	1.92	1.63	0.94	0.91	1.00
					20m	26.23	25.53	2.84	<b>1.41</b>	1.87	1.58	0.93	0.91	1.00
Nov	CARIACICA	26.03	24.98	3.83	4m	25.87	24.41	4.00	-0.16	1.81	1.38	0.89	0.94	1.00
					10m	25.70	24.44	3.72	-0.33	1.73	1.37	0.90	0.95	1.00
					20m	25.34	24.35	3.26	-0.68	1.80	1.42	0.90	0.93	1.00
Dec		27.25	26.32	3.72	4m	26.89	25.42	4.26	-0.35	1.89	1.40	0.90	0.94	1.00

					10m	26.65	25.28	3.95	-0.60	1.82	1.37	0.90	0.94	1.00
					20m	26.15	25.17	3.38	-1.09	1.96	1.57	0.90	0.92	1.00
<b>Feb</b>		28.27	27.14	3.59	4m	27.65	25.90	4.32	-0.63	1.77	1.43	0.93	0.95	1.00
					10m	27.40	25.85	3.99	-0.87	1.72	1.40	0.93	0.95	1.00
					20m	27.01	25.81	3.43	-1.26	1.86	1.52	0.93	0.93	1.00
<b>Nov</b>		24.77	24.10	3.16	4m	25.06	24.25	2.99	0.29	1.48	1.16	0.89	0.94	1.00
					10m	25.00	24.16	3.04	0.23	1.48	1.16	0.89	0.94	1.00
					20m	24.86	23.99	3.08	0.09	1.43	1.14	0.90	0.95	1.00
<b>Dec</b>	INMET-VIX	25.90	25.50	3.11	4m	25.94	25.12	3.21	0.04	1.40	1.02	0.90	0.95	1.00
					10m	25.88	25.09	3.26	-0.01	1.42	1.05	0.90	0.95	1.00
					20m	25.70	24.93	3.27	-0.20	1.42	1.08	0.90	0.95	1.00
<b>Feb</b>		26.73	26.00	3.17	4m	26.80	25.90	3.24	0.07	1.16	0.88	0.91	0.97	1.00
					10m	26.64	25.61	3.28	-0.10	1.12	0.86	0.91	0.97	1.00
					20m	26.51	25.50	3.30	-0.22	1.14	0.89	0.92	0.97	1.00

Table S5. Statistical metrics for RH2.

Month	Station	Mean <sub>OBS</sub>	Median <sub>OBS</sub>	SD <sub>OBS</sub>	Height	Mean <sub>MOD</sub>	Median <sub>MOD</sub>	SD <sub>MOD</sub>	MB	RSME	MAGE	r	IOA	FAC2
<b>Nov</b>		81.04	83.18	13.73	4m	74.54	78.76	15.23	-5.71	12.72	10.15	0.61	0.79	1.00
					10m	74.71	78.50	14.66	-5.54	12.44	9.94	0.62	0.79	1.00
					20m	75.76	78.86	13.59	-4.43	11.19	9.09	0.64	0.81	1.00
<b>Dec</b>	ASMA-VIX	77.18	78.42	12.35	4m	74.01	78.55	15.83	-3.18	11.62	8.95	0.71	0.82	1.00
					10m	74.59	78.27	15.02	-2.59	11.16	8.67	0.70	0.82	1.00
					20m	76.09	78.46	13.46	-1.09	10.37	7.96	0.68	0.82	1.00
<b>Feb</b>		77.36	79.37	12.17	4m	75.92	80.06	16.29	-1.44	8.95	6.89	0.85	0.90	1.00
					10m	76.68	80.09	15.60	-0.68	8.46	6.63	0.84	0.90	1.00
					20m	77.62	80.24	14.30	0.26	7.95	6.19	0.83	0.90	1.00
<b>Nov</b>	CARAPINA	81.74	84.95	13.91	4m	81.58	85.15	11.86	-0.16	7.65	6.16	0.84	0.91	1.00
					10m	81.53	84.64	12.33	-0.21	7.50	5.89	0.84	0.91	1.00
					20m	81.60	84.64	12.94	-0.14	7.34	5.61	0.85	0.92	1.00
<b>Dec</b>		80.15	83.23	12.67	4m	81.22	84.04	11.78	1.21	7.12	5.29	0.83	0.91	1.00

					10m	80.92	84.20	12.00	<b>0.92</b>	6.84	5.15	0.84	0.92	1.00
					20m	81.41	84.52	12.20	<b>1.42</b>	7.16	5.52	0.83	0.91	1.00
					4m	82.59	85.31	12.25	<b>1.95</b>	6.36	5.04	0.88	0.93	1.00
<b>Feb</b>		80.64	83.20	12.64	10m	83.49	86.96	12.49	<b>2.84</b>	6.26	5.06	0.90	0.94	1.00
					20m	83.52	87.13	12.94	<b>2.88</b>	6.54	5.24	0.89	0.93	1.00
					4m	73.73	77.53	16.87	<b>-1.12</b>	9.29	7.12	0.83	0.91	1.00
<b>Nov</b>		75.09	78.93	15.13	10m	73.76	77.90	16.21	<b>-1.11</b>	8.93	6.86	0.83	0.91	1.00
					20m	74.71	77.91	14.94	<b>-0.18</b>	8.12	6.32	0.84	0.92	1.00
					4m	71.73	77.43	18.06	<b>3.08</b>	12.76	8.71	0.78	0.88	0.95
<b>Dec</b>	CARIACICA	68.64	74.90	19.46	10m	72.15	76.81	17.35	<b>3.51</b>	12.79	8.72	0.78	0.87	0.95
					20m	73.57	77.10	15.64	<b>4.92</b>	13.21	9.00	0.78	0.85	0.94
					4m	74.32	79.22	18.40	<b>-0.41</b>	8.72	6.69	0.89	0.92	1.00
<b>Feb</b>		74.73	78.73	14.06	10m	74.76	79.07	17.58	<b>0.03</b>	8.29	6.36	0.89	0.93	1.00
					20m	75.61	79.75	16.21	<b>0.88</b>	7.91	6.08	0.87	0.93	1.00
					4m	80.15	83.48	13.52	<b>1.29</b>	8.92	7.35	0.82	0.90	1.00
<b>Nov</b>		78.86	81.00	15.53	10m	80.12	83.31	13.79	<b>1.26</b>	8.84	7.17	0.83	0.90	1.00
					20m	80.76	84.83	14.29	<b>1.90</b>	8.60	6.79	0.85	0.91	1.00
					4m	78.91	82.02	14.12	<b>2.12</b>	8.11	6.30	0.85	0.92	1.00
<b>Dec</b>	INMET-VIX	76.79	78.00	14.60	10m	78.93	81.77	14.19	<b>2.14</b>	8.00	6.29	0.86	0.92	1.00
					20m	79.78	82.63	14.32	<b>3.00</b>	8.37	6.58	0.85	0.91	1.00
					4m	80.60	84.06	14.42	<b>3.21</b>	7.70	6.17	0.85	0.93	1.00
<b>Feb</b>		77.46	79.00	14.97	10m	81.42	84.97	14.67	<b>4.09</b>	7.88	6.39	0.86	0.93	1.00
					20m	81.78	85.47	14.97	<b>4.46</b>	8.28	6.71	0.86	0.92	1.00

Table S6. Statistical metrics for NO<sub>2</sub>.

Month	Station	Mean <sub>obs</sub>	Media <sub>noBS</sub>	SD <sub>obs</sub>	Height	Mean <sub>mod</sub>	Media <sub>nmod</sub>	SD <sub>mod</sub>	MB	RSME	MAG <sub>E</sub>	NMB	NME	r	IOA	FAC2
Nov	ASMA-VIX	10.0	8.5	4.3	4m	19.4	17.6	9.5	<b>9.9</b>	12.4	9.9	98.7	98.7	0.60	0.45	0.57
					10m	17.9	16.5	8.9	<b>8.3</b>	10.6	8.4	83.3	83.9	0.69	0.54	0.70
					20m	17.9	15.3	9.7	<b>8.3</b>	10.8	8.4	83.4	83.8	0.76	0.56	0.67
<b>Dec</b>		5.7	5.6	1.3	4m	15.3	12.2	8.9	<b>9.6</b>	12.8	9.6	168.4	168.4	0.48	0.16	0.45

				10m	14.6	12.2	8.7	<b>8.9</b>	12.0	8.9	155.0	155.0	0.48	0.16	0.48	
				20m	14.7	12.2	9.1	<b>9.0</b>	12.3	9.0	156.7	156.7	0.50	0.16	0.48	
<b>Feb</b>		4.5	3.2	3.8	4m	17.8	14.0	9.8	<b>13.4</b>	<b>15.9</b>	<b>13.4</b>	299.3	<b>299.3</b>	0.51	<b>0.34</b>	<b>0.07</b>
					10m	16.9	12.3	9.8	<b>12.4</b>	15.2	12.4	278.4	278.4	0.47	0.34	0.10
					20m	16.5	11.5	9.8	<b>12.0</b>	14.8	12.0	268.7	<b>268.7</b>	<b>0.47</b>	0.34	0.10
<b>Nov</b>		23.1	21.1	9.5	4m	21.8	19.6	7.8	<b>-1.3</b>	8.1	5.8	-5.5	<b>25.3</b>	<b>0.59</b>	<b>0.77</b>	<b>0.93</b>
					10m	19.2	17.9	7.3	<b>-3.9</b>	8.6	6.6	-16.8	28.5	0.61	0.74	0.97
					20m	17.7	16.4	7.5	<b>-5.4</b>	9.1	7.2	-23.4	<b>31.2</b>	<b>0.65</b>	<b>0.74</b>	<b>0.93</b>
<b>Dec</b>	CARI ACIC A	19.1	17.1	8.4	4m	18.9	16.2	8.8	<b>-0.1</b>	4.9	3.8	-0.7	20.1	0.84	0.91	0.94
					10m	17.1	15.8	8.5	<b>-2.0</b>	5.5	4.7	-10.6	24.8	0.82	0.89	0.94
					20m	16.3	14.5	8.7	<b>-2.8</b>	6.0	5.4	-14.8	<b>28.3</b>	<b>0.81</b>	<b>0.87</b>	<b>0.90</b>
<b>Feb</b>		21.2	19.5	8.2	4m	20.6	19.0	8.8	<b>-0.6</b>	7.6	5.9	-3.0	27.8	0.61	0.78	0.93
					10m	18.8	16.9	8.7	<b>-2.4</b>	8.2	6.7	-11.2	31.8	<b>0.57</b>	<b>0.75</b>	0.90
					20m	18.0	16.7	8.9	<b>-3.2</b>	8.2	6.8	-15.1	<b>32.3</b>	<b>0.61</b>	0.76	<b>0.79</b>
<b>Nov</b>		19.9	19.9	6.6	4m	21.8	23.1	7.2	<b>2.0</b>	7.2	5.5	9.9	27.8	<b>0.45</b>	<b>0.69</b>	0.97
					10m	19.9	21.0	7.2	<b>-0.1</b>	6.2	4.7	-0.4	23.6	0.56	0.78	0.97
					20m	18.5	18.9	6.9	<b>-1.5</b>	6.9	5.5	-7.4	<b>27.8</b>	0.45	0.70	<b>0.93</b>
<b>Dec</b>	CENT RO- VIX	13.0	11.5	6.4	4m	19.9	18.5	8.2	<b>7.0</b>	11.3	7.8	53.6	<b>59.8</b>	0.28	0.53	<b>0.77</b>
					10m	18.3	17.5	8.2	<b>5.3</b>	10.7	7.3	40.9	56.7	<b>0.21</b>	<b>0.52</b>	<b>0.81</b>
					20m	17.8	17.2	8.9	<b>4.9</b>	10.7	7.3	37.7	<b>56.0</b>	0.27	0.55	<b>0.81</b>
<b>Feb</b>		14.5	14.7	4.5	4m	21.5	19.2	7.5	<b>7.0</b>	9.2	7.7	48.3	<b>53.1</b>	0.61	<b>0.55</b>	<b>0.90</b>
					10m	19.8	17.7	7.9	<b>5.3</b>	8.4	6.7	36.6	46.5	0.55	0.56	0.93
					20m	19.1	16.3	8.2	<b>4.6</b>	8.3	6.4	32.0	<b>44.0</b>	<b>0.55</b>	<b>0.57</b>	<b>0.93</b>
<b>Nov</b>		20.3	19.0	6.1	4m	27.5	28.2	8.9	<b>7.2</b>	12.7	9.4	35.6	<b>46.4</b>	<b>0.06</b>	<b>0.41</b>	<b>0.77</b>
					10m	24.2	24.1	7.8	<b>3.9</b>	10.1	8.1	19.4	39.8	0.11	0.47	0.80
					20m	22.2	21.4	7.5	<b>1.9</b>	9.6	8.1	9.5	<b>39.7</b>	0.06	0.43	0.90
<b>Dec</b>	ENSE ADA	16.4	15.2	4.8	4m	29.7	29.4	8.3	<b>13.4</b>	16.2	14.7	81.7	<b>89.8</b>	<b>0.10</b>	<b>0.30</b>	<b>0.55</b>
					10m	26.9	26.3	8.3	<b>10.5</b>	13.9	12.5	64.3	76.2	0.11	0.33	0.71
					20m	25.2	25.2	8.5	<b>8.8</b>	12.5	11.0	53.9	<b>67.1</b>	0.21	0.38	0.71
<b>Feb</b>		13.9	13.7	4.8	4m	29.7	29.9	8.0	<b>16.1</b>	18.2	16.3	116.2	<b>117.4</b>	0.25	<b>0.30</b>	<b>0.38</b>
					10m	27.0	27.0	8.2	<b>13.5</b>	15.9	13.7	96.9	98.9	0.26	0.33	0.52
					20m	25.3	25.1	8.6	<b>11.9</b>	14.8	12.6	85.6	<b>90.6</b>	<b>0.23</b>	<b>0.34</b>	<b>0.55</b>
<b>Nov</b>	IBES	14.8	12.8	6.4	4m	29.8	28.2	9.0	<b>15.0</b>	17.2	15.0	101.2	<b>101.2</b>	0.43	<b>0.42</b>	<b>0.47</b>

					10m	25.6	24.3	7.7	<b>10.8</b>	13.3	11.3	72.9	76.3	0.40	0.47	0.57
					20m	22.5	21.8	7.2	<b>7.7</b>	11.1	8.9	52.1	60.5	0.31	0.49	0.63
<b>Dec</b>		13.1	12.9	4.1	4m	30.5	31.1	5.6	<b>17.8</b>	18.5	17.8	136.0	136.0	0.38	0.27	0.26
					10m	27.3	27.5	5.8	<b>14.5</b>	15.7	14.5	111.1	111.1	0.30	0.30	0.45
					20m	25.0	24.7	6.1	<b>12.2</b>	13.7	12.2	93.3	93.4	0.26	0.33	0.61
<b>Feb</b>		13.0	12.3	3.9	4m	30.8	31.5	6.7	<b>17.8</b>	19.2	17.8	137.7	137.7	0.22	0.24	0.28
					10m	27.2	28.2	6.9	<b>14.2</b>	15.9	14.2	109.8	109.8	0.22	0.27	0.41
					20m	24.9	25.5	7.4	<b>12.0</b>	14.1	12.4	92.3	95.5	0.26	0.29	0.52
<b>Nov</b>		14.9	14.0	4.6	4m	25.2	21.6	10.9	<b>10.2</b>	12.9	10.3	68.3	68.6	0.76	0.51	0.70
					10m	22.9	20.2	10.0	<b>7.9</b>	10.8	8.2	53.1	54.6	0.73	0.57	0.80
					20m	21.8	19.0	10.3	<b>6.8</b>	10.3	7.5	45.8	50.3	0.71	0.58	0.80
<b>Dec</b>	JC	13.2	12.2	3.6	4m	20.1	18.5	8.8	<b>5.4</b>	7.5	5.7	41.2	43.2	0.32	0.58	0.90
					10m	18.2	16.4	8.8	<b>3.3</b>	6.3	4.4	25.0	33.7	0.29	0.63	0.94
					20m	17.8	14.7	9.7	<b>2.9</b>	6.6	4.4	21.9	33.5	0.34	0.64	0.94
<b>Feb</b>																
<b>Nov</b>		17.9	17.5	5.4	4m	20.3	20.7	7.8	<b>2.3</b>	8.4	6.2	13.1	34.4	0.30	0.53	0.87
					10m	18.4	16.7	7.8	<b>0.5</b>	8.2	6.5	2.8	36.0	0.27	0.53	0.83
					20m	15.8	13.9	7.5	<b>-2.1</b>	8.9	7.2	-11.5	40.2	0.13	0.45	0.73
<b>Dec</b>	LARA NJEIR AS	12.7	10.7	6.4	4m	18.8	17.6	8.1	<b>6.0</b>	13.2	9.4	47.4	74.2	-0.31	0.20	0.68
					10m	16.8	15.8	7.1	<b>4.1</b>	11.7	8.7	32.4	68.7	-0.32	0.20	0.71
					20m	16.0	14.3	7.8	<b>3.3</b>	12.3	9.3	25.7	73.0	-0.38	0.13	0.71
<b>Feb</b>		14.0	13.1	4.1	4m	20.6	18.8	7.4	<b>6.6</b>	9.2	7.1	46.8	51.0	0.47	0.48	0.83
					10m	19.6	18.0	7.1	<b>5.6</b>	8.5	6.6	39.7	47.0	0.44	0.51	0.83
					20m	18.1	15.9	7.4	<b>4.1</b>	7.9	6.1	29.5	43.8	0.43	0.53	0.83

Table S7. Statistical metrics for O<sub>3</sub>.

Month	Station	Mean <sub>OBS</sub>	Media <sub>OBS</sub>	SD <sub>OBS</sub>	Height	Mean <sub>MOD</sub>	Media <sub>MOD</sub>	SD <sub>MOD</sub>	MB	RSME	MAG <sub>E</sub>	NMB	NME	r	IOA	FAC2
Nov		38.8	38.8	14.0	4m	42.1	40.8	10.3	<b>2.3</b>	14.2	10.8	5.8	27.8	0.37	0.59	0.90



	ASMA				10m	42.2	41.0	9.2	<b>3.0</b>	14.2	10.8	7.7	27.9	0.36	0.56	0.90
	-VIX				20m	41.4	41.1	10.9	<b>2.0</b>	14.3	10.9	5.2	28.2	0.40	0.62	0.93
<b>Dec</b>	CARI	41.3	41.9	8.7	4m	46.5	46.4	7.9	<b>5.3</b>	15.1	11.2	12.9	27.1	-0.43	0.23	0.97
					10m	46.7	46.8	7.6	<b>5.5</b>	14.8	10.6	13.3	25.6	-0.40	0.27	0.94
					20m	47.8	47.8	7.8	<b>6.6</b>	15.1	10.5	15.9	25.5	-0.33	0.30	0.94
<b>Feb</b>	ACIC	39.8	40.3	9.1	4m	42.9	40.1	10.2	<b>3.1</b>	12.5	9.9	7.9	24.8	0.22	0.52	1.00
					10m	44.3	41.0	10.0	<b>4.5</b>	12.9	10.0	11.4	25.2	0.20	0.49	1.00
					20m	44.8	41.7	9.7	<b>5.0</b>	13.1	10.1	12.7	25.4	0.18	0.47	1.00
<b>Dec</b>	ENSE	36.4	35.4	7.3	4m	34.6	32.3	11.7	<b>-1.7</b>	11.9	8.7	-4.8	24.0	0.30	0.51	0.97
					10m	35.8	33.6	11.7	<b>-0.5</b>	12.0	8.7	-1.5	24.1	0.26	0.49	0.94
					20m	36.5	34.9	12.1	<b>0.1</b>	12.4	8.6	0.4	23.6	0.26	0.49	0.94
<b>Feb</b>	ADA	40.2	38.8	9.1	4m	31.8	33.6	7.9	<b>-8.4</b>	12.5	10.7	-21.0	26.7	0.42	0.54	1.00
					10m	33.2	32.7	7.2	<b>-7.0</b>	11.5	9.5	-17.4	23.7	0.39	0.54	1.00
					20m	34.4	35.7	8.1	<b>-5.9</b>	11.4	9.4	-14.6	23.3	0.37	0.56	1.00
<b>Dec</b>	IBES	40.2	40.1	7.8	4m	41.3	40.4	9.2	<b>1.0</b>	9.9	7.5	2.6	18.8	0.36	0.55	1.00
					10m	42.2	41.4	8.9	<b>1.9</b>	10.0	7.6	4.8	18.9	0.34	0.54	1.00
					20m	42.6	41.9	9.3	<b>2.3</b>	10.4	8.0	5.7	19.8	0.32	0.54	1.00
<b>Feb</b>		54.8	52.3	11.3	4m	38.9	39.1	7.7	<b>-15.9</b>	19.7	16.2	-29.0	29.5	0.29	0.47	0.97
					10m	40.3	40.1	6.8	<b>-14.5</b>	18.4	14.8	-26.5	27.1	0.30	0.48	0.97
					20m	40.4	39.6	6.5	<b>-14.4</b>	18.2	14.8	-26.3	27.0	0.32	0.48	0.97
<b>Dec</b>	LARA	42.7	41.7	9.8	4m	43.8	43.9	6.6	<b>1.5</b>	12.1	9.0	3.5	21.1	-0.04	0.32	1.00
					10m	45.0	44.8	5.5	<b>2.4</b>	11.7	8.8	5.6	20.7	-0.02	0.31	1.00
					20m	45.6	46.0	6.1	<b>3.2</b>	12.6	9.7	7.4	22.7	-0.11	0.29	1.00
<b>Feb</b>	NJEIR	37.2	33.0	8.2	4m	41.3	39.5	8.2	<b>4.1</b>	11.3	8.9	10.9	23.9	0.19	0.46	1.00
					10m	42.0	39.5	8.4	<b>4.8</b>	12.3	10.2	12.9	27.3	0.07	0.39	1.00
					20m	42.3	38.9	8.3	<b>5.1</b>	13.1	10.8	13.7	29.0	-0.08	0.28	1.00

Table S8. Statistical metrics for PM<sub>2.5</sub>.

Month	Station	Mean <sub>OBS</sub>	Media <sub>NOBS</sub>	SD <sub>OBS</sub>	Height	Mean <sub>MOD</sub>	Media <sub>NMOD</sub>	SD <sub>MOD</sub>	MB	RSME	MAG <sub>E</sub>	NMB	NME	r	IOA	FAC2
Nov		4.3	3.1	2.2	4m	8.6	8.3	3.4	<b>4.4</b>	5.9	4.7	102.7	109.3	0.09	0.34	0.50

					10m	7.8	8.0	2.5	<b>3.6</b>	4.8	3.9	83.3	90.7	<b>0.09</b>	0.39	<b>0.50</b>
					20m	7.4	7.3	2.5	<b>3.2</b>	4.5	3.7	74.8	85.8	<b>0.11</b>	0.40	<b>0.53</b>
<b>Dec</b>	ASMA-VIX	4.4	4.3	1.5	4m	7.8	7.0	3.0	<b>3.4</b>	5.0	3.6	75.4	81.5	<b>-0.27</b>	0.21	<b>0.61</b>
					10m	7.5	6.8	2.8	<b>3.1</b>	4.7	3.5	69.5	78.5	<b>-0.27</b>	0.21	<b>0.65</b>
					20m	7.3	6.4	2.8	<b>2.8</b>	4.5	3.3	63.6	73.1	<b>-0.25</b>	0.22	<b>0.65</b>
<b>Feb</b>		3.7	3.9	1.1	4m	9.4	7.7	4.2	<b>5.7</b>	7.0	5.7	152.1	152.8	<b>0.28</b>	0.21	<b>0.38</b>
					10m	9.1	7.3	4.6	<b>5.4</b>	7.0	5.5	144.5	146.2	<b>0.25</b>	0.20	<b>0.38</b>
					20m	8.4	6.8	4.0	<b>4.7</b>	6.1	4.8	125.8	127.9	<b>0.16</b>	0.21	<b>0.45</b>
<b>Nov</b>		11.8	11.4	3.4	4m	14.1	13.2	4.9	<b>2.2</b>	5.8	3.9	18.9	32.8	<b>0.21</b>	0.50	<b>0.93</b>
					10m	11.3	11.1	3.2	<b>-0.5</b>	3.8	3.2	-4.3	27.2	<b>0.36</b>	0.63	<b>1.00</b>
					20m	9.9	9.4	3.2	<b>-2.0</b>	4.3	3.6	-16.6	30.5	<b>0.33</b>	0.59	<b>0.97</b>
<b>Dec</b>	ENSE-ADA	10.7	10.7	2.6	4m	15.1	14.4	4.8	<b>4.4</b>	7.1	5.3	41.3	49.8	<b>-0.04</b>	0.28	<b>0.84</b>
					10m	13.0	12.8	3.8	<b>2.3</b>	5.1	4.0	21.2	37.2	<b>-0.02</b>	0.35	<b>0.84</b>
					20m	11.4	10.6	3.4	<b>0.7</b>	4.4	3.4	6.7	31.6	<b>-0.04</b>	0.33	<b>0.90</b>
<b>Feb</b>		9.8	9.6	1.9	4m	16.8	15.1	6.1	<b>7.0</b>	9.0	7.1	71.2	72.7	<b>0.35</b>	0.28	<b>0.72</b>
					10m	14.7	13.3	5.6	<b>4.8</b>	7.0	5.2	49.4	53.1	<b>0.42</b>	0.36	<b>0.83</b>
					20m	12.6	11.5	4.7	<b>2.8</b>	5.3	3.9	28.5	39.7	<b>0.32</b>	0.41	<b>0.93</b>

Table S9. Statistical metrics for PM<sub>10</sub>.

Month	Station	Mean <sub>obs</sub>	Media <sub>nobs</sub>	SD <sub>obs</sub>	Height	Mean <sub>mod</sub>	Media <sub>nmod</sub>	SD <sub>mod</sub>	MB	RSME	MAG <sub>E</sub>	NMB	NME	r	IOA	FAC2
<b>Nov</b>		20.1	21.3	6.8	4m	19.0	18.5	7.1	<b>-0.3</b>	8.2	6.8	-1.3	33.8	0.27	0.54	0.97
					10m	17.2	17.5	5.0	<b>-2.2</b>	7.6	6.2	-10.9	30.8	0.22	0.51	0.87
					20m	16.4	16.7	5.0	<b>-3.0</b>	7.9	6.6	-15.1	33.0	0.24	0.52	0.83
<b>Dec</b>	ASMA-VIX	16.8	16.8	3.5	4m	15.8	14.9	4.7	<b>-1.0</b>	6.4	5.2	-5.9	30.8	<b>-0.16</b>	0.25	0.94
					10m	15.0	13.9	4.5	<b>-1.7</b>	6.2	5.3	-10.4	31.9	-0.11	0.30	0.97
					20m	14.3	13.0	4.4	<b>-2.5</b>	6.2	5.5	-14.6	32.6	<b>-0.04</b>	0.33	0.97
<b>Feb</b>		16.2	15.4	4.0	4m	19.3	17.9	8.0	<b>3.1</b>	8.6	6.4	19.3	39.8	0.24	0.46	0.86
					10m	18.5	16.2	8.4	<b>2.3</b>	8.9	6.3	14.3	38.9	0.21	0.44	0.90
					20m	17.1	13.7	7.4	<b>0.9</b>	7.9	5.8	5.7	36.0	0.15	0.45	0.86

<b>Nov</b>		12.6	11.1	4.7	4m	15.7	14.8	3.8	<b>3.1</b>	5.3	4.4	24.4	34.8	0.50	0.63	<b>0.97</b>
					10m	15.8	14.6	4.1	<b>3.1</b>	5.2	4.3	24.8	34.3	0.56	0.67	<b>0.97</b>
					20m	15.2	13.7	4.4	<b>2.6</b>	5.5	4.4	20.2	35.1	0.43	0.61	<b>0.97</b>
<b>Dec</b>	CARA PINA	16.6	16.2	3.2	4m	15.1	14.4	3.2	<b>-1.6</b>	4.3	3.5	-9.4	20.8	0.21	0.53	<b>1.00</b>
					10m	14.8	14.6	3.2	<b>-1.8</b>	4.1	3.3	-11.1	19.9	0.36	0.60	<b>1.00</b>
					20m	14.7	13.9	3.7	<b>-1.9</b>	4.6	3.9	-11.5	23.5	0.24	0.53	<b>0.97</b>
<b>Feb</b>		15.5	14.5	4.1	4m	17.7	16.3	5.7	<b>2.2</b>	5.9	4.4	14.3	28.1	0.43	0.60	<b>0.97</b>
					10m	18.5	16.1	7.5	<b>3.0</b>	7.6	4.9	19.4	31.6	0.39	0.52	<b>0.93</b>
					20m	17.9	14.8	7.1	<b>2.4</b>	6.8	4.6	15.4	29.4	0.45	0.58	<b>0.93</b>
<b>Nov</b>		15.8	15.5	4.2	4m	23.3	23.6	6.9	<b>7.6</b>	10.3	8.0	47.9	50.9	0.28	0.42	<b>0.80</b>
					10m	20.5	20.0	5.8	<b>4.7</b>	7.5	5.9	29.6	37.5	0.35	0.54	0.93
					20m	17.9	17.4	5.0	<b>2.1</b>	5.5	4.6	13.3	28.9	0.40	0.63	<b>0.97</b>
<b>Dec</b>	CENT RO- VIX	14.6	14.2	2.6	4m	20.8	21.0	4.7	<b>6.2</b>	7.9	6.7	42.6	45.6	0.18	0.37	<b>0.94</b>
					10m	18.3	18.3	4.2	<b>3.7</b>	5.7	4.6	25.2	31.3	0.24	0.47	<b>0.97</b>
					20m	16.8	16.3	4.1	<b>2.2</b>	4.8	3.6	14.8	24.9	0.22	0.50	<b>0.97</b>
<b>Feb</b>		13.3	13.4	2.9	4m	24.2	22.7	8.6	<b>10.9</b>	13.5	10.9	82.1	82.1	0.34	0.29	<b>0.72</b>
					10m	21.4	20.6	7.8	<b>8.1</b>	10.9	8.4	61.2	63.4	0.36	0.34	<b>0.72</b>
					20m	18.7	17.0	6.3	<b>5.4</b>	8.2	5.9	40.7	44.8	0.28	0.37	<b>0.86</b>
<b>Nov</b>		29.9	28.2	9.7	4m	34.1	32.6	11.7	<b>4.6</b>	15.3	11.3	15.5	37.7	0.11	0.46	<b>0.83</b>
					10m	27.9	27.8	8.0	<b>-1.9</b>	11.5	10.0	-6.3	33.5	0.21	0.52	0.90
					20m	24.2	23.6	7.5	<b>-5.4</b>	12.0	10.2	-18.2	34.1	0.26	0.51	<b>0.93</b>
<b>Dec</b>	ENSE ADA	22.2	21.9	3.7	4m	35.2	32.7	9.6	<b>15.3</b>	18.9	15.8	69.0	70.9	-0.21	0.16	<b>0.90</b>
					10m	29.6	29.9	7.3	<b>9.1</b>	12.4	10.1	40.8	45.4	-0.29	0.19	0.94
					20m	25.5	24.1	6.2	<b>4.6</b>	8.9	6.7	20.9	30.1	-0.22	0.19	<b>0.97</b>
<b>Feb</b>		19.2	18.7	3.7	4m	38.3	36.9	11.8	<b>19.1</b>	22.3	19.4	99.3	101.1	0.20	0.20	<b>0.59</b>
					10m	33.1	33.0	10.9	<b>13.9</b>	17.4	14.4	72.5	75.1	0.28	0.27	0.69
					20m	28.2	27.6	8.9	<b>9.0</b>	12.8	10.4	47.0	54.4	0.18	0.30	<b>0.83</b>
<b>Nov</b>		21.5	21.0	9.2	4m	25.4	23.8	9.7	<b>3.8</b>	11.7	7.7	17.9	35.9	0.32	0.59	<b>0.90</b>
					10m	21.8	20.8	6.8	<b>0.2</b>	8.5	6.8	1.1	31.5	0.46	0.69	<b>0.93</b>
					20m	19.5	19.1	7.0	<b>-2.0</b>	9.2	7.0	-9.3	32.7	0.41	0.64	<b>0.93</b>
<b>Dec</b>	IBES	21.1	20.9	5.4	4m	25.4	23.6	8.7	<b>4.4</b>	11.6	7.8	20.9	36.9	-0.11	0.29	<b>0.87</b>
					10m	22.5	21.8	7.1	<b>1.4</b>	9.5	6.7	6.8	31.9	-0.10	0.33	<b>0.87</b>
					20m	20.2	19.3	6.9	<b>-0.8</b>	9.3	7.2	-3.9	34.2	-0.12	0.30	<b>0.87</b>

<b>Feb</b>		18.7	19.3	4.1	4m	29.8	26.7	12.5	<b>11.1</b>	17.0	11.5	59.7	61.6	0.06	0.24	0.72
					10m	26.5	23.9	11.5	<b>7.8</b>	14.3	10.0	42.0	53.6	0.06	0.26	0.76
					20m	23.5	19.8	10.5	<b>4.8</b>	12.2	8.4	25.7	45.1	0.03	0.29	0.83
<b>Nov</b>		19.9	19.3	6.0	4m	27.9	25.2	9.2	<b>8.0</b>	13.7	10.0	40.4	50.4	-0.04	0.31	0.77
					10m	23.1	23.0	5.7	<b>3.2</b>	9.1	7.4	16.0	37.2	-0.08	0.35	0.90
					20m	20.6	20.6	6.5	<b>0.7</b>	8.9	7.0	3.8	35.1	-0.02	0.35	0.93
<b>Dec</b>	JC	19.4	20.1	5.3	4m	26.2	23.7	8.9	<b>6.8</b>	14.0	9.6	35.1	49.4	-0.44	0.13	0.77
					10m	22.5	20.8	6.8	<b>3.1</b>	10.7	7.9	15.8	40.8	-0.42	0.14	0.87
					20m	20.0	18.1	6.0	<b>0.6</b>	9.6	7.5	3.1	38.7	-0.44	0.14	0.84
<b>Feb</b>		14.9	14.8	4.2	4m	31.2	28.8	13.7	<b>15.9</b>	21.1	15.9	106.3	106.3	0.14	0.20	0.76
					10m	26.6	22.9	12.0	<b>11.4</b>	16.8	11.4	76.2	76.2	0.16	0.22	0.79
					20m	23.8	20.2	10.2	<b>8.7</b>	13.9	9.0	58.4	60.2	0.13	0.25	0.83
<b>Nov</b>		22.4	20.7	9.1	4m	32.7	32.1	9.5	<b>10.3</b>	15.6	12.3	46.0	54.8	0.20	0.48	0.73
					10m	27.0	26.1	6.7	<b>4.6</b>	10.5	8.4	20.4	37.5	0.32	0.57	0.77
					20m	23.3	22.0	7.3	<b>0.9</b>	9.3	7.1	4.1	31.6	0.37	0.62	0.87
<b>Dec</b>	CENT RO- VV	20.5	19.8	4.6	4m	33.0	32.2	8.5	<b>12.4</b>	15.7	12.7	60.7	61.7	0.04	0.30	0.77
					10m	28.3	28.6	6.4	<b>7.8</b>	10.9	8.4	38.1	41.1	0.07	0.39	0.87
					20m	24.7	24.7	5.9	<b>4.2</b>	8.4	5.6	20.3	27.3	0.06	0.42	0.87
<b>Feb</b>		18.3	17.6	4.6	4m	37.4	33.7	13.0	<b>19.1</b>	23.4	19.2	104.4	104.7	0.07	0.22	0.52
					10m	32.5	29.3	10.8	<b>14.2</b>	18.1	14.4	77.7	78.8	0.12	0.28	0.66
					20m	28.5	25.4	10.0	<b>10.2</b>	15.2	11.0	55.5	60.1	-0.06	0.25	0.79

